SPIN-ORBIT AND MAGNETIC PROXIMITY LAYERS ON PAULI LIMITED SUPERCONDUCTING THIN FILMS

by

JOHN ERIC TKACZYK

B.S. Physics, Rutgers University
(1983)

SUBMITTED TO THE DEPARTMENT OF PHYSICS
IN PARTIAL FULFILLMENT OF THE REQUIREMENTS
FOR THE DEGREE OF

DOCTOR OF PHILOSOPHY IN PHYSICS

at the

MASSACHUSETTS INSTITUTE OF TECHNOLOGY
July, 1988

Signature of Author .....
Department of Physics
June, 1988

Certified by .....
P.A. Wolff
Professor, Department of Physics, MIT
Thesis Supervisor

Accepted by .....
G.F. Koster, Chairman
Departmental Graduate Committee
Department of Physics

SPIN-ORBIT AND MAGNETIC PROXIMITY LAYERS ON PAULI LIMITED SUPERCONDUCTING THIN FILMS

by

JOHN ERIC TKACZYK

Submitted to the Department of Physics
on June, 10 1988 in partial fulfillment of the
requirements for the Degree of Doctor of Philosophy in Physics

Abstract

Pauli-limited superconductors are characterized by conduction states with well defined spin and with singlet pairing which is characteristically perturbed by different spin-dependent interactions. It is known from the theory why spin-polarized tunneling is an excellent probe of the spin states in metals, and this technique is applied for the first time in a number of interesting cases for which spin-dependent scattering is introduced by impurity doping or by the deposition of a surface layer on a thin film. Tunneling is used as a probe of the resulting magnetic state of the local impurity moments, their interaction with superconductivity, and of the properties of these superconductors in large magnetic fields.

In the case of the heavy rare earths, the interaction between the impurity spin $\vec{S}_i$ and conduction electron spin $\vec{s}$ is found to be well described by the s-d exchange hamiltonian $H_{ex} = -J\vec{S}_i \cdot \vec{s}$. The exchange constant J between rare-earth impurities and the conduction states of the host is derived from the exchange enhanced Zeeman splitting of the superconducting density of states $2\mu_B B_{ex} = cJ\langle S_i \rangle$. Its value agrees with that obtained from fitting the Abrikosov-Gor'kov theory to the depaired tunneling conductance and decrease in T_c. The AG theory predicts that the initial decrease in T_c is proportional to the scattering rate calculated in the Born approximation $\Delta T_c \propto \hbar/\tau_{ex} = (\pi/2)c(\Omega N_o)J^2 S(S+1)$. These studies show conclusively that the exchange interaction is responsible for the effects seen in a related system, thin Aℓ films in contact with rare-earth oxides.

It is well known that in normal metals the exchange interaction induces a Ruderman-Kittel-Kasuya-Yosida (RKKY) spin polarization of the conduction electrons. A 3% polarization is measured for 1/4 monolayer of Gd at the *surface* of an Aℓ film in its normal state. When this same Gd/Aℓ bilayer is superconducting, no polarization is detected indicating the absence of the RKKY effect in BCS superconductors. This is the first experimental observation of this phenomenon which is due to the singlet nature of Cooper pairing. However, when the spin relaxation rate of the conduction electrons is large, the spin pairing of the superconductor is modified. This situation is realized in Gd/Aℓ/Pt structures where the Pt layer

is approximately two monolayers thick. The role of the Pt is to introduce spin-orbit scattering. In this case superconductivity is found to be compatible with the RKKY spin-polarization.

In doping thin films of V_3Ga and $A\ell$ with heavy elements, or in multilayer structures, the expected increase in spin-orbit scattering is sometimes absent. This along with other inconsistencies found in the literature suggest a deficiency in the present understanding of spin-orbit scattering. A review of the available literature and a discussion of the Z^4 dependence of the scattering rate is given where Z is the atomic number.

Thesis Supervisor: P.A. Wolff

Title: Professor of Physics

Acknowledgements

Here I would like to acknowledge the efforts of those people who contributed both directly and indirectly to the results presented in this thesis. Foremost, are my parents, Dorothy and John Tkaczyk, who nurtured in me a sense of curiosity (largely by tuning in to public television). Knowing they were always available to help during my graduate years at MIT provided important psychological support. My gratitude extends to my wife, Cecilia Tkaczyk, who assumed a large share of our domestic and financial responsibilities and chased me out the door each morning. Alternately, I would like to thank the Harvard Union of Clerical and Technical Workers for keeping Cecilia busy during those evenings and weekends I spent working. Jeff Quateman was a friend and housemate during my stay in Boston. Through his efforts I spent more time in the world outside the laboratory.

My advisor, Paul Tedrow, was always available with encouragement and new experimental approaches to the thesis topic. I thank him for also allowing me to explore some of my own ideas. Almost daily conversations with Jagadesh Moodera and Gary Gibson enriched my understanding of superconducting phenomena. In this same respect conversations with Bob Meservey were illuminating. From Terry Orlando I learned not only the physics of superconductors but also how to more effectively communicate what I have learned. I benefited from sharing in weekly group meeting, he and Dave Rudman organized. Terry Orlando served as the thesis reader and Peter Wolff as the Committee Chairman and I appreciate their patience during the completion of this thesis.

Because of the work of past students, Demetris Paraskevopoulos, John Kucera, and Xan Alexander, many of the experimental techniques were largely established when I began. Dick MacNabb provided Aℓ tunnel junctions and advice on lithography and vacuum deposition techniques. Mike Blaho helped in every aspect of the equipment maintenance and taught me electronic trouble shooting and soldering techniques. Xan Alexander and Dierk Rainer provided the tunneling and the basic critical field programs which are used extensively throughout this thesis. The high field user facilities of the Francis Bitter National Magnet Laboratory and advice of Bruce Brandt were also essential.

Thanks go to Donald E. Knuth for writing such superb typesetting software called TEX. I am grateful to Xin Hao and Mark Taylor for setting up the word processor. This research and my graduate education have been financially supported by the Department of Energy.

CONTENTS

Introduction

Superconducting tunneling is uniquely qualified as a probe for measuring the effect of spin-dependent perturbations on the conduction states of a metal. Such effects have been of interest for a long time and have been measured with a variety of techniques(1963,1985c). For example, in the normal state, g-factor shifts and spin-relaxation rates are measured using conduction electron spin resonance techniques which, in metals, are limited to studies of small particles by skin-depth attenuation(1969a,1985b,1984e). Knight shift measurements in superconductors can measure spin-relaxation rates but suffer from similar limitations(see references in 1978a). High sensitivity measurements involving superconductivity (but not tunneling) have studied moment formation at metal surfaces(1985d). This thesis presents a technique combining tunneling in thin films with superconductivity; this combination is shown to be a useful tool in the study of the spin-states of conduction electrons. Collected together are the results of the author's graduate research performed at the Francis Bitter National Magnet Laboratory, MIT in the years 1983-1988.

This introduction starts with an overview of the spin-polarized tunneling technique. There is an attempt to give the reader a feeling for the steps involved in collecting and analyzing the data and the typical numbers involved. Finally, the structure of the thesis itself is presented.

—Spin-Polarized Tunneling—

Spin-polarized tunneling will be considered here as any of the superconducting tunneling techniques which involve the Zeeman splitting $2\mu_B B_{int}$ of the density of states. Meservey, Tedrow and Fulde (1970) made the first observation of the Zeeman splitting of the density of states of aluminum and found it consistent with a g-factor of 2. This allowed the measurement of the spin-polarization of the conduction states in 3d and 4f ferromagnets (1973b,1980a). Subsequently, tunneling from ferromagnets allowed the total conductance to be separated into the contributions from the two spin directions(1982c). These individual spin conductances contain more information than the the total conductance allowing the discrimination of different effects present in the same sample. For example, spin-orbit scattering and Fermi liquid corrections effect the critical field in nearly the same way but are distinguishable in the tunneling conductance(1959a). Critical field studies demonstrated the importance of Fermi liquid corrections to the magnetic moment(1979a,1979b). However, a combination of critical field and spin-polarized tunneling measurements were necessary in order to make quantitative determinations of the parameters of the theory including the antisymmetric Fermi liquid parameter G^0 (1984b, 1985a). Finally, the spin relaxation rates in metals due to spin-orbit scattering(1979b) and exchange scattering (1965, 1988c) can be measured independently of one another due to the different symmetries of these processes under time reversal.

In addition to these quantitative measurements, spin-polarized tunneling has, in a particularly clear way, verified a number of fundamental properties of the superconducting state involving the electron spin. The early work on this point is summarized by Fulde(1973a). For instance, the lack of a Pauli paramagnetic response in BCS

superconductors is responsible for the Zeeman splitting of the density of states and the lack of the Ruderman-Kittel-Kasuya-Yosida(1954-1957)(RKKY) spin-polarization of itinerant electrons(1988c). Spin-mixing occurs in the presence of spin-orbit scattering(1971,1975a) and restores the RKKY effect in the superconducting state(1988c).

Spin-polarized tunneling has been a very useful technique in all these ways. However, in practice, spin-polarized tunneling has been restricted to studies involving mostly aluminum and is used by a relatively small community of physicists. There are real problems which account for this lack of dissemination. The main obstacle is the requirement of forming high quality tunnel junctions. Pb and Sn, which are among the favored materials for tunnel junctions, have intrinsic spin-relaxation rates which greatly exceed the Zeeman energy at the highest field for which these materials remain superconducting. Therefore, these materials are not suitable for spin-polarized tunneling.

Pauli-limiting is the condition in which the critical magnetic field is high enough that the Zeeman energy $2\mu_B B_{int}$ is greater than the spin-relaxation rate $\hbar/\tau_{sf}$ and is of the order of the superconducting energy gap. It is only in this case that spin-effects play an important role in observable properties. Consider that spin-relaxation at low temperatures is due to defects (e.g., vacancies) in the crystal and that the defect density is not easily reduced beyond a certain point by any simple processing methods. In addition, the main contribution to spin-relaxation in non-magnetic materials is spin-orbit scattering which may be expected to increase as $(\alpha Z)^4$ where $\alpha = 1/137$ and Z is the atomic number(see Section A.2 and 1978a). Therefore, one must look toward high critical fields in materials containing low-atomic-number elements to achieve the condition of Pauli-limiting.

A significant limiting factor in the critical field is the Meissner effect. The diamagnetic screening currents cost free energy relative to the normal state. However, in Type II and thin film superconductors, the screening currents are reduced due to field penetration. In the former, the surface energy of a superconducting/normal state interface is favorable for vortex flux penetration; for example, V_3Ga is a technologically important A15 superconductor which is in the extreme Type II limit, $\kappa = \lambda/\xi \sim 100$. It has a high critical current in practical conductors, $2\times10^4\, Amps/cm^2$ at 19 tesla and is used in the world's highest field superconducting magnet(1985e,1986b). The upper critical field is about 23 tesla, $2\mu_B B_{c2} \sim 2.3meV$, $\hbar/\tau_{so} \sim 1.1meV, \Delta \sim 2.4meV$ and even in the bulk this type II superconductor is Pauli limited. For a thin film superconductor oriented with the surface parallel to the field direction, significant field penetration occurs when the thickness of the film is of the order of the penetration depth and Pauli-limiting occurs when it is sufficiently thin. The critical field of a thin film is increased above that in the bulk ($B_c \sim 800G$ in $A\ell$) by the ratio of the penetration depth ($\lambda \sim 400\mathring{A}$) to the film thickness. $B_{c\|} = 2\sqrt{6}B_c\lambda/d$. The condition of Pauli-limiting occurs when $2\mu B_{\|} > \hbar/\tau_{so}$. This predicts for $A\ell$ ($\hbar/\tau_{so} \sim 50\mu eV, \Delta \sim 360\mu eV$), that Pauli limiting occurs in films of the order $50\mathring{A}$. In practice, in films less that $\sim 120\mathring{A}$ the Zeeman splitting is resolved.

Thin films of $A\ell$ were first shown to be Pauli-limited by Stongin and Kammercer (1966b). This became the system in which spin-polarized tunneling first showed its

potential. A review by Fulde(1973a) describes this early work and discusses other aspects of Pauli-limiting in thin films. Spin-polarized tunneling has also been observed in beryllium (1976), vanadium and V-Ti alloys (1978d,1988a), V_3Ga (1984a, 1987b), , and amorphous Ga (1978b, 1988a) all with some success. However, the most readily interpreted experimental results are obtained with ferromagnetic counter-electrodes and high quality junctions of this type are produced with very low yield or not at all. For materials without a favorable native oxide, tunnel barriers have been formed using deposited Al_2O_3 layers(1982a). The first observation of spin-polarized tunneling using a mechanically adjustable tunneling barrier(1987a) has been encouraging but further development is required. A recent advance has been made, the implications of which are not yet all realized (1988b). Moodera et al have used EuS, a ferromagnetic semiconductor, as an artificial tunnel barrier and have measured a large spin-polarization of the tunneling current. The use of such a barrier may provide or exceed the advantages of Fe counterelectrodes.

—This Thesis Research—

An important novel feature of the work presented in this thesis is that of "doping" to produce spin-orbit or exchange scattering. This is done by depositing a surface layer of some high Z or magnetic element,respectively, onto a Pauli-limited thin film superconductor. Since the films are thinner than the (bulk) spin-mean-free-path and coherence length, the spin-relaxation rate and energy gap, respectively, are constant characteristics of the conduction states throughout the film. It is only recently that the proper theoretical apparatus has been developed to treat this problem fully (1986a, 1988d). The work presented here is indebted to the first experiments of Tedrow and Meservey involving Pt layers at the surface of a 40$\AA$ film of $A\ell$ (1979b,1982b).

The goal is to derive information from experiment about the the scattering potentials U, V_{so}, J for transport, spin-orbit, and exchange scattering and relate these to the doping. Schematically, this process can be divided into the following steps.

$$\frac{dI}{dV} \overset{\text{tunneling theory}}{\Longleftrightarrow} DOS \overset{\text{Superconductor theory}}{\Longleftrightarrow} T_{co}, B_{int}, \hbar/\tau_{so}, \hbar/\tau_{ex} \overset{\text{Born approx.}}{\Longleftrightarrow} U(\vec{r}), V_{so}(\vec{r}), J(\vec{r})$$

Measurements are made of the conductance (*i.e.*, dI/dV) of a tunnel junction between a superconducting electrode and another superconductor or normal metal. Measurements are taken within a few meV of the Fermi surface. The theory of tunneling relates the conductance in a straightforward manner to the excitation spectrum or density of states (DOS) of the superconductor. In fact, in the case of a superconductor-insulator-normal junction the conductance is modified only by a convolution of the DOS with the derivative of the Fermi function and by the modulation of the lock-in amplifier. The former is a sharply peaked function with peak-width of the order of the temperature $k_B T$. Thus at temperatures obtained with pumped ^3He, (*i.e.* $T = 0.4K$), one measures the excitation spectrum of the system with an energy resolution of $34\mu eV$. In principle there is no loss of information as a reverse convolution can be performed. A $20\mu eV$ modulation is used to measure the conductance. Unlike the case of the normal state, the superconducting DOS will generally have structure sharper than kT.

In fact, the BCS superconducting DOS has a singularity at the gap edge below which no excitations are possible. However, generally the singularity will be broadened by residual pairbreaking effects. In thin films of aluminum $T_c \sim 2.4K$, the energy gap is $\Delta \sim 1.76 k_B T_c \sim 360 \mu eV$ and the intrinsic pairbreaking is of the order or less than $\hbar/\tau_{PB} \sim 0.05 k T_c \sim 10 \mu eV$.

However, it is not so much the sharpness of the density of states which makes spin-polarized tunneling an excellent probe of spin-dependent perturbations. For instance, the Zeeman splitting produced by a field of 1 tesla is $2\mu_B B \sim 115 \mu eV$, sufficiently large compared to the energy width of the Fermi surface (i.e. $\sim 3 \times k_B T$). Rather, it is the rigidity of the singlet pairing which is important. As shown in figure 1, the superconductor does not adjust the spin-up and spin-down populations when a magnetic field is applied (i.e. lack of Pauli paramagnetism). Thus the sharp structure in the superconducting density of states for one spin is shifted with respect to that of the other spin direction. The energy shift is the Zeeman splitting $2\mu_B B_{int}$. There is no mutual shift of this type at the Fermi level in a normal metal. A second exemplary property of superconductivity is that it distinguishes between perturbations depending on their transformation properties under time reversal. As a result one can distinguish between spin-orbit and exchange scattering.

In this thesis the superconducting DOS is obtained from the theory of Rainer, the computer programs for which were provided by Rainer and Alexander(1985a). The DOS is convoluted with the derivative of the Fermi function so as to account for the temperature broadening of the conductance, and the result is fit to the measured conductance. The input parameters to the theory include the energy scale of the superconductive pairing kT_{co}, and other parameters which have to do with quasiparticle properties. These are essentially normal state electronic parameters, for example, the internal magnetic field, the spin-orbit and exchange scattering rates. As in the theory of tunneling, the theory of weak-coupled superconductivity is quite straightforward (e.g. relative to band structure calculations). Rainer remarks, "The theory describes all superconducting phenomena very accurately with a relatively small amount of computational effort. The exceptional accuracy of the weak-coupling theory results from the existence of several small expansion parameters; the most important ones are $T_c/\Theta_{Debye}, 1/k_F \ell$, and $1/k_F \xi_0$, which in most superconductors are of the order 10^{-2} or smaller"(1985a). The superconducting transition temperature T_c can be measured resistively, but the other "normal state" parameters must be determined by the fit to the conductance data. The tunneling data may be supplemented with critical field measurements of the superconductor-normal phase boundary. The fits tend to be good, and the parameters are "orthogonal" in the sense that they are well determined and each parameter can be associated with a qualitatively different feature in the conductance. However, the problem which remains is to relate the "normal state" parameters obtained to the surface layer doping. To do this accurately requires something like a band structure calculation(1985c). A discussion of spin-orbit and exchange scattering in the normal state as calculated in the simplest (i.e. Born) approximation is given in appendix A.

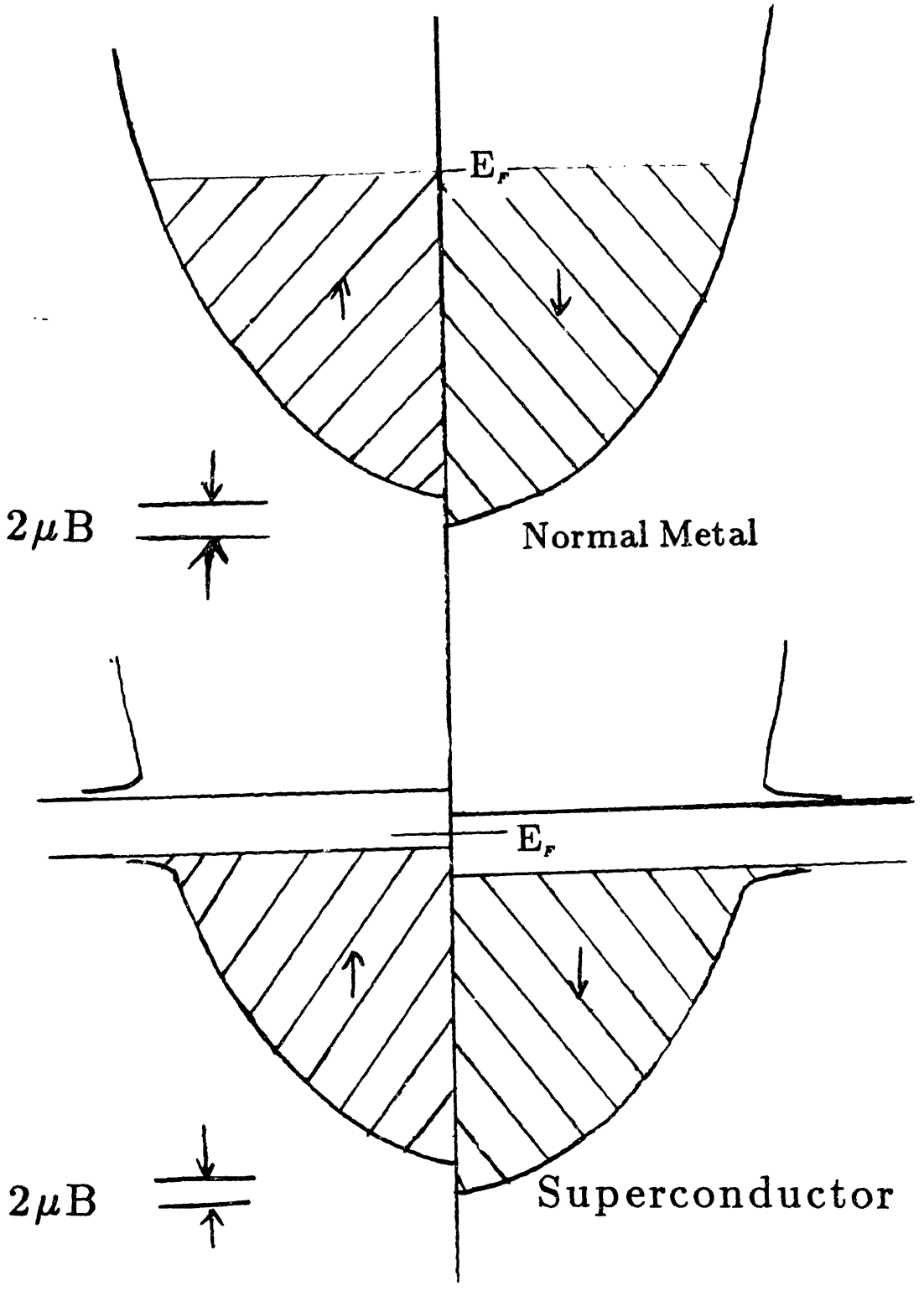

Fig. 1 The Zeeman splitting of the density of states can be observed in the superconductor.

—Thesis Summary and Structure—

The thesis is divided roughly into three sections— superconductivity and tunneling in chapter I and II, experimental results presented on the topics of exchange and spin-orbit scattering in chapters III and IV, respectively, and a discussion of the "normal state" parameters which enter the theory in appendix A. The critical field calculation and computer code is supplied in appendix B.

Chapter I gives an introduction to superconductivity and tunneling. The goal is to give a succinct physical picture wherever possible and to relate this picture to the mathematically rigorous theory. A description of superconductivity in terms of symmetry breaking is given so as to complement the the standard texts (Tinkham, 1975b; DeGennes, 1966a; Schrieffer, 1964). The order parameter and macroscopic Ginzburg-Landau (GL) equations (1950) are shown to be related to the microscopic theory, a generalized version of that due to Bardeen, Cooper, and Schrieffer (BCS) (1957). Pairbreaking and the associated decrease in T_c are given a physical interpretation. The Nambu-space formulation of perturbation theory in superconductors is developed to the point where a review by Maki on gapless superconductivity begins(1969b). A special feature of the Nambu formalism is that the whole normal state perturbation theory can be taken over to the superconducting state by simply replacing the scalar Green's function with a matrix Green's function. Because a Green's function approach is somewhat abstract, the field theoretic description of scattering in the Born approximation is given in A.2 with an emphasis on relating it to the more familiar Boltzmann transport theory in A.1. The off-diagonal part of the matrix Green's function corresponds to the superconducting order parameter. In chapter I, an attempt is made to understand the physical significance of this theory.

A description of experimental techniques and an analysis of the errors entering the conductance measurements are presented in chapter II. Chapter III describes data on junctions involving $A\ell$ films covered with a submonolayer of a rare-earth element or a $50\mathring{A}$ layer of a rare earth oxide. Three consequences of the exchange interaction are observed. Forward scattering from RE moments aligned with an applied magnetic field causes a Zeeman splitting of the conduction electron energy equivalent to that due to an effective "uniform exchange field", $B_{ex} = cJ(0)\langle S_z\rangle/g\mu_B$. Second, the depairing of the density of states due to (random) exchange scattering, $\hbar/\tau_{ex} = (\pi/2)c\Omega N_O J^2(0)S(S+1)$, is fit to the Abrikosov-Gorkov (AG) theory (1960) to obtain the exchange constant $J(0) \sim 10meV$. This value agrees within a factor of two with that obtained from the Zeeman splitting. The exchange constant for Ce is of the order of 100meV, and the pairbreaking appears to be anomalous in accord with other measurements(1967). When a Gd layer is sandwiched between two $20\mathring{A}$ $A\ell$ films, the exchange constant is found to be a factor of 2-3 larger than when deposited at the surface of a $40\mathring{A}$ film. This larger value is about the same as that obtained by Woolf and Reif for Gd impurities in Pb. In the case where the $A\ell$ film is in contact with Eu oxide(1986c,1987b), the exchange constant associated with scattering off the $A\ell$ /Eu oxide interface is very small with the result that one can have a large uniform exchange field (i.e. first order effect $B_{ex} \sim J$), while at the same time, the reduction in the T_c is negligible (i.e. second order effect $\hbar/\tau_{ex} \sim J(J/E_F)$). Finally, tunneling into the side of an $A\ell$ film

covered with a submonolayer of Gd reveals the presence of the localized RKKY spin-polarization in the normal state and its absence in the superconducting state. This result is attributed to the fact that the long range part of the spin-susceptibility in the BCS superconductor vanishes at low temperature. In addition, an Aℓ - $A\ell_2O_3$ - $Gd/Al/Pt$ tunnel junction was formed where the Gd thickness was 3 atoms/nm^{-2} and the Pt layer was approximately 2 monolayers thick. The role of the Pt is to introduce spin-orbit scattering. With the introduction of sufficient spin-orbit scattering, the long-range part of the spin susceptibility in the superconducting state can be of the order of that in the normal state. In this sample we observed the asymmetry associated with the RKKY spin-polarization in both the superconducting and normal states.

Chapter IV describes the fabrication and properties of V_3Ga films doped with high Z elements. It studies the effect of this doping on the magnitude of spin-orbit scattering. An increase in the spin-orbit scattering would have the effect of increasing the critical field, and this increase would be of technological interest. The critical field has been measured as a function of temperature, and analysis includes the possible role of Fermi liquid effects. For example, the role of the tricritical point is studied. This is the temperature below which the transition to the normal state is of first order; the critical field in this region is not described by perturbation theory to first order in the order parameter(i.e. GL theory). The equations determining the tricritical point are modified so as to include the Fermi liquid correction to the conduction electron magnetic moment. However, a detailed numerical analysis shows that critical field data cannot distinguish between these Fermi liquid effects and spin-orbit scattering. As a result one must turn to spin-polarized tunneling measurements for a better understanding. V_3Ga junctions with and without Fe counter-electrodes are used to set bounds on the spin-orbit scattering rate. Thin $A\ell$ films with submonolayer coverage of high Z elements provide additional data on how the doping affects the spin-orbit scattering rates. For 1$\AA$ Gd, little spin-orbit scattering is obtained. This is puzzling considering the large increase in spin-orbit scattering produced by 1$\AA$ Pt and the fact that 1$\AA$ Gd does produce significant exchange scattering. Possible explanations for the lack of an increase in the spin-orbit scattering rate are discussed.

Sections A.1 and A.2 derive the Fermi golden rule expression for the scattering rate $\hbar/\tau = 2\pi c\Omega N_O |V|^2$ in both the Boltzmann and field theoretic descriptions respectively. The origin of the atomic concentration c and unit cell volume Ω as factors in this expression is explained. Forward scattering acts as an effective uniform field and is included in the unperturbed part of the hamiltonian. Finally, an expression for the scattering rate in the Born approximation is obtained for impurities having internal structure (e.g. local moments). In section A.3, justification for the experimentally observed $(\alpha Z)^4$ dependence(1978a) of the spin-orbit scattering rate is explored. It appears that the matrix element entering into the scattering rate must be taken with a tight binding basis, as this most closely approximates the Bloch wave in the core region where the spin-orbit interaction makes its largest contribution. In this respect, spin-orbit scattering is different from transport scattering; the latter is calculated with a plane wave matrix element of a weak pseudopotential. Section A.4, motivates the use of the s-d model $H = -J\vec{S}\cdot\vec{s}$ for the exchange interaction between RE ions and

conduction electrons. The standard results following from the treatment of the s-d model in perturbation theory are derived. In first order, one has the uniform exchange field arising from forward scattering and a RKKY spin-polarization; second order corresponds to exchange scattering calculated in the Born approximation. Finally, the divergence in third order associated with the Kondo effect is pointed out. Apparently a new term, not present in the literature(1980b), is found in this derivation of the scattering rate taking into account both spatial and time correlations. When working in the Born approximation, one tries to express the square amplitude of the matrix element $|\sum_i \langle J\vec{S}_i \cdot \vec{s}\rangle|^2$ in terms of the impurity spin correlations $\sum_{i,} J^2\langle \vec{S}_i \cdot \vec{S}_j\rangle$; however, an additional term arises due to the non-commutivity of the impurity spin operators. The necessity of this term is made clear by taking the limit where only time correlations are considered. This corresponds to scattering in a magnetic field where spin-flip scattering is inelastic. The effect of spin correlations on the scattering rate can be measured by spin-polarized tunneling, and a general expression such as that derived in section A.4 is of interest.

Bibliography to the Introduction

1950 , V.L. Ginzburg, V.L., and L.D. Landau, Zh.Eksperim. i Teor. Fiz. **20**,1064 .

1954 , Ruderman, M.A., and C.Kittel, Phys.Rev. **96**, 99; T. Kasuya, Prog. Theor. Phys. Japan, **16**, 45 (1956); K. Yosida, Phys.Rev. **106**, 893 (1957).

1957 , J. Bardeen, L.N. Cooper, and J.R. Schrieffer, Phys.Rev. **108**,1175.

1960 , A.A. Abrikosov and L.P. Gor'kov, Zh.Eksperim. i Teor. Fiz **39**,1781 [Sov.Phys. JETP **12**,1243,1961].

1963 , Y. Yafet, Solid State Phys. **14**,1.

1964 , J.R. Schrieffer, *Theory of Superconductivity*, (Benjamin/Cummings Publishing Co., Reading, Mass.).

1965 , M.A. Woolf and F. Reif, Phys.Rev. **137**,A557.

1966a, P.G. DeGennes, *Superconductivity of Metals and Alloys*, Trans. P.A. Pincus, (W.A. Benjamin, NY).

1966b, M. Strongin and O.F. Kammercer, Phys.Rev.Lett. **16**,456.

1967 , A.S. Edelstein, Phys.Rev.Lett. **19**,1184.

1969a, J.R. Asik, M.A. Ball, and C.P. Slichter, Phys.Rev. **181**,645,662.

1969b, K. Maki, in *Superconductivity*, edited by R.D. Parks (Marcel Dekker, NY).

1970 , R. Meservey, P.M. Tedrow and P. Fulde, Phys.Rev.Lett. **25**,1270.

1971 , P.M. Tedrow and R. Meservey, Phys.Rev.Lett. **27**,919.

1973a, P. Fulde, Adv.Phys., **22**,667.

1973b, P.M. Tedrow and R. Meservey, Phys.Rev.B, **7**,318.

1973c, P.M. Tedrow and R. Meservey, Phys.Rev.B, **8**,5098.

1975a, R. Meservey, P.M. Tedrow, and R.C. Bruno, Phys.Rev.B **11**,4224.

1975b, M. Tinkham, *Introduction to Superconductivity*, R.E. Krieger Publishing, Huntington, NY, Reprinted 1980).

1976 , P.M. Tedrow and R. Meservey, Phys.Lett. **58A**, 237.

1978a, R. Meservey and P.M. Tedrow, Phys.Rev.Lett. **41**,805.

1978b, R. Meservey, P.M. Tedrow, and R.C. Bruno, Phys.Rev.B **17**,2915.

1978c, P.M. Tedrow and R. Meservey, Solid State Comm. **27**,1397.

1978d, P.M. Tedrow and R. Meservey, Phys.Lett. **69A**,285.

1979a, T.P. Orlando, E.J. McNiff, Jr., S. Foner, M.R. Beasley, Phys.Rev.B, **19**,4545.

1979b, P.M. Tedrow and R. Meservey, Phys.Rev.Lett. **43**,384.

1980a, R. Meservey, D. Paraskevopoulos, and P.M. Tedrow, Phys.Rev.B, **22**,1331.

1980b, C.M. Soukoulis and G.S. Grest, Phys.Rev.Lett. **21**,5119.

1982a, J.S. Moodera, R. Meservey, and P.M. Tedrow, Appl.Phys.Lett. **41**,488.

1982b, P.M. Tedrow and R. Meservey, Phys.Rev.B, **25**,171.

1982c, P.M. Tedrow, J.S. Moodera, and R. Meservey, Solid State Comm. **44**,587.

1984a, S.J. Bending, M.R. Beasley, and C.C. Tsuei, Phys.Rev.B, **30**,6342.

1984b, P.M. Tedrow, J.T. Kucera, D. Rainer, T.P. Orlando, Phys.Rev.Lett. **52**,1637.

1984c, P.M. Tedrow and R. Meservey, in *Advances in Cryogenic Engineering, Vol. 30*, Edited by A.R. Clark and P.R. Reed. (Plenum Publishing Corp.).

1984d, D.C. Vier, D.W. Tolleth, and S. Schultz, Phys.Rev.B, **29**,88.

1985a, J.A.X. Alexander, T.P. Orlando, D. Rainer, and P.M. Tedrow, Phys.Rev.B, **31**,5811; J.A.X. Alexander, (unpublished), Ph.D. thesis at MIT (1986).

1985b, D.M. Eigler and S. Schultz, Phys.Rev.Lett. **54**,1185.
1985c, R. Feder, *Polarized Electrons in Surface Physics*, (World Scientific Publishing, Singapore).
1985d, J.S. Moodera and R. Meservey, Phys.Rev.Lett. **55**,2082.
1985e, R.G. Sharma, Y. Tanaka and K. Tachikawa, Cryogenics, **25**,381; K. Tachikawa, Y. Tanaka, K. Inoue, K. Itoh, T. Asano, Y. Iijma, IEEE Trans. Mag. **21**, 1048.
1986a, A. Millis, D. Rainer, and J.A. Sauls, (preprint) to be published Phys. Rev. B, Aug. 1 1988.
1986b, T. Takeuchi, Y. Iijima, K. Inoue, and K. Tachikawa, J.Appl.Phys., **60**,1227.
1986c, P.M. Tedrow, J.E. Tkaczyk, and A. Kumar, Phys.Rev.Lett. **56**,1746.
1987a, J.E. Tkaczyk and P.M. Tedrow, Jap.J.Appl.Phys. **26**,1559.
1987b, J.E. Tkaczyk and P.M. Tedrow, J.Appl.Phys. **61**,3368.
1987c, J.E. Tkaczyk and P.M. Tedrow, IEEE Trans. Mag. **23**, 948.
1988a, G. A. Gibson and R. Meservey, private communication.
1988b, J.S. Moodera, X. Hao, G. Gibson, R. Meservey, submitted PRL.
1988c, J.E. Tkaczyk and P.M. Tedrow, This thesis and submitted PRL.
1988d, T.Tokuyasu, J.A. Sauls, D. Rainer, preprint.

Chapter I — Scattering in the Superconducting State

I.1 — An Introduction to Superconductivity

The free-energy difference between the superconducting and normal state is small $(f_N - f_S)/f_N \sim k_B T_c/E_F \sim 10^{-4}$. This means that there is no great change in the momentum distribution function of the electrons upon entering the superconducting state. Rather, it is the correlations between time reversed states which are responsible for the unique properties of the superconducting state. Unlike those induced by the repulsive Coulomb interaction, correlations induced by the electron-phonon interaction cannot be taken into account by simply renormalizing single-quasiparticle properties; there is a breakdown in the Fermi liquid description. This can be attributed to the fact that in the case of an attractive interaction, the interparticle scattering becomes phase coherent. The associated ground state is characterized by the breaking of the gauge symmetry of the hamiltonian. This symmetry breaking is parameterized by a complex number called the order parameter. The magnitude of the order parameter can be associated with the density of "superconducting" electrons. The phase of the order parameter is responsible for the remarkable fact that, in the superfluid, the whole is not simply the sum of its parts. Furthermore the macroscopic Ginzburg-Landau theory predicts that the phase is coupled to the electromagnetic vector potential, thus accounting for many of the magnetic properties of superconductors. Connection between the microscopic and macroscopic theories of superconductivity is made by identifying the order parameter in terms of microscopic variables. From an analogy to ferromagnetism, the BCS theory is shown to correspond to a mean field treatment with a spatially homogeneous magnetization.

—The Fermi liquid description—

A number of results explain the fact that the free electron picture describes many of the electronic properties of metals. For example, the interparticle interactions are taken into account in Landau's treatment of the Fermi liquid (Lifshitz and Pitaevskii). Landau considers the excitations of the whole system as a function of the strength of the interparticle coupling, the suggestion being that there is a one-to-one correspondence between the excitations of the interacting and non-interacting systems. Translational invariance allows a description in terms of a basis of elementary excitations or quasiparticles associated with a momentum $\vec{p}$ and dispersion $\varepsilon(\vec{p})$. The dispersion is not a simple function, but is a functional of the occupation $n(\vec{p'})$ of all the other quasiparticle states. Under the appropriate conditions described below, the quasiparticle description resembles a free-electron description with one-particle properties (e.g. mass, magnetic moment, etc.) renormalized due to (weak) residual interactions between quasiparticles. It is assumed that the quasiparticles have Fermi-Dirac statistics which leads to a discontinuity in the distribution function at $T = 0$. This discontinuity defines the Fermi surface, and its size is related to the mass renormalization. In the free electron limit $m = m_e$, and the distribution is a step function at $T = 0$.

Collisions between the quasiparticles arise due to the inter-quasiparticle coupling, and $\varepsilon(\vec{p})$ takes on an imaginary component $\hbar/\tau$. The requirement for this whole

picture to be self-consistent is that this energy uncertainty be small, not only with respect to the Fermi energy, but also with respect to the energy range ΔE over which the distribution function deviates from the step function . This is necessary if the quasiparticles are to be said to have a well defined dispersion $\varepsilon(\vec{p})$ which is a functional of the distribution $n(\vec{p})$. The crucial observation is that this is in fact the case for fermions at a sharp Fermi surface. The self-consistency argument goes as follows. Two quasiparticles involved in a scattering event must each find a place in the Fermi sea which doesn't violate the Pauli exclusion principle. This places a restriction on the "phase space" available for scattering processes. As a result, the scattering rate goes as $\hbar/\tau \sim \Delta E(\Delta E/E_F)$. If $\Delta E \ll E_F$, then

$$\hbar/\tau \ll \Delta E. \qquad I.1.1$$

It follows that the Fermi-liquid description is self-consistent, and quasiparticles are well defined.

As an example, consider how the effect of the coulomb interactions can be set in a quasiparticle description and how the residual interactions between quasiparticles act to renormalize one-particle properties. In particular, the effect on the magnetic moment is worked out since it can be measured by the technique of spin-polarized tunneling. This Fermi liquid correction plays an important role in the quantitative understanding of high field superconductivity.

The Hartree-Fock approximation is a technique by which the many-electron description is broken up into a set of independent particles interacting through self-consistent potentials. For example, the coulomb interaction is replaced by the Hartree potential and the exchange or Fock potential. The latter acts between pairs of electrons having the same spin direction such that around each electron there is an "exchange hole" where electrons of the same spin are absent. An electron and its associated exchange hole together constitute a quasiparticle. There still remain interactions between quasiparticles, but these can be taken into account by renormalization (e.g. the magnetic moment).

If one applies a magnetic field, there is a tendency for electrons to align their moments with the field. As a result of the coulomb interaction, the energy of an electron changes not only due to the Zeeman interaction $H_{Zee} = -\vec{\mu}_B \cdot \vec{B} = g\mu_B \vec{s} \cdot \vec{B}$, but also due to the change in electron occupation in the two spin directions $\Delta n_\uparrow$ and $\Delta n_\downarrow$.

$$\Delta\varepsilon_\uparrow = \mu_B B - \frac{G^\circ}{N_o}\Delta n_\downarrow$$

$$\Delta\varepsilon_\downarrow = -\mu_B B - \frac{G^\circ}{N_o}\Delta n_\uparrow$$

Here G°/N_o takes into account the Coulomb interaction of an electron with the other electrons in its exchange hole. G° is the antisymmetric Fermi liquid parameter. The effective Zeeman splitting $2\mu_{eff}B$ becomes

$$\Delta\varepsilon_\uparrow - \Delta\varepsilon_\downarrow \equiv 2\mu_{eff}B = 2\mu_B B - \frac{G^\circ}{N_o}(\Delta n_\downarrow - \Delta n_\uparrow). \qquad I.1.2$$

The change in density is given by that for the expression for Pauli paramagnetic response $(\Delta n_\downarrow - \Delta n_\uparrow) = N_o(2\mu_{eff}B)$. Thus,

$$2\mu_{eff}B = 2\mu_B B - 2\mu_{eff}BG^\circ.$$

Thus it has been shown that the strong bare coulomb interactions can be described within a quasiparticle picture, and that the weak inter-quasiparticle interaction is taken into account by a renormalization of the the magnetic moment $\mu_{eff} = \mu_B/(1+G^\circ)$.

—Broken Symmetry—

In a superconductor the effects associated with the attractive, phonon mediated electron-electron interaction cannot be described within the quasiparticle picture described above. The breakdown of the Fermi liquid theory is demonstrated by the fact that the distribution function is not sharp at $T = 0$, but closely resembles the Fermi distribution at $T = T_c$ (fig. I.1.1). The scattering rate is of the order of the width of the distribution function $\hbar/\tau \sim \Delta E \sim k_B T_c$, and thus the self-consistency argument described above (eq. I.1.1) is violated. The failure can be attributed to the fact that the attractive interaction tends to associate electrons in pairs which in the molecular limit have Bose-Einstein statistics (e.g. ^4He nuclei). Perhaps more importantly, the Fermi liquid is unstable with respect to the formation of a condensate (Cooper, 1956) which is characterized by a broken symmetry. Thus no one-to-one correspondence can be made between the excitations of the normal and superconducting fluids, and, in fact, the associated ground states can be shown to be orthogonal. These topics are made more explicit below.

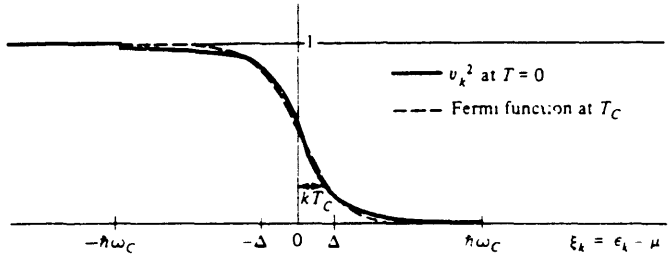

Fig. I.1.1— The distribution function of electrons in the superconductor at $T = 0$ is compared with that of the normal state at $T = T_c$ (from Tinkham, p. 29).

It is apparent from figure I.1.1 that, relative to the normal state, the superconductor has an excess of kinetic energy associated with the electron motion. Also the superconducting state has lower entropy than that of the normal state. Therefore, one comes to the conclusion that the low free-energy of the superconducting state is due to a lower potential energy. This will be shown to be the result of a phase-coherent use of the attractive electron-electron interaction. From the energy uncertainty implicit in the width of the distribution function, one may surmise that the range over which the coherence is maintained is of the order $\Delta x \sim \hbar v_F/k_B T_c$.

The phenomenon of broken symmetry in superconductors is equivalent in important ways to the alignment of spins in a ferromagnet below the Curie temperature.

In a ferromagnet each pair of spins contributes an energy $Je^{i\pi}$ to the energy of the system giving a total energy of the order $-NJ$ where N is the number of spins. Above the curie point, the spins are, on average, at arbitrary relative angles such that each pair contributes terms to the energy with arbitrary phase; there is a great deal of cancellation and no average gain in potential energy. The unique character of the ferromagnetic ground state results from the fact that it breaks the rotational symmetry of the hamiltonian $H = -J\vec{S}_i \cdot \vec{S}_j$. The ferromagnetic ground state cannot be obtained by the application of perturbation theory using basis states associated with the normal-state. In fact, as a result of the thermodynamic character of the phenomenon(i.e. $N \rightarrow 10^{23}$), the states characterized by random spin directions are orthogonal to the ferromagnetically aligned state. Also a ferromagnetic state with alignment in one direction is orthogonal to a ferromagnetic state with alignment in another. The scalar product between two ferromagnetic states goes as $[cos(\theta/2)]^N$ (Itzykson and Zuber, p.164). This vanishes for $N \rightarrow \infty$. Similarly, these ferromagnetic states are orthogonal to a helical arrangement of the spin directions. Thus the problem is that the Hilbert space associated with the hamiltonian is composed of a number of disjoint spaces, each characterized by some specific character of their spin arrangement. This character is described by an order parameter which may be a number or vector or some more complicated object.

A number of methods have been devised to cope with this problem. Perturbation theory is possible if one starts with a basis of states which break the symmetry of the hamiltonian in the appropriate way; that is, states which give non-zero expectation value of the order parameter. This is called the consistent or mean field approach, with the "field" referring to the order parameter. The trick here is to *guess* the appropriate order parameter. For a ferromagnet with spins constricted to the plane(X-Y model), the order parameter is a complex number with the magnitude and phase representing the magnetization and direction respectively. A complex number is also the appropriate order parameter for the superconductor. For example, the interaction $-J\vec{S}_i \cdot \vec{S}_j$ is replaced by $-J\vec{S}_i \cdot \langle\vec{S}\rangle$ where $\langle\vec{S}\rangle = (1/N)\sum_j \vec{S}_j$. Note that this implicitly assumes a basis set which breaks the symmetry of the hamiltonian since $\langle\vec{S}\rangle = 0$ in the paramagnetic state.

An alternate way of arriving at the self-consistent field method involves the introduction of a symmetry breaking term in the hamiltonian itself and then letting this term go to zero at the end of the calculation. For example, by including a magnetic field in the hamiltonian one obtains a macroscopic magnetization which leads to a ferromagnet polarized in the direction of the magnetic field. Finally, the renormalization group method takes a different approach. The system is divided into groups composed of a small number of spins. The spins in any one group are replaced by the average spin also called a "block" spin. The coupling between spins in different blocks is taken into account in terms of an effective coupling between block spins. The map between the original coupling constant and the coupling constant for block spins is then iterated until one obtains a super-block spin which effectively incorporates the properties of the whole system. This method makes the thermodynamic character of the ordering explicit by first considering only a small number of spins and then by

considering a geometrically growing number of spins. As the renormalization group is a more recent technique, most of the classic work in superconductivity was done with a suitable Green's function version of the self-consistent field method.

—The role of the phase in the condensate—

As discussed, successful application of the self-consistent field method requires the correct identification of the order parameter. An important clue as to the nature of the order parameter is implicit in the observation that the normal state is unstable with respect to the formation of bound pairs under an arbitrarily small attraction(Cooper,1956). In the molecular limit such pairs would have Bose statistics, and a Bose condensation would be possible. In spite of the fact that the electron pairs are not tightly bound but are highly overlapping, the order parameter of the superconductor is given by a continuity argument to be that of the Bose superfluid, a complex number, $|\Delta|e^{i\theta}$ with the magnitude representing the superfluid density and the gradient of the phase representing the superfluid velocity. As a result of this correspondence, the Bose superfluid and superconductor share properties such as zero viscosity(zero resistivity) and vortices/flux quantization and, if the particles are charged, the Meissner effect. Each of these properties may be viewed as a result following from the form of the order parameter(Huang).

The phase of the order parameter plays an important role as is demonstrated in the following. Consider quasiparticle states occurring at the surface of the (normal) Fermi sea. Coulomb interactions are assumed to be taken into account in the quasipartical mass, magnetic moment, etc. To a large extent, the phonon mediated electron-electron interaction can also be included in this way; however, the induced correlation between time reversed states is responsible for the breakdown in the Fermi liquid description and must be treated separately. Under the perturbative influence of the residual attractive interaction, a pair of time reversed states, $\{|k\uparrow\rangle|-k\downarrow\rangle\}$ is scattered into another pair $\{|k'\uparrow\rangle|-k'\downarrow\rangle\}$. For simplicity of notation, label these two pair-states as $(1,0)$ and $(0,1)$. Considering only scattering between these two degenerate pair-states, the eigenstates are obtained by diagonalizing the following perturbative part of the hamiltonian.

$$H'_{(2)} = \begin{pmatrix} 0 & -V \\ -V & 0 \end{pmatrix}$$

The solutions have eigenvalues $\pm V$ for states $\psi = (1, \mp 1)$ respectively. For scattering among three degenerate pair-states $\{|k\uparrow\rangle|-k\downarrow\rangle\}$, $\{|k'\uparrow\rangle|-k'\downarrow\rangle\}$, $\{|k''\uparrow\rangle|-k'\downarrow\rangle\}$ one must consider diagonalizing the following matrix:

$$H'_{(3)} = \begin{pmatrix} 0 & -V & -V \\ -V & 0 & -V \\ -V & -V & 0 \end{pmatrix}.$$

The solution consists of two states $(1,-1,0),(1,0,-1)$ at energy +V and one state $(1,1,1)$ at energy $-2V$. Notice that the lowest energy state has the special feature that each pair-state enters with the same phase $(1,1,1) = (1,0,0)+(0,1,0)+(0,0,1)$.

Furthermore, this state is orthogonal to the two states at energy $+V$. Similarly, if one includes N degenerate pair-states in the initial basis, the diagonalization yields $(N-1)$ states at energy $+V$ and only one state at $-(N-1)V$ which is obtained from the individual pair-states by a coherent superposition $|\psi\rangle = (1,1,\ldots,1)$. As a result the expectation value of the interparticle coupling $\langle\psi|H'|\psi\rangle$ is a sum of terms $(-V)+(-V)+\ldots+(-V)$ where no cancellation occurs among the terms. This remarkable result means that for $N \longrightarrow 10^{23}$ one expects a large binding energy Δ for even a relatively small attractive interaction V. Cooper generalized this result to a continuum normalization of the momentum eigenstates and considered scattering between the large number of degenerate states at the Fermi energy. He finds a non-analytic expression for the binding energy, demonstrating the impossibility of obtaining this result from perturbation theory starting from the normal state,

$$\Delta = \hbar\omega_D\, e^{-1/(V\,N)}.$$

To summarize this result, there exists a ground state which is unique in that it maintains a special phase relationship among its components $(1,1,\ldots,1)$. As a result, the scattering between components is phase coherent introducing a factor of N into the binding energy. One may have expected that the order parameter would be the binding energy or equivalently the number of electrons involved in the coherent superposition. Why then does the order parameter contain the phase factor $e^{i\theta}$? The answer lies in the fact that the phase prevents one from considering the whole as just the sum of its parts. This point has been emphasized by Anderson(1984). For instance, consider the system to be composed of the sum of a large number, say M, parts where there are N/M electrons in each. From this point of view, the total binding energy is $|\Delta| = M \times (1-N/M)V = -V(N-1)+V(M-1)$, that is, less by an amount V(M-1) from the binding energy for the system in which all the electrons participate in a single condensate. The discrepancy results because the phase relationships between different parts of the system were ignored.

—The relationship between the macroscopic and microscopic theories—

It remains to be shown how these ideas can be put into realistic calculations. There are two approaches. The macroscopic formalism developed by Ginzburg and Landau (1950) assumes a free energy expansion in terms of the order parameter. The symmetry properties of the system are incorporated in the form of this expansion. As the Ginzburg-Landau (GL) theory assumes the order parameter is small, the theory is restricted to regions near a second order phase boundary. Alternatively, the microscopic formalism identifies the order parameter as the expectation value of certain "anomalous" two-body operators. The self-consistency condition on these expectation values gives the connection to the coefficients in the GL free energy expansion. As an example, this procedure is carried out for the theory of Bardeen, Cooper and Schrieffer (BCS) (1957).

In the general perturbative treatment, the interparticle interaction enters to first order through the expectation value of the product of two creation and two annihilation operators(Fetter and Walecka, sect. 8).

$$\sum_q V(k+q, \ell-q|\ell,k)\langle c^\dagger_{k+q} c^\dagger_{\ell-q} c_\ell c_k\rangle$$

The expectation value is taken with respect to the ground state of the system in the absence of interparticle interactions. Wick's theorem is used to express this expectation value as the sum of the product of two-operator expectation values. For example, in the normal state one considers the Hartree terms $\langle c^\dagger_{k+q} c_k\rangle\langle c^\dagger_{\ell-q} c_\ell\rangle$ and the Fock term $\langle c^\dagger_{k+q} c_\ell\rangle\langle c^\dagger_{\ell-q} c_k\rangle$. The Pauli exclusion principle restricts the momentum transfer to $q = 0$ and $q = \ell - k$ respectively. These contribute in both the superconducting and normal state and are generally absorbed into the properties of the quasiparticles. However, there is an additional term, occurring in the superconductor, involving pairs of time-reversed states $\langle c^\dagger_{k\uparrow} c^\dagger_{-k\downarrow}\rangle\langle c_{-k\downarrow} c_{k\uparrow}\rangle$. These "anomalous" averages vanish for the ground state of the normal fluid. However, for the superconductor it is assumed that the expectation value is taken with respect to a state which does not have a definite number of particles. This state is chosen to reflect the broken gauge symmetry of the condensate. It is only by starting from such a state that the perturbation theory will converge.

The BCS hamiltonian includes only the interaction between these two time-reversed states.

$$H_{BCS} = \sum_{k\sigma}(\varepsilon_k - \mu) c^\dagger_{k\sigma} c_{k\sigma} - \sum_{kk'} V_{kk'} c^\dagger_{k'\uparrow} c^\dagger_{-k'\downarrow} c_{-k\downarrow} c_{k\uparrow}.$$

That a mean field treatment is appropriate is suggested by the fact that the hamiltonian can be written in terms of the spin-operators $S^-_k \equiv c^\dagger_{k\uparrow} c^\dagger_{-k\downarrow}$, $S^+_k \equiv c_{-k\downarrow} c_{k\uparrow}$.

$$H_{BCS} = \sum_k (\varepsilon_k - \mu)(1 - 2S^z_k) - \sum_{kk'} V_{kk'}(S^x_k S^x_{k'} + S^y_k S^y_{k'}).$$

The mean field hamiltonian is equivalent to the interaction of the spins with an effective molecular field.

$$H_{MF} = -\sum_k \vec{B}^{mol}_k \cdot \vec{S}_k, \quad B^{mol}_k = 2(\varepsilon_k - \mu)\hat{e_z} + \sum_{k'} V_{kk'}(\langle S^x_{k'}\rangle \hat{e_x} + \langle S^y_{k'}\rangle \hat{e_y}) \qquad I.1.3$$

The order parameter becomes

$$\Delta_k \equiv -\langle S^+_k\rangle = \langle c_{k\uparrow} c_{-k\downarrow}\rangle.$$

The solution proceeds by obtaining the eigenstates of the mean field hamiltonian and applying statistical mechanics to calculate the thermal average (Tinkham, DeGennes). This yields the self-consistency equation,

$$\Delta_k = -\sum_\ell V_{k\ell} \frac{\Delta_\ell}{2E_\ell} tanh(E_\ell / 2k_B T).$$

A spatially uniform, non-trivial solution exists only for $T < T_c = \Delta(0)/(1.764)k_B$. Here $\Delta(T = 0)$ sets the scale of the pairing interaction; the free energy difference between the superconducting and normal states is $\frac{1}{2}N_o|\Delta|^2$.

The connection between the macroscopic and microscopic formalisms is achieved through the self-consistency relation. For the spatially uniform case, the Landau free energy expansion takes the form

$$F = a(T)|\Delta|^2 + b|\Delta|^4 + \text{higher order terms, where } a(T) = a_o(T - T_c), \qquad I.1.4$$

which describes the BCS superconductor at temperatures near T_c (Fig. I.1.2). Above T_c the free energy has a minimum at $|\Delta| = 0$. For $b < 0$ the system undergoes a first order transition to the superconducting state. For $b > 0$, the transition is second order and the order parameter grows with a square root dependence $\Delta(T) = (a_o(T_c - T)/2b)^{1/2}$. The self-consistency relation can be expanded near T_c to give $\Delta(T) = \Delta(0)(1 - T/T_c)^{1/2}$. One thereby obtains the correspondence between the microscopic theory and the coefficients in the GL free energy expansion $a_o \rightarrow N_o/2T_c$, $b \rightarrow N_o/4\Delta^2(0)$.

In the spatially inhomogeneous case one may have thought that the free energy expansion takes the form

$$F = a|\Delta(\vec{r})|^2 + b|\Delta(\vec{r})|^4 - \frac{\hbar^2}{2m^*}|\vec{\nabla}\Delta(\vec{r})|^2 + \cdots.$$

However, this form is not invariant under a local U(1) (also called gauge) transformation.

$$\Delta(\vec{r}) \rightarrow e^{ie^*\omega(\vec{r})}\Delta(\vec{r})$$

To insure gauge invariance, the gradient in I.3 is replaced with the covariant derivative $\vec{D} = \vec{\nabla} - (ie^*/\hbar c)\vec{A}$. $\vec{A}$ is the electromagnetic vector potential which transforms as $A^\mu(\vec{r}) \rightarrow A^\mu(\vec{r}) + \partial^\mu\omega(\vec{r})$ under a change of gauge. The superconducting state is characterized by the breaking of gauge invariance. As a result the phase of the order parameter, ϕ, becomes coupled to the vector potential as is evident in the GL equations. These are obtained by setting the functional derivative of the free energy with respect to Δ to zero (Tinkham, chap.4).

$$a\Delta + 2b|\Delta|^2\Delta + \frac{\hbar^2}{2m^*}\nabla^2\Delta = 0$$

$$J = \frac{e^*}{m^*}|\Delta|^2(\hbar\vec{\nabla}\phi - \frac{e^*}{c}\vec{A})$$

These equations reveal the two length scales involved in the variation of the order parameter. The magnitude, whose square represents the density n of superconducting electrons, varies over the coherence length ξ. The phase, current and magnetic field are all coupled and vary over the penetration depth λ.

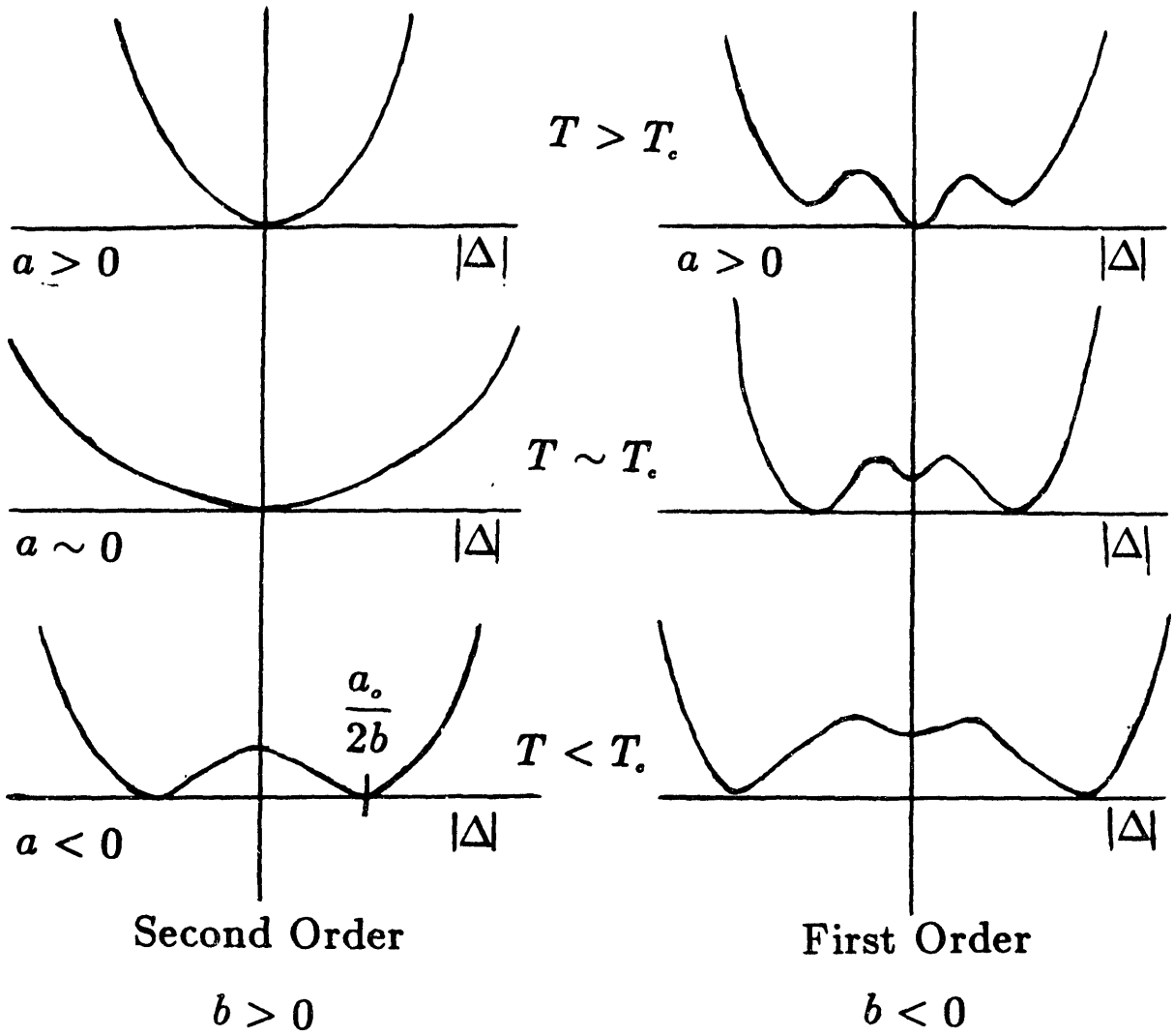

Fig. I.1.2 The Ginzberg-Landau free energy is plotted as a function of $|\Delta|$. The transition to the superconducting state (i.e. $\Delta \neq 0$) can be first or second order depending on the sign of b.

$$\xi(T) = \frac{\hbar^2}{2m^*|a(T)|}, \ \lambda = \frac{m^* c^2}{4\pi e^{*2} n}.$$

Gorkov(1959) showed the correspondence between the microscopic and macroscopic formalisms by deriving the GL equations from a BCS-type theory generalized to account for the spatial variation of the order parameter. As in the spatially homogeneous case worked out above, Gorkov's derivation employed an expansion of the self-consistency relation near T_c so as to determine the coefficients of the GL free energy expansion.

I.2 Pairbreaking and Impurity Scattering

Superconductivity is characterized by the pairing of time reversed states. With the introduction of perturbations which are not time reversal invariant, these states become non-degenerate and the superconducting transition temperature is reduced. Such perturbations are referred to as pairbreakers. An important distinction can be made between two limits called non-ergodic and ergodic pairbreaking. These two limits are characterized by different thermodynamic behavior and densities of states. In particular, ergodic pairbreaking is associated with gapless superconductivity near a second order phase boundary. After discussing these topics from a physical point of view, the microscopic theory will be introduced up to the point where Maki's review (1969) of gapless superconductivity begins. The results of the microscopic theory can be expressed in terms of T_{co} and certain "normal state" properties such as the scattering rates discussed in appendix A. In order to illustrate the microscopic formalism and further demonstrate the role of time reversal, the self-energy of a superconductor with spin-orbit and exchange scattering will be calculated in the Born approximation.

—Anderson's Theorem—

A basic observation is that, to a good approximation, the hamiltonian of a closed system is invariant under a time reversal transformation. From this observation and the fact that the hamiltonian determines the time evolution of a system,

$$\psi(\vec{r},t) = e^{-iHt/\hbar}\psi(\vec{r}) \qquad I.2.1$$

it can be shown that the time reversal operator takes the form $K = i\sigma_y C$ where C represents the complex conjugation operator. This form is chosen specifically to insure the invariance of the spin-orbit interaction (section A.3) which is part of the Dirac hamiltonian(Falicov). Because of the invariance property of the hamiltonian, the time reversal operator commutes with the hamiltonian, and states connected by the time reversal operator are degenerate. This is Kramers' theorem.

However, if the system is divided into two parts, then the hamiltonian is not necessarily invariant under a time reversal transformation applied only to one of the parts. For example, the interaction of electrons with an externally applied magnetic field is not invariant, unless one considers a comprehensive transformation which includes the reversal of the currents in the laboratory magnet supplying the "external" field. Similarly, the weak coulomb interaction between itinerant and localized electrons is described by the exchange interaction(section A.4) and this interaction is not invariant under time reversal of the itinerant system only.

Anderson (1959) suggested that the pairing in a superconductor is between time reversed states and that the introduction of perturbations which are time reversal invariant do not have a drastic effect on the transition temperature. In order to give a physical argument of why this is so, an inspection of the superconducting wavefunction is required. The discussion in section I.1 leads to the conclusion that, in analogy to the Bose condensate, the wavefunction of the superconductor is described by the product of two-electron orbitals where each orbital enters with the same phase. However, the antisymmetrization property of the wavefunction under interchange of any two

fermions must be incorporated into this scheme. One might consider the following wavefunction.

$$\psi_n = \{\phi(\vec{r}_1,\vec{r}_2;\sigma_1,\sigma_2)\phi(\vec{r}_3,\vec{r}_4;\sigma_3,\sigma_4)\ldots\phi(\vec{r}_{n-1},\vec{r}_n,\sigma_{n-1},\sigma_n) - \phi(\vec{r}_1,\vec{r}_3;\sigma_1,\sigma_3)\phi(\vec{r}_2,\vec{r}_4;\sigma_2,\sigma_4)\ldots\phi(\vec{r}_{n-1},\vec{r}_n,\sigma_{n-1},\sigma_n) + \cdots\}$$

The two-electron orbital $\phi(\vec{r}_1,\vec{r}_2;\sigma_1,\sigma_2)$ is antisymmetric under interchange of $\vec{r}_1$ and $\vec{r}_2$. This wavefunction is discussed by Leggett(1975) and is in fact the projection of the BCS wavefunction onto a n-particle manifold(Schrieffer, Sec. 2.4). It is generally the case in metals that the spatial part of the the orbital is symmetric. This is apparently due to the fact that the $\ell = 0$ part of the interparticle potential dominates. This corresponds to isotropic or s-wave scattering(see review by Leggett, 1975). Since the spatial part of the wavefunction is symmetric, it follows that the two spins form a singlet.

$$\phi(\vec{r}_1,\vec{r}_2;\sigma_1,\sigma_2) = u(\vec{r}_1,\vec{r}_2)(\uparrow\downarrow - \downarrow\uparrow)/\sqrt{2}$$

At this point the form of $u(\vec{r}_1,\vec{r}_2)$ is rather general being restricted only by the requirement that it be symmetric. However, as will be shown, the lowest binding energy will correspond to a $u(\vec{r}_1,\vec{r}_2)$ which is characterized by the pairing of time reversed states.

To evaluate the binding energy it is easier to work in the momentum space representation.

$$u(\vec{r}_1,\vec{r}_2) = \frac{1}{V}\sum_{kq} u(\vec{k},\vec{q})e^{i(\vec{k}+\vec{q})\cdot\vec{r}_1 - i(\vec{k}-\vec{q})\cdot\vec{r}_2} = \frac{1}{V}\sum_{kq} u(\vec{k},\vec{q})e^{i\vec{q}\cdot(\vec{r}_1+\vec{r}_2)+i\vec{k}\cdot(\vec{r}_1-\vec{r}_2)}$$

The wavevectors $\vec{k}$ and $\vec{q}$ are associated with the relative and center of mass motions of the Cooper pair respectively. Because of the antisymmetry property under interchange of electrons, one requires $u(-\vec{k},\vec{q}) = u(\vec{k},\vec{q})$. Therefore, one can rearrange the expansion of $\phi(\vec{r}_1,\vec{r}_2;\sigma_1,\sigma_2)$ so as to make the Cooper pairing in momentum space explicit.

$$\phi(\vec{r}_1,\vec{r}_2;\sigma_1,\sigma_2) = \sum_{kq} u(\vec{k},\vec{q})e^{i(\vec{k}+\vec{q})\cdot\vec{r}_1}e^{-i(\vec{k}-\vec{q})\cdot\vec{r}_2}(\uparrow\downarrow - \downarrow\uparrow)/\sqrt{2}$$

$$= \sum_{kq}\frac{u(\vec{k},\vec{q})}{\sqrt{2}}\left[e^{i(\vec{k}+\vec{q})\cdot\vec{r}_1}e^{-i(\vec{k}-\vec{q})\cdot\vec{r}_2}\uparrow\downarrow - e^{-i(\vec{k}-\vec{q})\cdot\vec{r}_1}e^{i(\vec{k}+\vec{q})\cdot\vec{r}_2}\downarrow\uparrow\right]$$

$$= \sum_{kq}\frac{u(\vec{k},\vec{q})}{\sqrt{2}}\left[|\vec{k}+\vec{q},\uparrow\rangle_1|-\vec{k}+\vec{q},\downarrow\rangle_2 - |-\vec{k}+\vec{q},\downarrow\rangle_1|\vec{k}+\vec{q},\uparrow\rangle_2\right]$$

The condensate is formed with pairs of electrons $|\vec{k}+\vec{q},\uparrow\rangle|-\vec{k}+\vec{q},\downarrow\rangle$. The binding energy per pair $\Delta(q)$ is maximized for $q \equiv |\vec{q}| = 0$. One reason is that the kinetic

energy associated with the center of mass motion is minimized for $q = 0$. Naively one might expect that $\Delta(q) \sim \Delta(0) - \hbar^2 q^2/2m$. However, it is a property of the superconductor that the decrease in binding energy is more rapid and is, in fact, linear in q. As will be shown, this is due to a loss of the potential energy associated with the coherent interparticle scattering which characterizes the superconducting ground state. In section I.1 it was found that the binding energy of the superconducting condensate was of the order of NV where V is the attractive interparticle coupling strength (i.e. BCS pair-potential) and N was the number of pairs participating in the condensate. The factor of N appears due to the phase coherence between pair-states. The numbers of pairs $N(q)$ of the type $|\vec{k}+\vec{q},\uparrow\rangle|-\vec{k}+\vec{q},\downarrow\rangle$ decreases proportionally with q due to the energy difference between the two members of the pair $\delta E = 2\hbar^2 kq/m$ and the fact that the density of states goes as a square root of the energy.

$$N(q) = \frac{N_o}{\sqrt{E_F}}\sqrt{E_F - \frac{2\hbar^2 k_F q}{m}} \sim N_o(1 - q/k_F)$$

The binding energy decreases with q due to a loss of the potential energy and with q^2 due to a gain in kinetic energy.

$$\Delta(q) = VN(q) - \frac{\hbar^2 q^2}{2m} = \Delta(0) - \Delta(0)\left(\frac{\delta E}{E_F}\right)^{\frac{1}{2}} - \delta E\left(\frac{\delta E}{E_F}\right)$$

This result is maintained in the continuum normalization (Cooper, 1956; see also Schrieffer, p.33), and it has important consequences for this discussion. Cooper remarks, "Thus, the elementary excitations of the pair might correspond to the splitting of the pair rather than to increasing the kinetic energy of the pair."

Now consider a system where time reversal invariance is violated by a perturbative term H' in the hamiltonian. In this case $H'K = -KH'$ and the first order energy contribution δE is opposite for time reversed pairs. For example, in a magnetic field the time reversed states $k\uparrow, -k\downarrow$ are separated by an energy difference $\delta E = 2\mu B$. The basic point is that in the superconductor the pairing of these non-degenerate time reversed states is energetically favorable as compared to pairing degenerate states at the Fermi level (Fig. I.2.1). There is a competition between the single-particle Zeeman energy and the many-body potential energy and the latter always wins out. The pairing of time reversed states pays an energy price $\delta E(\delta E/E_F)$ whereas the pairing of degenerate states at the Fermi level pays the much larger price $\Delta_o(\delta E/E_F)^{1/2}$. Thus the (S-wave) superconductor is always characterized by the pairing of time reversed states. Relative to the normal state, the superconducting state (with time reversed pairing) has a binding energy $\Delta = \Delta_o - \delta E$. Therefore, the T_c is reduced with the introduction of the pairbreaker H', and the normal state becomes favorable for $\delta E \sim \Delta_o$.

Ergodic verses Non-ergodic

Another way of looking at the depression of T_c is to consider that the the energy difference between time reversed states corresponds to a phase difference which grows

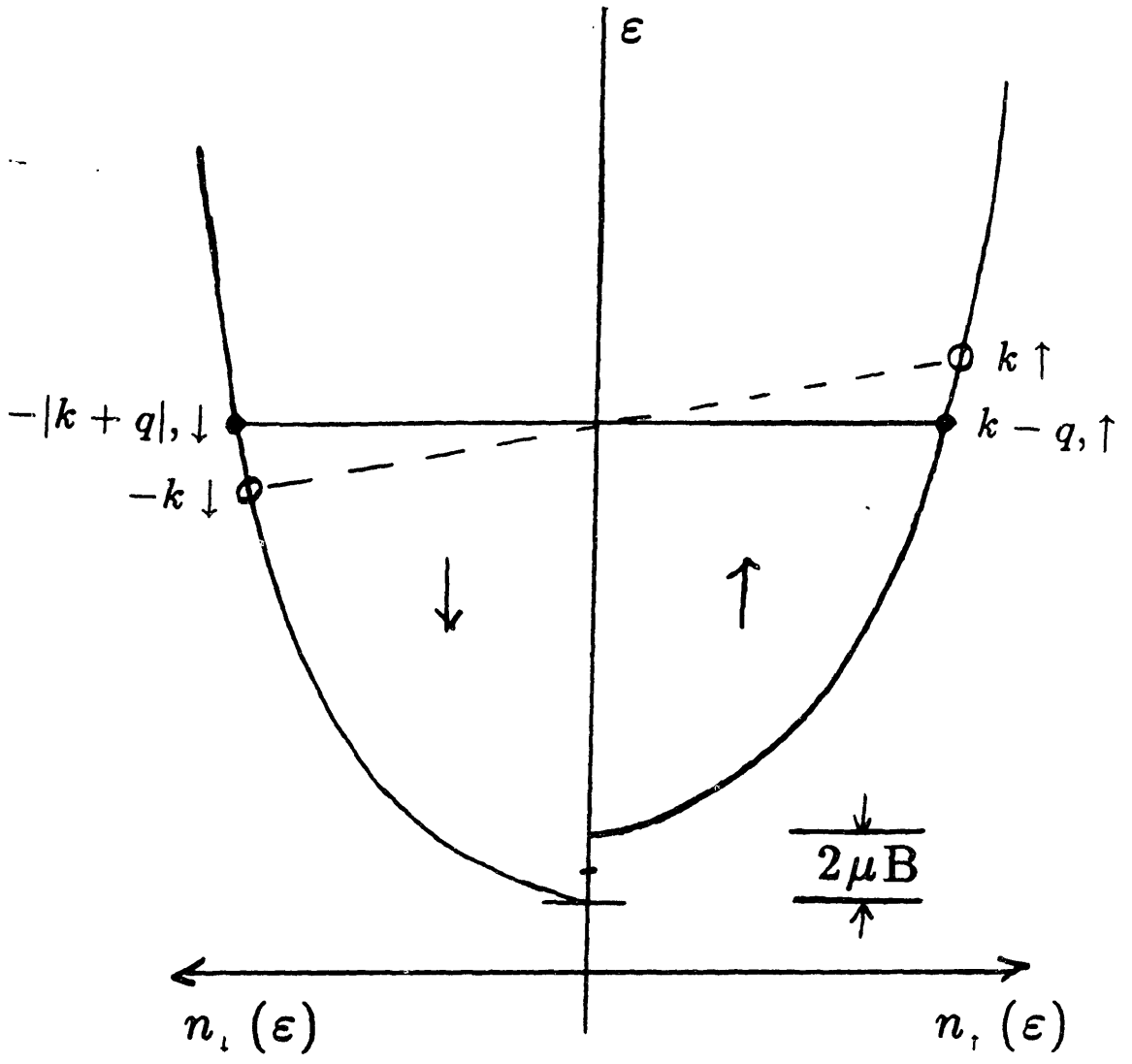

Fig. I.2.1 Due to the coherent nature of the superconductor, the pairing of non-degenerate time reversed states is energetically favored.

in time in accord with equation I.2.1. When the phase difference is of order unity, the pair no longer contributes to the binding energy of the condensate and the pair is said to have become unbound. This picture in terms of a phase difference is used by Tinkham(chapt. 8), and is based on a more rigorous treatment by DeGennes(chapt. 8). As discussed just above, the superconductor maintains the density of paired states by pairing non-degenerate time reversed states. As shown by DeGennes, the energy range δE over which this pairing takes place is determined by the time t_{PB} over which the pairs remain phase correlated $\delta E \approx \hbar/t_{PB}$. He introduces the correlation function $g(t) \equiv \langle K^{\dagger}(0)K(t)\rangle$ where K is the time reversal operator. One can show that $K(t) = e^{i[H,K]t/\hbar}K(0)$ where the commutator is related to the energy difference between time reversed states. For a time reversal symmetric hamiltonian $K(t) = K(0)$ and $g(t) = 1$ for all t. As a result, $t_{PB} = \infty, \delta E = 0$ and the Cooper pairing occurs among degenerate states.

In the case where the hamiltonian breaks time reversal invariance, one must distinguish between two limits. In the non-ergodic limit the phase difference evolves continuously; in the ergodic limit the phase difference grows diffusively. For example, consider a superconducting film oriented with its surface parallel to a magnetic field with a film thickness much less than the magnetic penetration depth. The internal field is nearly that of the applied field. Due to the Zeeman interaction of the magnetic field on the spins, time reversed states are not degenerate. The phase difference grows at a rate $d\phi/dt = 2\mu B/\hbar$. The non-ergodic limit corresponds to a system in which there is no spin-flip mechanism (e.g. spin-orbit scattering). After a "pairbreaking time" $t_{PB} = \hbar/2\mu B$, the phase difference reaches a value of unity. As a result, the transition temperature is reduced by the associated pairbreaking rate $T_c(B) \sim T_{co} - 2\mu B/k_B$.

The ergodic case corresponds to the limit of strong spin-flip scattering $\tau_{sf} \ll (d\phi/dt)^{-1}$. As such, the phase difference grows in a diffusive fashion. On average the phase change between any two spin-flip scattering events grows by an amount $\tau_{sf}(d\phi/dt)$. This corresponds to the size of one step taken in a random walk. After a time t, the number of steps taken is t/τ_{sf}, and the distance from the starting point is of the order $\tau_{sf}(d\phi/dt) \times (t/\tau_{sf})^{1/2}$. This is the product of the size of each individual step times the square root of the number of steps. Thus the phase difference grows more slowly than in the non-ergodic case. Again, pairbreaking occurs after a time t_{PB} when the phase difference is of order unity.

$$t_{PB} = \tau_{sf}(\tau_{sf}\frac{d\phi}{dt})^{-2} = \frac{\hbar}{(2\mu B)^2\tau_{sf}} \qquad I.2.2$$

The transition temperature is reduced by the pairbreaking rate $T_c \approx T_{co} - (\pi/4)\hbar/t_{PB}$. The factor of $\pi/4$ is taken from the Abrikosov-Gorkov (AG) theory in the limit of weak pairbreaking. The pairbreaking rate is generally normalized to the energy scale of the superconducting pairing, that is, T_c or T_{co} or $\Delta_o = 1.764k_BT_{co}$.

$$\rho_{AG} = \frac{\hbar}{\pi k_B T_c t_{PB}}, \; PP0 = \frac{\hbar}{k_B T_{co} t_{PB}}, \; \alpha_{Maki} = \frac{\hbar}{\Delta_o t_{PB}}$$

The original AG calculation was for the case of magnetic impurities; however, the

theory is now known to apply to a wide range of pairbreaking situations(Maki, 1969). For magnetic impurities, the pairbreaking time becomes the exchange scattering rate $\hbar/\tau_{ex} = (\pi/2)c\Omega N_o J^2(0)S(S+1)$ (see A.4). When the impurity spins are aligned in a magnetic field, there is a corresponding non-ergodic pairbreaking due to forward scattering off the impurities. This is equivalent to an effective Zeeman interaction from a "uniform exchange field" $B_{ex} = c\langle S_z\rangle J(0)/g\mu$. Therefore, non-ergodic pairbreaking corresponds to the forward scattering and the ergodic pairbreaking corresponds to random scattering.

There are important differences between the ergodic and non-ergodic cases. Among these are the effect on the density of states (DOS) and thermodynamics of the system. The DOS of the BCS superconductor has an energy gap above which there is a square root singularity and below which no single particle excitations exist. When a non-ergodic perturbation is applied, the gap in the density of states is shifted relative to the Fermi level. For example, for a uniform magnetic field the DOS for up and down spin directions are shifted in opposite directions, and the relative shift is the Zeeman splitting(Fig. I.2.2). As a result excitations are possible for $\Omega_G = \Delta - \mu B$. In the ergodic limit, where both a field and strong spin-flip scattering are present, the Cooper pair acquires a resonance width. The singularity in the density of states is broadened by $\hbar/t_{PB}$, and excitations are possible above $\Omega_G \sim \Delta - \hbar/t_{PB}$. It is important to note that in both cases the order parameter Δ is not the same as the spectroscopic gap Ω_G for single particle excitations.

The thermodynamic properties are strongly dependent on the DOS. In doing thermodynamics in mean field theory, one first solves for the excitation spectrum of the system (i.e. DOS) using a general value of Δ. Then, using the appropriate particle statistics (e.g. Fermi-Dirac), one solves the self-consistency condition to obtain the value for Δ as a function of the thermodynamic variables T,P,B, etc. The different DOS obtained in the non-ergodic and ergodic cases yield different thermodynamic behavior. Most startling is the fact that in the ergodic case the transition to the normal state is second order, and, as a result, the spectroscopic gap may go to zero before the order parameter. This is the phenomenon of gapless superconductivity which shows that the absence of low energy excitations in the BCS superconductor is not the reason for superfluid behavior(e.g. zero resistance).

Alternately, the non-ergodic case is characterized by a first order transition and gapless superconductivity does not occur. To illustrate this point, consider again the Zeeman interaction from an applied magnetic field. At $T = 0$ the pure superconductor has zero spin-susceptibility due to the singlet nature of the Cooper pairing(Yosida,1958). The spin-susceptibility as a function of $|\vec{q}|$ is shown in figure I.2.3 (Anderson and Suhl, 1959). As a result, in a magnetic field the free energy of the superconducting state is raised relative to the Pauli paramagnetic, normal state. The susceptibility of the latter is $\chi_N = (g\mu)^2 N_o/2$. At the "Pauli limiting field" B_P, the superconducting condensation energy $N_o\Delta^2/2$ equals the polarization energy $(\chi_N - \chi_S)B^2/2$.

$$B_P = \frac{\sqrt{2}\Delta_o}{g\mu} = 1.86\ T_c(tesla/K) \qquad I.2.3$$

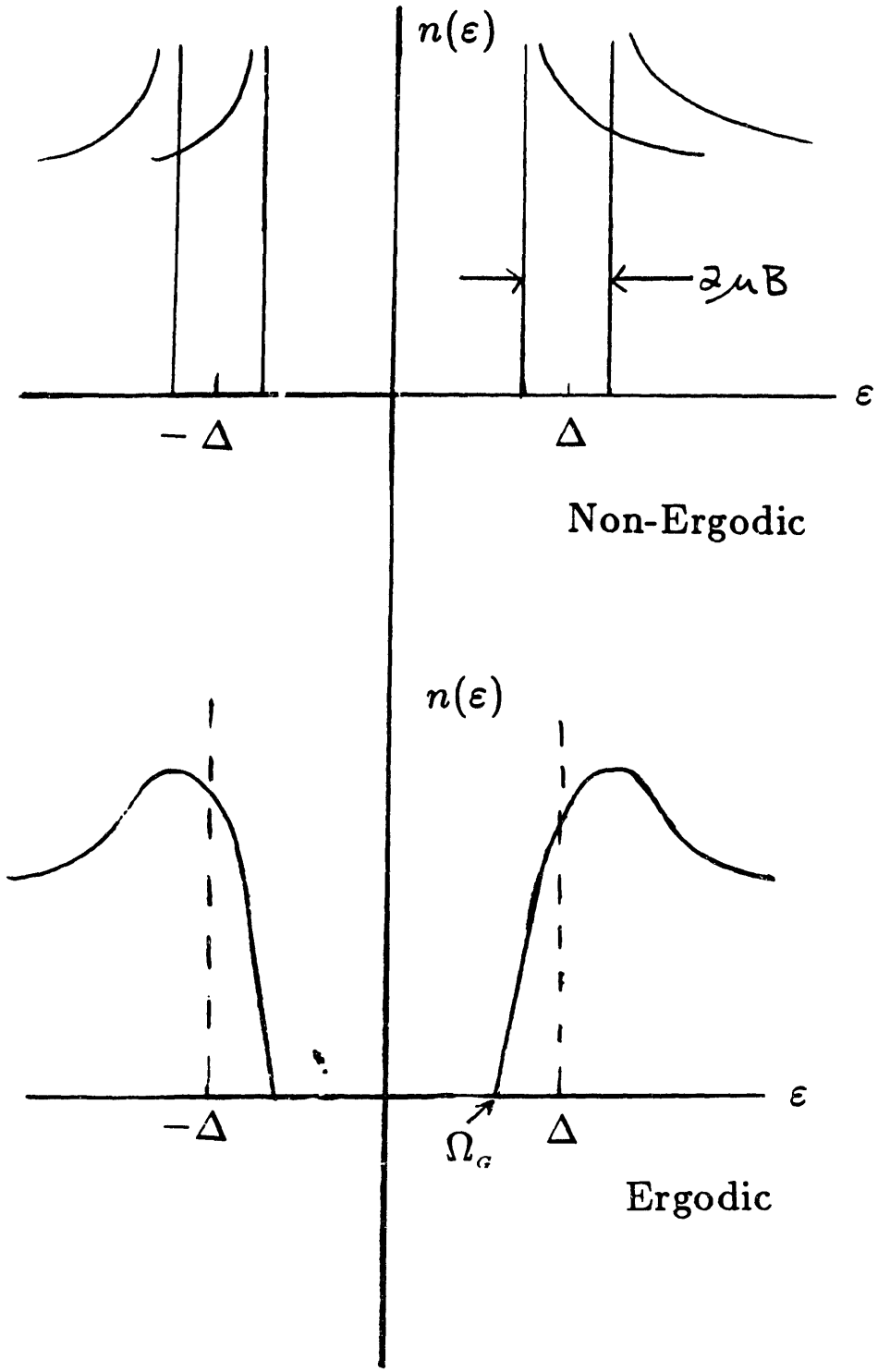

Fig. I.2.2 The density of states of a superconductor is perturbed differently by ergodic and non-ergodic pairbreakers.

This is the limiting field introduced by Clogston(1962) and Chandrasekhar(1962) as the upper limit on the superconducting critical magnetic field. Sarma (1963) showed that the transition to the normal state was of first order.

When Clogston introduced the Pauli-limiting field, he suggested that many-body correction to the spin-susceptibility would alter the Pauli limit. Experimentally, the necessity of including such Fermi liquid effects was found in the work of Orlando, McNiff, Foner, Beasley (1979), Tedrow and Meservey(1979), and Orlando and Beasely(1981). However, as pointed out by Rainer, it is the correction to the Zeeman splitting (not susceptibility) which ends up in the expression I.2.3 for the Pauli limiting field. The Fermi liquid correction due to coulomb interactions was worked out as an example in section I.1 and was interpreted in terms of a renormalized magnetic moment $\mu = \mu_B/(1+G^o)$. Equivalently, one can retain the quasiparticle moment as μ_B and consider the effect in terms of an effective internal field $B_{int} = B(1+G^o)$. In either case the Pauli limit becomes $B_P = (\sqrt{2}\Delta_o/g\mu_B) \times (1+G^o)$.

For $T \neq 0$, thermal fluctuations break up some number of Cooper pairs. The unbound quasiparticles can align their spins antiparallel to the applied magnetic field and contribute to the spin susceptibility. The density of single particle excitations which may respond to the applied field is described by the Yosida function Y(t) which is shown in figure I.2.4. Since the excitations must be thermally excited above the energy gap, Y(t) is a function of reduced temperature $t = T/T_c$. As a result, the Fermi liquid effects also have a temperature dependence. Since only unbound quasiparticles can respond to the field, $(\Delta n_\downarrow - \Delta n_\uparrow) = Y(t)N_o(2\mu_{eff}B)$. Substitution of this in equation I.1.2. yields

$$2\mu_{eff}B = 2\mu_B B - 2\mu_{eff}B\ Y(t)\ G^o$$

This gives the magnetic moment as a function of the reduced temperature $\mu_{eff} = \mu_B/(1+Y(t)G^o)$. Similarly, the susceptibility becomes $\chi_S(t) = \mu(t)(\Delta n_\downarrow - \Delta n_\uparrow)/B = \chi_N Y(t)/(1+Y(t)G^o)$. Details are provided by Leggett(1965), Alexander, Orlando, Rainer and Tedrow(1985), and Gibson(1988).

The fact that the superconductor at $T \neq 0$ has a non-zero spin-susceptibility means that the system can respond to the applied magnetic field. This enters into the self-consistency condition for the order parameter with the result that above the "tricritical" temperature, $T_{c3} = 0.556T_{co}$, the transition to the normal state is second order(Engler and Fulde). As one might expect, the introduction of spin-flip scattering into the system lowers this tricritical temperature. In the ergodic limit, the entire T,B phase boundary is associated with second order transitions.

For temperatures greater T_{c3}, the transition is of second order and is described by a Landau free energy expansion of the form given by I.1.4. The coefficients of the expansion are functions of T and B and need to be calculated with the microscopic theory. This is accomplished by expanding the self-consistency condition to second order in the order parameter. The second order transition occurs for $a(T,B) = 0$, $b(T,B) > 0$. The tricritical point is determined by the condition $a(T,B) = 0$, $b(T,B) = 0$. The calculation by Engler and Fulde for T_{c3} will be extended to include Fermi liquid effects in chapter IV.

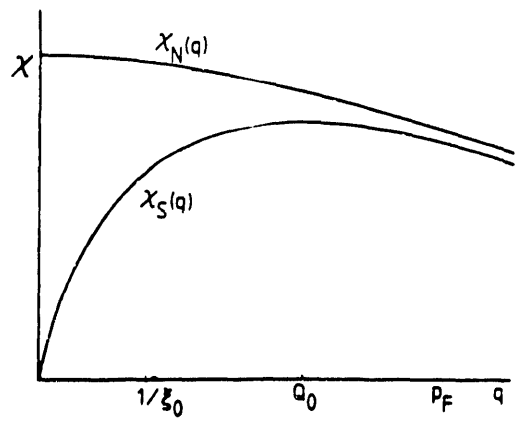

Fig. I.2.3 The spin-susceptibility is plotted verses wavevector for the superconductor and normal metal where $Q_o = (3\pi k_F^2 \xi_o^{-1})^{1/3}$ (from Anderson and Suhl, 1959).

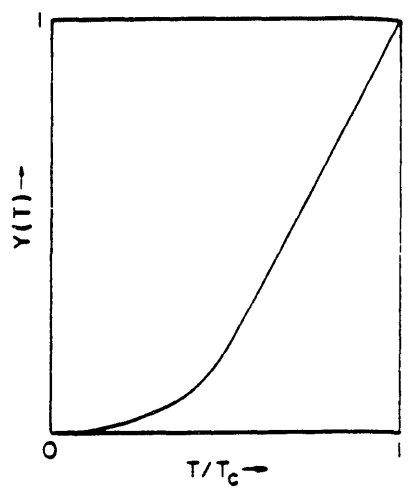

Fig. I.2.4 The Yosida function verses reduced temperature (from Leggett, 1973).

A first order transition occurs for $b(T,B) < 0$; however, the order parameter appears discontinuously at the transition, and a free energy expansion in a *small* order parameter is not justified in general. A numerical solution of the self-consistency condition is required in this region. A numerical solution is also needed for the area of the T,B phase diagram not near the phase boundary. It is important to note that one advantage of tunneling as opposed to critical field measurements is that tunneling gives information throughout the superconducting phase diagram and is not restricted to the phase boundary. Introduced below is the microscopic theory from which these GL coefficients are calculated.

—The Microscopic Theory—

A generalization of the BCS-type mean field theory is necessary in order to treat scattering from localized impurities and other perturbations which are spatially inhomogeneous. Even for a uniform magnetic field, the vector potential is a function of position leading to spatial variations in the order parameter (e.g. vortices). The discussion of scattering in the normal state presented in appendix A is extended here to superconductors. The following is derived from a number of sources, the most pertinent of which are Bruno(1972), Maki(1969), Vonsovsky et al(1982), and DeGennes(1966, chapt. 5).

In section I.1, the order parameter was identified in terms of an anomalous average of the type $\Delta_k = \langle c_{k\uparrow} c_{-k\downarrow} \rangle$. In order to take into account spatial variations it is advantages to work in a coordinate representation. Furthermore, dynamics will be included by working in a time representation; even if the impurity scattering is elastic, this procedure will allow calculations for $T \neq 0$. One introduces the field operators in the Heisenberg representation with respect to a grand canonical ensemble.

$$\psi_\alpha^\dagger(\vec{r},t) = e^{i(H-\mu N)t/\hbar} \left(\sum_{\alpha\beta} \langle \vec{r}|k\alpha\rangle c_{k\alpha}^\dagger \right) e^{-i(H-\mu N)t/\hbar}$$

The order parameter becomes $\Delta(x) = \langle \psi_\uparrow(x)\psi_\downarrow(x)\rangle$ where $x \equiv (\vec{r},t)$. The unperturbed mean field hamiltonian corresponding to I.1.3 becomes

$$H_o = \int d\vec{r} \left\{ \sum_\alpha \psi_\alpha^\dagger(\vec{r}) \left(\frac{-\hbar^2\nabla^2}{2m} - \mu \right) \psi_\alpha(\vec{r}) + \Delta(\vec{r})\psi_\uparrow^\dagger(\vec{r})\psi_\downarrow^\dagger(\vec{r}) + \Delta^*(\vec{r})\psi_\downarrow(\vec{r})\psi_\uparrow(\vec{r}) \right\}$$

Gorkov(1958) introduced a perturbation theory for superconductors using the anomalous averages $F_{\uparrow\downarrow}(x_1,x_2) \equiv -i\langle T\psi_\uparrow(x_1)\psi_\downarrow(x_2)\rangle$ along with the usual Green's function $G_{\alpha\beta}(x_1,x_2) \equiv -i\langle T\psi_\alpha(x_1)\psi_\beta^\dagger(x_2)\rangle$. Averages of the sort $F_{\uparrow\uparrow}$ correspond to triplet pairing and are not considered. Averages of the sort $G_{\uparrow\downarrow}$ are considered since spin-flip processes are possible from spin-orbit and exchange scattering.

Nambu(1960) introduced a notation which allows one to apply to superconductors the same diagrams found in the perturbation theory used for normal metals. For example, the diagrams in A.2 will be used to describe scattering in superconductors. Consider the four component spinor.

$$\psi^\dagger(x) \equiv \left(\psi_\uparrow^\dagger(x),\ \psi_\downarrow^\dagger(x),\ \psi_\uparrow(x),\ \psi_\downarrow(x)\right);\quad \psi(x) \equiv \begin{pmatrix} \psi_\uparrow(x) \\ \psi_\downarrow(x) \\ \psi_\uparrow^\dagger(x) \\ \psi_\downarrow^\dagger(x) \end{pmatrix}$$

One defines a matrix Greens' function which involves the outer product of these spinor operators $\widehat{G}(x_1;x_2) = -i\langle T\psi(x_1)\psi^\dagger(x_2)\rangle$. The associated 4×4 "Nambu" space is conveniently spanned by the product of two sets of the 2×2 Pauli matrices. One set $\sigma_1, \sigma_2, \sigma_3, \sigma_0$ will be associated with the spin degrees of freedom and the other $\rho_1, \rho_2, \rho_3, \rho_4$ with what is called the particle-hole degrees of freedom.

$$\rho_1 = \begin{pmatrix} 0 & 1 \\ 1 & 0 \end{pmatrix},\ \rho_2 = \begin{pmatrix} 0 & -i \\ i & 0 \end{pmatrix},\ \rho_3 = \begin{pmatrix} 1 & 0 \\ 0 & -1 \end{pmatrix},\ \rho_0 = \begin{pmatrix} 1 & 0 \\ 0 & 1 \end{pmatrix}$$

This particle-hole degree of freedom enters because time reversed states which start at the Fermi level are shifted in energy by a pairbreaking perturbation so that one is above and one is below the Fermi level. The product space is defined as in the following example.

$$\rho_3\sigma_1 = \begin{pmatrix} \sigma_1 & 0 \\ 0 & -\sigma_1 \end{pmatrix} = \begin{pmatrix} 0 & 1 & 0 & 0 \\ 1 & 0 & 0 & 0 \\ 0 & 0 & 0 & -1 \\ 0 & 0 & -1 & 0 \end{pmatrix}$$

The unperturbed hamiltonian I.2.3 takes the compact form

$$\widehat{H_o} = \int d\vec{r}\psi^\dagger(\vec{r})(\varepsilon\rho_3 + \rho_1\sigma_2\Delta)\psi(\vec{r})$$

where $\varepsilon = -(\hbar^2\nabla^2/2m) - \mu$ and Δ has been chosen to be real and independent of position. The 2×2 unit matrices σ_o, ρ_o are usually not written; for example, $\rho_3 \equiv \rho_3\sigma_o$. As shown in section I.1, the vector potential couples to the phase of the order parameter; therefore, Δ can not be chosen to be real in the perturbed system.

Any external potential $U_{\alpha\beta}(\vec{r})$ is easily related to its counterpart $\widehat{U}$ in the Nambu notation. One defines $\widehat{U}$ such that

$$\int d\vec{r}\sum_{\alpha\beta}\psi_\alpha^\dagger(\vec{r})U_{\alpha\beta}(\vec{r})\psi_\beta(\vec{r}) = \frac{1}{2}\int d\vec{r}\psi^\dagger(\vec{r})\widehat{U}(\vec{r})\psi(\vec{r}).$$

The factor of $1/2$ enters as an artifact of the Nambu notation but divides out at the end of the calculation. A little matrix algebra and the relation $\psi_\alpha U_{\alpha\beta}\psi_\beta^\dagger = -\psi_\beta^\dagger U_{\beta\alpha}^{tr}\psi_\alpha$ shows that

$$\widehat{U} = \begin{pmatrix} U_{\alpha\beta} & 0 \\ 0 & -U_{\alpha\beta}^{tr} \end{pmatrix}$$

Note that the spin operator has a transpose given by $-\vec{\sigma}^{tr} = \sigma_2 \vec{\sigma} \sigma_2$. The matrix operator corresponding to spin is usually denoted by $\hat{\vec{\alpha}}$ where $\hat{\alpha}_x = \rho_3 \sigma_1$, $\hat{\alpha}_y = \sigma_2, \hat{\alpha}_z = \rho_3 \sigma_3$. Similarly, one can show that the matrix momentum operator is $\hat{\vec{p}} = \vec{p} \rho_3$.

The advantage of Nambu notation is that Wick's theorem applied in the normal way to bracketed products of the spinor operators automatically gives both the normal $G_{\alpha\beta}$ and anomalous $F_{\alpha\beta}$ Green's functions used by Gorkov (Vonsovsky et al, Chap.3). For example, Wick's theorem applied to the average $\langle T\psi^\dagger(x_1)\psi^\dagger(x_2)\psi(x_3)\psi(x_4)\rangle$ gives the sum $\langle T\psi(x_4)\psi^\dagger(x_1)\rangle\langle T\psi(x_3)\psi^\dagger(x_2)\rangle - \langle T\psi(x_3)\psi^\dagger(x_1)\rangle\langle T\psi(x_4)\psi^\dagger(x_2)\rangle$. Each factor is a matrix Green's function of the form

$$\hat{G}(x_1;x_2) = -i\langle T\psi(x_1)\psi^\dagger(x_2)\rangle = \begin{pmatrix} G_{\uparrow\uparrow} & G_{\uparrow\downarrow} & 0 & F_{\uparrow\downarrow} \\ G_{\downarrow\uparrow} & G_{\downarrow\downarrow} & F_{\downarrow\uparrow} & 0 \\ 0 & F^\dagger_{\uparrow\downarrow} & G^\dagger_{\uparrow\uparrow} & G^\dagger_{\uparrow\downarrow} \\ F^\dagger_{\downarrow\uparrow} & 0 & G^\dagger_{\downarrow\uparrow} & G^\dagger_{\downarrow\downarrow} \end{pmatrix}$$

In a perturbative treatment one tries to expand the Green's function of the perturbed system in terms of the unperturbed Green's function. This is most easily done in momentum and frequency space. The equation of motion for the matrix Green's function in the unperturbed system is

$$(i\frac{d}{dt} - \hat{H}_o)\hat{G}_o(\vec{r}_1 - \vec{r}_2, t_1 - t_2) = \delta(\vec{r}_1 - \vec{r}_2)\delta(t_1 - t_2)$$

and the Fourier transform of this is

$$(i\hbar\omega - \varepsilon_k \rho_3 - \Delta_k \rho_1 \sigma_2)\hat{G}_o(k,\omega) = 1$$

where $\varepsilon_k = \hbar^2 k^2/2m - \mu$. The Green's function becomes

$$\hat{G}_o(k,\omega) = (i\hbar\omega - \varepsilon_k \rho_3 - \Delta_k \rho_1 \sigma_2)^{-1} = \frac{-i\hbar\omega - \varepsilon_k \rho_3 - \Delta_k \rho_1 \sigma_2}{\hbar^2\omega^2 + \varepsilon_k^2 + \Delta_k^2}$$

The fact that $\hat{G}\hat{G}^{-1} = \hat{1}$ is easily verified in this notation by noting that the square of a Pauli matrix is the unit matrix and that $(\rho_3\sigma_o)(\rho_1\sigma_2) = -(\rho_1\sigma_2)(\rho_3\sigma_o)$.

$$(i\hbar\omega - \varepsilon_k \rho_3 - \Delta_k \rho_1 \sigma_2) \times (-i\hbar\omega - \varepsilon_k \rho_3 - \Delta_k \rho_1 \sigma_2) = \hbar^2\omega^2 + \varepsilon_k^2 + \Delta_k^2$$

For a $T \neq 0$ calculation one sums over the Matsubara frequencies $\hbar\omega = 2\pi k_B T(n + 1/2); n = 0, \pm 1, \pm 2, \ldots$ (Lifshitz and Pitaevskii, Chapt.IV; Mattuck, Chapt. 14). The poles of the Green's function correspond to elementary excitations. For example, the poles of $\hat{G}_o$ give $E_k = i\hbar\omega_k = \pm\sqrt{\varepsilon_k^2 + \Delta_k^2}$. There is a square root singularity above the gap Δ_k.

This is about the point at which Maki(1969) picks up the discussion in his review of gapless superconductivity. He proves a generalized version of Anderson's theorem which was discussed from a physical point of view earlier in this section. The proof is

rather straightforward in this mathematical context. "If a static external perturbation does not break the time-reversal symmetry and does not cause a long-range spatial variation of the order parameter [i.e., $\Delta_k(\vec{r}) \simeq$ const.], the thermodynamic properties of the superconductor remain unchanged in the presence of the perturbation." The word "static" refers to elastic scattering. So as to not rewrite Maki's review, this section will conclude by simply completing the correspondence with appendix A. The effect of spin-orbit and exchange scattering will be considered as these illustrate the role of time-reversal.

In the Nambu notation, spin-orbit and exchange interactions are given by

$$\langle k'|\hat{H}_{so}|k\rangle = \frac{iv_{so}(\vec{q})}{|k|^2}(\vec{k'} \times \vec{k}) \cdot \hat{\vec{\alpha}}\rho_3$$

$$\langle k'|\hat{H}_{ex}|k\rangle = J(\vec{q})S_i \cdot \hat{\vec{\alpha}}$$

In correspondence with the discussion in A.2, the self-energy in the Born approximation becomes

$$\hat{\Sigma}(k,\omega) = V \int \frac{d\vec{k'}}{(2\pi)^3} \langle k|\hat{H}'|k'\rangle \; \hat{G}(k') \; \langle \; k'|\hat{H}'|k\rangle$$

where $\hat{G}(k') \equiv (i\hbar\tilde{\omega} - \varepsilon_k\rho_3 - \tilde{\Delta}_k\rho_1\sigma_2)^{-1}$ is the Green's function of the perturbed system. One has terms of the form

$$Spin-orbit \longrightarrow \hat{\vec{\alpha}}\rho_3 \left[\frac{i\hbar\tilde{\omega} + \varepsilon_k\rho_3 + \tilde{\Delta}_k\rho_1\sigma_2}{\hbar^2\tilde{\omega}^2 + \varepsilon_k^2 + \tilde{\Delta}_k^2}\right]\vec{\alpha}\rho_3$$

$$Exchange \longrightarrow \hat{\vec{\alpha}} \left[\frac{i\hbar\tilde{\omega} + \varepsilon_k\rho_3 + \tilde{\Delta}_k\rho_1\sigma_2}{\hbar^2\tilde{\omega}^2 + \varepsilon_k^2 + \tilde{\Delta}_k^2}\right]\vec{\alpha}$$

In the spin-orbit case one makes use of the commutation properties $(\rho_3\sigma_0)\hat{\vec{\alpha}} = +\hat{\vec{\alpha}}(\rho_3\sigma_0)$ and $(\rho_1\sigma_2)\hat{\vec{\alpha}}(\rho_3\sigma_o) = -\hat{\vec{\alpha}}(\rho_3\sigma_o)(\rho_1\sigma_2)$. In the exchange case, $(\rho_1\sigma_2)\hat{\vec{\alpha}} = +\hat{\vec{\alpha}}(\rho_1\sigma_2)$ and the sign change makes all the difference.

$$\hat{\Sigma}_{so}(k,\omega) = V \int \frac{d\vec{k'}}{(2\pi)^3} \left|\frac{v_{so}(\vec{q})(\vec{k'} \times \vec{k}) \cdot \vec{s}}{|k|^2}\right|^2 \left[\frac{-i\hbar\tilde{\omega} - \varepsilon_k\rho_3 + \tilde{\Delta}_k\rho_1\sigma_2}{\hbar^2\tilde{\omega}^2 + \varepsilon_k^2 + \tilde{\Delta}_k^2}\right]$$

$$\Sigma_{ex}(k,\omega) = V \int \frac{d\vec{k'}}{(2\pi)^3} \left|J(\vec{q})\vec{S}_i \cdot \vec{s}\right|^2 \left[\frac{-i\hbar\tilde{\omega} - \varepsilon_k\rho_3 - \tilde{\Delta}_k\rho_1\sigma_2}{\hbar^2\tilde{\omega}^2 + \varepsilon_k^2 + \tilde{\Delta}_k^2}\right]$$

The momentum space integration is performed by the usual separation into an integration over energy and over constant energy surfaces

$$V\int\frac{d\vec{k'}}{(2\pi)^3}\rightarrow VN_o\int\frac{d\Omega}{4\pi}\int_{-\infty}^{\infty}d\varepsilon_{k'}.$$

Since the scattering considered is elastic, the energy ε_k doesn't appear in the scattering potentials. The energy integrations are determined by the residues in the complex plane and terms odd in ε_k don't contribute.

$$\int_{-\infty}^{\infty}d\varepsilon_k\frac{-i\hbar\tilde{\omega}\pm\tilde{\Delta}_k\rho_1\sigma_2}{\left(\varepsilon_k-i\sqrt{\hbar^2\tilde{\omega}^2+\tilde{\Delta}_k^2}\right)\left(\varepsilon_k+i\sqrt{\hbar^2\tilde{\omega}^2+\tilde{\Delta}_k^2}\right)}=\pi\frac{i\hbar\tilde{\omega}\mp\tilde{\Delta}_k\rho_1\sigma_2}{\sqrt{\hbar^2\tilde{\omega}^2+\tilde{\Delta}_k^2}}$$

Thus the self-energy is of the form.

$$\Sigma_{\binom{\circ\circ}{\times\times}}(k,\omega)=\frac{\hbar}{2\tau_{\binom{\circ\circ}{\times\times}}}\frac{i\hbar\tilde{\omega}\mp\tilde{\Delta}_k\rho_1\sigma_2}{\sqrt{\hbar^2\tilde{\omega}^2+\tilde{\Delta}_k^2}}$$

where the scattering rates are those calculated as in equation A.1.10. With this result Maki goes on to demonstrate how one calculates the density of states and expands the self-consistency equation near the phase boundary. For spin-orbit scattering there is no change in T_c. For exchange scattering the T_c is reduced from its value T_{co} in the unperturbed superconductor due to ergodic pairbreaking. The implicit relation between T_c and T_{co} was first obtained by Abrikosov and Gorkov.

$$ln(T_{co}/T_c)=\psi(\frac{1}{2}+\frac{\rho_{AG}}{2})-\psi(1/2). \qquad I.2.4$$

Here ψ is the digamma function and $\rho_{AG}=\hbar/\pi T_c\tau_{ex}$. This corresponds to the relation $a(T,\rho_{AG})=0$ where $a(T,\rho_{AG})$ is the coefficient in the free energy expansion (Eq. I.1.4). The non-ergodic case is taken into account by adding a term to the unperturbed hamiltonian. For example, the Green's function in the case of a pure superconducting thin film in a parallel magnetic field is

$$\hat{G}_o(k,\omega)=[i(\hbar\omega+iI\rho_3\sigma_3)-\varepsilon_k\rho_3-\Delta_k\rho_1\sigma_2]^{-1}$$

where $I=\mu B$. It is easily seen that the elementary excitations (i.e. poles of $\hat{G}_o$) occur at $E_k=i\hbar\omega=\sqrt{\varepsilon_k^2+\Delta_k^2}-I$. In the limit of strong spin-orbit scattering $\hbar/\tau\gg k_BT_{co}$ one regains the ergodic results (eq. I.2.2) with $\hbar/t_{PB}=3I^2/2(\hbar/\tau_{so})$ (Maki and Tsuneto,1964). Similarly, one can treat combined spin-orbit and exchange scattering(Fulde and Maki,1966). In the "dirty limit", $\hbar/\tau_{tr}\gg k_BT_{co}$, orbital effects from the $\vec{p}\cdot\vec{A}$ interaction can be viewed as ergodic pairbreaking (Werthamer, Helfand, and Hohenberg,1966; Maki,1966). The condition of Pauli limiting occurs when the spin-orbit scattering rate is less than the Zeeman energy associated with the upper critical field, a situation reviewed by Fulde(1973).

Bibliography I

Abrikosov, A.A., and L.P. Gor'kov, Zh.Eksperim. i Teor. Fiz. **39**,1781 (1960); Sov.Phys. JETP **12**,1243 (1961).

Alexander, J.A.X., T.P. Orlando, D.Rainer, and P.M. Tedrow, Phys.Rev.B **31**,5811 (1985).

Anderson, P.W., J.Phys.Chem.Sol. **11**,26 (1959).

Anderson, P.W., and H. Suhl, Phys. Rev. **116**, 898 (1959).

Anderson, P.W., *Basic Notions of Condensed Matter Physics*, (Benjamin/Cummings Publishing, Menlo Park, CA, 1984).

Bardeen, J., L.N. Cooper, and J.R. Schrieffer, Phys.Rev. **108**,1175 (1957).

Bruno, R.C., *The Magnetic Field Behavior of Superconductors*, Ph.D. thesis MIT, (1972).

Chandrasekhar, B.S., Appl.Phys.Lett. **1**,7 (1962).

Clogston, A.M., Phys.Rev.Lett. **9**,266 (1962).

Cooper, L.N., Phys.Rev. **104**,1189 (1956).

DeGennes, P.G., *Superconductivity of Metals and Alloys*, Trans. P.A. Pincus, (W.A. Benjamin, NY, 1966).

Engler, H., P. Fulde, Phys.Kondens.Materie **7**, 150 (1968).

Falicov, L. M., *Group Theory and its Physical Applications*, Compiled by A. Luehrmann, (University of Chicago Press, Chicago, 1966).

Fetter, A.L. and J.D. Walecka, *Quantum Theory of Many-Particle Systems*, (McGraw-Hill Book Co., NY, 1971).

Fulde, P., and K. Maki, Phys.Rev. **141**,275 (1966).

Fulde, P., Adv.Phys. **22**,667 (1973).

Gibson, G., (unpublished), Ph.D. thesis at MIT (1988).

Ginzberg, V.L., and L.D. Landau, Zh.Eksperim.i Teor. Fiz. **20**,1064 (1950).

Gorkov, L.P., Sov.Phys. JETP **36**,1364 (1959).

Huang, K., *Quarks, Leptons & Gauge Fields*, (World Scientic Publishing, Singapore, 1982).

Itzykson, C., and J.B. Zuber, *Quantum Field Theory*, (McGraw-Hill Inc., NY, 1980).

Leggett, A.J., Phys.Rev. **140**,A1869 (1965).

Leggett, A.J., Rev.Mod.Phys. **47**,331 (1975).

Lifshitz, E.M., and L.P. Pitaevskii, *Statistical Physics*, Trans. J.B. Sykes and M.J. Kearsley, (Pergamon Press, NY, 1980).

Maki, K., and T.Tsuneto, Progr.Theoret.Phys. **31**,945 (1964).

Maki, K., Phys.Rev. **148**,362 (1966).

Maki, K., in *Superconductivity* edited by R.D. Parks, (Marcel Dekker, NY, 1969)

Mattuck, R.D., *A Guide to Feynman Diagrams in the Many-Body Problem*, 2^{nd} edition, (McGraw-Hill, NY, 1976).

Orlando, T.P., E.J. McNiff, Jr., S. Foner, M.R. Beasley, Phys.Rev.B **19**,4545 (1979).

Orlando, T.P., and M.R. Beasley, Phys.Rev.Lett. **46**,1598 (1981).

Sarma, G., J.Phys.Chem.Solids, **24**,1029 (1963).

Schrieffer, J.R., *Theory of Superconductivity*, (Benjamin/Cummings Publishing Co., Reading, Mass., 1964).

Tedrow, P.M., R. Meservey and B.B. Schwartz, Phys. Rev. Lett. **24**, 1004 (1970).
Tedrow, P.M., and R. Meservey, Phys.Rev.Lett. **43**,384 (1979).
Tinkham, M., *Introduction to Superconductivity*, R.E. Krieger Publishing, Huntington, NY, 1980).
Vonsovsky, S.V., Y.A. Izyumov, E.Z. Kurmaev, *Superconductivity of Transition Metals*, Trans. E.H. Brandt and A.P. Zavarnitsyn, (Springer-Verlag, NY 1982).
Werthamer, N.R., E. Helfand, and P.C. Hohenberg, Phys.Rev. **147**,295 (1966).
Yosida, K., Phys.Rev. **110**,769 (1958).

Chapter II — Experimental Techniques

II.1 Spin-Polarized Tunneling

In this first section a brief description of the spin-polarized tunneling technique is given. This includes information as to how the conductance reflects the density of states (DOS) as well as a description of the experimental apparatus and measurement procedure. For the most part the description will only serve to compliment information available elsewhere. However, a more complete analysis of the errors which enter into the conductance measurement is given here. Two texts on the subject of tunneling are those by Solymar(1972) and Wolf(1985). Spin-polarized tunneling and the special superconducting properties of thin $A\ell$ films are reviewed by Fulde (1973). Three Ph.D. dissertations and an senior thesis include detailed discussion of these techniques (Paraskevopoulos, 1976; Alexander, 1986; Gibson, 1988; Kucera, 1983).

The tunneling current between a superconductor and normal metal separated by a insulating barrier was first measured by Giaever (1960). The conductance $G = dI/dV$ of a superconductor-insulator-normal (S-I-N) metal junction has a peak at the superconducting energy gap and a trough around zero bias voltage (Fig. II.1.1). This suggested to Giaever that the tunneling conductance was proportional to the superconducting density of states which has a square root singularity above and vanishes below the superconducting gap energy.

$$\rho_S(E) = \begin{cases} \Delta/\sqrt{E^2 - \Delta^2} & E > \Delta \\ 0 & E < \Delta \end{cases}$$

The proportionality can be understood from the viewpoint that the transition probability of moving an electron from one electrode to the other is described by a Fermi golden rule expression $(2\pi/\hbar)|M|^2\rho_f$ where M is the associated matrix element and ρ_f is the density of final states. On closer inspection the relationship between the tunneling conductance and density of states is surprisingly subtle (Bardeen, 1961; Harrison, 1961). In regard to Giaever's measurements Harrison (p.87) remarks, "It seems remarkable that the simple experimental result depends so directly upon the subtleties of the many-particle system. In any case, we do not expect this essential breakdown of the independent-particle model to occur in tunneling involving normal metals, ... Neither, then, do we expect to find the simple proportionality of the ac conductance to the density of states."

However, under certain restrictions which appear to apply to planar tunnel junctions (see section 2.2 of Wolf), the ratio of the tunneling conductance in the superconducting state to that in the normal state is given by the convolution of the superconducting density of states with the derivative of the Fermi distribution. The derivative $\partial f/\partial eV$ is a sharply peaked function with a peak width given by the thermal energy kT ($\sim 40\mu V$ at $T = 0.5$ K).

$$G_{SIN}/G_{NIN} = \int_{-\infty}^{\infty} \rho_S(E) \left[\frac{\partial f(E - eV)}{\partial eV}\right] dE \qquad II.1.1$$

A somewhat different expression for the tunneling conductance between superconductors (i.e. S-I-S tunneling) predicts a peak in the conductance at an energy corresponding to the sum of the energy gaps of the two electrodes. A helpful aid in understanding the relationship between the tunneling conductance and the density of states of the two electrodes is provided by the so called "semiconductor model" which is described in detail by Tinkham (section 2-8), and Solymar.

Previous experiments have established the fact that the superconducting density of states of a thin Aℓ film is split into spin-up and spin-down parts by an applied magnetic field B (Meservey, Tedrow and Fulde, 1970; Fulde, 1973). The splitting energy at low temperature and field is $2\mu B$ where μ is the electron magnetic moment. The resulting density of states is shown schematically in figure II.1.2(a). If the Aℓ film is part of a tunnel junction with a normal metal counter electrode, a conductance (dI/dV) curve such as shown in figure II.1.2(b) would be observed as a function of voltage. The DOS splitting of $2\mu B$ is reflected in the dI/dV curve. If the counterelectrode is Fe, a curve such as figure II.1.2(c) would be observed (Tedrow and Meservey, 1971). The asymmetry arises from the polarization of the electrons at the Fermi surface of the Fe. This asymmetry makes possible the determination of the spin-dependent densities of states of the superconductor (Tedrow, Moodera, and Meservey, 1982). Note that if the counter electrode is another thin Aℓ film, no splitting will be observed in the dI/dV curve with magnetic field applied to the junction (Tedrow and Meservey, 1971; Meservey, Tedrow and Bruno, 1975), because both films will have their densities of states split by the same amount and spin is conserved in the tunneling process. However, if one film should have different splitting from the other, the peak at the sum of the gaps will be split by the difference in the effective Zeeman splitting of electrons in the two electrodes (figure II.1.2(d). This previously unobserved situation can arise if one superconductor has very large spin-orbit scattering and a high magnetic field is applied (see section III.4), or if the two superconductors are in different (effective) magnetic fields. In chapter III, the exchange interaction from magnetic impurities is found under certain conditions as an effective magnetic field acting on the spins of the electrons only. Thus, in S-I-N tunneling, the total splitting of the density of states is observed, while in $S_1 - I - S_2$ tunneling, the difference in splitting of the densities of states of the two superconductors S_1 and S_2 is observed.

—The tunneling circuit and sources of error—

Sample fabrication will be discussed in the next section and in the following chapters. However, the typical junction configuration is shown in figure II.1.3. Junction areas are of the order $2.7 \cdot 10^{-3} cm^2$. Generally samples with and without the perturbative surface layer are formed. The conductance is measured with the circuit shown schematically in figure II.1.4. Superimposed on a DC bias applied between the two electrodes is a (constant-amplitude) AC modulation voltage $\partial V = 20\mu eV$ at 500 Hz from the oscillator of a Princeton Applied Research A124 lock-in amplifier. The AC current amplitude ∂I through the junction is measured across the resistor R_s with the lock-in amplifier. The bias voltage is slowly swept from $-3\Delta/e \rightarrow +3\Delta/e$, and the rate of the sweep is set such that the output of the lock-in amplifier changes by at most a few percent of the full scale deflection during one integration time constant.

Integration times of more than 300ms did not improve the signal to noise ratio.

Since ∂V is (approximately) constant, the output of the lock-in amplifier is taken to be proportional to the conductance $\partial I/\partial V$. The conductance value at a bias voltage of 3mV ($\sim 10\Delta$) corresponds approximately to the normal state conductance (figure II.1.5). The ratio of the conductance at any arbitrary bias voltage to that at 3mV is expressed by equation II.1.1 and is sometimes referred to as the normalized conductance (i.e. normalized to the normal state conductance). This of course assumes that the normal state conductance is independent of bias voltage (Ohmic behavior) which from figure II.1.5 is seen to be an adequate approximation over the $\pm 3mV$ region most studied.

The constancy of the modulation ∂V across the junction is only approximate. An equivalent circuit is shown in figure II.1.6. Since the junction resistance is a function of bias voltage, the part of the input modulation V_{in} across the junction changes (i.e. $\sim R_j/(R_j + R_s)$). In order for these changes to be negligible, the lead resistance and R_s must be much less than the junction resistance R_j. Junction resistances of the order $1K\Omega$, lead resistances $< 100\Omega$, and $R_s \sim R_j/50$ are typical and sufficient in order to neglect this source of error.

For larger values of the junction resistance, the input signal to the lock-in ∂I measured across R_s is reduced in absolute magnitude such that the signal to noise ratio increases. However, in certain cases (e.g. V_3Ga junctions) the junction resistances are not under experimental control. In such cases there is the possibility of a phase shift between V_{in} and V_{out}. Ideally one would like $\partial I \equiv V_{out}/R_s = V_{in}/R_j$. However, due to the close spacing of the electrodes in a tunnel junction $\sim 10^{-9}$m, the capacitance is significant

$$C \sim \frac{\epsilon(Area)}{d} \sim \frac{(10^{-11}F/m)(10^{-7}m^2)}{(10^{-9})} = 10^{-9} \sim 1nF$$

The resulting phase shift raises the possibility that the real part of V_{out} is not linear in $1/R_j$. The output voltage can be written

$$V_{out} = \frac{V_{in}R_s}{Z} = V_{in}R_s\frac{1 + i\omega CR_j}{R_s(1 + i\omega CR_j) + R_j}$$

For $\omega CR_s \ll 1$ and $R_s/R_j \ll 1$ one can easily show

$$\partial I \equiv \frac{\Re e(V_{out})}{R_s} = \frac{V_{in}}{R_j}\left[1 - \frac{R_s}{R_j}(1 - (\omega CR_j)^2)\right]$$

Typically, $R_s \sim 10\Omega, R_j \sim 1k\Omega, \omega = 500Hz$ and $\omega CR_s \sim$ [4]. Thus, this source of error can be ignored for the most part.

Finally, one must consider the effects of the $20\mu eV$ RMS modulation. Because the voltage swings $V_1 = 34\mu eV$ to either side the DC bias voltage V_o, any asymmetric non-linearity (e.g cubic terms in the I(V) taylor expansion about V_o) is not averaged to zero and thereby distorts the conductance measurement. Generally, it is believed that these errors can be neglected as long as $eV_1 < kT$ ($\sim 40\mu eV$ at $T = 0.5k$). However, thermal effects are accounted for in the data analysis by convoluting the theoretical

DOS with the derivative of the Fermi distribution as in equation II.1.1. Furthermore, there is structure in the DOS sharper than kT. Thus, it is appropriate to consider the error in $G = dI/dV$ produced by the non-zero modulation amplitude V_1. The current through the junction at a time t when the voltage is $V(t) = V_o + V_1 \sin\omega t$ is given by

$$I(t) = \int_0^{V(t)} dxG(x) = I_o + \int_{V_o}^{V_o + V_1 \sin\omega t} dxG(x)$$

where $I_o = \int_0^{V_o} dxG(x)$ is the current for just the DC voltage V_o. One can expand the conductance about V_o in a taylor series with the result

$$I(t) = I_o + G(V_o)V_1 \sin\omega t + \frac{1}{2}V_1^2 G'(V_o)\sin^2\omega t + \frac{1}{6}V_1^3 G''(V_o)\sin^3\omega t$$

let $\sin^2\omega t = (1 - cos2\omega t)/2, \sin^3\omega t = (3\sin\omega t - \sin 3\omega t)/4$

$$I(t) = I_o + V_1 G(V_o)\sin\omega t + \frac{1}{4}V_1^2 G'(V_o)[1 - cos2\omega t] +$$

$$+\frac{1}{24}V_1^3 G''(V_o)[3\sin\omega t - \sin 3\omega t] + \cdots$$

The lock-in amplifier picks out the coefficient of the $\sin\omega t$ term which is

$$I_\omega = V_1 G(V_o) + \frac{1}{8}V_1^3 G''(V_o) + \cdots$$

To lowest order one obtains the conductance at the DC bias voltage (i.e. $I_\omega/V_1 = G(V_o)$). The lowest order error in the conductance measurement due to the non-zero modulation amplitude is given by the next term $V_1^2 G''(V_o)/8$. Thus, the error decreases faster than the magnitude of the signal (which goes as V_1). For $V_1 = 50\mu eV$, the conductance is distorted at peaks where d^3I/dV^3 is large. In decreasing the modulation to $30\mu eV$, the curves are noticeably sharper. In decreasing from 30 to $20\mu eV$ there is little change and one can be relatively sure that the error due to the modulation can be neglected.

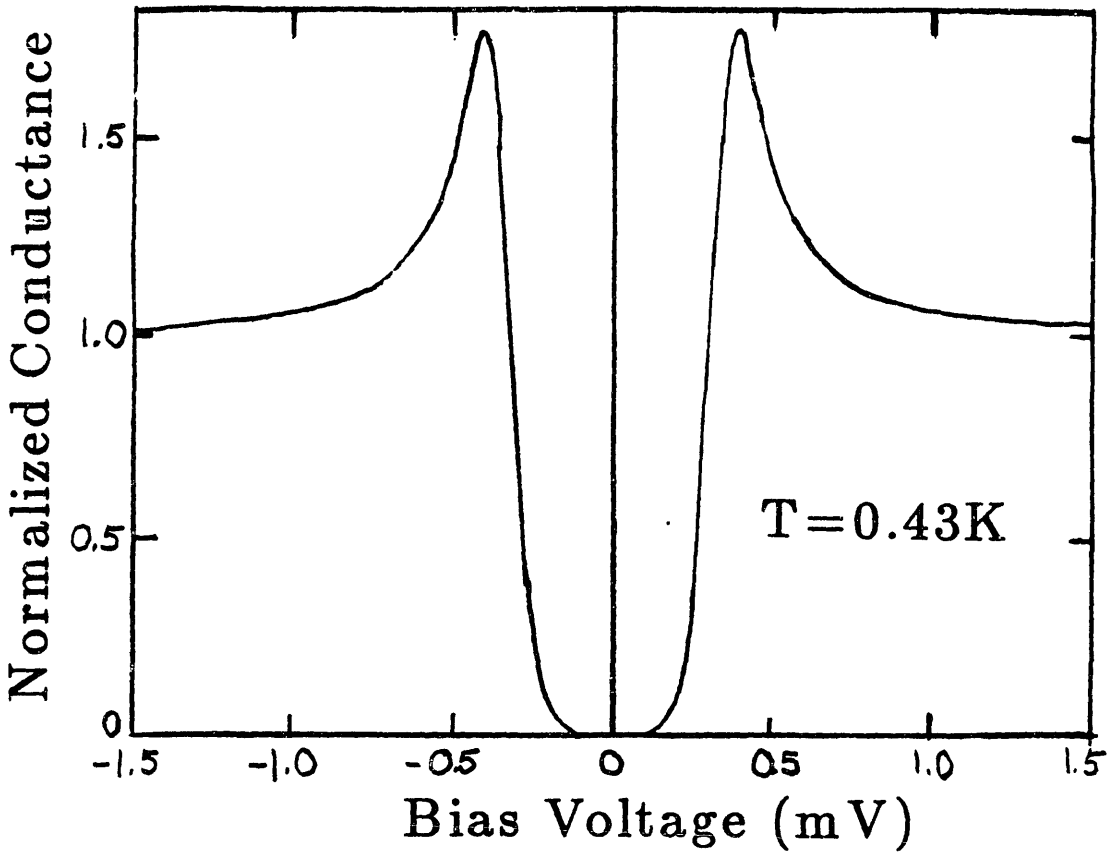

Fig. II.1.1 The measured tunneling conductance of a S-I-N tunnel junction where the superconducting electrode is a 40$\mathring{A}$Aℓ film and the normal electrode Ag.

Fig. II.1.2 (next page) (a) BCS density of states split into spin-up and spin-down parts by a magnetic field B. (b) Schematic tunneling conductance vs. voltage of a junction between a thin Aℓ film and a normal metal in a magnetic field B. (c) Schematic tunneling conductance vs. voltage of a junction between a thin Aℓ film and a ferromagnetic metal film in a magnetic field. (d) Schematic tunneling conductance vs. voltage of a junction between a thin Aℓ film in a magnetic field B and a thin Aℓ film in a magnetic field B+B*.

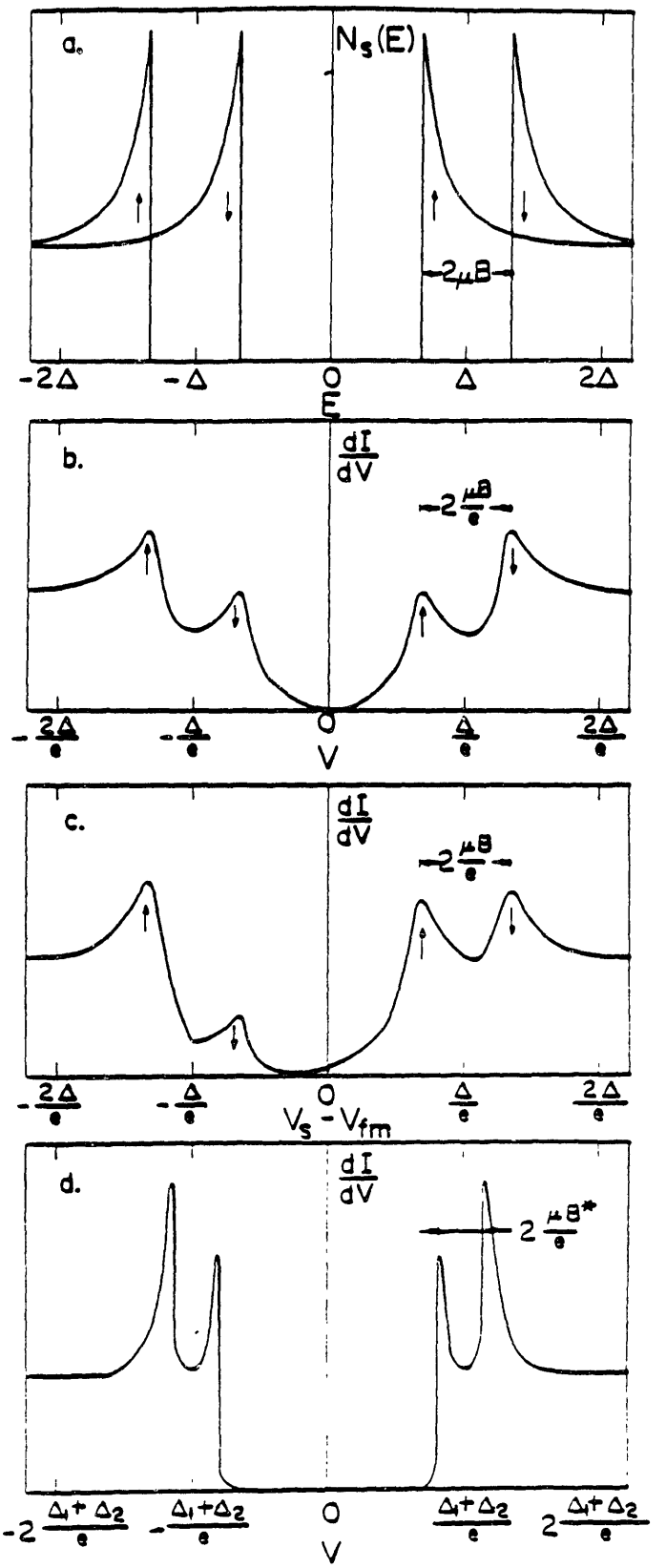
a.
$N_s(E)$
$2\mu B$
-2Δ
$-\Delta$
0
Δ
2Δ
E
b.
$\frac{dI}{dV}$
$2\frac{\mu B}{e}$
$-\frac{2\Delta}{e}$
$-\frac{\Delta}{e}$
0
$\frac{\Delta}{e}$
$\frac{2\Delta}{e}$
V
c.
$\frac{dI}{dV}$
$2\frac{\mu B}{e}$
$-\frac{2\Delta}{e}$
$-\frac{\Delta}{e}$
0
$\frac{\Delta}{e}$
$\frac{2\Delta}{e}$
$V_s - V_{fm}$
d.
$\frac{dI}{dV}$
$2\frac{\mu B^*}{e}$
$-2\frac{\Delta_1+\Delta_2}{e}$
$-\frac{\Delta_1+\Delta_2}{e}$
0
$\frac{\Delta_1+\Delta_2}{e}$
$2\frac{\Delta_1+\Delta_2}{e}$
V

Fig. II.1.3 Sample Configuration.

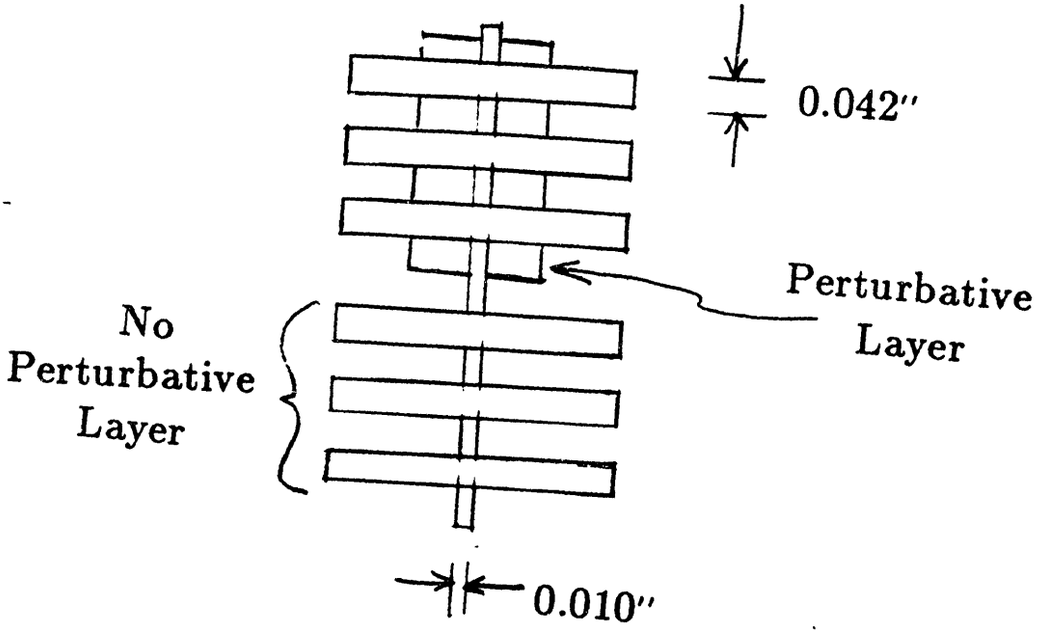

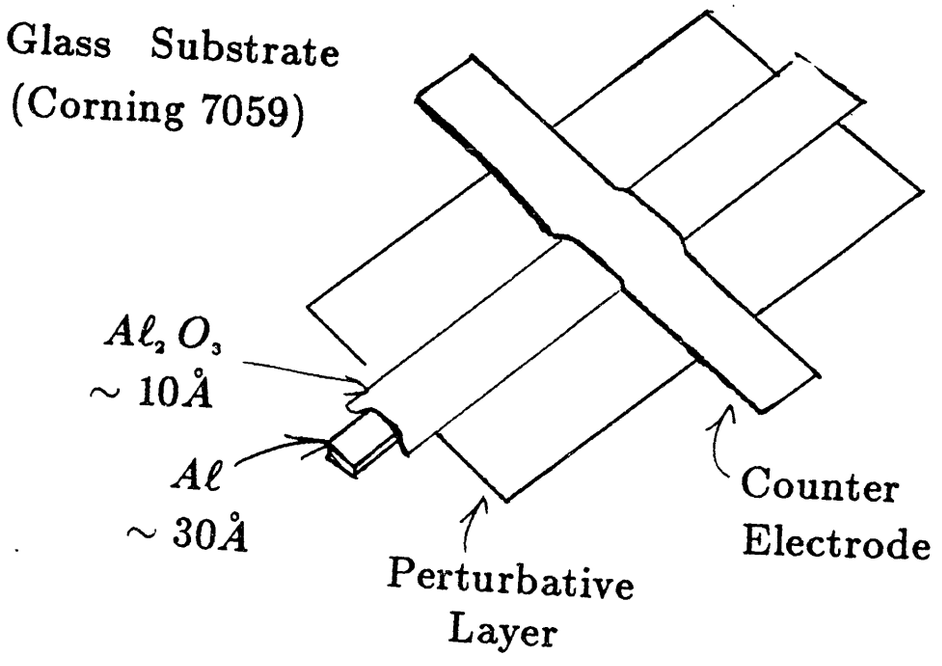

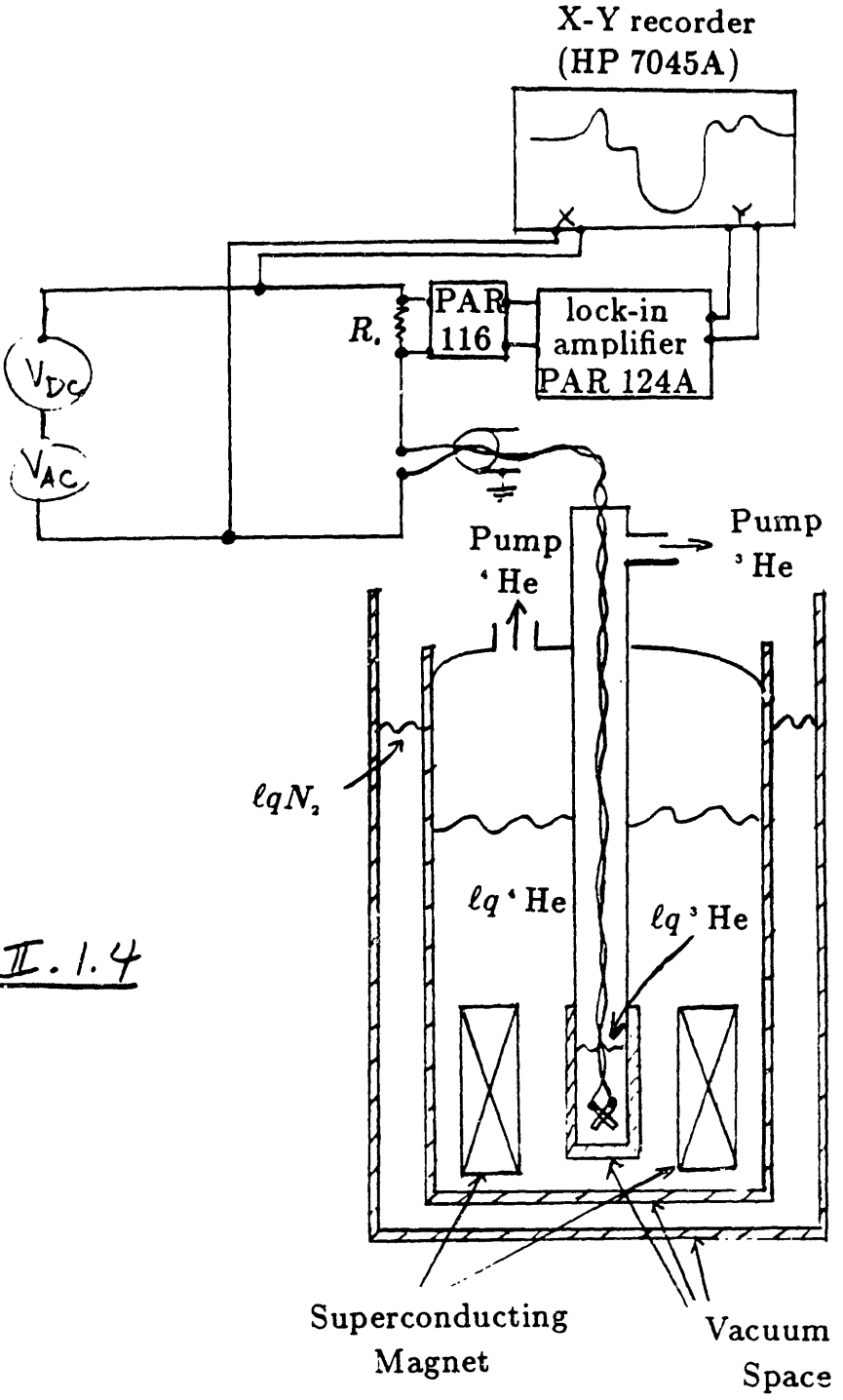
X-Y recorder
(HP 7045A)
X
Y
R_s
PAR
116
lock-in
amplifier
PAR 124A
V_{DC}
V_{AC}
Pump
^{4}He
Pump
^{3}He
$\ell q N_2$
$\ell q\ ^4$He
$\ell q\ ^3$He
Superconducting
Magnet
Vacuum
Space

Fig II.1.4

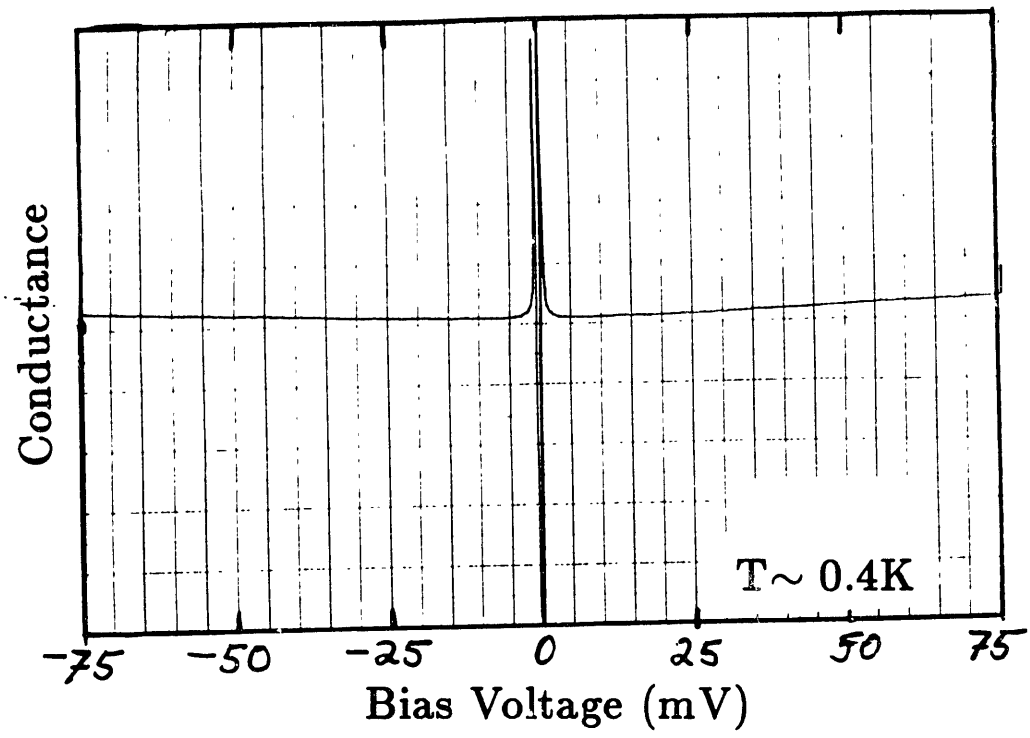

Fig. II.1.5 The measured tunneling conductance of an $Al - Al_2O_3 - Al$ junction. The curvature of the normal state conductance is possibly due to barrier height effects (see Wolf, section 2.3.1).

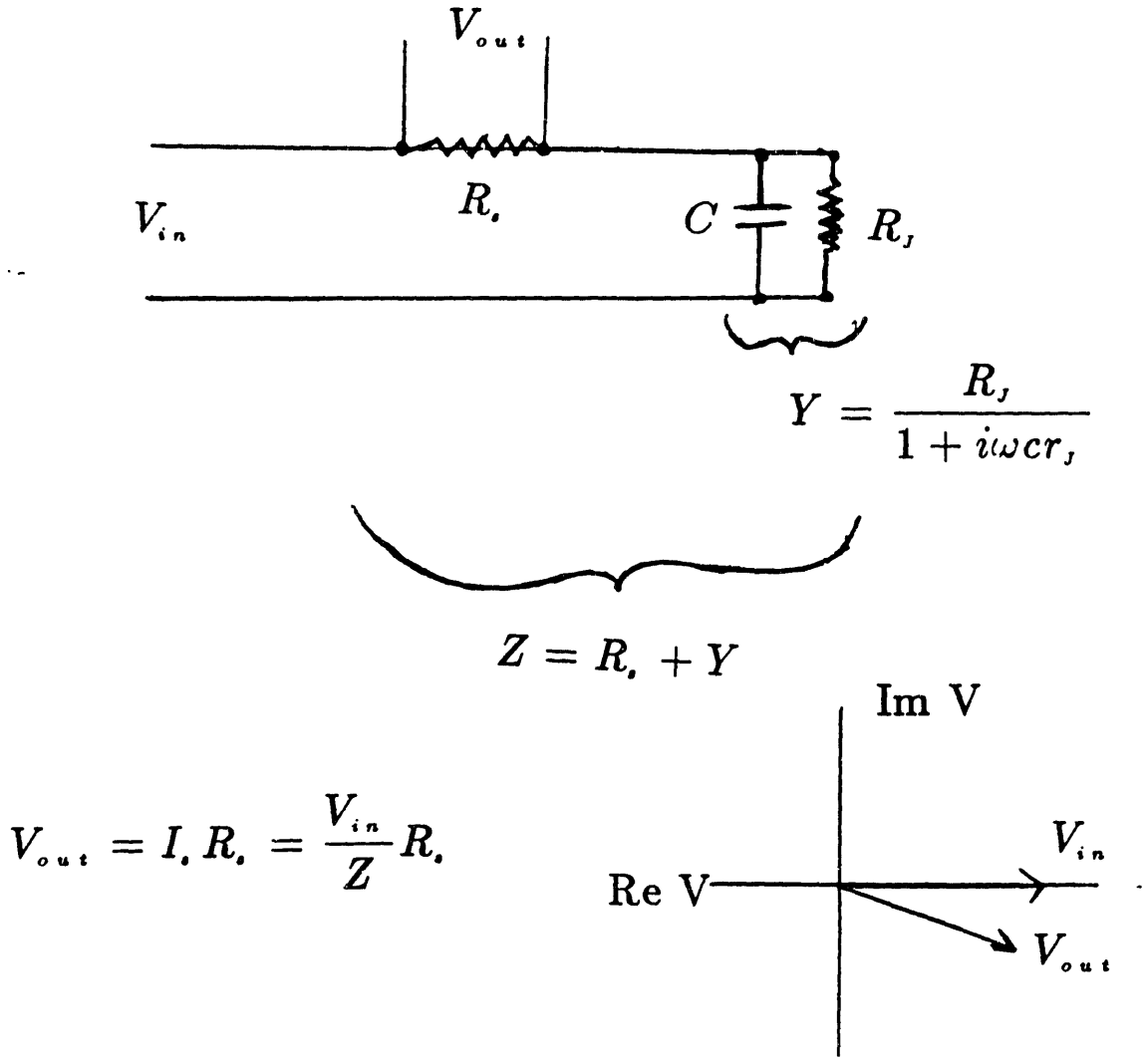

Fig. II.1.6 Equivalent circuit for measuring the tunneling conductance of a junction with capacitance C and resistance R_J. It is assumed that the capacitance and resistance of the leads are negligible.

II.2 Thin Film Preparation

—$A\ell$ Thin Films—

Thin $A\ell$ films have been produced by R. MacNabb at the Francis Bitter National Magnet Laboratory (FBNML) for a number of years for the use in experiments involving superconductivity, tunneling, fluctuations and localization. The substrates consist of a barium aluminum borosilicate glass produced under the name Corning 7059. The product literature says that this glass was developed particularly for thin film applications, and they quote a "typical surface smoothness" of less than $60\mathring{A}$. This literature also mentions that the glass is chemically inert due to the absence of alkali ions (such as those in soda-lime glass). The absence of high atomic number or magnetic species in the glass assures that the spin-orbit and exchange scattering rates of the electrons in the $A\ell$ film are not significantly changed by the contact of the film with the substrate. This is apparently not the case in Pb doped glass substrates (Lindelof and Wang, 1986).

The substrates are cleaned by vapor degreasing in isopropyl alcohol. Upon removal from the degreasing apparatus, the substrates are shaken to remove the remaining solvent rather than allowing it to evaporate. The evaporation process tends to concentrate the organic contaminants redepositing them as splotches on the substrate surface. The cleaned substrates are clamped onto a Cu sample holder which is placed in the evaporator with the samples approximately 10-20 inches away from the electron beam and thermal evaporation sources. An overnite pumpdown brings the system pressure to $\sim 10^{-7}$torr. Substrates and shadow masks are cooled to liquid nitrogen temperatures, and $A\ell$ is evaporated from a W filament. The film thickness is monitored with a quartz crystal oscillator calibrated by also measuring the thickness of a film with an optical interferometer technique. Meservey and Tedrow (1971) describe in situ measurements of the $A\ell$ film resistance as a function of thickness and find that the films become continuous at approximately $10-20\mathring{A}$. The final deposited thickness is usually $40\mathring{A}$. Before forming the tunnel barrier, the sample is heated with lamps located outside the evaporator. When the samples reach room temperature, oxygen is introduced into the system reaching a partial pressure of $\sim$ 70mtorr. A DC glow discharge is set up with a bias voltage of $\sim 1.8kV$. If the counter electrode was to be Fe, an oxidation time of approximately 40 seconds gave junction resistances of $\sim 1k\Omega$. For Ag or $A\ell$, less oxidation time was needed ($\sim$ 30 seconds) to obtain the same junction resistance. The resistivity of the $40\mathring{A}$ film after oxidation is of the order of $30\mu\Omega$. Electrical contact to the samples were made with evaporated Sn-Pb solder pads and # 44 gauge Cu magnet wire anchored with silver paint.

—V_3Ga Films—

Bulk V_3Ga is a superconductor with a transition temperature of 16.5K and is a member of a class of superconducting compounds (A15's) which have high critical temperatures, fields and currents. The A15 crystal structure is characterized by chains of atoms which are closely spaced. This apparently results in a peak in the density of states at the Fermi level which is partially responsible for the high T_c (Klein, Boyer, Papaconstantopoulos, and Mattheiss, 1978). A review of the A15 superconductors is given by Dew-Hughes (1975). The understanding of the electronic and phonon

structure and the relation to superconductivity is reviewed by Dew-Hughes (1979) and Vonsovsky, Izyumov, and Kurmaev (1982).

The A15's have a molecular formula A_3B, and the stability of this compound is controlled by the relative stability of the sigma phase A_5B_3, or A_3B_2. V_3Ga is unique in that it is stable on both the Ga rich and poor sides of the stoichiometric composition. The transition temperature is maximum at stoichiometry and the decrease in Tc in the off stoichiometric material has been associated (see discussion Bending, 1986) with the decrease in the density of states due to disorder(Tesdardi, 1978).

Hammond (1975) has developed a technique for making A15 films by electron beam codeposition of the A and B elements. V_3Ga films 200-500nm thick have been made at Stanford University using the techniques of Hammond (Bending, Beasley, and Tseui, 1984). The critical field of some of these films, doped with heavy elemental impurities, has been measured at the FBNML for the purpose of studying spin-orbit scattering from bulk distributed impurities (Tedrow, Tkaczyk, Meservey, Bending and Hammond, 1985).

Following these studies, thin films of V_3Ga down to 6nm thick have been fabricated at the FBNML with the intent of studying the effect of a surface layer on the spin-orbit scattering. The deposition geometry is shown in figure II.2.1. Single crystal sapphire substrates are vapor degreased and mounted to a Nb sample holder. The sample holder is threaded by a 0.025in W heater wire insulated with ceramic tubes. The use of stainless steel clamping screws restricts the substrate temperature to less than 700 degrees centigrade. Molybdenum screws allow applications involving substrate temperatures above 1000C. In order to prevent the screws from fusing to the Nb sample holder, the high temperature lubricant MoS_2 is used. The substrate temperature is measured with an alumel-chromel thermal couple and is recorded throughout the deposition. Substrate temperatures of $\sim$ 500C were found to be optimum for films 10nm thick.

The sample holder with three substrates is mounted $\sim$ 14in from the deposition sources. Deposition rates were monitored by separate crystals for the V and Ga sources. In fact, due to the frequent failure of the crystals covered with Ga, two crystal monitors were pointed at the Ga source. A shutter could be switched from one crystal to the other so that a fresh crystal would be available without venting the system to atmospheric pressure. The positioning of the substrates between the two e-gun sources (Temescal SFIH-270) containing V and Ga produces a phase spread. Comparison of the T_c of the three samples allows adjustment of the respective V and Ga deposition rates so as to maximize the Tc and thereby achieve stoichiometry of the V_3Ga compound. After mounting the substrate holder into the system, the bell jar was lowered and the system evacuated overnight. Usually the system was baked out for 3-5 hours. In the morning the charges were outgassed by depositing some material with the substrate shutter closed. The vanadium was found an effective getter of the residual gases; the pressure after the V deposition would be lower than before. This outgassing was followed by the cooling of the cryopaneling with liquid nitrogen. The base pressure before deposition was generally $\sim 4 \cdot 10^{-8}$ torr. Due to the large pumping speed of the two 6in vapor diffusion pumps, the pressure during the deposition only

rose to $8 \cdot 10^{-8} - 2 \cdot 10^{-7}$ torr. Cryopaneling prevents the system from warming during the deposition which would tend increase the pressure.

After depositing the V_3Ga film, the substrate heater is turned off. When the film has cooled below 200 C, a 20Å layer of Aℓ is deposited as an oxidation barrier. The samples are then cooled below 100C and are removed from the system. The resistive transitions for films from 6-100nm thick are shown in figure II.2.1. The T_c determined by the midpoint of the resistive transition decreases with a decrease in the film thickness (figure II.2.3). The proportionality to 1/d suggests that stress and possibly interdiffusion at the substrate/film interface is responsible for the decrease in transition temperature. The width of the transition is fairly constant until the film thickness is of the order of the coherence length $\xi \sim 30Å$. The temperature dependence of the resistivity is very much like that of the bulk material (Ramakrishnan, Nigam, and Chandra, 1986). Scatter plots of resistivity and residual resistivity ratios against T_c are shown in figures II.2.4,5 for 100Å V_3Ga films.

To form tunnel junctions on these films, the samples are mounted into the evaporation system used to form the thin Aℓ films. Another 20Å layer of Aℓ is deposited over the whole substrate at room temperature. This is exposed to an oxygen glow discharge for 1 minute. The edges of the V_3Ga film are covered with a thick insulating layer of SiO (600Å) which also serves to define the junction area ($\sim 3 \cdot 10^{-3} cm^2$). Finally, 600Å of Fe is deposited at room temperature as a counter electrode, and then the samples are stored in a rough vacuum until needed. The yield of low leakage junctions with a junction resistance below 100kΩ is low $\sim$ 1:50.

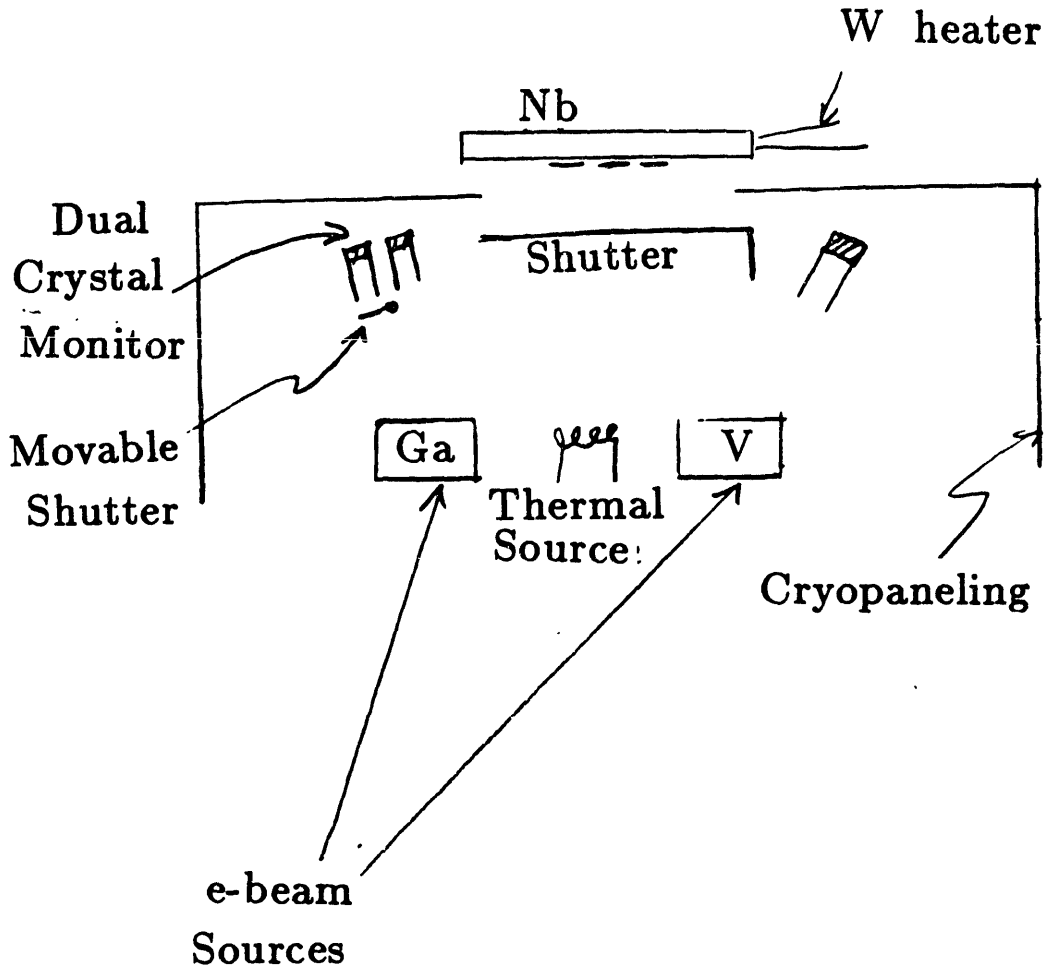

Fig. II.2.1 Schematic representation of the deposition configuration.

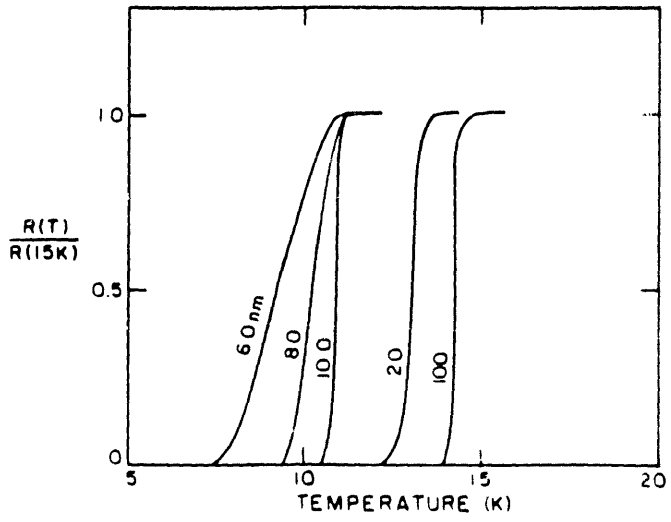

Fig. II.2.2 The resistive transition for films of V_3Ga of varying thicknesses.

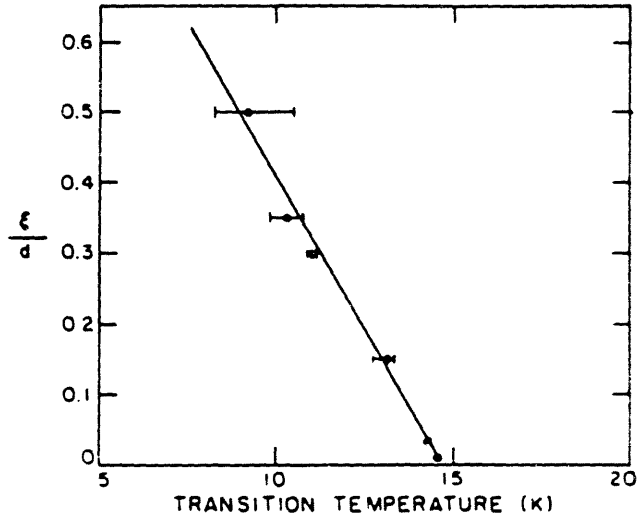

Fig. II.2.3 The midpoint and width of the resistive transition is shown as a function of the inverse thickness.

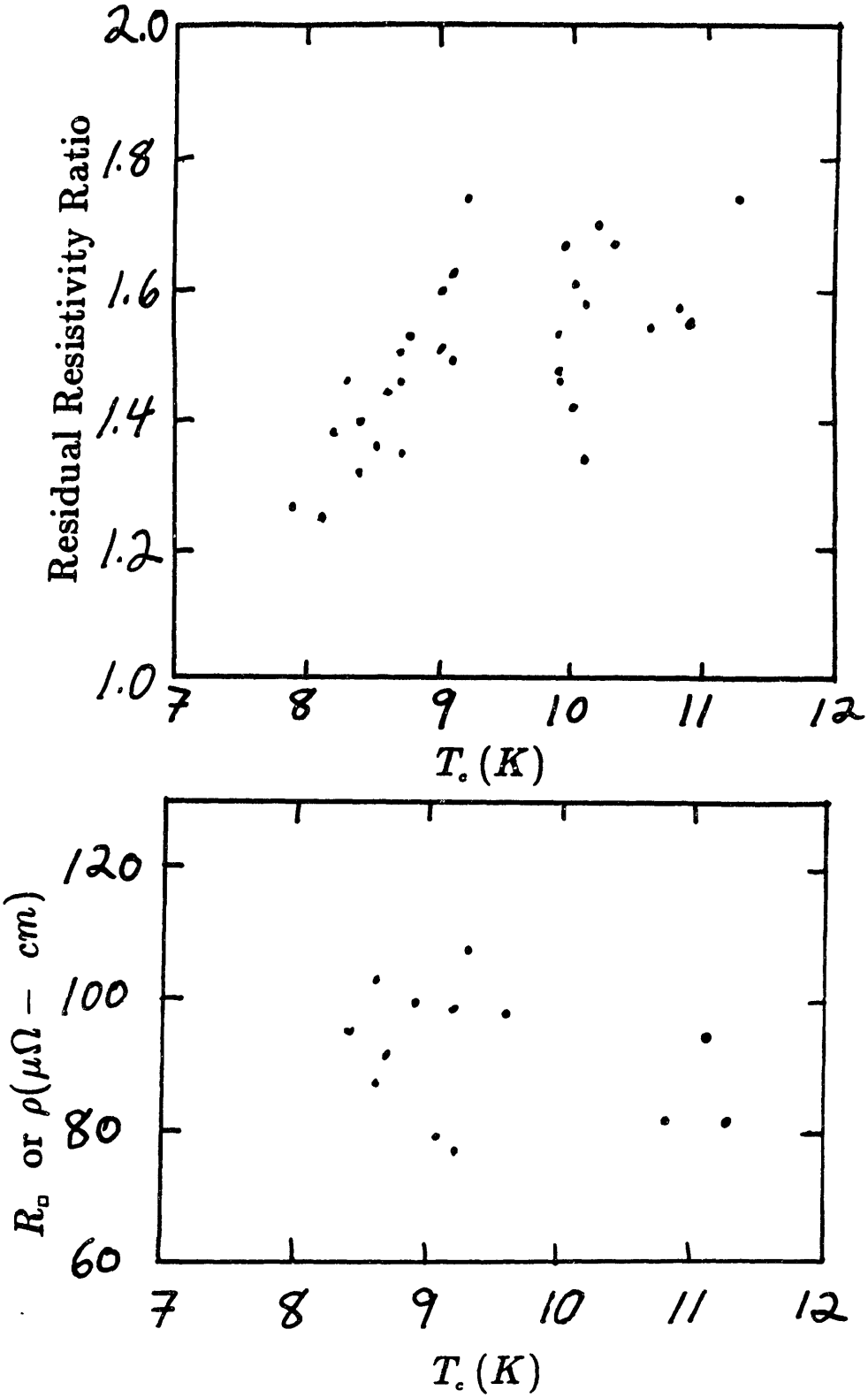

Fig. II.2.4,5 The residual resistivity ratio (R/R(T=15K)) and resistivity as a function of T_c for 100Å V_3Ga films.

Bibliography II

Bardeen, J., Phys. Rev. Lett. **6**, 57 (1961).

Bending, S.J., M.R. Beasley, and C.C. Tsuei, Phys. Rev. B **30**, 6342 (1984).

Bending, S.J., M.R. Beasley and E.L. Wolf, Phys. Rev. B **35**, 115 (1987).

Dew-Hughes, D., Cryogenics (Aug. 1975) p. 435.

Dew-Hughes, D., in *Treatise on Materials Science and Technology, Vol. 14, Metallurgy of Superconducting Materials*, edited by T. Luhman and D. Dew-Hughes, (Academic Press, Inc., London, 1979).

Fulde, P., Adv.Phys. **22**,667 (1973).

Giaever, I., Phys. Rev. Lett. **5**, 147 (1960).

Gibson, G., unpublished, Ph.D. thesis, M.I.T. (1988).

Harrison, W.A., Phys. Rev. **123**, 85 (1961).

Hammond, R.H., IEEE Trans. Mag. **MAG-11**, 201 (1975).

Klein, B.M., L.L. Boyer, D.A. Papaconstantopoulos, and L.F. Mattheiss, Phys. Rev. B **18**, 6411 (1978).

Kucera, J.T., unpublished, undergraduate thesis, M.I.T., (1983).

Lindelof, P.E., and S. Wang, Phys. Rev. B **33**, 1478 (1986).

Meservey, R., P.M. Tedrow, and P. Fulde, Phys. Rev. Lett. **25**, 1270 (1970).

Meservey, R., and P.M. Tedrow, J. Appl. Phys. **42**, 51 (1971).

Meservey, R., P.M. Tedrow and R.C. Bruno, Phys. Rev. **11**, 4224 (1975).

Ramakrishnan, S., A.K. Nigam, and G. Chandra, Phys. Rev. B **34**, 6166 (1986).

Solymar, L., *Superconductive Tunnelling and Applications*, (Wiley-Interscience, NY, 1972).

Tedrow, P.M., and R. Meservey, Phys. Rev. Lett. **26**, 192 (1971).

Tedrow, P.M., J.S. Moodera and R. Meservey, Solid State Commun. **44**, 587 (1982).

Tedrow, P.M., J.E. Tkaczyk, R. Meservey, S.J. Bending and R. Hammond, IEEE Trans. Mag. **MAG-21**, 1144 (1985).

Testardi, L.R., and L.F. Mattheiss, Phys. Rev. Lett. **41**, 1612 (1978).

Tinkham, M., *Introduction to Superconductivity*, R.E. Krieger Publishing, Huntington, NY, 1980).

Vonsovsky, S.V., Y.A. Izyumov, and E.Z. Kurmaev, *Superconductivity of Transition Metals* Trans. E.H. Brandt and A.P. Zavarnitsyn, (Springer-Verlag, NY, 1982).

Wolf, E.L., *Principles of Electron Tunneling Spectroscopy*, (Oxford University Press, NY, 1985).

Chapter III— Magnetic Proximity Layers

Superconductivity and magnetism in combination show a variety of effects which are interesting because they involve a competition between different broken symmetries. Magnetism tends to align electron spins in the same direction whereas superconductivity binds pairs of electrons in a singlet spin state. The practical aspect is that this competition yields detailed information about the electronic system which is not obtainable from normal-state measurements (Maple, 1976, 1984). For example, the sensitivity of superconductivity to exchange scattering allows the study of impurity magnetism in the extreme dilute limit. One can then follow this into a less dilute regime where correlations between spins become important. Also questions of moment formation and the detailed nature of the exchange interaction between itinerant electrons and local moments are probed by superconductivity. One can distinguish between the Kondo and non-Kondo regimes of the s-d exchange interaction and even distinguish these from cases where the familiar s-d interaction is not appropriate (e.g. valence fluctuations and resonant scattering). In fact, the variety of possible magnetic behavior and the role of impurity correlations challenges present theoretical efforts in the field of heavy fermion systems. Of course there is also the other side of the coin. The interaction between superconductivity and magnetism elucidates the nature of existing superconducting phenomena and may lead to entirely new types of superconductivity (see review by Maple, 1986). For example, the magnetic properties are among those unusual characteristics of high temperature (Shirane et al, 1987) and heavy fermion (Fulde and Keller, 1987; Lee et al, 1986) superconductors which suggest non-BCS pairing mechanisms and possible triplet pairing.

The traditional method of studying the combination of superconductivity and magnetism by measuring thermodynamic effects such as the critical field and specific heat has yielded significant results. However, such measurements are restricted to the superconducting/normal phase boundary. In this chapter, the technique of spin-polarized tunneling is introduced for the first time for the investigation of these phenomena. The entire superconducting region in the temperature verses field phase space is open to study. Furthermore, the tunneling conductance provides a measure of the excitation spectrum (i.e. density of states) which is more closely connected to the hamiltonian than are thermodynamic properties. Finally, tunneling is sensitive to properties within only a few atomic layers of the surface and is therefore, ideally suited to the study of surface magnetism questions (Feder, 1985) and to phenomena involving a localized response (e.g. the RKKY effect). Again, the other side of the coin is that proximity effect tunneling has been suggested by Meservey as a method of detecting non-conventional superconductivity (see discussion Ashaver, Kieselmann, and Rainer, 1986; Buchholtz and Zwicknagle, 1981). The initial published results have stimulated development of a model (Tokuyasu, Sauls and Rainer, 1988) based on some recently developed theoretical techniques which describe the effect of magnetically active surfaces in contact with superconductors (A. Millis, D. Rainer, and J.A. Sauls, 1986).

As this is the first use of this technique, the simplest possible magnetic systems are studied. Rare earth impurities at the surface and inside thin $A\ell$ films are found to be

well described by the s-d exchange hamiltonian. The usefulness of this technique lies in the fact that three different consequences of the exchange interaction are observed in the same system. Quantitative information is obtained, and in some cases the same information is obtained in more than one way so as to show the consistency of the results. In more complicated magnetic impurity systems, the abundance and redundancy of information may be necessary in order to distinguish between different models of impurity magnetism. One may anticipate the use of these techniques in the study of Ce compounds and heavy fermion materials for surface magnetism and moment formation questions.

III.1 Exchange Effects in Superconductors

This section begins with a discussion of the consequences of the s-d exchange hamiltonian and reviews the theoretical and experimental literature on the interaction between superconductivity and magnetism. After giving this perspective on the field, the relevant experimental results of the thesis research are then summarized so as to convey the significance of these results.

—Consequences of the Exchange Interaction—

The magnetic moment of impurities in s-p metals is generally associated with the unfilled core orbitals of the impurity. As discussed in A.4, residual interactions between the core and conduction states result in a fluctuation of the spin direction such that below some temperature $T_{f\ell}$ these fluctuations dominate the thermal fluctuations and the susceptibility saturates. For the rare-earths, the magnetic moment is due to the unfilled 4-f shell which is localized and only weakly coupled to the conduction electrons due to effective shielding. Thus the fluctuation temperature is small and the coupling is well described by the s-d exchange hamiltonian.

$$H_{ex} = -\int d\vec{r} J(\vec{r}) \vec{S} \cdot \vec{s} \qquad III.1.1$$

This defines the exchange constant J where $\vec{S}$ is the impurity spin and $\vec{s}$ is the electron spin with magnitude 1/2. Note that in the literature this expression can be found with factors of 2 and 1/2 which must be taken into account when comparing the results presented here with those found elsewhere. Generally(Davidov et al, 1973), it is assumed that the form factor (see A.1) can be taken as a constant on the Fermi surface (i.e. $J(\vec{q}) = J(\vec{q} = 0)$). This corresponds to a spatial dependence given by a delta function or is equivalent to including only S-wave scattering. For most of the rare-earths, the coupling is weak and positive $J(0) \sim 10 - 100meV$, arising from the direct exchange term (Maple, 1970; Sugawara and Eguchi, 1967) and depending on the host.

Tunneling is used here for the first time to probe three consequences of the s-d exchange interaction on the conduction electrons in the same system. These are conveniently described by how they enter into perturbation theory and are discussed in section A.4. The results which are used extensively in the data analysis are summarized here for convenience. If the impurity moments are aligned, there is a forward scattering contribution $\langle k\sigma|H_{ex}|k\sigma\rangle$ which can be included in the unperturbed hamiltonian and

which splits the energy of the spin-up and spin-down electrons. This is equivalent to a Zeeman splitting from an effective magnetic field

$$B_{ex}(q=0) = cJ(0)SB_S(\eta)/g\mu \qquad III.1.2$$

where $B_S(\eta)$ is the Brillouin function, and $\eta = \mu B/k_B T$. The Pauli paramagnetic response to such a field would be a uniform magnetization of the conduction electron system such as considered by Zener(1951). However, there are (non-spin-flip) first order contributions between different momentum states $\langle k'\sigma|H_{ex}|k\sigma\rangle$ which along with the forward scattering contribution localizes the response (Ruderman-Kittel-Kasuya-Yosida, 1954-1957) (RKKY). The linear response is given in terms of the spin-susceptibility χ of the electron system and the effective exchange field $B_{ex}(q)$.

$$M(r) = \int d\vec{r'}\chi(\vec{r}-\vec{r'})B_{ex}(\vec{r'}) = \sum_q \chi(\vec{q})B_{ex}(\vec{q}). \qquad III.1.3$$

For the free electron gas $\chi(\vec{q})$ is about constant out to $2k_F$ where it goes to zero; thus the response is localized to within a distance $\sim 1/k_F$ from the impurity.

To second order in J, one considers both spin-flip and non-spin-flip parts of equation III.1.1. In a magnetic field the spin-flip part is inelastic, and from A.4.2 and A.4.3 one obtains the following scattering rate for the s-d model hamiltonian.

$$\hbar/\tau_{ex} = \frac{\pi}{2}(\Omega N_o)cJ^2(0)S\{S + (1 - B_S(\eta)tanh(\eta/2))\} \qquad III.1.4$$

This neglects correlations among different impurity sites but includes time correlations induced by the magnetic field. The zero field limit gives the expression obtained from the Fermi golden rule $\hbar/\tau_{ex} = 2\pi(\Omega N_o)cJ^2(0)|\langle\vec{S}\cdot\vec{s}\rangle|^2$ by replacing the matrix element with $(1/3)S(S+1)s(s+1) = (1/4)S(S+1)$. In the high field limit the factor $S(S+1)$ is replaced by the S^2. For example consider Gd, $S = 7/2$. The field has a relatively small effect on the scattering rate since $S(S+1) = 15.75$ and $S^2 = 12.25$. However, for Ce, $S = 1/2$, and the field reduces the scattering rate by a factor of 3. In either case the *spin-flip* part of the exchange scattering rate goes to zero in a large magnetic field; that is, the spin-relaxation rate goes to zero. Again, from equation A.4.2 and A.4.3 an expression for the spin-flip scattering rate is found by including only those terms arising from $S^{\pm}S^{\mp}[2/(1+e^{\mp})]$. The upper and lower signs give the same scattering rate.

$$\hbar/\tau_{sf} = c\pi(N_o\Omega)J^2(0)SB_S(\eta)/sinh(\eta) \qquad III.1.5$$

Having introduced the results III.1.2-III.1.5 which will be used in the data analysis, it is appropriate to next present a brief survey of the phenomena involving the interplay of superconductivity and magnetism. This puts the spin-polarized tunneling measurements presented in this chapter into perspective with the work of other researchers.

—Superconductivity and Magnetism—

The first experiments involving superconductivity and magnetic impurities were done by Matthias, Suhl, and Corenzwit (1958) who showed that the decrease in T_c

of La for different rare earth impurities correlated with the magnitude of the spin of the impurity rather than with the magnetic moment. This indicated the relevance of the exchange interaction to Herring (1958) and Suhl and Matthias (1959). Anderson (1959) made the more general connection between the decrease in T_c and the violation of time reversal invariance. Abrikosov and Gor'kov (1961) presented a powerful Green's function calculation treating exchange scattering in the Born approximation and made the significant prediction that near a second order transition to the normal state, the excitation spectrum had no gap. Woolf and Reif (1962, 1965) measured the tunneling conductance of lead films with $\sim$ 1% Gd impurities and confirmed the presence of this gapless state. Subsequently there has been a large volume of theoretical and experimental work exploring the great variety of phenomena associated with the interaction of superconductivity and magnetism.

For the moment consider only uncorrelated moments which represents the situation in the extreme dilute impurity limit. It is the sensitivity of superconductivity to the exchange interaction which makes this limit a region accessible to experiment. A treatment of scattering beyond the Born approximation leads to "bound states" lying below the energy gap (Rusinov, 1969). These are observed in some impurity systems (e.g. Mn in Pb) through tunneling measurements of the density of states(Bauriedl, Ziemann, and Buckel, 1981; Tsang and Ginsberg, 1980). Rusinov's calculations ignore the non-commutivity of the spin operators which is associated with the Kondo effect (an assumption which is justified in systems where the Kondo temperature is much lower than the superconducting transition temperature). Kondo effects from single impurities are treated by the theory of Müller-Hartmann and Zittartz (1971). Work continues up to the present, for example, to deal with valence fluctuating impurities in superconductors(Li, Gong, and Holz, 1987; Schlottmann, 1982), strong-coupling effects (Schachinger, Daams, and Carbotte, 1980) and scattering from magnetically active surfaces(Tokuyasu, Sauls, and Rainer, 1988; Millis, Rainer, and Sauls, 1986).

Maple (1976, 1984) has introduced a categorization of the possible situations which is useful, but represents an oversimplification for some systems. He suggests that there are three possibilities. The simplest case corresponds to a well defined moment with a positive exchange constant (i.e. the impurity and itinerant spins tend to align). The intrinsic spin fluctuation temperature $T_{f\ell}$ is much smaller than the superconducting transition temperature $T_{f\ell} \ll T_{co}$. The effect of magnetic impurities in this limit is that discussed in section I.2 with a pairbreaking rate $\hbar/\tau_{PB}$ which is temperature independent. In particular the density of states and reduction of T_c (eq. I.2.4) are described by the Abrikosov-Gor'kov theory which treats the scattering in the Born approximation. It will be shown that this is the situation which describes the heavy rare earths at the surface of an $A\ell$ film. The second possibility is where the moment is still well defined $T_{f\ell} \ll T_{co}$, but where the exchange constant is negative and Kondo effects are important $T_K \sim T_{co}$. Here the Abrikosov-Gor'kov theory still applies but with a temperature-dependent pairbreaking parameter. Finally, when the transition temperature is of the order of the fluctuation temperature, the effect of the impurity is not described by pairbreaking but by what has been called pair weakening. Maple gives examples of systems which typify these categories and reviews the use of

T_c and specific heat measurements as a function of impurity concentration as a way to distinguish among them. He makes the point that superconductivity is a superb probe of local moment formation due to its sensitivity to interactions which affect the correlations between time reversed states.

In addition to these results associated with uncorrelated impurities, a large literature has developed investigating the question of magnetic ordering in superconductors. The first work was done by Gor'kov and Rusinov (1964). One can divide this topic into the consideration of temporal and spatial correlations. Temporal correlations may be induced, for example, by an applied magnetic field which aligns the impurity spins. As described by equation III.1.2, the forward scattering from aligned spins acts like an effective magnetic field acting on the conduction electron spins. The most startling consequence is that predicted by Jaccarino and Peter(1962) and observed in $Eu_xSn_{1-x}Mo_6S_8$ (Meul et al, 1984; Fischer el al, 1985). In this system, the sign of J is such that the exchange field is opposite the applied field; there is mutual cancellation, and this results in the phenomenon of magnetic field-induced superconductivity. A second effect of temporal correlations is that, as noted in equation III.1.5, the spin-flip part of the exchange scattering rate can be "frozen out" by a magnetic field. The significance of this is that the spin relaxation rate is reduced, thereby allowing the resolution of the Zeeman splitting $2\mu B$ in spin-polarized tunneling which would otherwise be smeared due to spin-mixing. Keller and Brenda (1970) calculated the effect of temporal correlations on the pairbreaking rate and found equation III.1.4 to be appropriate in the strong correlation limit. The density of states has been calculated by Bruno and Schwartz (1973) and a general list of references can be found in the review by Fulde and Keller (1982).

Spatial correlations between spins are expected in impurity systems at higher doping levels. These correlations may be due to an applied magnetic field or to inter-impurity spin interactions. Long-range correlations have the greatest effect on superconductivity since the free energy $-(1/2)\chi(q)B_{ex}^2(q)$ of the superconducting state is raised relative to that of the normal state. This fact can be seen from figure I.2.3 which shows that the susceptibility of the superconductor is less than that of the normal state for $q < Q_o \sim (\xi k_F^2)^{1/3}$. Correlations on a spatial scale longer that $1/Q_o$ tend to reduce the transition temperature (Anderson and Suhl, 1959). In particular, ferromagnetic correlations reduce T_c more than antiferromagnetic correlations.

A separate but related question is whether correlations can be mediated by the polarization of the conduction electron system. Again figure I.2.3 shows that the polarization of the conduction electrons $M(q) = \chi(q)B_{ex}(q)$ is reduced in the superconducting state relative to that in the normal state for spatial variations greater than $1/Q_o$. Thus inter-impurity spin interactions are reduced. A two volume review provides additional details and references on magnetically ordered superconductors (Maple and Fischer, 1982). There are a number of compounds with a sublattice of rare earth elements weakly coupled to the conduction electron system which show antiferromagnetic ordering. The most recent system of this type is the family of high T_c superconductors (Lee et al, 1988). Coexistent ferromagnetism and superconductivity is rare but exists in $HoMo_6Se_8$ (Lynn, et al, 1984) and $ErRh_4B_4$ (Moncton et al,

1980; Sinha et al, 1982). A theory (Bulaevskii et al, 1983; Fulde and Keller, 1982) of this latter phenomenon involves the modification of the indirect RKKY coupling between local moments in a superconductor. Other unusual effects are found in $CePb_3$ (Lin, et al, 1985) and the heavy fermion superconductors(Brandt and Moshchalkov, 1985; Stewart, 1984) and it appears that a full understanding of exchange effects from a lattice of local moments has yet to be formulated (Lee, et al, 1986; Fulde, Keller and Zwicknagl, 1987).

Tunneling provides detailed information giving the excitation spectrum of the system directly with good energy resolution. Measurements are not restricted to the superconducting/normal phase boundary as in the case of critical field and T_c studies. Furthermore, spin polarized tunneling provides spin-resolution which lends itself to a quantitative analysis of exchange and spin-orbit effects. Whereas bulk polycrystaline materials have traditionally been used to study the interaction of superconductivity and magnetism, the use of thin films provides a level of control not otherwise possible. Spin-dependent perturbations of the electron states can be introduced by the deposition of the appropriate surface layer. For example (Tedrow and Meservey, 1979), the deposition of one-half monolayer of platinum onto a thin film of Al increases its spin-orbit scattering rate by a factor of 30. A similar approach using magnetic surface layers to introduce exchange scattering is presented below.

—Summary of Experimental Results—

In this chapter experiments on two types of systems involving superconductivity and magnetism are described. The first, in section III.1, consists of thin $A\ell$ films in contact with rare-earth oxides(REO). The study of this system was initiated in order to verify the observation of a "bound state" associated with the interface between a superconductor and a ferromagnetic insulator (DeWeert and Arnold, 1985; Stageberg, Cantor, Goldman, Arnold, 1985). The bound state was not observed; however, this investigation lead to significant results (Tedrow, Tkaczyk, and Kumar, 1986), but at the same time there were aspects which were not understood. A large Zeeman splitting equivalent to that produced by a magnetic field of $B^* \sim 1-3$ tesla was observed for conduction electrons of an REO/$A\ell$ bilayer. The otherwise obvious role of the exchange interaction was not clear because no significant decrease in the superconducting gap was observed. One would expect such a decrease due to ergodic pairbreaking. An alternate explanation is that the Zeeman interaction arises due to a coupling of the electrons of the $A\ell$ film to the magnetization of the REO.

In order to decide which of these two mechanisms, exchange or magnetization, was responsible for the enhancement of the Zeeman splitting $2\mu B^*$, an experimental program was initiated to study $A\ell$ films deliberately depaired by the deposition of a submonolayer of (unoxidized) rare-earth elements onto the $A\ell$ film surface. In section III.3, the study of this RE/$A\ell$ bilayer system is described. The quantitative results obtained lead to the conclusion that the field B^*observed in the REO/$A\ell$ system arises from the exchange interaction. In addition, a number of other consequences of the exchange interaction are observed and studied quantitatively. The exchange constant J is obtained in two ways. First the depaired conductance in zero field is fit by the Abrikosov-Gor'kov theory to obtain the exchange scattering rate from which J

is extracted. Second, the rare earth moments are aligned at low temperature in a small magnetic field. Scattering from aligned spins results in an effective Zeeman splitting of the conduction electron energy. This is measured, and a second determination of J is made in a way which does not involve the AG theory. The two values are found to agree within a factor of 2. Comparison is made to results reported in the literature on $REAl_n$ laves compounds and to rare earth impurities in other hosts.

In section III.4, additional results from the RE/Al system are presented. For the experiments described above, the tunneling was directed into the side of the Al film opposite the side covered with the rare earth submonolayer (i.e. RE/Al $\longleftarrow$). If instead one probes the conduction states at the surface with the rare earth (i.e. $\longrightarrow$ RE/Al), then one observes an asymmetry in the conductance associated with the RKKY spin polarization of the conduction electrons. However, the asymmetry was observed only in the case where the RE/Al electrode was in the normal state, demonstrating the modification of the RKKY result in superconductors. In addition, about 2 monolayers were added to form an RE/Al /Pt electrode; the Pt layer supplies sufficient spin-orbit scattering so as to return the spin-susceptibility of the superconductor to the normal-state value. The RKKY spin-polarization is then observed in both the superconducting and normal states in this electrode.

III.2—Rare Earth Oxide Proximity Effect

The samples were made by vacuum evaporation onto liquid-nitrogen-cooled glass substrates(Corning 7059). First, 1-5 nm of the rare earth (RE) metal was evaporated. The substrate was warmed to room temperature and the RE was exposed for 1 minute to an oxygen glow discharge in an oxygen pressure of $\sim$ 70millitorr and a voltage bias of 1.8 kV. After the substrate was cooled again, an Al film 4-10 nm thick was evaporated. Oxidation of this film provided the tunnel barrier. A counter electrode of either Al or Fe was then added. Identical control junctions without the REO were made at the-same time on the same substrate. The junctions were cooled to 0.4K with an immersion ^{3}He cryostat. The magnetic field was supplied by either a superconducting solenoid or a water-cooled Bitter magnet and was applied parallel to the plane of the films.

—Observation of an enhanced splitting—

The first measurements were made on junctions where the rare earth was Eu. Both the divalent and trivalent oxides (i.e. EuO and Eu_2O_3) are relatively stable and are expected to be present in the glow discharged Eu film (Massenet, Capiomont, and Van Dang, 1974). For convenience, such films will be labeled EuO. These films were found to be transparent and insulating at room temperature. In figure III.2.1, the conductance of an EuO/Aℓ-Aℓ_2O$_3$-Aℓ junction in zero field and 0.43K is shown. Both electrodes are superconducting and the conductance of the junction shows features associated with superconductor-insulator-superconductor (S-I-S) tunneling. There is a peak at the sum of the energy gaps $\Delta_B + \Delta_T$ where Δ_B is the gap of the bottom electrode (i.e. EuO/$A\ell$) and Δ_T is the gap of the top electrode. The conductance is close to ideal in that the zero bias conductance is negligible on the scale of the normal state (i.e. high bias voltage) conductance. This indicates the absence of conductance paths through the junction barrier which do not involve tunneling. For example, an ohmic short would contribute conductance at zero bias.

This same junction at higher temperature but still in zero field shows a difference peak at the voltage $|\Delta_T - \Delta_B|/e \sim 0$ indicating that the gap of the bottom electrode is not significantly depressed by the contact with the REO. There is apparently no ergodic pairbreaking. This may have been expected since in the REO's the 6s and 5d electrons of the RE bind with the oxygen 2p states forming an insulating gap in the band structure and leaving only localized 4f states at the Fermi level. The band gap of EuO is $\sim$ 1.1 eV. Therefore, the conduction states of the $A\ell$ cannot propagate into the oxide and the interaction with the RE moments is restricted to surface scattering effects. One may have thought effects associated with this surface scattering to be small, but this turns out not to be the case.

A small magnetic field is applied in the plane of the junction with the result shown in figure III.2.2. The peak at the sum of the gaps splits into two peaks. In S-I-S tunneling the splitting of the peak at the sum of the gaps is given by the difference in the effective Zeeman splitting in the two electrodes. The data suggest that the bottom electrode is Zeeman split by an effective field $2\mu(B + B^*)$ whereas the top electrode is split by only the applied field $2\mu B$. The enhancement B^* is presumably due to the contact of the bottom $A\ell$ film with the REO. Whereas S-I-S tunneling

shows the difference in the Zeeman splitting in the two electrodes, the total Zeeman splitting $2\mu(B + B^*)$ in the bottom electrode (i.e. superconducting) is observed in superconductor-insulator-normal (S-I-N) junctions. In figure III.2.3, the conductance of a EuO/$A\ell$ - $A\ell_2O_3$- Fe junction is shown in an applied field of $B = 3.10$ tesla along with the conductance of the control junction in a higher magnetic field $B = 3.94$ tesla. The curves are nearly identical indicating that the internal fields acting on the conduction electrons of the $A\ell$ film are equal. One concludes that the field enhancement of the bottom electrode is $B^* = 0.84$ tesla.

The broadening of the conductance peaks in a magnetic field is due to ergodic pairbreaking. There are (orbital + magnetic field), (spin-orbit + magnetic field), and exchange scattering contributions to the total pairbreaking rate. These contributions are called "pairbreakers" and broadening of the conductance is called "depairing". In figure III.2.3, the conductance peaks are equally well resolved in the two cases indicating that the contact with the rare earth does not introduce any more or less depairing than that due to a magnetic field of magnitude $B + B^*$. This result is borne out by the fact that the critical field of the $EuO/\ A\ell$ film is reduced by B^* (fig. III.2.4).

The magnitude of B^* compares with the internal magnetization of bulk EuO (fig. III.2.5); however, the field dependence is more closely related to that of a Brillouin function. The conductance of a Gd_2O_3 /$A\ell$ - $A\ell_2O_3$- Fe junction has been measured as a function of the applied field and the saturation value of B^* can be 2-3 tesla(figure III.2.5). These curves have been separated by the procedure described by Tedrow, Moodera and Meservey, (1982) in order to obtain the Zeeman splitting. The field dependence of B^* is shown in figure III.2.6 for two values of the temperature and the saturation curve approximately follows a $S = 7/2$ Brillouin function. The field dependence of B^* is shown in figure III.2.8 for three samples differing in the $A\ell$ film thicknesses $d_{A\ell}$. The saturation value of B^* follows approximately an inverse relationship to the aluminum film thickness. This implies that there is a constant interaction H' between the conduction electrons of the $A\ell$ film and the surface of the rare earth oxide. Since the bulk spin mean free path is much larger than the film thickness, the effective energy splitting of the conduction states goes as the interaction times the area divided by the "normalization" volume; thus, $\Delta E \propto 1/d_{A\ell}$. This behavior is characteristic of what may be called a proximity effect. This terminology makes an analogy with the "Cooper limit" for the proximity effect between a normal metal and a superconductor. Cooper (1961) states, "The essential observation made here is that this average will be decreased if the electron normalization volume is increased while the ...interaction acts over only a part of the volume".

—Two possible mechanisms—

Two possible interactions H' which will be considered are the exchange interaction and the magnetization. As discussed in sections I.2 and A.4, the forward scattering part of the exchange interaction acts like an effective uniform field. The first possible explanation then involves the overlap of conduction electrons with 4-f orbitals present at the surface of the REO. Alternatively, the magnetization of the REO, which originates from the magnetic moment of the unfilled 4-f shells in the REO, acts on electrons which penetrate some distance beyond the REO-$A\ell$ interface. This penetration is nec-

essary due to the fact that the demagnetization factor of a thin film is zero; that is the magnetization exists only inside the REO and there is a negligible fringing field. This penetration could be either due to tunneling into the oxide or a consequence of surface roughness. However, the surface roughness can't be too large due to the extreme sensitivity of $A\ell$ to perpendicular magnetic fields (fig. III.2.9). A perpendicular component of a few hundred gauss would produce a pairbreaking rate which is easily detectable.

Three subtle observations suggest that the coupling is to the magnetization μM of the REO. Several measurements of different EuO/$A\ell$ bilayers show a sample dependent variation in the value of B^*, but generally B^* is of the order of μM. Second, the absence of any significant effects at zero field is easier to understand by assuming that the coupling is not of the exchange type. It one assumes that the local rare-earth moments are randomly oriented at zero field, there would be no average magnetization to which to couple. However, the presence of exchange scattering between the $A\ell$ quasiparticles and rare-earth spins would still cause depairing. Finally, the tunneling curves in an applied field B shows depairing (i.e. broadening) identical to that seen in the control junction in an applied field $B + B^*$. The depairing caused by an magnetic field on an $A\ell$ film is due partially to the perturbative effect on the orbits of the quasiparticles, but the exchange field acts only on the spins of the quasiparticles.

The possibility of an exchange coupling provides a somewhat less direct explanation for these observations. The value of the Zeeman splitting $2\mu B^*$ is generally of the order 0.1-0.3 meV which corresponds to a field of $B^* \sim 1-3$ tesla. The exchange coupling between conduction electrons and rare-earth ions has been estimated to be about 100meV, 10^3 times our observed splitting(Penney, Shafer, Torrance, 1972; Maple, 1970; Taylor and Darbey, 1972). A proximity model described by DeGennes(1966) in which the coupling is to the exchange field can account qualitatively for the results. In this model the coupling would be reduced by the ratio of the lattice spacing in the REO to the thickness of the $A\ell$ film and by interface degradation (such as $A\ell$ oxide between the $A\ell$ and REO). The lattice spacing enters since it is approximately the tunneling distance into the oxide $\sim k_F^{-1}(2E_F/E_g)^{1/2} = 2.7\mathring{A}$ where $E_g \sim 1eV$ is the band gap of the REO, $E_F \sim 10eV$ is the Fermi energy of $A\ell$, and $k_F^{-1} \sim 0.6\mathring{A}$. The observation that B^* is inversely proportional to the $A\ell$ thickness supports such a proximity effect model.

The most convincing support for the relevance of the exchange mechanism is that the maximum value of B^* is obtained for Gd_2O_3. The saturation values of B^* for all the REO/$A\ell$ bilayers studied are given in table III.1 and plotted against atomic number in figure III.2.10. The scatter in the value of B^* from one sample to the next for the same REO can be associated with the sensitivity of surface scattering to the details of the REO/Aℓ interface. For example, when the Gd_2O_3 film was formed by evaporating Gd_2O_3 powder from a W boat, the value of B^* was significantly reduced (sample 6131). However, different samples from the same deposition have B^* with the same value within 10% (samples 5891, 6079). This suggests that identification and monitoring of the appropriate deposition and oxidation conditions would account for the scatter in detail.

The most difficult thing to explain about the proposed exchange mechanism is why there is no significant pairbreaking in zero field. One explanation assumes that the REO films are composed of magnetically ordered domains. The size of the domains would be of the order of the film thickness. For example, the divalent europium oxide EuO is a well studied ferromagnet (Mauger and Godart, 1986) with a curie temperature of $T_c \sim$ 70K and most of the trivalent rare earth oxides RE_2O_3 are antiferromagnets with Neel temperatures of the order T_N ~1-4 K(Taylor and Darby, 1972). The following explanation based on magnetically ordered domains will later be rejected in favor of a much simpler one; however, it played an important role in the initial thinking about the REO/Al proximity effect (Tkaczyk and Tedrow, 1987) and appears to be relevant in a recently studied system (Moodera et al, 1988). Therefore, the implications of having magnetically ordered domains are briefly considered.

The domains must remain with their moments in the plane of the film since any moment perpendicular to the Al film would cause easily detectable depairing of the tunneling conductance. The exchange interaction from a *lattice* of spins oriented in the same direction will cause an effective field according to equation III.1.2. However, no scattering is induced by a well ordered lattice of aligned spins. The absence of ergodic pairbreaking is explained by the fact that a *uniform* exchange field induces only the non-ergodic effect. The observation that B^* goes to zero as the applied field is reduced is then the result of randomization of the magnetically ordered domains and the fact that the quasiparticles are expected to average the exchange field over the spin-mean-free-path. In samples where the EuO was formed on top of a Al film rather than on the glass substrate, splitting in zero field was sometimes observed. This has also been observed by Moodera et al in the case where EuS was used as a tunnel barrier. This phenomenon would correspond to domains retaining alignment in zero field.

As shown in figure III.2.3, the depairing due to the applied field B_1 plus the enhancement B^* is equivalent to that due to an equivalent magnetic field $B_2 = (B_1 + B^*)$. A magnetic field induces orbital depairing but the exchange field acts only on the electron spin. Therefore, in order to expound that the exchange interaction is the cause of B^*, one must explain the magnitude of the depairing. Since an Al film in an increasing magnetic field at 0.4K undergoes a first order transition, the perturbative effect on the spins in more important than on the orbits. In this respect the pairbreaking due to the coupling to the exchange field or to a magnetic field would be identical. Thus the universality of pairbreaking near the phase boundary may admit an exchange coupling scheme.

These results were published in three papers (Tedrow, Tkaczyk, and Kumar, 1986; Tkaczyk and Tedrow, 1987a,b) which presented the discussion above but failed to resolve which mechanism, exchange or magnetization, is the cause of the field B^*. The most important objection to the possibility that the exchange interaction is the correct mechanism is the apparent absence of ergodic pairbreaking. Samples with unoxidized rare earth submonolayers were fabricated in an attempt to obtain additional data concerning the quantitative aspects of exchange scattering. After presenting these results on RE/Al bilayers, the exchange interaction will be identified as the

cause of B^*, and the role of ergodic pairbreaking is elucidated. Tokuyasu, Sauls and Rainer(1988) have developed a theoretical proximity effect model describing these results. They find that the coupling to the magnetization is weak and can not account for B^*. They also conclude that the exchange interaction is responsible for B^*.

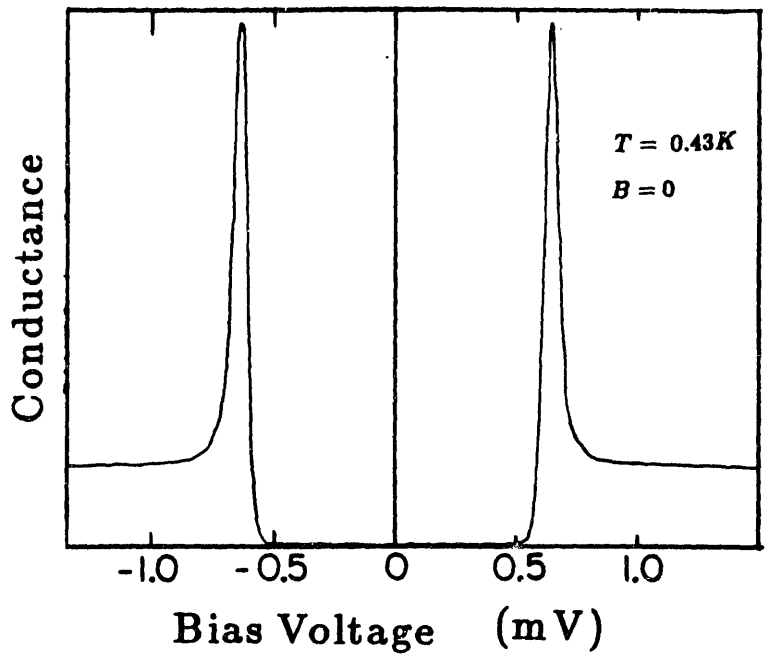

Fig. III.2.1 The measured tunnel conductance of a $EuO/Al-Al_2O_3-Al$ junction in zero field (sample 5833).

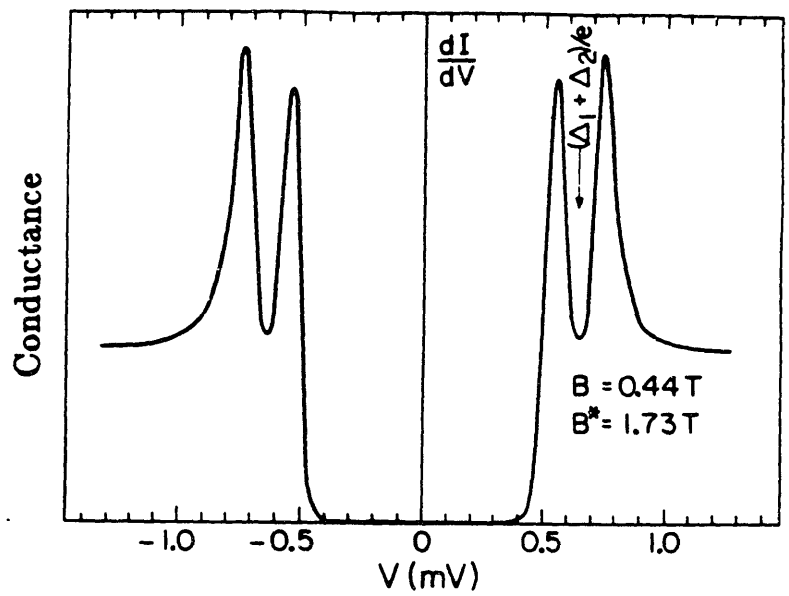

Fig. III.2.2 The measured tunneling conductance for a $EuO/Al-Al_2O_3-Al$ junction in an applied field of B=0.44T and showing a voltage splitting equivalent to 1.73T (sample 5833).

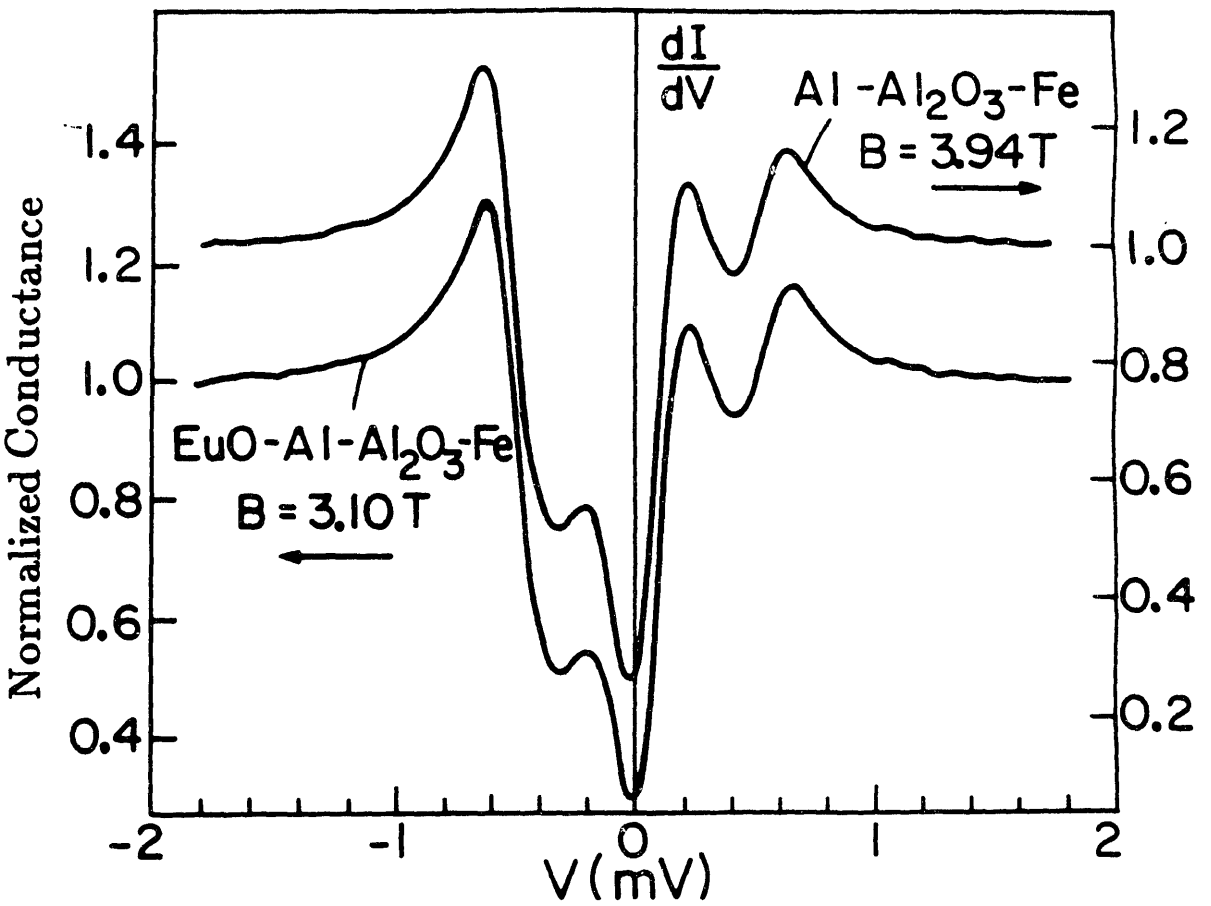

Fig. III.2.3 The normalized conductances of a $EuO/Al-Al_2O_3-Fe$ junction in an applied field of 3.1T and an $Al-Al_2O_3-Fe$ junction in an applied field of 3.94T (sample 5854).

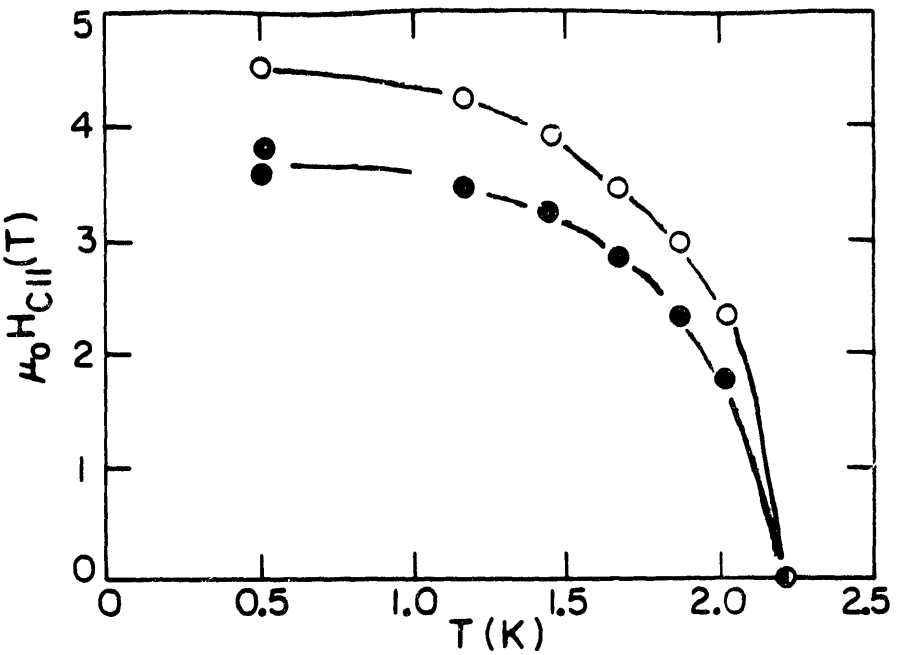

Fig. III.2.4 The critical magnetic field verses temperature for two similar Aℓ films, one of which (solid circles) was in contact with EuO (sample 5833).

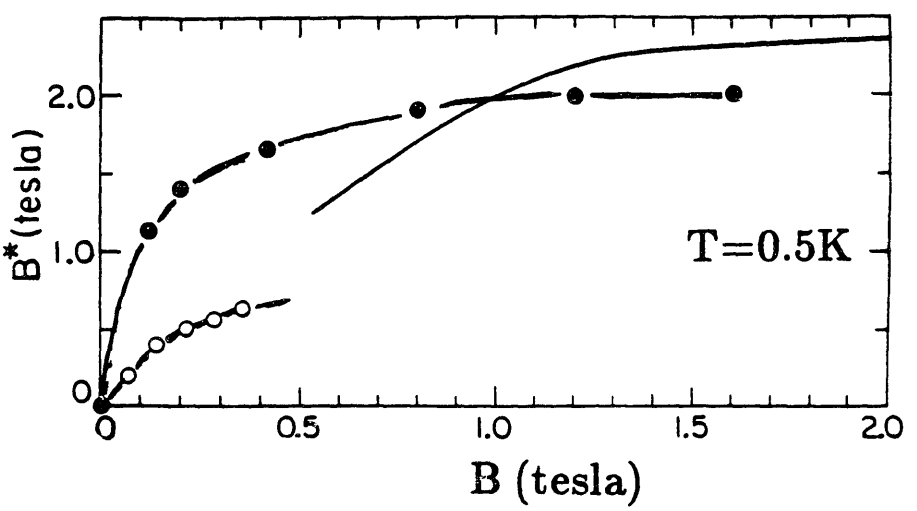

Fig. III.2.5 Observed values of B* verses applied field B for two EuO/Aℓ films. The magnetization for EuO (Shapira et al, 1973) is shown by the solid line (samples 5854, 5883).

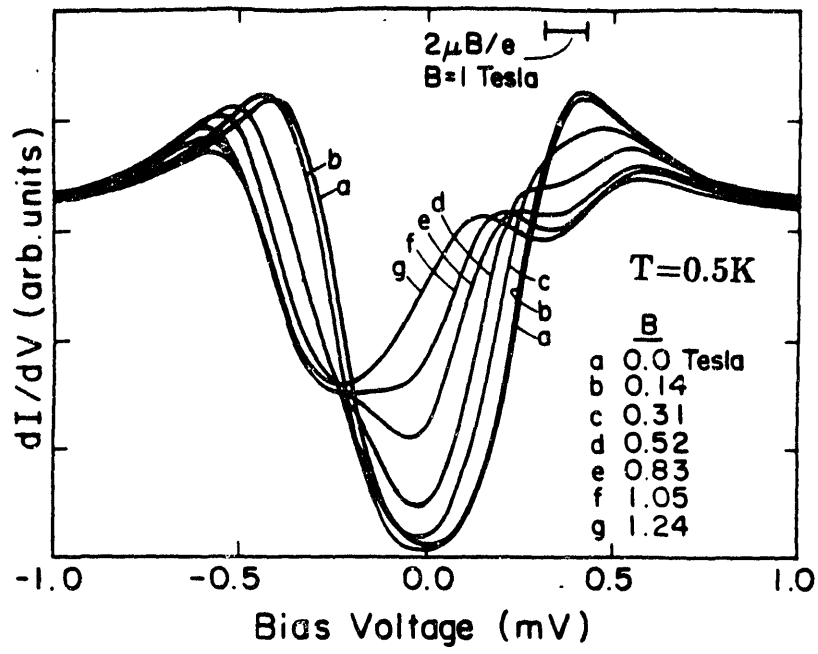

Fig. III.2.6 Measured conductance of a $Gd_2O_3/Al - Al_2O_3 - Fe$ junction for several values of the applied magnetic field (sample 5890).

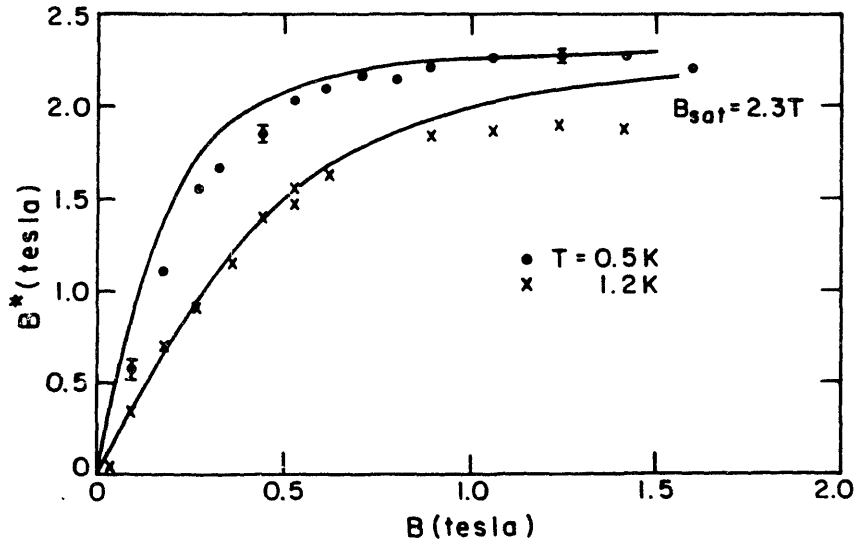

Fig. III.2.7 Comparison of the field dependence of B* with the $S = 7/2$ Brillouin function (sample 5974).

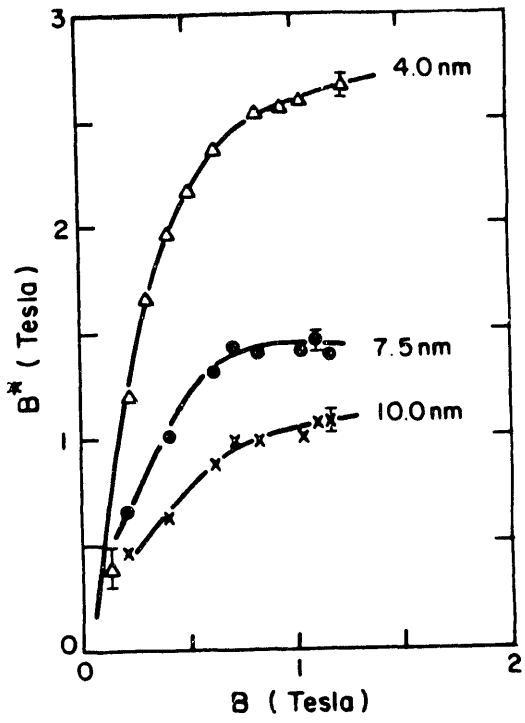

Fig. III.2.8 B^* as a function of the applied field for three $A\ell$ film thicknesses of a $Gd_2O_3/A\ell$ bilayer (samples 5890, 5963).

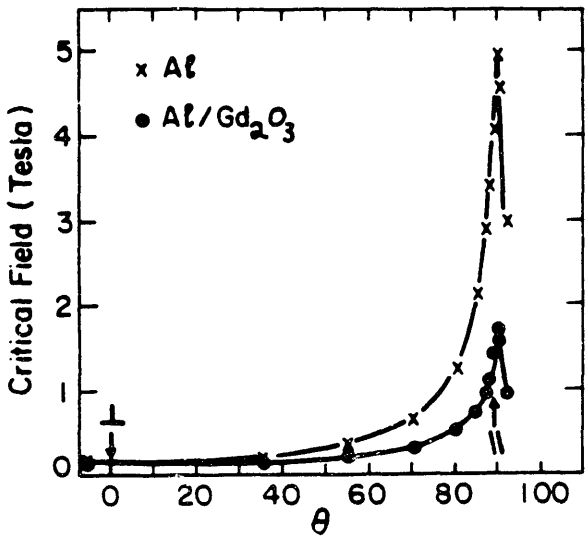

Fig. III.2.9 Angular dependence of the critical field at $T = 0.45$K (sample 5974). The orientation $\theta = 90°$ corresponds to the magnetic field parallel to the surface of the $A\ell$ film.

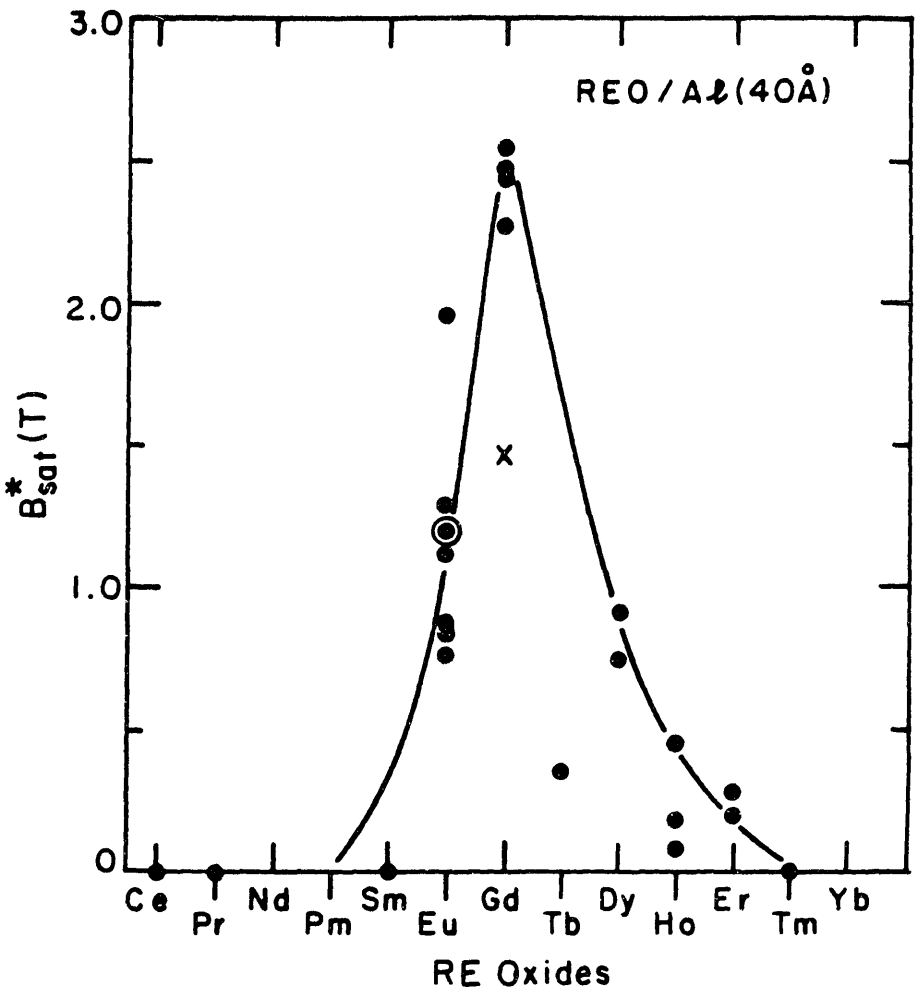

Fig. III.2.10 The saturation value of B* for all of the rare-earth oxides studied and also EuS as designated by ⊙. (See Table III-1.) The point designated by × corresponds to Gd_2O_3 evaporated from a boat.

III.3 Submonolayer Rare-Earths

In the last section, data were presented for the rare earth oxides in contact with thin Aℓ films. It was concluded that there is an enhancement of the Zeeman splitting in the Aℓ film due to the interaction of the conduction electrons with the REO. Furthermore, the extra field B^* was found to be inversely proportional to the film thickness in accord with a proximity model. However, the nature of the interaction at the interface was not resolved. There are two possibilities: the exchange interaction or the magnetization. In this section a tunneling study of Aℓ films covered with submonolayer of an unoxidized rare earth element is presented. The pairbreaking due to rare earth spins will be found to be consistent with the Abrikosov-Gor'kov (AG) theory, and values of the exchange constant are derived for a number of samples of most of the rare earths. The exchange constant is obtained in two different ways. The first method consists of fitting the AG theory to the depaired conductances in zero field. The exchange constant is also obtained without using the AG theory by measuring the Zeeman splitting. The two values obtained are found to agree within a factor of 2 of each other. This supplies strong support that exchange scattering from rare earth spins can be treated by the s-d exchange hamiltonian in the Born approximation. These are the assumption entering into the AG theory. The s-d exchange hamiltonian represents the magnetic limit of the Anderson model, and the validity of the Born approximation implies the absence of the Kondo effect (see discussion in section A.4). Furthermore, the quantitative analysis suggests that scattering from a submonolayer of rare earth at the surface is the same as scattering from bulk impurities.

With this improved quantitative understanding of depairing due to exchange scattering, the data on the rare-earth oxides are reexamined. On closer inspection, it is found that the Aℓ films in contact with the REO show a small amount of depairing on the order of the "background" depairing of an undoped $A\ell - A\ell_2O_3 - Fe$ junctions. This small effect was overlooked in the initial study of the REO/Aℓ system because the oxide most studied was that of Eu. For Eu the exchange constant is particularly small and it is possible to have a large first order effect $B_{ex} \propto cJ$ while still having a small second order effect $\Delta T_c \sim \hbar/k_B\tau_{ex} \propto cJ(J/E_F)/k_B < 0.05K$. Finally, the identification $B^* = B_{ex}$ is made and the data on the two systems (i.e. REO/Aℓ and RE/Aℓ) are combined in a single plot of B^* verses $\hbar/\tau_{PB}$. A plot of this kind may be of more general value to studies of moment formation and surface magnetism questions because it distinguishes between changes in the concentration c of impurities and product JS of the exchange constant and impurity spin. In fact, the product JS can be determined without knowing the Aℓ film thickness or the factional RE coverage.

—Pairbreaking in the RE/Aℓ system—

Samples were formed by first depositing the rare earth on a cryogenically cooled glass substrate followed immediately by a 40Å strip of Aℓ . The Aℓ was oxidized to form a tunnel barrier and Fe or Ag cross strips were deposited to complete the tunnel junction. The deposition of the submonolayer rare earth was monitored using the standard quartz oscillator technique giving a thickness error of $\sim 3\%$. Depositions using a rotating chopper gave a relative error between differing thicknesses of better than 1%. For example, a thickness reading of 0.1nm Gd is equivalent to an areal number density

of 3 atoms/nm^2 or 0.31 atomic layers using a metallic radius of 0.18nm. Comparison of the perpendicular and parallel field pairbreakers determines the thickness of the unoxidized part of the Aℓ film to be about 3.0 $\pm$ 0.2 nm (Aoi, Meservey, and Tedrow, 1974). Therefore, a thickness reading of 0.1nm Gd in contact with a oxidized Aℓ film corresponds to an effective impurity concentration $c = 1.7 \pm 0.1\%$.

The conductance in zero field is shown for four Gd/Aℓ - $A\ell_2O_3$- Ag junctions made at the same time with 0,1,2,3 Gd ions/nm^{-2} (figure III.3.1). Qualitatively the effect of pairbreaking on the conductance is clear. The peaks in the conductance associated with the singularity in the BCS density of states are rounded, and the conductance at zero bias increases indicating the introduction of states below the energy gap of the undoped Aℓ film. Fits to the conductance were generated from the computer program of Rainer and Alexander (Alexander et al, 1985; Alexander, 1986) and these show excellent agreement with the data. Two parameters T_{co} and $PP0 = \hbar/k_B T_{co}\tau_{ex}$ were varied in order to obtain the fit and the values are listed in table III.2 (sample 6310). T_{co} is nearly constant and the scattering rate increases linearly with Gd coverage. This is the expected result for bulk impurities where the concentration is given by the ratio of the number of impurity atoms to the number of atoms of the host. The proportionality of the pairbreaking rate to the concentration implies an inverse dependence on the film thickness $\hbar/\tau_{PB} \propto c \propto 1/d$. This is not an obvious result. In fact, some theories predict and some experiments imply that the pairbreaking rate from a surface should be proporitonal to $1/d^2$ (Wong and Ketterson, 1986; Tokuyasu, Sauls and Rainer, 1988; Hauser, Theuerer, and Werthamer, 1966).

From the AG equation (eq. I.2.4) one can estimate the transition temperature T_c. This estimate is found (see Table III.2) to be in excellent agreement with the resistively determined transition temperature (figure III.3.2). This agreement of the conductance data taken at $T = 0.43K$ and the resistance measurement at $T = 1 \sim 2K$ means that the AG pairbreaking parameter $\rho_{AG} = \hbar/\pi k_B T_c \tau_{ex}$ and the scattering rate $\hbar/\tau_{ex}$ are temperature independent over this range indicating the absence of Kondo effects. This result agrees with the conductance measurements of Woolf and Reif (1965) who determined that the AG theory, which treats the scattering in the Born approximation, adequately describes the effect of ~1% Gd in thick Pb films.

The "control" junction $A\ell - A\ell_2O_3 - Ag$ with no RE was also fit to the theory so as to obtain the intrinsic pairbreaking rate τ_{PB}^{-1} for the 40Å Aℓ film. This was generally found to lie between 1.5 and $4 \cdot 10^{10} sec^{-1}$ for junctions with Ag counter electrodes. To some extent this intrinsic pairbreaking rate ($\hbar/\tau_{PB} \sim 10$ to 26μeV) is an artifact of not correcting for the $20\mu eV$ modulation of the bias voltage used to measure the conductance. As noted previously (Tedrow and Meservey, 1973) when Fe counter electrodes are used, the fringe magnetic field from the Fe counter electrode depairs the conductance significantly. The pairbreaking rate of the control junctions with Fe counter electrodes was found to be larger ($\hbar/\tau_{PB} \sim 19 - 47\mu eV$). For this reason an indication has been made in Table III.2 of the material used for the counter electrode (Fe or Ag). For a $RE/A\ell - A\ell_2O_3$-(Ag or Fe) junctions the contribution to the pairbreaking rate from exchange scattering was obtained by subtracting off the pairbreaking rate of the associated control junction $A\ell - A\ell_2O_3$-(Ag or Fe). The

resulting values for the exchange scattering rates are given in table III.3. Equation III.1.4 is then inverted to yield the exchange constant (Table III.3). The exchange constant J(0) corresponds to the form factor of section A.1, eq. A.1.10, and is the spatial average of the exchange interaction multiplied by the number of lattice sites in the crystal. The density of states was taken from the specific heat γ of bulk Al(Corruccini and Gniewek, 1976) $N_o = 1.084 \cdot 10^{34} cm^{-3} erg^{-1}$.

—The RE spins are aligned with a magnetic field—

With the application of a small magnetic field, a large Zeeman splitting $2\mu(B+B^*)$ of the density of states is observed (fig. III.3.3). Since ergodic pairbreaking is clearly present, one can make the identification $B^* = B_{ex}$ where B_{ex} is given by equation III.1.2. The magnitude of B^* and its dependence on the applied field are shown in figure III.3.4. The splitting corresponding to the sample with lowest Gd coverage appears to saturate for an applied field of $B \sim 1.5$ tesla. For higher applied fields the Gd/Aℓ bilayer goes normal. One would expect that spin-flip terms are frozen out when $\mu B/kT$ is sufficiently large to saturate the splitting (see eq. III.1.5). Therefore, the theory without an exchange spin-flip contribution was used to fit the conductance in a field of 1 tesla (fig. III.3.5).

The fitting parameter $T_{co} = 2.4K$ was taken as that determined in zero field (figure III.3.1, table III.2). The Fermi liquid parameter $G^o = 0.3$ was taken as the value for undoped Aℓ films (Alexander et al, 1985). The orbital effects were neglected as they are small: the contribution $C_F(\mu B/k_B T_{co})^2/1.764)$ to PPO from orbital pairbreaking in an applied magnetic field of $B = 1$ tesla is of the order of 0.01 using the value of $C_F = 0.2$ appropriate for Aℓ . The parameters $b_{so} = \hbar/3\tau_{so}\Delta_o, PP0$, and $B_{int} = B+B^*$ were allowed to vary so as to obtain the best fit which is shown in figure III.3.5. The best fit value of the spin-orbit scattering rate $b_{so} = 0.09$ is not much different from that of undoped Aℓ films $b_{so} = 0.05$. One may expect that some of the increase is due to spin relaxation effects associated with the spin-flip part of the exchange interaction from impurity spins which are not completely saturated . The low value of the spin-orbit scattering rate is a puzzling result considering that the increase in spin-orbit scattering produced by 1nm^{-2} of Pt is of the order $b_{so} = 0.24$ (Tedrow and Meservey, 1979). Questions on the spin-orbit scattering rate are addressed in chapter IV. The value of the pairbreaking rate $\hbar/\tau_{PB} = k_B T_{co} PP0 = 42\mu eV$ (i.e. PP0 = 0.21) is not much different from the value obtained in zero field $\hbar/\tau_{PB} = 36\mu eV$ (i.e. PP0 = 0.18). This in accord with the discussion of equation III.1.4.

A number of curves were generated with some of these parameters held constant ($T_{co} = 2.4, b_{so} = 0.09, PP0 = 0.21$), but with different values of B_{int}. From a comparison of these with the conductance data of figure III.3.3, the exchange field as a function of applied field was determined (figure III.3.4). The saturation of B_{ex} suggests a functional dependence like that of a Brillouin function. The solid line through the data is a spin 7/2 Brillouin function but with an argument $\mu_{eff}B/KT$ where $\mu_{eff} = \mu_B/2$. The factor of 1/2 represents a deviation from the behavior expected for a free trivalent ion and may be due to the interaction between 4f and conduction states. This same functional dependence was scaled up by a constant factor to obtain the solid lines in figure III.3.4 for Gd coverages of 2 and 3 nm^{-2}. The saturation value

of B^* was used in equation III.1.2, to obtain a second determination of the exchange constant J(0). These values are listed in Table III.3.

Thus, the exchange constant has been obtained in two ways. The first method involved the AG theory. The depairing of the conductance or the decrease of the transition temperature (eq. I.2.4) due to exchange scattering (eq. III.1.3) gives the absolute value $|J(0)|$. Second, the Zeeman splitting of the density of states gives a value of J(0) in a way which doesn't involve the AG theory (eq. III.1.2). The values determined in these two ways are compared in Table III.3 and agree within a factor of two. This can be considered good agreement granted the necessary approximations made in the AG theory and for this simple way of treating surface scattering (i.e. like impurity scattering in the bulk). The sign of the exchange constant J is such that the internal field is increased relative to the applied field. Due to the sign of the DeGennes factor $(g_L - 1)$ (Table III.4) this corresponds to J is positive for the heavy rare earths and negative for the light rare earths. This is in accord with the NMR (Knight shift) and electron spin resonance data of Jaccarino et al (1960) for $REA\ell_2$ Laves compounds and with the spin-disorder resistivity data of Sagawara and Eguchi (1966) for RE impurities in Lanthanum. The exchange constant was obtained for a number of samples covering most of the rare earth elements. These results are found in Table III.3 and are plotted in figure III.3.6. The exchange constant is of the order of 10 meV for the heavy rare earths and Sm. The especially small exchange constant for Eu and the large value for Ce is in agreement with the work of other researchers (Maple, 1970; Sagawara and Eguchi, 1966).

—Additional Experimental Concerns—

The large variability of the exchange constant between different evaporations of the same species as shown in figure III.3.6 may possibly be attributed to surface disorder and contamination. The presence of small amounts condensed gases on the substrate is likely considering that the substrates were cryogenically cooled. To test the possibility of a surface contamination effect, a clean surface was produced by first depositing 20Å Aℓ and then the rare earth submonolayer followed by another 20Å Aℓ. When depositing Gd in this sequence, between two 20 Å Al films, the scattering rate was found to be a order of magnitude larger than the values obtained with the same (as deposited) coverage of Gd at the surface (sample 6321 in Table III.3). Similarly, Eu deposited between two 20Å Aℓ layers results in an increased scattering rate (sample 6320). Associating this increased scattering rate with a change in J corresponds to an exchange constant $\sim 2 - 3$ times larger. This larger value is in accord with the results of Woolf and Reif. Using their data and equation III.1.4 one can calculate the exchange constant for (bulk distributed) Gd impurities in Pb. From figure 2 and 7 in their paper, one concludes that the scattering rate from 1% Gd is $\hbar/\tau_{ex} \sim 0.23meV$. Using a free electron density of states $N_o \sim 6.6 \cdot 10^{33} cm^{-3} erg^{-1}$ and unit cell volume $\Omega = (4.95 \cdot 10^{-8} cm)^3$ one obtains an exchange constant $J(0) = 27$ meV.

Thus there is a clear progression. The exchange scattering rate is largest when deposited on a fresh Aℓ surface and then immediately covered with more Aℓ. The scattering rate is less when deposited on the cryogenically cooled glass substrate and then covered with Aℓ, and it is smallest when the rare earth is deposited and then

purposely oxidized as described in section III.2.

Since the scattering rate goes as $\hbar/\tau_{ex} \propto cJ^2$ one may consider a simple but basic question: is it the concentration c or the exchange constant J which is being changed by surface degradation and oxidation. The first possibility corresponds to the "insulation" of a fraction of the rare earth ions from the itinerant electronic system. For example, in the rare earth oxides there is a gap in the band structure; conduction electrons can't propagate, and there is no overlap of the 4-f and conduction electronic wavefunctions except at the surface. The second possibility corresponds to a change in the coupling between local and itinerant electrons. As discussed in section A.4, the exchange constant has positive and negative contributions from "direct" coulomb and mixing interactions respectively. The balance between these may be changed if the crystal fields and valence of the ion are changed. In this way the effective exchange constant may be changed, and this may account for the smaller scattering rate for the rare earths at the surface.

As a way of resolving this question, it is suggested that the effect of changing the concentration can be distinguished from that of changing the exchange constant by plotting B_{ex} verses $\hbar/\tau_{ex}$. As the concentration of impurities is increased both $B_{ex} \propto cJS$ and $\hbar/\tau_{ex} \propto cJ^2S(S+1)$ increase, but the ratio $B_{ex}/(\hbar/\tau_{ex}) \propto 1/J(S+1)$ remains constant. Thus data from a number of samples with differing concentrations of impurities, but with a constant product $J(S+1)$, will plot on as straight line with slope $J(S+1)$. This is shown for several values of the product $J(S+1)$ in figure III.3.7. The data for Eu and Gd submonolayers at the surface of a Aℓ film (samples 6227, 6310) and inside the Aℓ film (samples 6320, 6321), respectively, are plotted on this same graph in figure III.2.8. It appears that the product $J(S+1)$ has a larger value for RE ions inside the Aℓ film. Some caution should be used in drawing conclusions from this limited amount of data especially considering the large error bars. However, this example demonstrates the use of this type of plot for investigation of surface magnetism and moment formation questions. An analysis of this type does not appear in the reference literature due to the requirement of having data for both B_{ex} and $\hbar/\tau_{ex}$ on the same samples.

It is believed that the error bars can be reduced. The major contribution to the error in B_{ex} arises from the extrapolation of the low field data to find the saturation value of B^*. Generally, the internal field $B + B^*$ reaches the critical field of a 40Å Aℓ film before B^* saturates. Thus, errors in $B, T, and B^*$ at low field introduce a relatively large error in the extrapolated value of B^*_{sat}. Errors in B, T could be reduced by introducing independent calibrated thermometer and Hall sensor. An easy error to make is to let the level of the ^{3}He bath drop down below the sample at which point the ^{3}He vapor pressure no longer gives the sample temperature. It should also be noted that as shown in fig. III.2.9, the misalignment of the junction with the applied field can reduce the measured B^*. The errors in $\hbar/\tau_{ex}$ arise primarily from the necessity of subtracting off a large "background signal" $PP0 \sim 10 - 47\mu eV$. That is the pair-breaking rate obtained for the control junctions (those without any RE) is itself of the order of the exchange scattering rate. Contributions to this background include the $20\mu V$ modulation of the lock-in amplifier and the fringing magnetic field of Fe

counter electrodes. In low noise junctions there is room to reduce the modulation. Since the conductance error introduced by the modulation goes as the modulation amplitude squared, only a small decrease in the amplitude is necessary. Contributions to the background may also arise due to fundamental physical effects such as disorder-enhanced correlation effects (Dynes, Garno, Hertel, Orlando; 1984) or lifetime broadening (Dynes, Narayanamurti, and Garno, 1978). According to the supplier, the concentration of magnetic impurities (Fe, Co, Ni) in the starting Aℓ material itself is less than 10^{-6}. Additional errors are introduced by taking the conductance data on an analogue X-Y plotter. The plotter can be found to be noticeably misaligned such that the axes are not perpendicular. This problem could be corrected by dedicating an X-Y plotter to the project, or, preferably, taking the data digitally on a computer. Initial attempts to interface the computer to the measurement apparatus were plagued by noise associated with digital electronics. The effect of the noise was to overmodulate the voltage bias of the junction.

—Origin of the rare earth oxide effect—

An significant feature of plotting B^* verses $\hbar/\tau_{ex}$ is that the impurity concentration divides out of the ratio. Thus the data from both the RE/Aℓ and REO/Aℓ systems can be combined on one plot. This is done for Eu and Gd data in figure III.3.9. The data suggest that the oxidation doesn't so much change the product $J(S+1)$ but rather changes the concentration c. The REO contributes an effective concentration of $c \sim 0.5\%$. Another fact obtained from figure III.3.9 is that the exchange constant is approximately determined *without having to know the RE or Aℓ film thicknesses.* For Eu, $J \sim 3.5$meV and for Gd, $J \sim 10-15$meV. The values agree with those calculated in table III.3 assuming an Aℓ film thickness of 30Å.

The exchange constant is a factor of ~ 3 less for Eu than for the heavy rare earths and Sm. This has the important consequence that B^* can be of the order of 1 tesla without a significant decrease in T_c. The expected decrease is given by $\Delta T_c \sim (\pi/4)\hbar/k_B\tau_{ex}$ which is given as an alternate abscissa in figures III.3.7 and III.3.9. As shown in figure III.3.9, the decrease in T_c for EuO is less than 0.05K. For comparison the decrease in T_c due to the fringing magnetic field of the Fe counter electrode is of the order of 0.2K. Thus the enhancement of the Zeeman splitting in the REO/Aℓ system discussed in section III.1 can be attributed to the exchange interaction between the conduction electrons of the Aℓ and the rare earth spins at the surface of the REO. The absence of significant ergodic pairbreaking is explained by the fact that the exchange constant is small relative to the Fermi energy ($E_F \sim 10eV$). To see this, consider that $B^*_{sat} = cJS$ is observable only if it is of the order of the Pauli field $B_P \sim k_B T_{co}/\mu_B$. In this case the associated decrease in the transition temperature is of the order of

$$\Delta T_c/T_{co} = \frac{\pi}{4k_B T_{co}} \times 2\pi c(\Omega N_o)J^2 S(S+1) \sim J(S+1)(\Omega N_o).$$

This is negligible if $J/E_F \ll 1$. The exchange constant is small $\sim 10meV$ for rare earths at the surface of an Aℓ film and is especially small for Eu, accounting for the observations presented in section III.2.

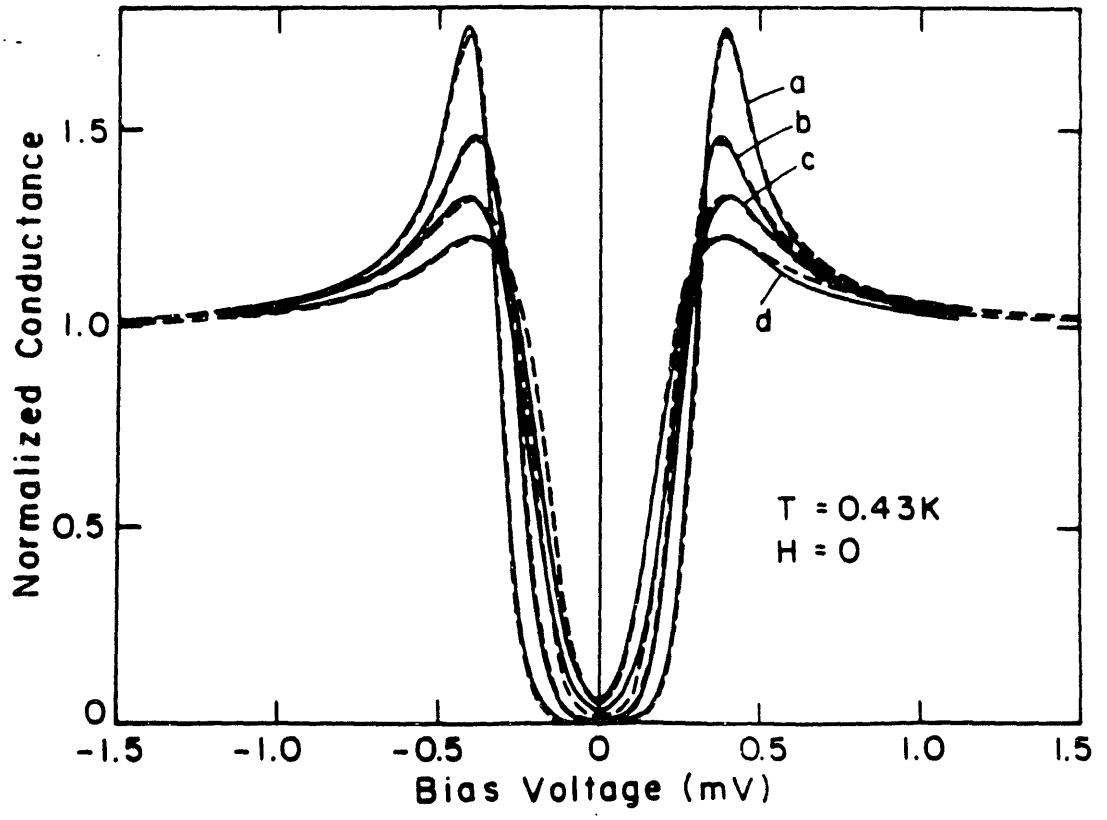

Fig. III.3.1 The measured tunneling conductance (solid) and fits of the AG theory (dashed) of $Gd/Al - Al_2O_3 - Ag$ junctions a,b,c,d corresponding to Gd coverages of 0,1,2,3 ion/nm^2 (sample 6310).

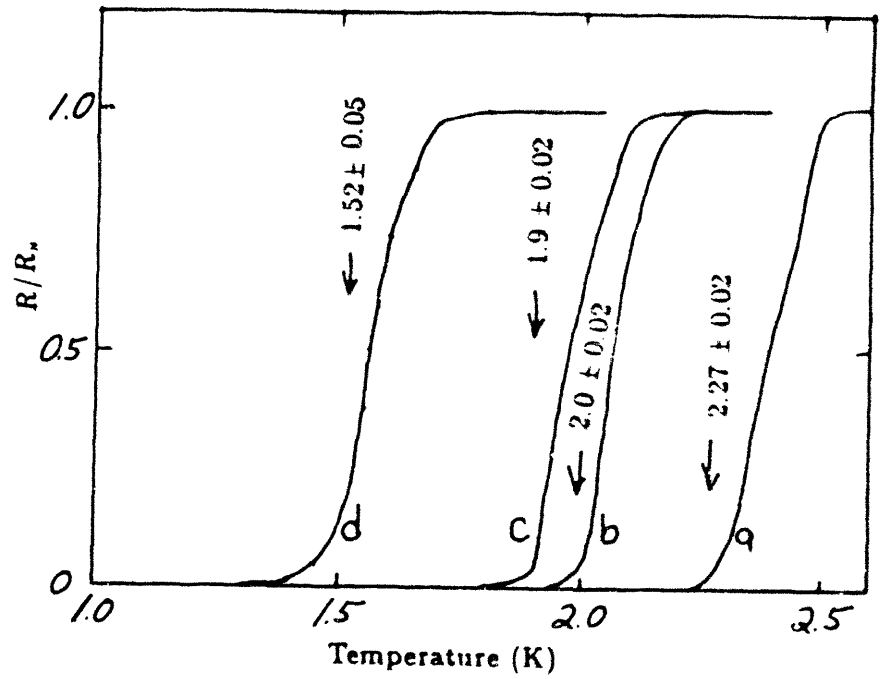

Fig. III.3.2 The $B = 0$ resistance verses temperature for the Gd/Aℓ electrodes corresponding to the junctions a,b,c,d in figure III.2.1 (sample 6310).

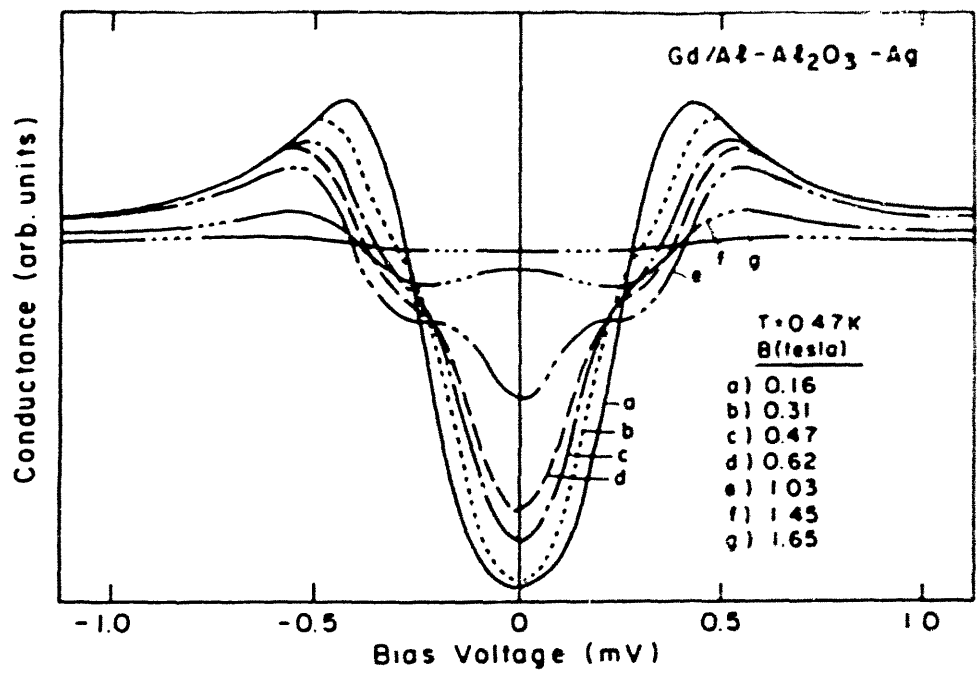

Fig. III.3.3 The conductance for several applied fields. The junction is the same as that used in figure III.2.1 with Gd coverage of 1 ion/nm^2 (sample 6310).

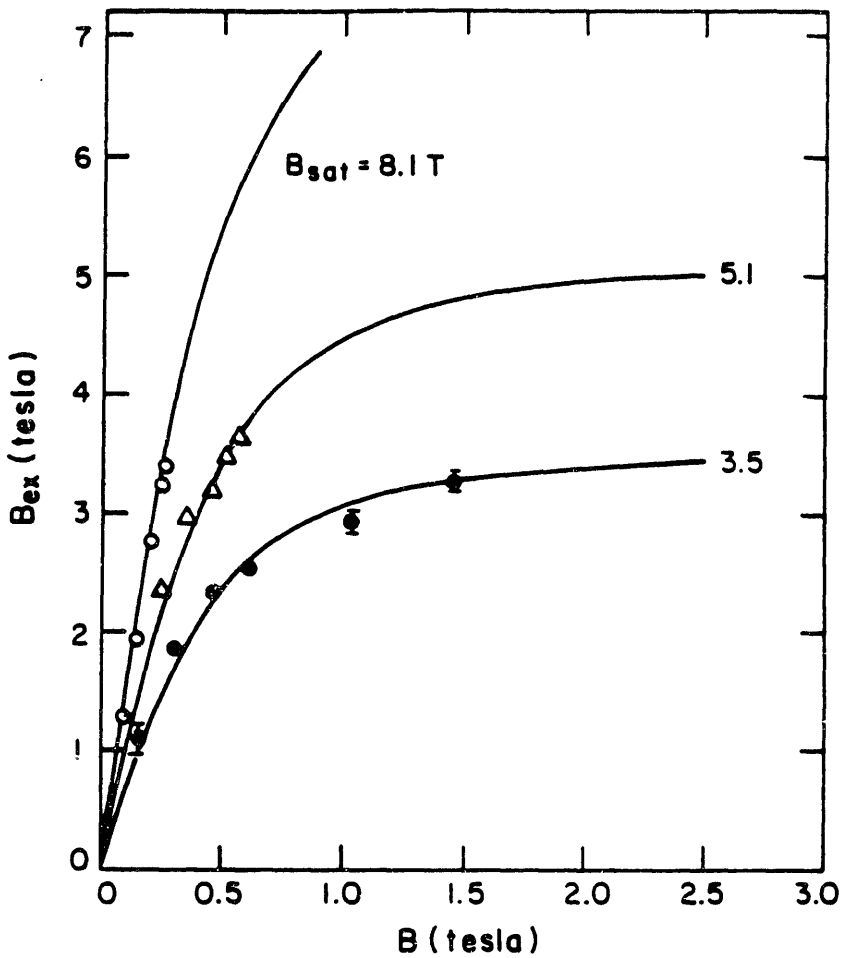

Fig. III.3.4 The uniform exchange field as a function of the applied magnetic field is obtained from the Zeeman splitting of the conductance for the junctions corresponding to b,c,d in figure III.2.1. The curve drawn through the points corresponding to the lowest Gd coverage saturates at $B_{ex} \sim 3.5$ tesla. This curve was scaled by a constant factor to obtain the saturation curves for greater coverages (sample 6310).

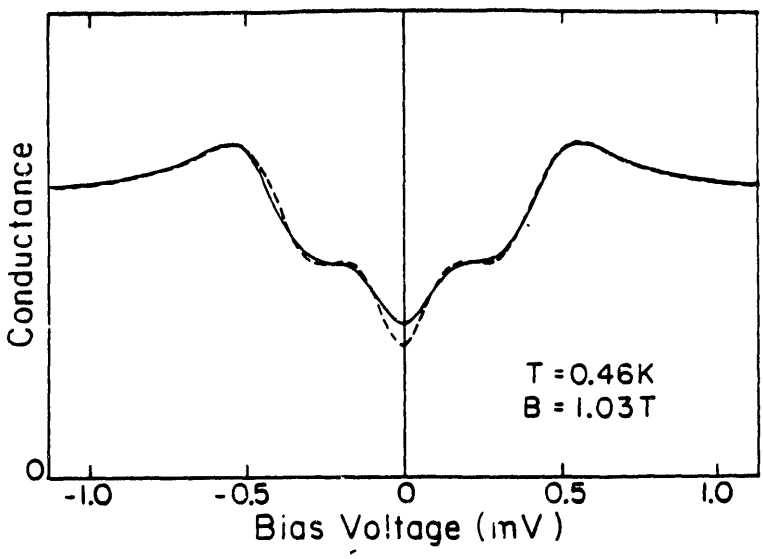

Fig. III.3.5 The conductance of the $Gd/A\ell - A\ell_2O_3 - Ag$ junction corresponding to the lowest Gd coverage (curve b in figure III.3.1) shows a large Zeeman splitting in an applied field of $B = 1.03$ T. The fit (dashed) is derived from the theory of Rainer and does not include the spin-flip part of the exchange scattering (sample 6310, 1 Gd ion/nm^2).

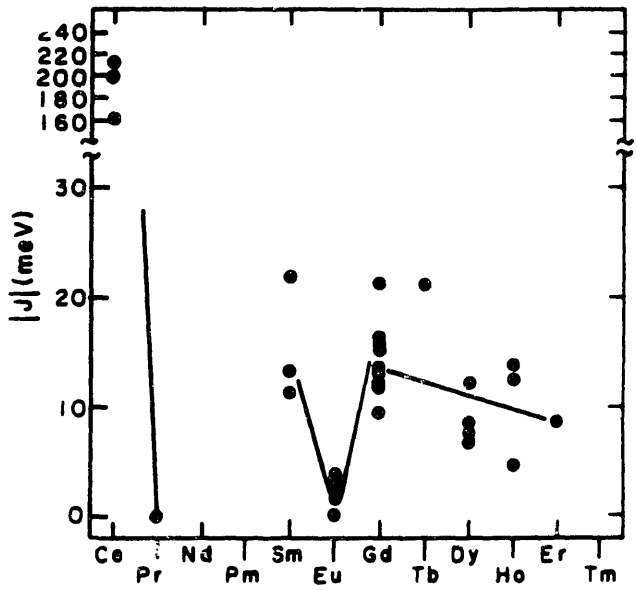

Fig. III.3.6 The exchange constant for a rare earth at the surface of Aℓ film determined by fitting the zero field conductance to the Ag theory and by measuring the Zeeman splitting of the density of states.

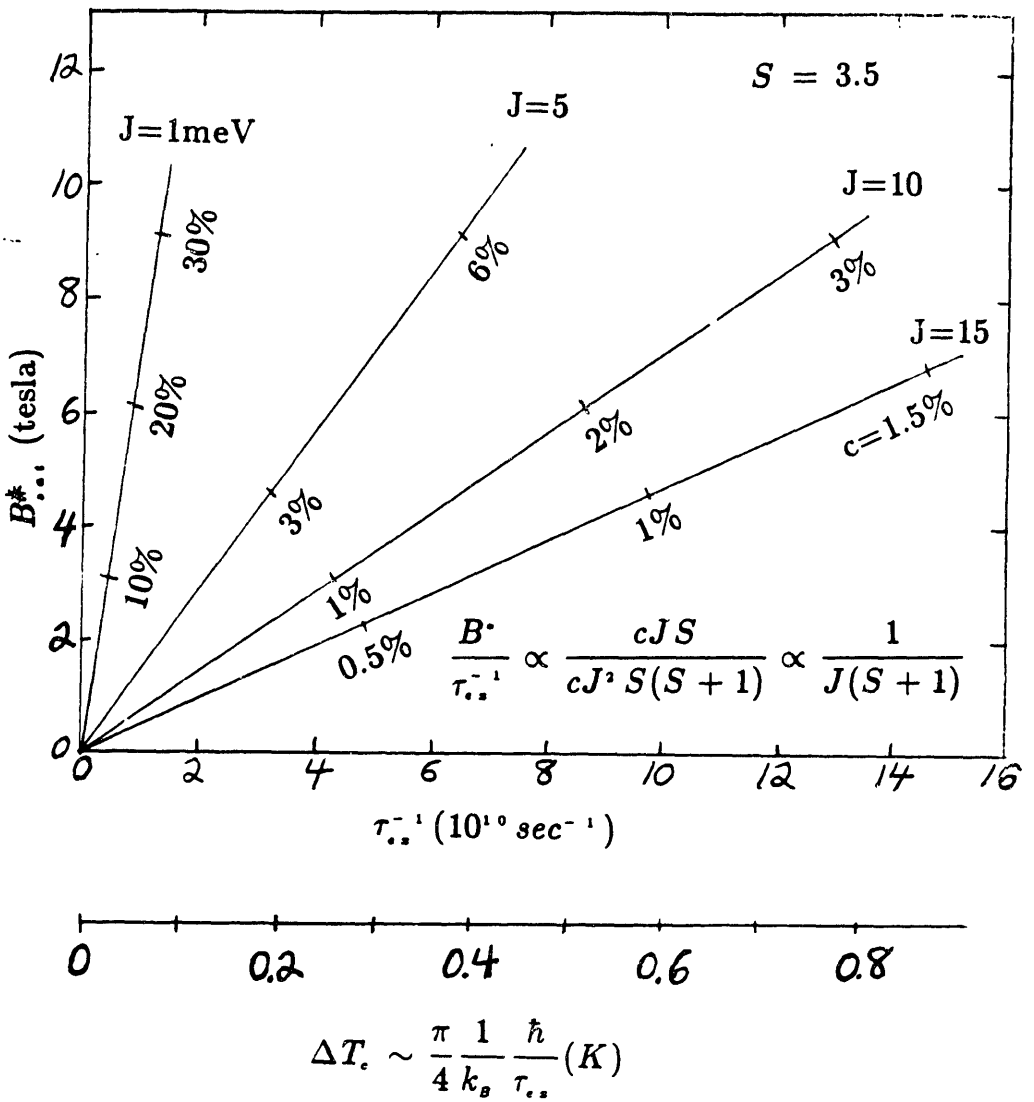

Fig. III.3.7 Comparison of the saturation value of B* versus the scattering rate and on the decrease in T_c for several values of the exchange constant and assuming $S = 3.5$. The numbers along each line give the effective impurity concentration.

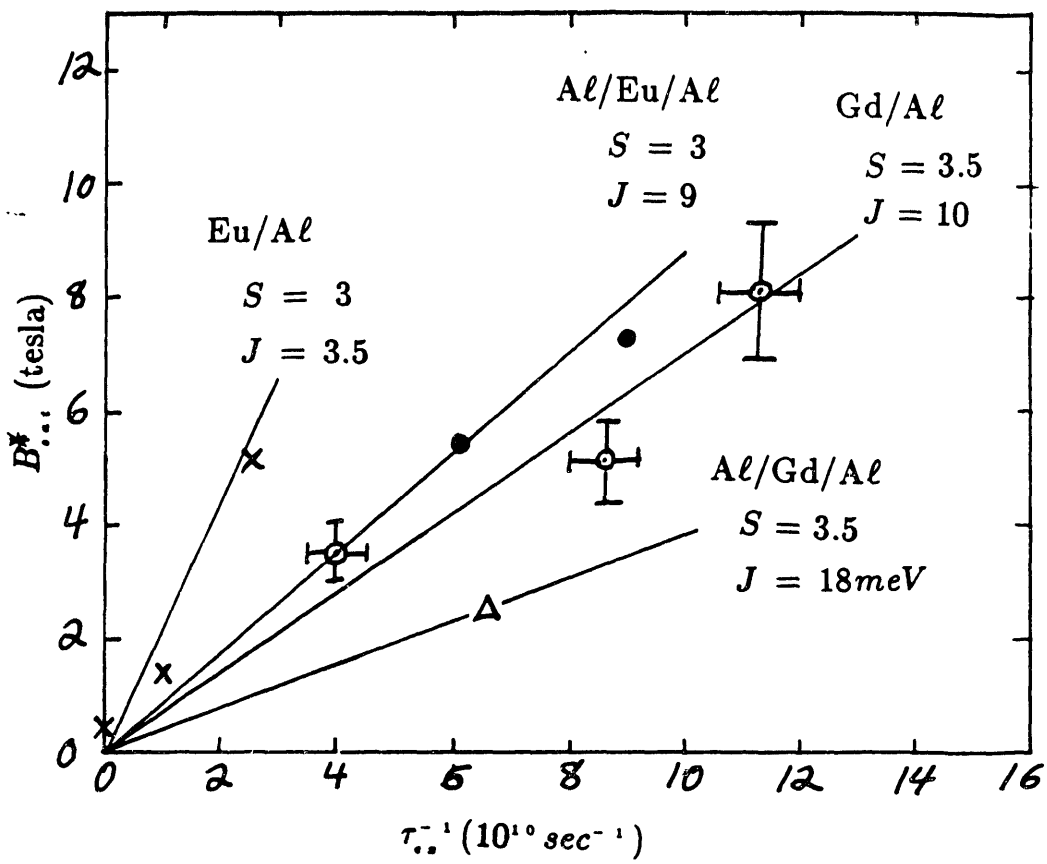

Fig. III.3.8 The exchange constant is determine by plotting B* verses τ_{ex}^{-1} for Eu at the surface (x), Eu inside (•), Gd at the surface (○), and Gd inside (△) of a 40Å Aℓ film (Samples 6227, 6091, 6320, 6310, 6321).

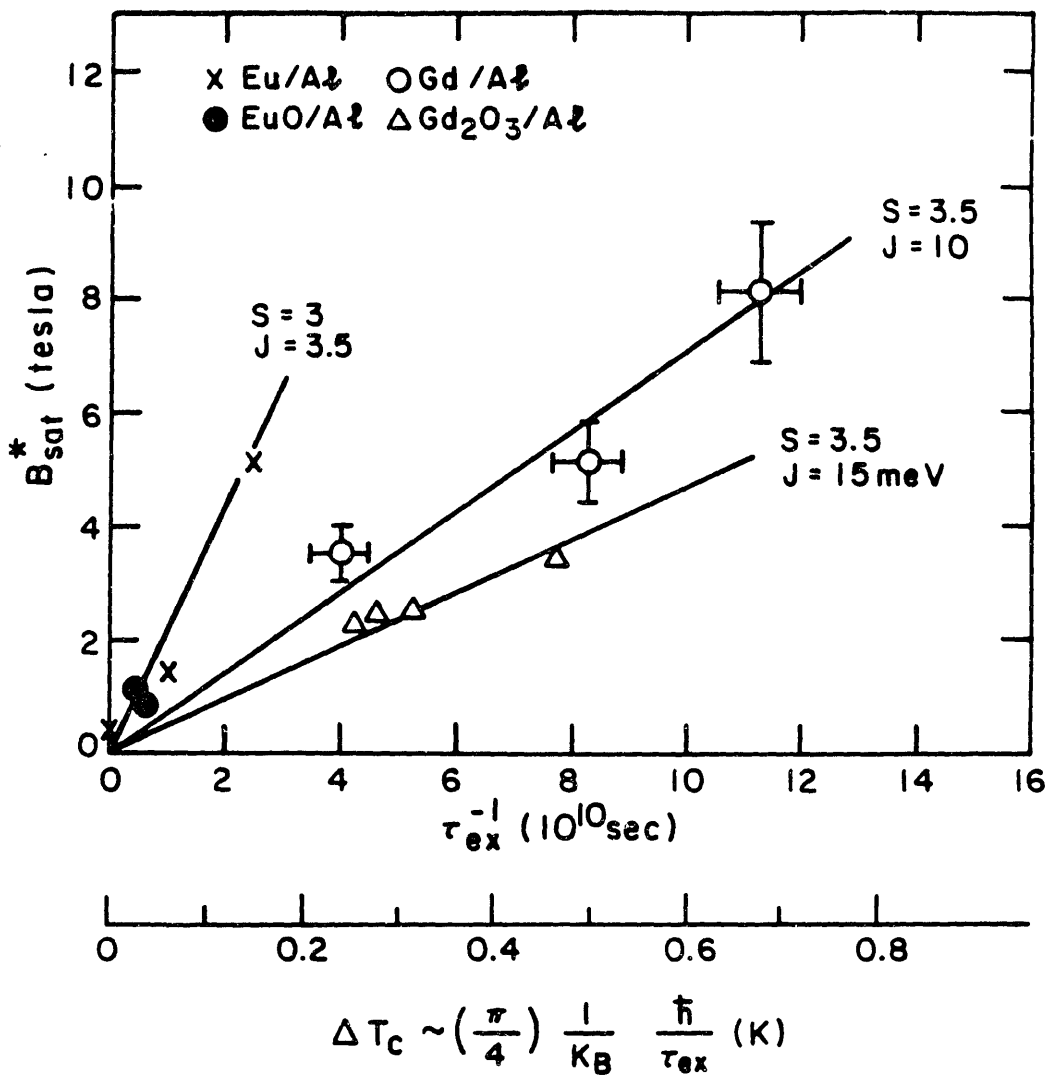

Fig. III.3.9 Comparison of oxidized and unoxidized rare earth proximity layers on Aℓ.

III.4 RKKY Effect in Superconductors

In this section additional results for the Gd/Aℓ system are presented. Spin-polarized tunneling is used to detect for the first time the Ruderman-Kittel-Kasuya-Yosida (RKKY) spin-polarization of the conduction electrons localized at the surface of an Aℓ film covered with a submonolayer of Gd. The important role of spin-orbit scattering is demonstrated. In the limit of weak spin-orbit scattering the polarization is observed only in the normal state. The absence of spin-polarization in the superconducting state is attributed to the reduced value of the long range part of the susceptibility, a property following from singlet pairing. When the spin states of the electrons are mixed by a two monolayers of Pt, the RKKY effect is detected in both the superconducting and normal states. As expected ($k_B T/E_F \ll 1$), the spin relaxation rate can be large enough to destroy the Zeeman splitting of the electron energies at the Fermi level without decreasing the RKKY effect. Since the RKKY effect plays a role in long range magnetic ordering, these results are pertinent to recent theoretical dialogue concerning the influence of spin-orbit scattering in coexistent superconductor/ferromagnetic phases (Bulaevskii et al, 1986; Anderson, 1985; Fulde and Keller, 1982).

—Pairbreaking at a surface—

In sections III.2 and III.3, two consequences of the exchange interaction were studied, the exchange enhanced Zeeman splitting $2\mu B_{ex}$ and the scattering rate $\hbar/\tau_{ex}$. In order to present a straightforward discussion of the third consequence, the RKKY effect, is it necessary to consider a more detailed physical picture of how the planar geometry used in all these experiments is different and how it is the same as bulk distributed impurities. In addition, a more detailed physical picture is needed because there are rather subtle points which are brought out for the first time in these experiments concerning the length scales involved in the tunneling investigation of electronic properties.

An important result obtained in section III.2 and III.3 was that the splitting and scattering rate scaled as the concentration c = # impurity atoms $\times a_o/d$ where a_o, and d are the lattice constant and thickness of the Aℓ film, respectively. This makes sense in the simple picture of the RE/Aℓ system as an infinite square well with a short range perturbation $H' = -J(r)\vec{S}\cdot\vec{s}$ at the surface (fig. III.4.1). The range δ of the perturbation may be that $2\pi k_F^{-1} \sim 3.6\mathring{A}$ associated with the overlap of local and itinerant states. In the REO/Aℓ system, δ may correspond to several atomic layers due to a disordered interface or due to tunneling of electrons into the oxide. For the latter possibility δ is of the order $k_F^{-1}(2E_F/E_g)^{1/2}$ where E_g is the band gap of the oxide. In section III.2 the tunneling distance into EuO was estimated to be $\delta = 2.7\mathring{A}$.

The states of the film can be decomposed into the product of plane waves traveling parallel and perpendicular to the film surface. However, symmetry considerations suggest the use of sine wave eigenstates instead of plane waves for motion perpendicular to the surface. For states traveling nearly perpendicular to the surface $|k_\perp| \sim k_F$, the first order perturbative shift in the energy at the Fermi level is given by $E^{(1)} = \pm(1/2)JS\delta/d$. This is the Zeeman shift observed with spin-polarized tunneling and corresponds to scattering events at the surface which connect plane wave states

traveling to the right with those traveling to the left ($k_\perp \uparrow$ to $-k_\perp \uparrow$). These two states together make up the standing wave (i.e. sine wave). This first order energy shift is responsible for a non-ergodic pairbreaking effect leading to a first order transition. Of course, for states traveling at an angle significantly off perpendicular the Zeeman splitting is reduced. However, these contribute an exponentially small tunneling current due to the additional distance they must tunnel through the junction barrier.

If one considers specular scattering from the surface only, then there are spin-flip scattering events ($k_\perp \uparrow$ to $-k_\perp \downarrow$) which cause pairbreaking which is described by nether the ergodic nor non-ergodic theories. This unique possibility of this planar geometry is considered by Tokuzasu, Sauls and Rainer (1988). They show that the pairbreaking rate goes inversely with the *square* of the film thickness and that the transition to the normal state is always second order. They define a pairbreaking parameter $\rho = (\hbar v_F / 4\pi k_B T_{co} d) tan(\Theta/2)$ where Θ is the angle by which an electron spin is rotated when scattered by the surface. The transition temperature decreases by $\Delta T_c = 2.8 T_{co} \rho^2$. If the surface layer is disordered so that there is diffuse scattering, then there are matrix elements connecting not only k to $-k$ but also k to $-k'$. In light of the measurements presented in section III.3, this diffuse scattering case can be described by the standard ergodic pairbreaking theory such as that of Abrikosov and Gor'kov (1960). The scattering rate goes inversely with the sample thickness. A more rigorous theoretical model, of this latter situation has not yet been treated in the literature. Falkovsky(1983) has reviewed normal state transport phenomena at metal surfaces and concludes, "that a more complete theory is necessary if the effects of surface scattering in transport phenomena are to be adequately understood". Further complications arise due to the fact that real metal surfaces are not described by a infinite potential. A text on this latter subject is available (Garcia-Moliner and F. Flores, 1979) and some of the original work was done by Lang and Kohn (1970). However, for the purposes of the results presented here the simple model described above is sufficient.

—The distance probed by tunneling—

The density of states $dN_\uparrow(\vec{k}_F)/dE$ is a measurable quantity which contains information about the hamiltonian of the electronic system. For example, specific *features* in the density of states have been identified with the exchange interaction (e.g. the enhanced Zeeman splitting and ergodic depairing effect). The density of states is function of position and can have variations as small as the Fermi wavelength. However, since the (bulk) spin mean free path is much larger than the film thickness the Zeeman splitting and exchange scattering rate are uniform throughout the film.

The energy gap is a feature in the density of states which is a signature of the correlations between time reversed states associated with superconductivity. Even in the case of gapless superconductivity, the density of states has features (a dip at zero energy and a peak at about an energy $k_B T_c$) which are associated with superconductivity. These features in the density of states can only vary over a length scale of the coherence length. That is, two measurements of the DOS at two positions separated by a distance less than the coherence length will indicate approximately the same energy gap. Since the coherence length is much larger than the film thickness these features

are uniform throughout the film.

Tunneling probes the density of states within a few Fermi wavelengths of the surface. This is a fact that is usually assumed, but to the author's knowledge, is never addressed rigorously in the literature. The Fermi wavelength is involved due to the wave nature of the tunneling process. It is a common misconception that in superconducting tunneling the appropriate length scale involves the coherence length. The reason this is not the case is because the superconducting coherence factors drop out of the tunneling matrix element. In order to convince the reader of this point, a discussion of how this misconception arises will be given first.

Consider how superconductivity affects the results obtained using another *local* probe of the electronic system: the nuclear magnetic resonance (NMR) relaxation rate. The spin relaxation of the nuclear moment arises because the hyperfine interaction between electrons and the nucleus includes spin-flip terms of the form $I_+ s_-$. The hyperfine interaction is highly localized being associated with the nuclear region. In the superconductor, however, the scattering rate α_S is altered from that in the normal state α_N by the so called coherence factor.

$$\frac{\alpha_S}{\alpha_N} \sim (uu' - vv')^2$$

where

$$(uu' - vv')^2 = (1 + \frac{\Delta}{EE'})/2$$

The presence of the coherence factors give the scattering rate a unique temperature dependence which was important in substantiating the BCS theory. A discussion is given by Tinkham (section 2-9). For the purposes here, consider the case where the system is inhomogeneous. The coherence factor, which involves the energy gap, can vary only on length scales larger than the coherence length. In this sense the measurement of the NMR relaxation rate in a superconductor draws in information about the electronic system from a distance of the order of the coherence length whereas, in the normal state only the nuclear region is probed.

Thus one can understand the misconception that superconductivity will alter the distance probed by tunneling. However, the coherence factors divide out of the tunneling matrix elements(See Tinkham, section 2-8). Tinkham remarks, "...it appears on the face of it that the tunneling current will depend on the nature of the superconducting ground state as well as on the density of available excited states; but this turns out not to be true ...the characteristic coherence factors of the superconducting wavefunction, u_k and v_K, have dropped out". In the superconducting and normal states, tunneling probes only the density of states within a few Fermi wavelengths of the surface.

—The RKKY effect in superconductors—

The discussion so far has been restricted to the case where the tunneling was directed into the surface of the Aℓ film opposite the side covered with Gd. Since the thickness of the film is much smaller than the (Bulk) mean free path and the coherence

length, the Zeeman splitting and energy gap, respectively, are uniform throughout the film. However, in the normal state one expects a RKKY spin-polarization within a few Fermi wavelengths of the RE ions. Tunneling directed into the Gd/Aℓ surface serves as a probe of this localized feature of the density of states.

In terms of the infinite square well model presented above one can understand the RKKY effect in this planar geometry. As discussed the surface scattering events $k\uparrow \longrightarrow -k\uparrow$ are responsible for the energy shift between up and down spins $2\mu B_{ex} = cJS$. One might consider the resulting difference in the magnitude of the normal state DOS for the two spin directions $(2\mu B_{ex}/E_F)N_o$. This uniform polarization of the conduction electrons is the same as that considered by Zener (1951) for the bulk case. However, as shown by RKKY (1954-1957) the non-forward scattering ($k\uparrow \longrightarrow -k'\uparrow$) alters this result and in particular localizes the response (see section A.4). It is only recently that the RKKY interaction a metal surface has been considered theoretically. For example, Gumbs and Glasser (1986) use the infinite barrier model presented above. Also, Zheng and Lin (1987) consider the RKKY interaction at the surface of a semi-infinite rare earth metal.

Consider tunneling in a junction in the case that one electrode has spin-polarized itinerant electrons. The tunneling probability then differs for the two spin directions. As a result the conductance measured in an applied field is asymmetric with respect to zero bias voltage. The asymmetry has been measured for a number of 4f (Meservey, Paraskevopoulos, and Tedrow, 1980) and 3d (Meservey, Paraskevopoulos, and Tedrow, 1976; P.M. Tedrow and R. Meservey, 1973) metals from which it has been concluded that the degree of asymmetry is proportional to the magnetic moment of the itinerant electrons at the surface of the film.

In figure III.4.2 the conductance of an Aℓ -$A\ell_2O_3$-Gd/Aℓ junction is shown for two values of the applied field. In curve a, the applied field is below the critical field of both electrodes. No asymmetry is observed. In the case of $S_1 - I - S_2$ tunneling, the conductance is split by the difference $2\mu B_{ex}$ in the Zeeman splitting of electrons in the top and bottom electrodes. The curve b was taken above the critical field of the top electrode. The bottom electrode remains superconducting but the spin states are Zeeman split by the applied magnetic field $2\mu B = 0.41$ meV. The conductance is asymmetric indicating a 2.9±0.6% polarization of the itinerant electrons in the (normal state) top electrode. This is the expected order of magnitude considering that the polarization observed in Gd metal is $\sim 13\%$ and the sample has $\sim 1/3$ atomic layer coverage of Gd. The asymmetry is a large effect in comparison to other features routinely measured by tunneling, for instance, those due to phonons.

The fact that the conductance is symmetric in the case where the top electrode is superconducting demonstrates the lack of a RKKY response in the superconductor. The important difference between the superconducting and normal states is that the long range part of the response function (i.e. susceptibility) is significantly depressed in the superconductor. One understands this simply in terms of the singlet pairing of the superconductor. From figure I.2.3 one observes that the response for length scales greater than $Q_o^{-1} \sim (k_F^{-2}\xi_o)^{1/3}$ is suppressed. Specifically, the lack of a uniform (i.e. $q = 0$) response is responsible for the absence of Pauli paramagnetism in BCS

superconductors. This latter fact in $A\ell$ has been verified in Knight shift experiments, but only after a series of conflicting experimental results (Hammond and Kelly, 1967; Fine, Lipsicas, and Strongin, 1969; Meservey, Tedrow, and Bruno, 1975). The result presented here represents the first evidence for the lack of the q-dependent response associated with the RKKY effect in superconductors.

For curve b in figure III.4.2, where the polarization is observed, one may attempt to construct a more detailed physical picture of the tunneling process. Since the RKKY spin-polarization is not uniform, but oscillatory, one may consider whether 1) the tunneling electron sees an average DOS's or 2) if different electrons see different DOS's depending on the closeness to the Gd atom. The question is probably more meaningful if rephrased as follows: what is the minimum length scale over which the tunneling process will average the density of states in the plane of the junction. Considering the images produced by the scanning tunneling microscope (STM), this length scale is at least on the order of a few angstroms and uncertainty principle arguments suggest the Fermi wavelength. However, it is important to note that the tunneling results reported here are not sensitive to this length scale. No matter what this scale is, the polarization observed in the tunnel conductance is the average of the polarization. This is because of the additivity of conductances in parallel. Consider the case where the averaging length scale is of the order of the Fermi wavelength and where the polarization $P(\vec{r})$ is a function of position. The measured conductance for a bias voltage E is given by

$$\sigma(E) = \frac{1}{A}\int d\vec{r}\left[\left(\frac{1+P(\vec{r})}{2}\right)f(E-\mu B_{int}) + \left(\frac{1-P(\vec{r})}{2}\right)f(-E-\mu B_{int})\right]$$

$$= \left(\frac{1+\overline{P}}{2}\right)f(E-\mu B_{int}) + \left(\frac{1-\overline{P}}{2}\right)f(-E-\mu B_{int})$$

where $\overline{P} = (1/A)\int d\vec{r}P(\vec{r})$ is the average polarization over the area of the junction. Here the internal field B_{int} is taken as a constant. The functions $f(\pm E - \mu B_{int})$ are the spin-up (+) and spin-down (−) contributions to the total conductance $\sigma(E)$ for $P = 0$. Thus, the polarization obtained from the conductance of a planar junction is the areal average $\overline{P}$.

The local polarization $P(\vec{r})$ may possibly be measured in a spin-polarized scanning tunneling microscope such as that proposed by Tedrow and Meservey. Such a device would combine the STM with the spin-polarized tunneling techniques developed by these researchers and used throughout this thesis. A first step toward a SPSTM is the observation of spin-polarized tunneling in a tunnel junction with a mechanically adjustable tunnel barrier. A device for such has been constructed suitable for ^{3}He cryogenics and large magnetic fields. Operation of this device, including spin-polarized tunneling, have been reported at the 18th International Conference on Low Temperature Physics (Tkaczyk and Tedrow, 1987). A copy this paper along with a description of this device and the first observation of spin-polarized tunneling using a mechanically adjustable tunnel barrier are given in appendix C.

—The influence of spin-orbit scattering—

Tedrow and Meservey have experimentally demonstrated the effect of a Pt surface layer on the critical field (1979) and the DOS (1982) of thin Aℓ films. They conclude that the Pt layer is a very effective at introducing spin-orbit scattering. The spin-orbit scattering rate $\hbar/\tau_{so} = 3\Delta b_F$ is found to increase by 1.6 meV for each 1$\AA$ of Pt. A deposited layer of 1$\AA$ of Pt is equivalent to a coverage of 6.6 atoms/nm^2. Note that the scattering rate $\hbar/\tau_{so} = 1.6meV$ is large in the sense that in order to resolve the Zeeman splitting $2\mu B$ the field B must be of the order $\sim 1.6meV/2\mu_B = 13.8$ tesla.

A junction of the form Aℓ -$A\ell_2O_3$-Aℓ /Pt was prepared with 40$\AA$ Aℓ films and a Pt thickness of 4$\AA$ which corresponds to approximately 2 monolayers. The electron spin states of the top electrode can be considered to be well mixed. That is the Zeeman splitting will not be resolved for fields less than $\sim$ 55 tesla. The conductance in an applied magnetic field of B=2.12 tesla is shown in figure III.4.3. Both electrodes are superconducting and the sum-gap peak is split as is characteristic of S-I-S tunneling when the Zeeman splitting of the electrons in the two electrodes is not equal. In fact the energy splitting observed corresponds to the Zeeman splitting of the bottom Aℓ film appropriate for the applied field $2\mu B$ = 0.25 meV. One concludes that the Zeeman splitting of the top electrode is not resolved due to spin mixing.

An important point to make is that the Pauli principle restricts spin-orbit scattering to states within k_BT of the Fermi level. Therefore, most electron states are still spin split by the Zeeman interaction due to the applied magnetic field or the uniform exchange field. Only those states at the Fermi surface are spin mixed. As a result the RKKY spin-polarization of the conduction electrons in the normal state is essentially unaffected by spin-orbit scattering. This is shown in figure III.4.4 where the conductance for a Aℓ -$A\ell_2O_3$ – $(3nm^{-2})$Gd/Aℓ /Pt is shown for an applied field of B=3.33T. This junction is from the same sample set as that for the junction used for figure III.4.3 and was made at the same time in the same way (except for the Gd deposition). For this value of the applied magnetic field, the top electrode is normal. The Zeeman splitting of the bottom electrode is observed along with an asymmetry corresponding to a polarization of P=4.1±0.6% of the top electrode. This polarization is somewhat larger than that observed in the case without Pt (P=2.9±0.6%, figure III.4.2), but is consistent with the $\sim$ 20 % error resulting from taking the data on the scale where the whole conductance curve fits on one page. For a more quantitative study, these errors could be substantially decreased by measuring the peak heights separately.

In another sense, the data show that the spin-relaxation introduced by the spin-orbit scattering greatly effects the spin response of the normal state. For if there was no spin relaxation at the Fermi surface there would be no way for spin-up electrons to change into spin-down electrons when the applied magnetic field made it energetically favorable to do so. The system would be kinetically limited from reaching thermal equilibrium and there would be no Pauli paramagnetism. This lack of states at the Fermi level which will flip there spin is exactly the case for the BCS superconductor. In the superconductor, such a spin-flip would cost significant potential energy associated with the coherent electron-electron scattering in superconductors (see section I.2). In

this sense the lack of the Pauli paramagnetism in superconductors is analogous to the lack of (DC) resistance. However, the analogy suffers, for example, in the case of gapless superconductivity. For the gapless state there are single particle excitations at the Fermi level which undergo spin and momentum relaxation. The spin relaxation results in a non-zero spin susceptibility; but, the DC conductivity remains zero due to the fact that the superconducting electrons "short out" the resistive single particle excitations.

The q-dependent susceptibility of a superconductor with spin-orbit and exchange scattering contributions has been worked out by Kaufman and Entin-Wohlman (1976). With the introduction of sufficient spin-orbit scattering

$$\hbar/\tau_{so} \sim 3\Delta,\ b_F = \hbar/3\Delta_o\tau_{so} \sim 1,$$

the spin susceptibility of the superconductor can be of the order of that in the normal state(see review by Fulde and Keller, 1982). In such a case one would expect the presence of a Pauli paramagnetic response to an applied magnetic field and the RKKY response to a local exchange potential. The Knight shift measurements in the heavy element superconductor Hg(Reif, 1967) demonstrates the former. The latter fact is demonstrated for the first time in figure III.4.5 for the same junction used for figure III.4.4 (Aℓ -$A\ell_2O_3$-Gd/Aℓ/Pt). The conductance is shown in an applied field B = 2.12 Γ for which both electrodes are superconducting. This is the same field used in figure III.4.3 where the conductance of the control junction (i.e. no Gd) is shown. The features associated with S-I-S tunneling are displayed (e.g. the difference gap) along with asymmetry associated with a polarization of P=3.3±0.6% in the *superconducting* Gd/Aℓ/Pt electrode. This is of the order of that in the normal state (P=4.1±0.6%, fig. III.4.4) and close to the value in the normal state but without Pt (P=2.9±0.6%, fig. III.4.2).

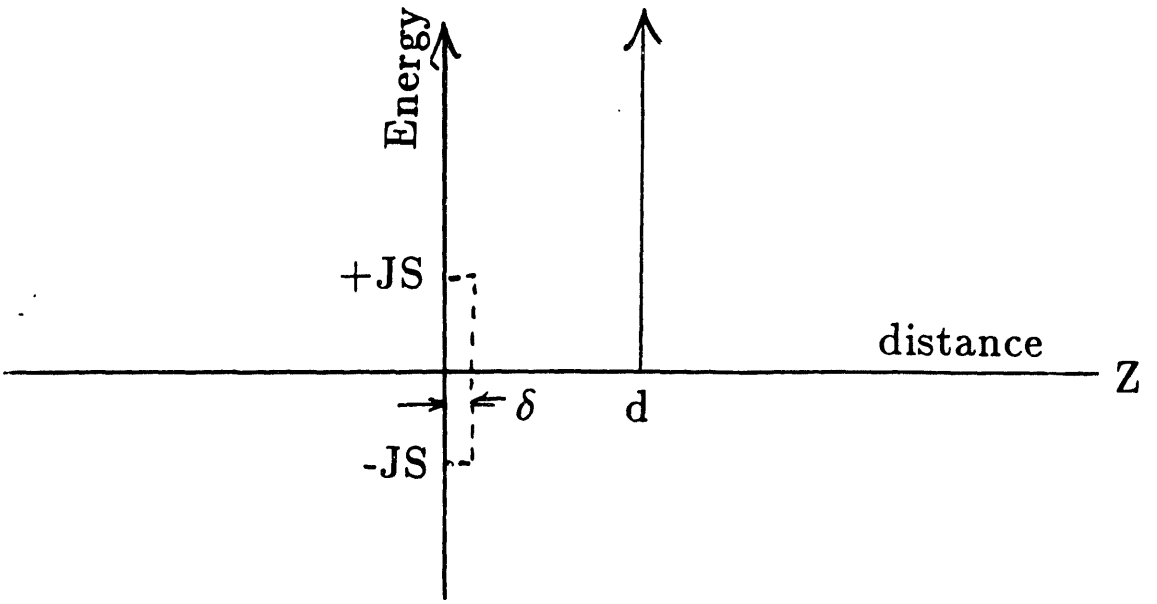

Fig. III.4.1 A schematic representation of an Aℓ film with a spin-dependent potential at the surface. $H_{ex} = -J\vec{S}_i \cdot \vec{s}$.

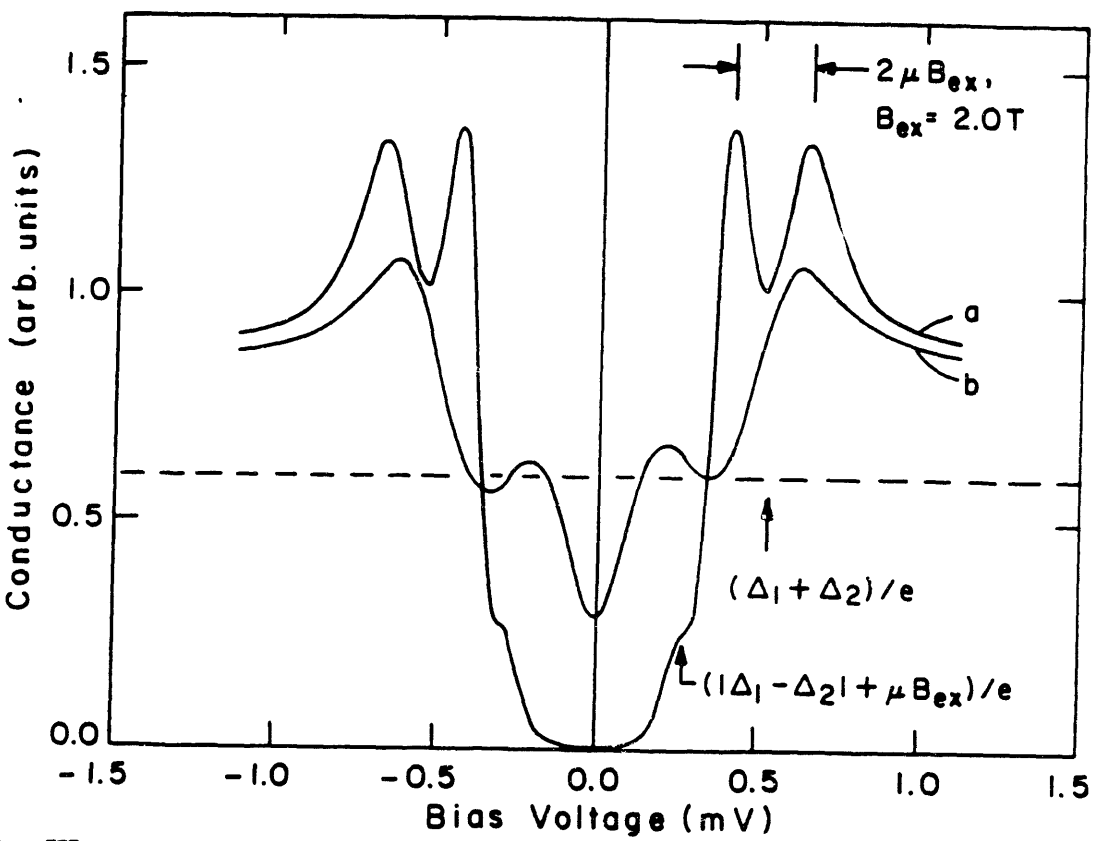

Fig. III.4.2 The conductance of an $A\ell - A\ell_2O_3 - Gd(3nm^{-2})/A\ell$ junction measured in an applied magnetic field for which the top electrode (Gd/Aℓ) is (a) superconducting $B = 0.17$T, and (b) normal $B = 3.72$T.

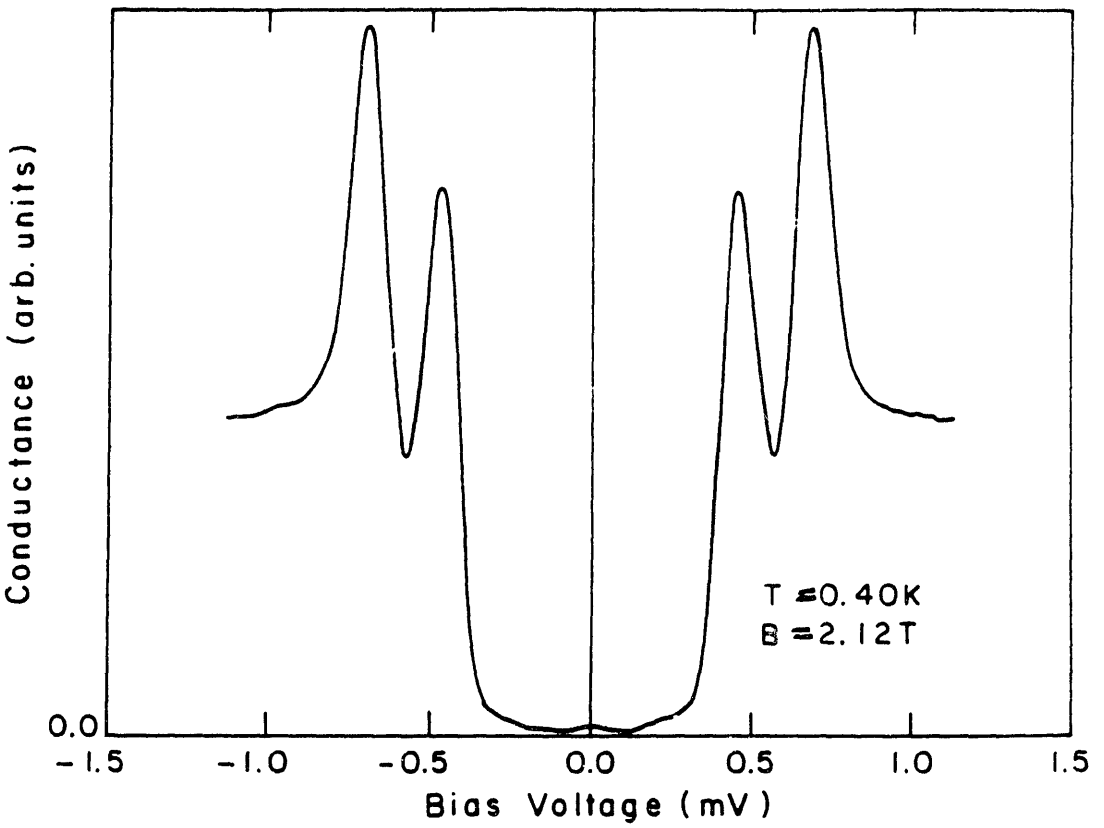

Fig. III.4.3 The conductance of an $A\ell - A\ell_2O_3 - A\ell/Pt$ junction where the 2 monolayers of Pt mixes the spin-states of the top electrode. The voltage splitting in the sum gap peak corresponds to the Zeeman splitting of electrons in the bottom electrode $2\mu B = 0.25$meV.

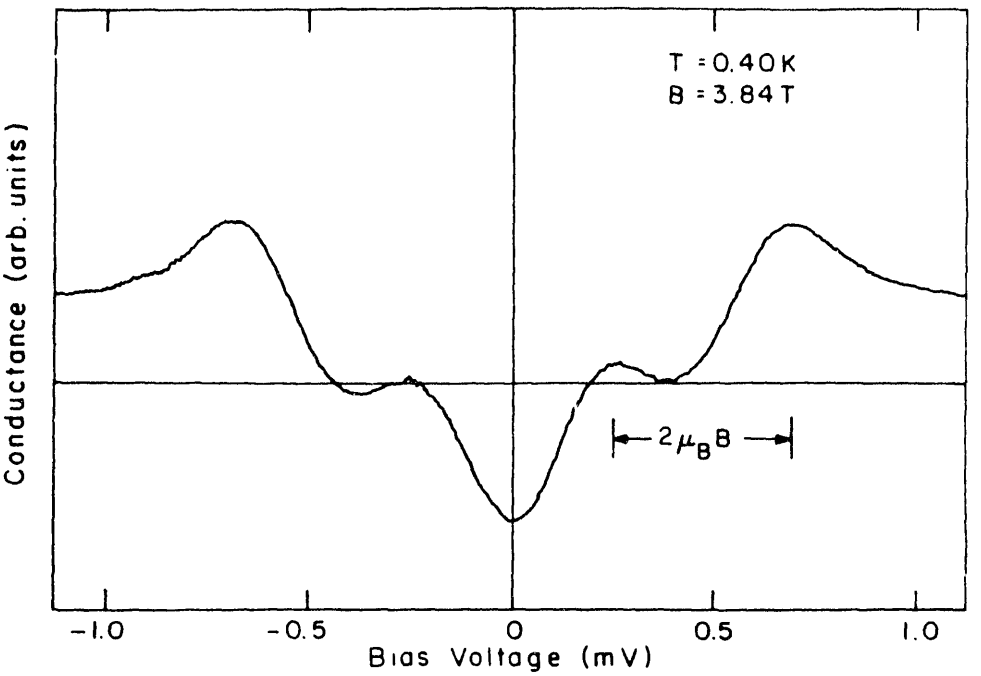

Fig. III.4.4 The conductance of an $Al-Al_2O_3-Gd/Al/Pt$ junction measured in a field where the top electrode is normal. The conductance of the corresponding control junction (i.e. no Gd) is shown in figure III.4.3.

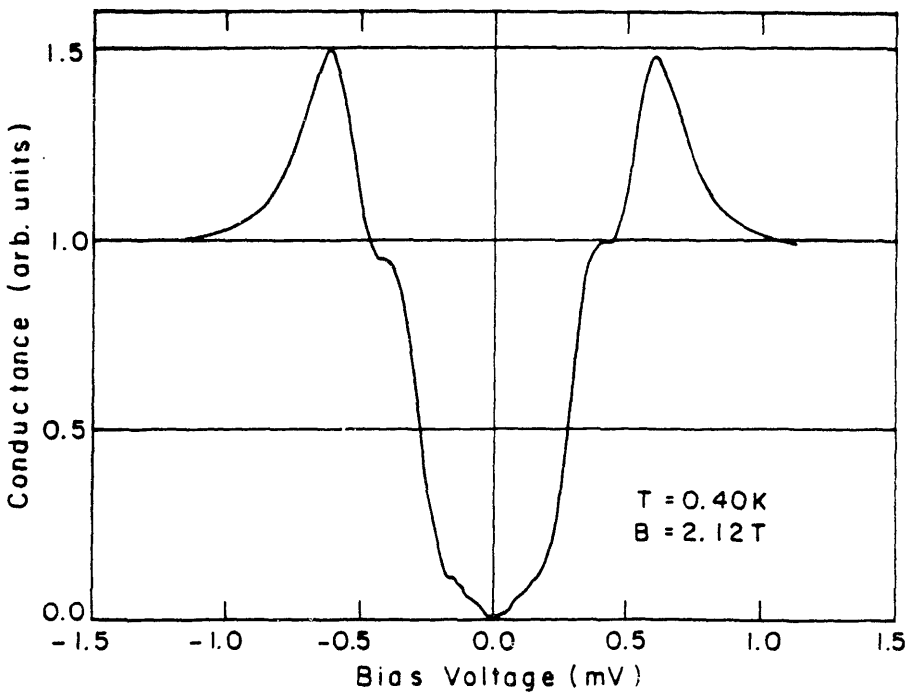

Fig. III.4.5 The conductance of the same junction used in figure III.4.4 but in a lower magnetic field for which the top electrode is superconducting.

Table III—1 Rare Earth Oxides

REO	Sample	Comments	B^*_{sat} (tesla)	REO	Sample	Comments	B^*_{sat} (tesla)
Ce	6109		0(a)	Gd	5890		2.54
	6117		0		5963	75Å $A\ell$ (d)	1.47
	6133	in air (b)	0		5963	100Å $A\ell$ (d)	1.11
Pr	6159		0		5974		2.27
Sm	6069		0		5987	(f)	3.4
	6262		0(a)		6079	1Å Gd (c)	2.47
Eu	5833		1.29		6079	3Å Gd (c)	2.43
	5854		0.84		6131	powder (e)	1.46
	5874		1.12	Tb	5914		0.35
	5883		1.96	Dy	5956		0.74
	5891	10Å Eu (c)	0.78		6253		0.91
	5891	25Å Eu (c)	0.87	Ho	5905		0.08
EuS	6308	sulfide (g)	1.2		6024		0.18
					6039	in air (b)	0.45
				Er	5965		0.20
					6259		0.28
				Tm	5952		0

The saturation value of a number of REO/Aℓ bilayers is shown. Unless indicated otherwise, the REO was formed by depositing 50Å of the RE and oxidizing in a DC oxygen plasma, and the Aℓ film thickness before forming the tunnel barrier was 40Å.

a) $B^* \sim 0$ and significant spin-orbit scattering present.
b) oxidized in an air glow discharge
c) RE film thickness before oxidation
d) Aℓ film thickness
e) REO powder evaporated from a W boat
f) This film is clearly depaired due to exchange scattering.
g) EuS powder evaporated from a W boat, no oxidation.

Table III—2 Depairing of Zero Field Conductance

RE	Sample	Thickness (Å)	PP0[a]	$T_{co}(K)$	$T_c(K)$ (AG theory)	τ_{PB}^{-1} $(10^{10} sec^{-1})$	$T_c(K)$ (resistive)
Ce	6113	1.26(4)	0.85(2)	2.80(5)	0.38	31.15	
Ce	6118	0.59(6)	0.70	2.90	1.05	26.60	
	6118	none	0.16	2.85	2.48	5.97	
Ce	6267	0.60(33)	0.71	2.80	0.98	26.04	
	6267	none	0.19	2.80	2.37	6.96	
Sm	6233	0.95(5)	0.29	2.80	2.14	10.06	
	6233	none	0.22	2.65	2.18	7.63	
Sm	6284	0.73(3)	0.33	2.60	1.89	11.24	
	6284	none	0.12	2.60	2.35	4.08	
Eu	6227	2.00(5)	0.20	2.80	2.35	7.33	
Eu	6227	5.02(12)	0.24	2.80	2.25	8.80	
Gd	6003	1.00(2)	0.56	2.25	1.16	16.50	
	6003	none	0.20	2.40	2.02	6.13	
Gd	6155	0.96(5)(b)	0.42	2.20	1.42	12.09	
Gd	6266	0.99(3)(b)	0.62	2.50	1.13	20.28	
	6266	none(b)	0.12	2.60	2.35	4.08	
Gd	6310	1.00(3)(b)	0.41	2.40	1.58(5)	12.88(59)	1.52(5)
Gd	6310	0.66(2)(b)	0.30	2.50	1.88(6)	9.82(52)	1.90(2)
Gd	6310	0.33(1)(b)	0.18	2.35	2.01(6)	5.54(42)	2.00(2)
	6310	none(b)	0.050	2.35	2.26(6)	1.54(34)	2.27(2)
Tb	6230	0.98(5)	0.76	2.65	0.76	26.46	
	6230	none	0.13	2.65	2.37	4.52	
Tb	6272	1.02(5)	0.37	2.45	1.70	11.86	
	6272	none	0.14	2.45	2.18	4.49	
Dy	6229	0.99(5)	0.28	2.55	1.97	9.35	
	6229	none	0.20	2.70	2.26	7.09	
Ho	6226	3.01(8)	0.40	2.80	1.86	14.66	
Ho	6226	5.24(12)	0.75	2.80	0.84	27.47	
Er	6232	2.57(13)	0.27	3.0(2)	2.34	10.60	
	6232	none	0.21	3.0(2)	2.49	8.24	

continued ...

Table III—2 (Continued)

RE	Sample	Thickness (Å)	PP0[a]	$T_{co}(K)$	$T_c(K)$ (AG theory)	τ_{PB}^{-1} ($10^{10} sec^{-1}$)	$T_c(K)$ (resistive)
Rare earth oxides							
EuO	5854	50	0.11	2.60	2.37	3.74	
	5854	none	0.09	2.60	2.41	3.06	
EuO	5874	50	0.10	2.70	2.49	3.53	
	5874	none	0.09	2.60	2.41	3.06	
Gd_2O_3	5890	50	0.25	2.55	2.03	8.35	
Gd_2O_3	5974	50	0.22	2.55	2.10	7.34	
Gd_2O_3	5987	50	0.30	2.75	2.07	10.80	
Gd_2O_3	6079	1	0.23	2.55	2.07	7.67	
Metals between two 20Å $A\ell$ films							
Eu	6320L	1.00(3)	0.30	3.20	2.41	12.56	
Eu	6320K	0.66(2)	0.23	3.20	2.60	9.63	
	6320	none	0.09	3.05	2.83	3.59	
Gd	6321	0.13(1)[b]	0.28	2.75	2.12	10.10	

The conductance in zero field was fit with the AG theory to obtain the scattering rate and transition temperature. In sample set 6310 the transiton temperature was also obtained from the resistance verses temperature curve. Unless otherwise indicated, the junctions were formed with Fe counterelectrodes (i.e. RE/Aℓ -Aℓ_2O_3 - Fe).

a) $PP0 = \hbar/\tau_{PB} k_B T_{co} = (\pi T_c/T_{co})\rho_{AG}$

b) Ag counterelectrodes

Table III—3 Rare Earth Submomolayers

RE	Sample	$c^{(a)}$	τ_{ex}^{-1} $(10^{10} sec^{-1})$	$\lvert J^{(b)} \rvert$ (meV)	B^*_{sat} (T)	$J^{(c)}$ (meV)
Ce	6113	0.0199	25.2	163.7		
	6118	0.0093	20.6	216.5		
	6267	0.0095	19.1	206.3		
Pr	6174	0.0081	none			
Sm	6233	0.0157	2.4	11.1	3.3(e)	-13.5
	6284	0.0121	7.2	21.8		
Eu[d]	6227	0.0228	1.0	3.6	1.4	2.4
	6227	0.0573	2.5	3.6	5.1(e)	3.4
	6091	0.0114	none		0.45	1.5
Gd	6003	0.0166	10.4	12.0		
	6155	0.0160	6.0	9.3		
	6266	0.0164	16.2	15.1		
	6310	0.0166(12)	11.3(7)	12.5(6)	8.1(12)(e)	16.1(12)
	6310	0.0110(8)	8.3(6)	13.2(8)	5.1(7)(e)	15.3(23)
	6310	0.0055(4)	4.0(5)	12.9(9)	3.5(5)	21.0(33)
Tb	6230	0.0168	21.9	21.2		
	6272	0.0175	7.4	12.1	3.5(e)	7.7
Dy	6229	0.0172	2.3	8.4	2.5	6.8
Ho	6226	0.0531	8.7	11.5	4.3(e)	4.7
	6226	0.0925	21.5	13.7		
Er	6232	0.0461	2.4	8.6		
Metals between two 20Å $A\ell$ films						
Eu	6320	0.0068	6.04	16.4	5.4(e)	30.6
	6320	0.0114	8.97	15.4	7.3(e)	24.7
Gd	6321	0.0022	6.51	26.1	2.5	37.6

a) $c = \frac{d_{RE}}{30A} \frac{\rho_{RE}}{2.7g/cc} \frac{26.79}{MW_{RE}}$

b) $J^2 = (3.63 \cdot 10^{-10}(meV)^2 sec)/c\tau_{ex} I(I+1)(g_L - 1)^2$, where $I = |\vec{S} + \vec{L}|$.

c) $J = B^*_{sat}/c(8.64T/meV)I(g_L - 1)$

d) For Eu, $I \to 3, (g_L - 1) \to 1$.

e) The B^* verses B curve was extrapolated with a Brilliuon function to estimate the saturation value of B^*.

Table III—4 Trivalent Rare Earth Ions

RE	S	L	I= $\lvert\vec{S}+\vec{L}\rvert$	I(I+1)	$(g_L - 1)$	density (g/cc)	molecular weight
Ce	0.5	3.0	2.5	8.75	-0.14	6.70	140.12
Pr	1.0	5.0	4.0	20.0	-0.20	6.77	140.91
Nd	1.5	6.0	4.5	24.75	-0.27	7.01	144.24
Sm	2.5	5.0	2.5	8.75	-0.72	7.52	150.35
Eu	3.0	3.0	0.0	0.0		5.24	151.96
Gd	3.5	0.0	3.5	15.75	1.00	7.9	157.25
Tb	3.0	3.0	6.0	42.0	0.50	8.23	158.92
Dy	2.5	5.0	7.5	63.75	0.33	8.55	162.50
Ho	2.0	6.0	8.0	72.0	0.25	8.80	164.93
Er	1.5	6.0	7.5	63.75	0.20	9.07	167.26
Tm	1.0	5.0	6.0	42.0	0.17	9.32	168.93

$g_L = 3/2 + [S(S+1) - L(L+1)]/2I(I+1)$

Abrikosov, A.A., and L.P. Gor'kov, Zh.Eksperim. i Teor. Fiz. **39**,1781 (1960); Sov.Phys. JETP **12**,1243 (1961).

Alexander, J.A.X., T.P. Orlando, D. Rainer, and P.M. Tedrow, Phys. Rev. B, **31**, 5811 (1985).

Alexander, J.A.X., (unpublished), Thesis at MIT (1986).

Anderson, P.W., J.Phys.Chem.Sol. **11**,26 (1959).

Anderson, P.W., and H. Suhl, Phys. Rev. **116**, 898 (1959).

Anderson, P.W., Phys. Rev. Lett. **55**, 1805 (1985); and the following reply to this comment (p. 1807).

Aoi, K., R. Meservey, and P.M. Tedrow, Phys. Rev. B, **9**, 875 (1974).

Ashauer, B., G. Kieselmann and D. Rainer, J.Low Temp. Physics, **63**, 349 (1986).

Bauriedl, W., P. Ziemann, and W. Buckel, Phys.Rev.Lett. **47**, 1163 (1981).

Brandt, N.B., and V.V. Moshchalkov, Adv.Phys. **33**, 373 (1984).

Bruno, R.C., and B.B. Schwartz, Phys.Rev. B **8**, 3161 (1973).

Buchholtz, L.J., and G. Zwicknagl, Phys. Rev. B **23**, 5788 (1981).

Bulaevskii, L.N., A.I. Buzdin, S.V. Panjukov, and M.L. Kulic', Phys.Rev. B **28** 1370 (1983).

Bulaevskii, L.N., A.I. Buzdin, and M. Kulic, Rapid Comm. **34**, 4928 (1986).

Cooper, L.N., Phys.Rev.Lett. **6**,689 (1961).

Corruccini, R.J., and J.J. Gniewek, in *Handbook of Physics and Chemistry*, edited by R.C. Weast, (CRC Press Inc., Cleveland, 1976), p. D-169.

Davidov, D., K. Maki, R. Orbach, C. Rettori, and E.P. Chock, Solid State Commu. **12**, 621 (1973).

DeGennes, P.G., Phys. Lett. **23**, 10 (1966).

DeWeert, M.J., and G.B. Arnold, Phys.Rev.Lett. **55**, 1522 (1985).

Dynes, R.C., V. Narayanamurti, and J.P. Garno, Phys. Rev. Lett. **41**, 1509 (1978).

Dynes, R.C., J.P. Garno, G.B. Hertel, and T.P. Orlando, Phys. Rev. Lett. **53**, 2437 (1984).

Falkovsky, L.A., Adv. Phys. **32**, 753 (1983).

Feder, R., editor, *Polarized Electrons in Surface Physics*, (World Scientific Publishing Co., Singapore, 1985).

Fine, H.L., M. Lipsicas, and M. Strongin, Phys. Lett. **29**, A366 (1969).

Fischer, Ø., H.W. Meul, M.G. Karkut, G. Remenyi, U. Welp, J.C. Piccoche, and K. Maki, Phys.Rev.Lett. **55**, 2972 (1985).

Fulde, P., and J. Keller, in *Superconductivity in Ternary Compounds II*, edited by Ø. Fischer and M.B. Maple, (Springer-Verlag, NY, 1982).

Fulde, P., J. Keller, and G. Zwicknagl, Solid State Phys. (April, 1987).

Garcia-Moliner, F., and F. Flores, *Introduction to the theory of solid surfaces*, (Cambridge University Press, NY, 1979).

Gor'kov, L.P., and A.I. Rusinov, Zh. Eksperim. i Teor. Fiz. **46**, 1363 (1964) [trans. Soviet Phys. JETP **19**, 922 (1964)].

Gumbs, G., M.L. Glasser, Phys. Rev. B **33**, 6739 (1986).

Hauser, J.J., H.C. Theuerer, and N.R. Werthamer, Phys. Rev. **142**, 118 (1966).

Herring, C., Physica **24**, S184 (1958).
Hammond, R.H., and G.M. Kelly, Phys. Rev. Lett. **18**, 156 (1967).
Jaccarino, V., B.T. Matthias, M. Peter, H. Suhl, and J.W. Wernick, Phys. Rev. Lett. **5**, 251 (1960).
Jaccarino, V., and M. Peter, Phys.Rev.Lett. **9**, 290 (1962).
Kaufman, M., and O. Entin-Wohlman, Physica **84B**, 77 (1976).
Keller, J., and R. Benda, J.Low Temp. Phys. **2**, 141 (1970).
Lang, N.D., and W. Kohn, Phys. Rev. B **1**, 4555 (1970).
Lee, B.W., J.M. Ferreira, Y. Dalichaouch, M.S. Torikachvili, K.M. Yang, and M.B. Maple, Phys.Rev.B., **37**, 2368 (1988).
Lee, P.A., T.M. Rice, J.W. Serene, L.J. Sham, and J.W. Wilkins, Comments on Cond.Mat. Phys., **12** , 99 (1986).
Li, J., C. Gong, A. Holz, Phys. Rev. B, **36**, 5230 (1987).
Lin, C.L., J. Teeter, J.E. Crow, T. Mihalisin, J. Brooks, A.I. Abou-Aly, and G.R. Stewart, Phys.Rev.Lett. **54**, 2541 (1985).
Lynn, J.W., J.A. Gotass, R.W. Erwin, R.A. Ferrell, J.K. Bhattacharjee, R.N. Shelton and P. Klavins, Phys.Rev.Lett. **52**, 133 (1984).
Maple, M.B., Solid State Comm., **8**, 1915 (1970).
Maple, M.B., Appl.Phys. **9**, 179 (1976).
Maple, M.B., Ø. Fischer, editors, *Superconductivity in Ternary Compounds*, Vol. I and II, (Springer-Verlag, NY, 1982).
Maple, M.B., in *Moment Formation in Solids*, Edited by W.J.L. Buyers, (Plenum Press, NY, 1984).
Maple, M.B., Physics Today **39**, 72 (March, 1986).
Massenet, O., Y. Capiomont, and N. Van Dang, J. Appl. Phys., **45**, 3593 (1974).
Matthias, B.T., H. Suhl, E. Corenzwit, Phys.Rev.Lett. **1**, 92 (1958).
Mauger, A., and C. Godart, Phys. Reports **141**, 51 (1986).
Meservey, R., P.M. Tedrow, and R.C. Bruno, Phys. Rev. B **11**, 4224 (1975).
Meservey, R., D. Paraskevopoulos, and P.M. Tedrow, Phys. Rev. Lett. **37**, 858 (1976).
Meservey, R., D. Paraskevopoulos, and P.M. Tedrow, Phys. Rev. B **22**, 1331 (1980).
Meul, H.W., C. Rossel, M. DeCroux, Ø. Fischer, G. Remanyi, and A. Briggs, Phys.Rev.Lett. **53**, 497 (1984).
Millis, A., D. Rainer, and J.A. Sauls, Phys.Rev B, (Aug. 1 1988).
Moncton, D.E., D.B. McWhan, P.H. Schmidt, G. Shirane, W. Thomlinson, M.B. Maple, H.B. MacKay, L.D. Woolf, Z. Fisk, and D.C. Johnston, Phys.Rev.Lett. **45**,2060 (1980).
Moodera, J.S., X. Hao, G. Gibson, and R. Meservey, submitted PRL (1988).
Müller-Hartmann E., J. Zittartz, Phys.Rev.Lett. **26**,428 (1971); E. Müller-Hartmann, in *Magnetism*, vol. 5, edited by H. Suhl, (Academic Press, NY, 1973).
Penney, T., M.W. Shafer, and J.B. Torrance, Phys. Rev. B **5**, 3669 (1972).
Reif, F., Phys. Rev. **106**, 208 (1967).
Ruderman, M. A., and C. Kittel, Phys.Rev. **96**, 99 (1954); T. Kasuya, Prog.Theo.Phys. Japan, **16**, 45 (1956); K. Yosida, Phys.Rev. **106**, 893 (1957).
Rusinov, A.I., Sov.Phys.JETP **29**, 1101 (1969).

Schachinger, E., J.M. Daams, and J.P. Carbotte, Phys. Rev. B **22**, 3194 (1980).
Schlottmann, P., Phys. Rev. B **26**, 558 (1982).
Shapira, Y., S. Foner, R.L. Aggarwal, and T.B. Reed, Phys. Rev. B **8**, 2316 (1973).
Shirane, G., Y. Endoh, R.J. Birgeneau, M.A. Kastner, Y. Hidaka, M. Oda, M. Suzuki, and T. Murakami, Phys. Rev. B **59**, 1613 (1987).
Sinha, S.K., G.W. Crabtree, D.G. Hinks, and H. Mook, Phys.Rev.Lett. **48**, 950 (1982).
Stageberg, F., R. Cantor, A.M. Goldman, and G.B. Arnold, Phys.Rev B, **32**, 3292 (1985).
Stewart, G.R., Rev.Mod.Phys. **56**, 755 (1984).
Sugawara, T., and H. Eguchi, J.Phys. Soc. Japan, **21**, 725 (1966).
Sugawara, T., and H. Eguchi, J.Phys. Soc. Japan, **23**, 965 (1967).
Suhl, H., and B.T. Matthias, Phys.Rev. **114**, 977 (1959).
Taylor, K.N.R., and M.I. Darby, *Physics of Rare Earth Solids*, (Chapman & Hall LTD, London, 1972).
Tedrow, P.M., and R. Meservey, Phys. Rev. B **7**, 318 (1973).
Tedrow, P.M., and R. Meservey, Phys. Rev. Lett. **43**, 384 (1979).
Tedrow, P.M., and R. Meservey, Phys. Rev. B **25**, 171 (1982).
Tedrow, P.M., J.S. Moodera and R. Meservey, Solid State Comm. **44**, 587 (1982).
Tedrow, P.M., J.E. Tkaczyk, and A. Kumar, Phys.Rev.Lett. **56**,1746 (1986).
Tkaczyk, J.E., J.J. Appl. Phys. **26**, 1559 (1987).
Tkaczyk, J.E., and P.M. Tedrow, J.Appl.Phys. **61**,3368 (1987); IEEE Trans. Mag. **23**, 945 (1987).
Tokuyasu, T., J.A. Sauls, and D. Rainer, preprint (1988).
Woolf, M.A., and F. Reif, Phys.Rev. **137**, A557 (1965).
Tsang, J.K., D.M. Ginsberg, Phys.Rev. B **22**, 4280 (1980).
Wong, H.K., and J.B. Ketterson, J. Low Temp. Phys. **63**, 139 (1986).
Zener, C., Phys. Rev. **81**, 440 (1951).
Zheng, H., and D.L. Lin, Phys. Rev. B, **36**, 2204 (1987).

Chapter IV — Spin-Orbit Scattering

The scattering of conduction electrons from impurities, defects and surfaces is accompanied by a rotation in the electron spin due to the spin-orbit interaction. This spin-orbit scattering has a characteristic effect on the critical magnetic field and density of states (DOS) of a Pauli-limited superconductor. A fit of the theory to measurements of the critical field and DOS yields the spin-orbit scattering rate of the conduction electron states. Pauli limiting is the condition in which the critical field is sufficiently large such that the Zeeman energy $2\mu B$ is greater than the spin relaxation rate and is also of the order of the superconducting energy gap. It is in this limit that one expects spin effects to be important.

From straight-forward considerations (see section A.3) one expects a rapid increase in spin-orbit scattering as a function of atomic number Z. This is presumably the reason that V_3Ga and $A\ell$ have a small value of the spin-orbit scattering rate. In the following, bulk impurities or surface layers of high Z elements are added in an attempt to study their effect on the spin-orbit scattering rate. Previous experimental results suggest that, for s-p metals like Li, Na, and $A\ell$, the spin-orbit scattering increases approximately as Z^4 where Z is the atomic number of the impurity or surface layer. However, for V_3Ga no increase in the spin-orbit scattering rate was observed with the doping. This suggests that the conduction electron states of this d-band metal do not reach the core region of the impurity where the spin-orbit interaction makes its largest contribution.

IV.1 The Present Understanding of Spin-Orbit Scattering

Spin-orbit scattering enters phenomenologically into the theories of superconductivity, localization, and conduction electron spin resonance (CESR). The phenomenological parameter is usually either the scattering rate $\hbar/\tau_{so}$ or the spin-flip probability ε at a surface. For example, Dyson remarks (1955, p. 350), "we do not introduce the spin-orbit coupling explicitly, but we assume a relaxation-time U ... and a probability $[1 - exp(-t/U)]$ that the final spin state will be randomly distributed relative to the initial spin state." In the absence of theoretical calculations of $\hbar/\tau_{so}$ or ε for model systems, the analysis of a wide variety of experimental results has suffered. In particular, an understanding of the scattering rate for different elemental impurities in s-p and d band metals is lacking, as is an understanding of variety of surface and interface relaxation times (Eigler and Schultz, 1982).

The Pauli paramagnetic response of a normal metal to an applied magnetic field does not occur instantaneously but is limited by the spin relaxation time, T_1, of the electron spins. A closely related time T_2 is the inverse width at half maximum of the spin resonance line. Possibly the first interest in mechanisms responsible for electron spin relaxation in metals was generated by the difficulty in observing the conduction electron spin resonance (Griswold, Kip, Kittel, 1952; Feher and Kip, 1955). Overhauser (1953) listed several possible mechanisms, and Elliott (1954) considered effects due to spin-orbit interaction in more detail. However, they considered plane wave matrix elements of the spin-orbit interaction in calculating the scattering amplitude and concluded that spin-orbit scattering makes a negligible contribution to spin relaxation at low temperature. Experiments of Feher and Kip (1955) were the first to suggest

that spin-orbit scattering from impurities (and defects) does make a major contribution to T_2^{-1}. They showed that the (temperature independent) resonance width T_2^{-1} in Li increased with the impurity content. Subsequently, Pines and Slichter (1955) used atomic matrix elements to give an upper bound on the spin-orbit scattering rate.

Surface scattering effects on the resonance width were worked out by Dyson (1955) and Walker (1971) who introduced the probability ε that a surface scattering event will result in a spin-flip. In particular, for samples with dimensions small compared with the skin depth, the surface scattering contribution to the linewidth is $T_s^{-1} = 4V/\varepsilon v_F S$ where V is the volume and S the surface area. Meservey and Tedrow (1978) compiled results from Knight shift, critical field and spin-polarized tunneling measurements and showed that ε was given approximately by $(\alpha Z)^4$ both in magnitude and in the dependence on atomic number.

This result (i.e. $\varepsilon \sim d/v_F \tau_{so} \sim (\alpha Z)^4$), which can be understood from the model presented in section A.3, is predicted (without explanation) by Abrikosov and Gor'kov (1962), and is also substantiated by a variety of more recent measurements. Weak localization effects in thin films have been shown to be sensitive to the spin-orbit scattering time (Bergmann, 1982). Alexander, Tedrow and Orlando (1986) find good agreement between scattering rates determined in the same sample from weak localization properties and from the superconducting tunneling DOS. The spin-orbit scattering rate of Mg films of different thicknesses d have been measured by Lindelof and Wang (1986). They find that the scattering rate is proportional to 1/d and they associate the proportionality constant with ε . The surface relaxation probability ε for films deposited on lead glass is larger than that for films deposited on soda glass. This suggests that the Pb at the surface of the Mg film participates in spin-flip scattering. Similarly, Bergmann and Horriar-Esser (1985) found that, for Mg films with a Au submonolayer deposited on the film surface, $\hbar/\tau_{so}$ varied inversely with the Mg film thickness. Alternately, Tedrow and Meservey (1979, 1982) showed that the spin-orbit scattering rate $\hbar/\tau_{so}$ of a thin $A\ell$ film increased linearly with Pt surface coverage up to 4meV for one monolayer of Pt. Recently, Eigler and Schultz (1985) have used CESR to follow the increase in $\hbar/\tau_{so}$ as a function of Xe and Kr adsorbed onto a 400 $\AA$ Li film and have found a linear dependence of ε verses rare gas coverage up to a few monolayers. Xe produced a larger effect than Kr as is consistent with the rapid increase in the spin-orbit interaction with atomic number suggested above. They report that calculations of the spin scattering cross sections are being attempted by Lu, Sham and Shore.

An early review on some aspects of CESR in metals is given by Yafet (1963) but very little is said about the effect of impurity scattering on the spin relaxation rate. An extensive experimental investigation of this question in Li and Na hosts was carried out by Asik, Ball, and Slichter (1969). Their data are plotted in figure IV.1.1 as a function of the atomic number of the impurity. They find that the experimentally measured scattering rates can be accounted for (within a factor of $\sim$ 5) by using a Fermi golden rule expression with a matrix element $V_{so} \sim (1/3)a_{np}^2 \lambda_{np}$. Here a_{np} is the overlap integral between a plane wave and the lowest filled p orbital, and λ_{np} is the atomic spin-orbit splitting of this p orbital obtained from atomic spectra. In

figure IV.1.1, it is shown that the spin-orbit scattering rate increases as Z^4 and that the gross magnitude can be accounted for by taking one seventh of the atomic matrix element (compare with fig. A.3.1).

However, there is a body of experimental results concerning the magnitude of the spin relaxation rate which is hard to understand. Asik, Ball and Slichter attempt to explain the peaks in the scattering rate (shown in fig. IV.1.1) in terms of the valence difference between the host and the impurity. They calculate changes in the overlap integral a_{np} due to the screening of the excess charge but find that the theory does not account for the existence or position of this peak. Ferrell and Prange (1966) associate the peak with a p-wave resonance in analogy to the d-wave resonance found for transition metal impurities dissolved in s-p metals (Friedel, 1958). A phase shift analysis (Ball, Asik and Slichter, 1969) is found to account for the existence of the peak but not its position. Stesmans and Sambles (1980) have measured the probability ε for Cu and Ag foils. They find that, "All these values fall substantially below those predicted from simple theory based on spin-orbit coupling. It is indicated that a reconsideration of previous ε interpretations is necessary." In regard to the magnitude of ε for Xe and Kr adsorbed onto Li, Eigler and Schultz (1985) conclude that, "The results indicate that there is a large pileup of conduction-electron density deep within the rare-gas adsorbate core ...".

It is generally believed that the residual resistivity and spin-orbit scattering are closely related. For example, this is implicit in Dyson's remark (1955, p. 350) "... spin-orbit coupling exists and very occasionally, about once in every 10^5 collisions in the case of sodium, causes the spin state to change during a collision." However, some experimental evidence suggests that spin-orbit scattering is not simply proportional to transport scattering. Orlando et al (1979) have derived values of the scattering rates from critical field measurements on Nb_3Sn and found the spin mean free path to be smaller than the transport mean free path. In Ga films (Meservey, Tedrow and Bruno, 1978), comparison before and after annealing at 77K showed no significant difference in the spin-orbit scattering rate in the amorphous and polycrystaline phases in spite of the fact that the resistivity differed by a factor of 7.8. There is, however, a report where the spin-orbit scattering rate of Mg and Ag films is found to be proportional to the resistivity (Bergmann and Horriar-Esser, 1985).

Thus, in summary, the experimental evidence suggests that the intrinsic spin relaxation in both s-p and d band metals arises from the spin-orbit interactions with surfaces and defects. The general trend is that the scattering rate depends on atomic number approximately as Z^4. Impurities and surface layers on s-p metals cause a significant increase in the spin-orbit scattering rate if the atomic number of impurity and host differ significantly. These results can be understood to be the result of coupling near the core of the ions; unlike transport scattering, these results can not be understood within a pseudopotential picture which neglects core effects (see A.3). However, beyond this, no theoretical understanding exists, and calculations of the scattering rate for model systems have not been attempted (e.g. a monolayer of Pt at the surface of a Aℓ film; a vacancy in bulk Pb).

In addition, the effect of impurities and surface layers in d band metals has not

been explored experimentally (Yafet, 1968; Gossard, Heeger, and Wernick, 1967). It is known that transport scattering in d band metals can not be accounted for by a simple pseudopotential picture; resonant scattering plays an important role (Harrison, 1969, 1970). One may expect that spin-orbit scattering is just that much more complicated in d-band metals. In fact, it is only recently that a related question has been addressed: "How does the spin-orbit interaction effect the g-factor of conduction states in d-band metals?" (Ohlsen and Calais, 1987). Another related calculation is that of the spin-dependent cross section of *free* electrons scattered from a metallic surface (Achermann and Feder, 1984; Feder, 1985). These theoretical techniques need to be applied to the problem of spin-orbit scattering in metals from impurities and surfaces.

—Spin-orbit scattering in superconductors—

The history of spin-orbit scattering in superconductors begins with NMR measurements in Hg (Reif, 1957) and Sn (Androes and Knight, 1959) which indicated that the spin susceptibility of these superconductors does not extrapolate to zero as $T \rightarrow 0$. This result is in contradiction with the calculation of Yosida (1958) which predicts a vanishing susceptibility which follows from the singlet pairing of the BCS theory. Ferrell (1959) followed by Anderson (1959) suggested that spin-mixing due to the spin-orbit interaction at surfaces modifies the spin pairing so as to allow a non-zero spin susceptibility at $T = 0$. Abrikosov and Gor'kov (1962) presented a detailed calculation giving the spin susceptibility as a function of $\hbar/\tau_{so}$ and made the incidental comment that the ratio of the spin-orbit scattering rate to the transport scattering rate is of the order $(\alpha Z)^4$.

Chandrasekhar (1962) and Clogston (1962) pointed out that the BCS superconductor (i.e. $\hbar/\tau_{so} = 0$) has a upper limit to the critical field due to the Pauli paramagnetism of the normal state (see section I.2). However, experimental evidence suggested that spin-orbit scattering relaxes this "Pauli limit" (Neuringer and Shapira, 1966). Werthamer, Helfand and Hohenberg (1966) and Maki (1966) calculated the critical field in the presence of spin-orbit scattering using the field theoretic methods of Abrikosov and Gor'kov(1962) and Maki (1964). As explained in section I.2, the part of the critical field where the transition is second order can be described by a low order Ginzberg-Landau free energy expansion $F = a(T,H)|\psi|^2 + b(T,H)|\psi|^4$. The critical field is determined by the condition a=0. The tricritical temperature (below which the transition is first order) is determined by the condition $a = 0, b = 0$ and is calculated by Engler and Fulde (1968). The critical field of bulk type II superconductors was found to be pretty much consistent with the theory (Hake, 1967). Subsequently, a number of more quantitative experimental tests of the theory showed Fermi liquid effects to be important (Orlando, McNiff, Foner, Beasley, 1979; Tedrow and Meservey, 1979). Inclusion of such effects brought critical field and spin-polarized tunneling measurements into accord (Alexander, Orlando, Rainer, Tedrow, 1985).

It is convenient to introduce at this point the dimensionless parameters which enter the theory of critical fields. The spin-orbit scattering rate is parameterized by dividing by the energy gap $b_{so} = \hbar/3\tau_{so}\Delta$ or the transition temperature $\lambda_{so} = 2\hbar/3\pi\tau_{so}k_B T_c$ ($\lambda_{so} = 1.12 b_{so}$). The effect of the magnetic field on the electron orbits (i.e. the $\vec{p} \cdot \vec{A}$ interaction) is opposite in sign for the two members of the Cooper

pair. Therefore, this orbital effect is a pairbreaking interaction. In the "dirty limit" (i.e. where mean free path ℓ is less than the coherence length ξ), the pairbreaking is ergodic. The orbital pairbreaking rate $\hbar/\tau_{PB}$ depends on the geometry. For a thin film oriented with the field parallel to the film surface, $\hbar/\tau_{PB} = \mu_B^2 B c_F/\Delta_o$ where $c_F = D(ed)^2\Delta_o/6\mu_B^2\hbar$ is a commonly used dimensionless parameterization (SI units); for example, used by Fulde (1973). Here $D = \ell v_F/3$ is the diffusion constant and d the film thickness. For a film oriented perpendicular to the applied field, $\hbar/\tau_{PB} = eDB = 4k_B B/\pi S$ where S is the slope of the critical field at T_c ($S = 10.972/D$ in kG/K with D in cm^2/sec units). Note that by measuring the parallel and perpendicular critical field of a thin film, one may determine the diffusion constant and film thickness (d in $\AA$ is given by $282(c_F S/T_c)^{1/2}$ where S is in tesla/K.

In the next section data are presented for thin V_3Ga films with third element impurities or surface layers. Information about the spin-orbit scattering rate of V_3Ga will be extracted from an analysis of critical field data. Since the critical field of V_3Ga is Pauli limited, it is expected that the linearized theory cannot be applied to the low temperature data where the transition is first order. For this reason, it is of interest to know the tricritical temperature. However, the calculation of Engler and Fulde needs to be modified to include the Fermi liquid renormalization of the Zeeman energy. This has been done by the "lifting" procedure described by Alexander et al which amounts to replacing the Zeeman energy by the renormalized Zeeman energy $2\mu_B/(1+G^o)$. The resulting equations are found in Appendix B along with the computer code to execute the calculation of the critical field and tricritical temperature. In figure IV.1.2,3 the tricritical temperature normalized to T_c is plotted verses the orbital depairing parameter c_F and for different values of the spin-orbit scattering rate and for different values of G^o. The curves for $G^o = 0$ are the same as those displayed by Engler and Fulde (1968).

Unlike critical field measurements, which are necessarily confined to the phase boundary, the S-I-N tunneling provides information at any point in the H-vs.-T phase diagram. In order to avoid complications due to vortices, the theory is at present restricted to measurements on films thinner than the coherence length and with the field applied parallel to the film surface. When the normal metal is a ferromagnet, the total conductance can be split into individual conductances corresponding to the two spin projections. This allows a direct observation of the spin-mixing due to spin-orbit scattering and permits a measurement of b_{so} (Tedrow, Moodera, and Meservey, 1982). A computer subroutine which does the separation is given in appendix B. Such spin-polarized tunneling measurements on aluminum have produced values of b_{so} which differ by a factor of four from earlier values obtained by fitting critical fields (Tedrow and Meservey, 1982). It has been proposed that fitting both critical field and tunneling data provides the necessary and sufficient information required to obtain the material parameters uniquely (Alexander, Orlando, Rainer, and Tedrow, 1985). The strong paramagnetic limiting and yet high critical field of V_3Ga make it an interesting material in which to test the theory. Such a study is also of current technological interest since V_3Ga is of interest as a material for making very high field, superconducting magnets (Tachikawa, et al, 1985; Takeuchi, Iijima, Inoue, and

Tachikawa, 1986).

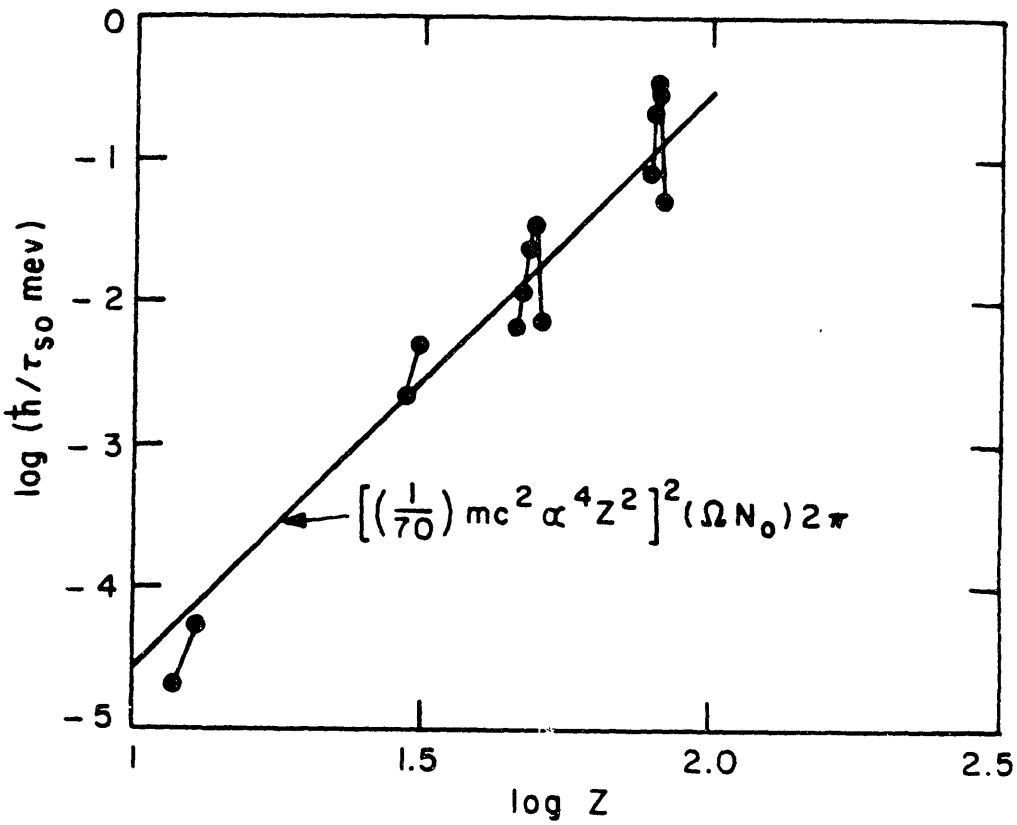

Fig. IV.1.1 The spin-orbit scattering rate per unit impurity concentration as measured by Asik, Ball and Slichter (1969).

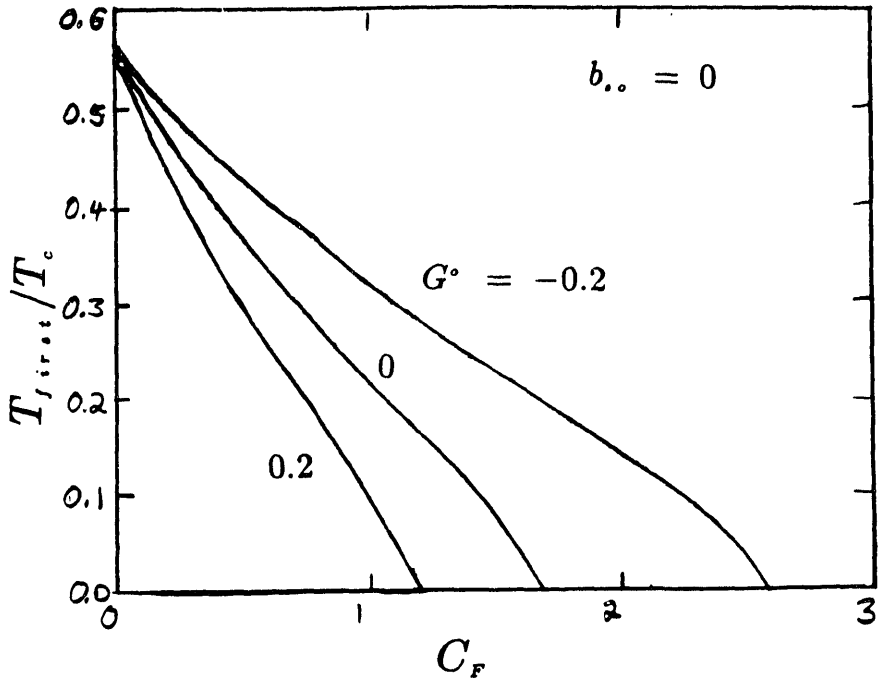

Fig. IV.1.2 The ratio of the tricritical temperature to the transition temperature for different values of the Fermi liquid parameter and for $b_{\circ\circ} = 0$

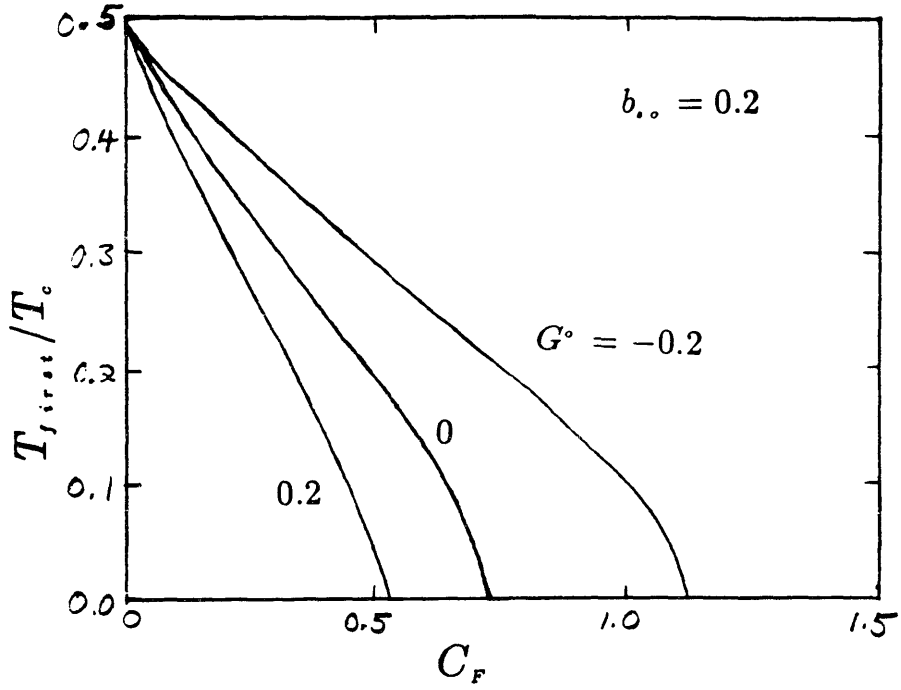

Fig. IV.1.3 Same as figure IV.2.1 except that $b_{\circ\circ} = 0.2$.

IV.2 V_3Ga Thin Films

V_3Ga thin films, 6 to 500nm thick, have been made for the purpose of investigating the role of spin-orbit scattering in this A15 superconductor. Either 1 percent dopings or thin surface layers of high-atomic-number elements have been added to these samples in an attempt to modify the spin-orbit scattering rate in this paramagnetically limited material. Critical fields are presented and material parameters are obtained by fitting to a modified high field theory. Tunneling conductance data are shown to be consistent with the value of spin-orbit scattering obtained. The uniqueness of the parameters obtained in this manner is discussed in light of Fermi-liquid effects. Comparisons are drawn with bulk V_3Ga . Although the zero-field properties are affected by the addition of a third element, the magnetic field dependent properties are unchanged. Some of these results have been published elsewhere (Tedrow, Tkaczyk, Meservey, Bending and Hammond, 1985; Tkaczyk and Tedrow, 1986, 1987).

—Introduction—

In addition to its use as a practical material in high field magnets, V_3Ga is of interest in terms of understanding superconductivity in high magnetic fields. As is apparent in the theory (section I.2), such an understanding gives information about quasiparticle properties of electrons in the *normal* metal. In particular, spin-dependent properties are obtained which cannot be easily measured with normal state experiments. V_3Ga is a superconductor in the dirty limit ($\xi_o/\ell \sim (\xi/\ell)^2 \sim 2$) with a critical field of 23 tesla which is limited by the presence of Pauli paramagnetism in the normal state. Because it elucidates the role of spin-orbit scattering and Fermi liquid effects, the Pauli limit represents an interesting regime in the theory of superconductors in a magnetic field. Pauli limiting also exists at lower fields in aluminum for which critical field data and the spin-separated tunneling conductance have been fit with the theory yielding a self consistent set of material parameters. As such, the work on Aℓ films (Alexander et al, 1985) serves as a verification of the theory at low fields. To date, no similarly complete application of the theory has been reported for metals more complicated than aluminum or for fields typical of the critical field of V_3Ga (for work on Ga films see Gibson, 1988).

Based on the published values of the electron-phonon coupling parameter, Orlando and Beasley (1981) have shown that the critical field of V_3Ga at zero temperature implies the presence of spin-fluctuations arising from electron-electron interactions. Foner, McNiff, Moehlecke, and Sweedler (1981) come to a similar conclusions based on the whole critical field curve and call for additional research. On the other hand, Schopohl and Scharnburg (1985) find that "isotropic scattering can account for the low H_{c2} observed, making it unnecessary to invoke spin-fluctuations." A direct test of the present theory requires measurements to be done on films of thickness less than the coherence length and penetration depth. The coherence length in V_3Ga is 3nm (Foner et al, 1981) which presents an obstacle to such a test. The penetration depth is of the order of 500nm. Here the fabrication and characteristics of V_3Ga films of thickness down to 6nm are reported. Critical field measurements are presented and analyzed as a function of thickness. Additional information about the value of the spin-orbit scattering rate is derived from tunneling data.

As the critical field of V_3Ga is paramagnetically limited, theory predicts that the introduction of spin-orbit scattering can lead to a higher critical field. That the increase would be of technological interest is shown in figure IV.2.1. The critical field of V_3Ga and Nb_3Sn are shown, both of which are used in present high field superconducting magnets. The theory is used to predict the critical field for the hypothetical case where the spin-orbit scattering of V_3Ga is changed to $b_{so} = 1.2$ with other parameters unchanged. The resulting critical field rises above that of Nb_3Sn. From the experimental data reviewed in the last section, it would appear that spin-orbit scattering is a rapidly increasing function of atomic number. As such, one may expect that a small concentration (about 1%) of large Z elements uniformly dispersed into the material, or as thin layers in contact with thin films of V_3Ga , will increase the critical field. It has been shown that only eighty percent of a monolayer of Pt deposited onto a thin, aluminum film more than doubles the critical field(Tedrow and Meservey, 1982). However, such properties as critical field and superconducting transition temperature are sensitive to the degree of long-range order of the A15 crystal structure(Dew-Hughes, 1975). Therefore it is expected that results similar to those found for aluminum may be difficult to achieve in V_3Ga .

—500nm V_3Ga Films—

Previous work (Tedrow, Tkaczyk, Meservey, Bending and Hammond, 1985) on V_3Ga films 500nm thick has included assessing the effect on the critical field of 1 to 2% elemental impurities of Pb, Pt, Sn, Nb, and Ta. Here we present a quantitative analysis of these data. These films made at Stanford University were formed by electron beam codeposition of V_3Ga and the impurity onto sapphire substrates heated to 750C. The simultaneous production of samples with a range of composition yielded comparisons of impurity doped films both on and off stoichiometry. The films off stoichiometry have higher resistivity and lower transition temperatures (figure IV.2.2). It was found that in off-stoichiometry V-Ga (Ga rich) the 1% Nb samples had higher T_c's than the undoped off stoichiometry material (figure IV.2.3). This increase in T_c was a significant effect; at the highest gallium concentration produced, 30%, the T_c of the Nb doped sample was 11.75K as compared to 8.6K for the undoped V-Ga. However, in the stoichiometric material the doped samples had lower T_c's than the pure V_3Ga .

This zero-field effect on T_c indicates that the impurities influenced the V_3Ga A15 structure. However, analysis of the critical fields and tunneling data shows no evidence of significantly increased spin-orbit scattering (figure IV.2.4). In fact, when plotted in reduced variables, as in figure IV.2.5, the critical fields are almost identical. Critical field measurements were made up to 20 Tesla with the field oriented perpendicular to the surface of the film. Parameters obtained by fitting the critical fields are given in Table IV.1. Fermi-liquid effects were ignored for these fits by setting $G^o = 0$. The strong paramagnetic limiting of the critical field of V_3Ga makes a quantitative analysis difficult because in this limit the critical field is not characterized by linear temperature behavior near T_c. In addition, the transition becomes of first order below a relatively high tricritical temperature. Using only data above the tricritical temperature, fits were optimized by minimizing the statistical variance utilizing a computerized, gradient search of the parameter space (Appendix B).

The similarity in the parameters derived from the critical field of doped and undoped films indicates that there is no field-dependent perturbation due to the impurities. This is unexpected in light of the zero-field effect on T_c. Since substrate temperature was optimized for V_3Ga crystal growth, the possibility arises that the third element is excluded from such growth and segregates to the grain boundaries. Similarly, Asik, Ball and Slichter (1969) find that certain large Z elements introduced as impurities in Li and Na do not increase the spin-orbit scattering rate, and they attribute this result to a lack of solubility of these elements. However, such a solubility argument is hard to reconcile with the change in T_c.

In the non-stoichiometric, Ga-rich, material, the Nb dopant apparently participates by assuming vacant vanadium sites, thereby reducing distortion of the A15 lattice resulting in the observed increased T_c. Nb forms a superconducting A15 compound with gallium with a reported T_c of 20.3K (Dew-Hughes, 1975). An XPS study directed toward detecting the position of the impurity in the A15 lattice was inconclusive because of a lack of standards with which to compare observed energy shifts and also because of lack of the necessary sensitivity for detecting 1 percent effects.

Attempts to form tunnel junctions with artificial $A\ell_2O_3$ or SiO_2 on V_3Ga proved difficult. We were not successful at fabricating the high quality junctions with Fe counter electrodes needed for spin-polarized tunneling. Measurements of a Pb-SiO_2-V_3Ga (Pt) junction in fields up to the critical field are shown in figure IV.2.6. The observation of Zeeman splitting in the conductance is an indication of low spin-orbit scattering. The first observation of splitting in V_3Ga was made by Bending, Beasley and Tsuei (1984). The tunneling conductances resemble those of a thin film in a parallel field in spite of the vortex structure present. The degree of resemblance is shown by comparison with conductance curves generated from the *thin film* theory (figure IV.2.7). The parameters needed as input to the theory are those typically obtained from the critical fields ($S = 4.2T/K, b = 0.2, G^o = 0$). In addition the gap was taken as $\Delta = 1.9k_BT_c$. It should be emphasized that figure IV.2.6 is not a fit to the data (figure IV.2.5) since the theory does not take vortices into account. However, the resemblance can be understood to be appropriate at low fields as a consequence of extreme type II behavior; the Ginzberg-Landau parameter is large, $\kappa = \lambda/\xi \sim 100$. Thus V_3Ga is in the Abrikosov state in fields above $H_{c1} \sim H_{c2}^*/\kappa^2 = 40$ Gauss where $H_{c2}^* \sim 40T$ is the orbital upper critical field. Above H_{c1}, the vortex lattice spacing is less than the penetration depth resulting in a relatively uniform field in the V_3Ga . For fields less than the Pauli limited critical field H_{c2}, the contribution from the normal cores is a factor κ^{-2} smaller than that from the superconducting regions.

—Thinnest Films—

The doping of V_3Ga with impurities has paradoxically shown a decrease in T_c and an increase in transport scattering, but without the associated increase in spin-orbit scattering. As already mentioned the placement of sub-monolayer coverings of Pt on 4nm Al films was successful at significantly increasing the spin-orbit scattering rate and critical field. Given a spin mean free path of 20nm in V_3Ga one may expect to see some similar effect for V_3Ga films of thickness less than 10nm. Films of V_3Ga of thicknesses 6 to 100nm thick have been made using techniques similar to those

used for making the 500nm thick films. The 1/4" x 1/2" sapphire substrates were heated to a temperature of 500°C. This is 250°C less than the typical temperature used for the samples made at Stanford. Attempts to make these very thin samples at higher substrate temperatures yielded non-conducting material which may be due to island formation or interdiffusion at the substrate/film interface. Three substrates were placed in line between the separated V and Ga sources for each evaporation. Comparison of the T_c's of the resulting films allows one to achieve stoichiometry by adjusting the respective rates to obtain the maximum T_c. The deposition rate was typically 0.6nm/sec and pressure during the evaporation was in the high 10^{-8} Torr range.

Aluminum was evaporated over some of the V_3Ga films as a protective layer. Substrate temperature during these overlayer evaporations was below 200C. An aluminum thickness as much as 3 to 6 nm was required to achieve high transition temperatures in the thinnest V_3Ga film. In addition the deposition of a layer of Ta either on the exposed film surface or on the $A\ell_2O_3$ substrate under the V_3Ga has been seen to increase the T_c of the film by 10%. An XPS depth profile shows the presence of magnetic vanadium oxides both at the surface and at the film-substrate interface (figure IV.2.8,9). VO_2 is of particular concern since it is magnetic and is expected to depress the superconducting transition temperature. One may suspect that the Aℓ and Ta serve as an oxygen barrier. XPS shows both both unoxidized and oxidized Aℓ is present.

A system of masks and shutters has been developed for the simultaneous deposition of two films onto the same substrate differing only by the presence of a third element overlayer on one. Such a pair of films allows an unambiguous determination of the effect, or lack thereof, which the third element has on thin V_3Ga films. A few samples with alternating layers of V_3Ga and the third element have been made. The substrate temperature during the fabrication of these structures was kept at 500C.

As has been observed previously in other A15 films (Orlando et al, 1979), samples with higher zero-field transition temperatures are found with higher residual resistivity ratio, lower resistivity and narrower transitions. Variations in residual pressure, annealing times, cooling rates and the presence of mask shadows or compositional variations at edges each could have their own effect on such properties. Emphasis has been placed on maximizing T_c and sample quality by varying substrate temperature and film composition. For such 10nm thick films the residual resistivity and resistivity ratio lie in the respective ranges 80-100 $\mu\Omega - cm$ and 1.3-1.7 (figures II.2.4,5). The transition widths are about 0.5K which is comparable to bulk values.

The resistive transitions are shown for samples of various thicknesses in chapter II (figures II.2.2,3). The zero-field transition temperature decreases with decreasing film thickness. Presumably, the factors influencing the change in T_c are diffusive contaminants, especially oxygen, and strain at the substrate-film interface. Localization may also play a role in the decrease of T_c. The depth profile in figure IV.2.8 may indicate some interdiffusion at the film/substrate interface. The field dependent properties of these films are remarkably similar. The slope of H_{c2} at T_c increases with decreasing T_c in such a way that the coherence length remains approximately constant

($\xi^2 = 4.61 \cdot 10^{-11}/T_c S$, where ξ is in centimeters and S is in kG/K). The pair of 8nm films listed in Table IV.1 were made on the same substrate. In these films, the width of the constant temperature, ramped field transition narrowed when the temperature was decreased (figure IV.2.10). This suggests a strong fluctuation contribution to the width rather than the effect of inhomogeneities or edges. Of the 8nm thick samples the one with a 0.5nm Ta overlayer has the higher T_c. Yet, values of the coherence length and b_{so} are nearly identical. Similarly, in pairs of 10μm V_3Ga films differing only by 1nm in the aluminum overlayer thickness, the sample with the greater coverage of Aℓ had the higher T_c. However, a comparison of the critical fields shows no field dependent effect due to additional Aℓ . Similarly, samples with alternating layers of V_3Ga and the impurity showed changes in T_c, but no field dependent effects.

—Analysis of Critical fields—

An important point should be made concerning the uniqueness of the critical field fits when Fermi-liquid effects are considered to play a role. The parameters entering into the expression for the perpendicular critical field are T_c, b_{so} S (i.e. slope at T_c) and G^o. The possible presence of Fermi-liquid effects (i.e. $G^o \neq 0$) forces one to use tunneling measurements for a correct quantitative analysis of these films. The reason is that spin-orbit scattering and Fermi liquid effects have the same influence on the shape of the critical field. This point is illustrated in figure IV.2.11. Having chosen particular values b_{so} and G^o, critical field curves were calculated for different values of T_c and S until the statistical variance with respect to the data was minimized. Points below the tricritical temperature where the transition is first order were excluded from the calculation of the variance. In this way the best fit to the data (by only varying a subset of the available parameters) was obtained for each point in a 100 point grid in the parameter space formed by b_{so} and G^o. A contour map of the variance, based on a linear interpolation from this grid, is shown in the figure. One may trade off b_{so} for G^o and still achieve the same quality fit of the theory. This result indicates the need for more data to determine the values of G^o and b_{so} uniquely. In a similar analysis, minimizing the variance with respect to either b_{so} or G^o shows that the slope at T_c and, therefore, the orbital depairing parameter are in fact well determined by the perpendicular critical field. In spite of a measured strong-coupling parameter of $\Delta/kT_c \sim 1.9$, (equals 1.72 for a BCS superconductor) strong-coupling effects were not considered in the data analysis.

The parallel critical field for each of these films was higher than the perpendicular critical field (figure IV.2.12). For samples less than two times the penetration depth, oriented parallel to the field, there is significant penetration of the field from the surface without the formation of a normal, vortex core. There may also be some degree of surface superconductivity which supports a higher parallel critical field. A quantitative analysis is complicated by spin effects which are ever present at these high fields. As the film thickness approaches the coherence length, one expects a crossover to a two-dimensional regime characterized by a spatially uniform order parameter which vanishes at T_{co} with a square-root dependence on $T_c - T$. This behavior is evidenced in the parallel critical fields for thicknesses below 10nm (figure IV.2.13). Near T_{co}, where the coherence length diverges, the parallel critical field vanishes as a square-root. The

theory in the thin film limit is well developed, but is restricted to film thicknesses less than $1.8 \times \xi = 5.5nm$ for V_3Ga . However, in spite of being somewhat outside the regime of validity, several parallel critical field fits were attempted for samples 10nm thick.

The perpendicular and parallel field were fitted to the theory as shown in figure IV.2.14 (sample VGA060 in Table IV.1). Two values of the spin-orbit scattering rate were chosen to illustrate the fact that the Fermi liquid corrections affect the shape of the critical field of V_3Ga in approximately the same way as spin-orbit scattering. In addition the importance of taking the tricritical temperature into account is demonstrated. For $b_{so} = 0.05$ good fits with $G^o = 0.11$ were obtained to the parallel and perpendicular critical field data above the tricritical temperature (as indicated by the arrow). Using the same orbital pairbreaking parameters, ($c_F = 0.44, S = 5.02$ T/K) the same data was fit with $b_{so} = 0.2$ and with no Fermi liquid effects (i.e. $G^o = 0$). Note that without taking the tricritical temperature into account one would attempt to include the low temperature data and arrive at the fit (curve a) shown with $b_{so} = 0.2$ and $G^o = 0$. However, it is clear from figures IV.2.14 and IV 2.11 that the critical field data cannot be used to distinguish between $b_{so} = 0.2$ and $b_{so} = 0.05$. The analysis of critical field data in the past has underestimated the importance of the first order transition in the low temperature regime.

And yet the orbital parameter is well determined (e.g. the critical field near T_c). From a comparison of the orbital pairbreakers obtained in figure IV.2.14 for the perpendicular and parallel orientations, one can infer a value for the film thickness of 12.6nm. This is acceptable in light of the fact that a 10nm thick film is not truly in the thin film limit.

—Conclusions—

It has been shown that the critical field of V_3Ga films down to 6nm in thickness resembles that of the bulk. The T_c decreases with decreasing film thickness but the slope of the critical field at T_c increases such that the coherence length is constant. Although changes in T_c were observed when these films were doped, or covered with third elements, no field dependent effects have been seen which are attributable to the impurity, in spite of the care taken to form two samples on the same substrate differing only in the presence of the impurity. The absence of the effect which these sample preparation methods were expected to have on the spin-orbit scattering rate is not understood. The spin mean free path $l_{so} = \xi_o/b_{so}$ is of the order of 25nm in V_3Ga . This implies that the conduction electrons should frequently encounter the added scattering sites in the 1% doped material. The large atomic number of the impurities suggests a strong spin-orbit scattering cross section. Surfaces are thought to be very effective in spin scattering so that heavy surface layers on 10nm films should provide frequent spin-flip scattering events. For the available data, it appears that the conduction electrons don't reach the core region of the impurities where the spin-orbit interaction is strong. This could be due to a lack of solubility such as that described by Asik, Ball, and Slichter. Alternately, there may be another explanation based on the d-band character of the conduction electrons. A microstructural explanation would for example place the high Z impurities in grain boundaries, insulated from the

conduction electrons. Further experiments should be done in a simpler d-band metal such as vanadium. For example, one could measure the critical field of thin films of V(Pt) alloys. However, in such a study one would still have to address the solubility question.

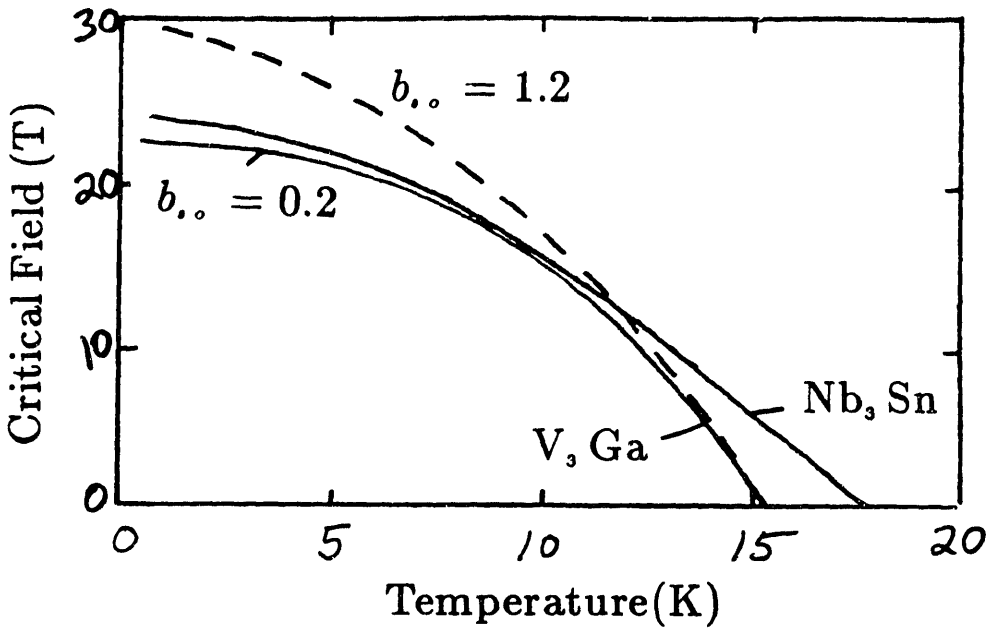

Fig. IV.2.1 Comparison of the critical fields of V_3Ga and Nb_3Sn and a calculation (dashed) with T_c and S typical of V_3Ga but with $b_{,o} = 1.2$ instead of $b_{,o} = 0.2$.

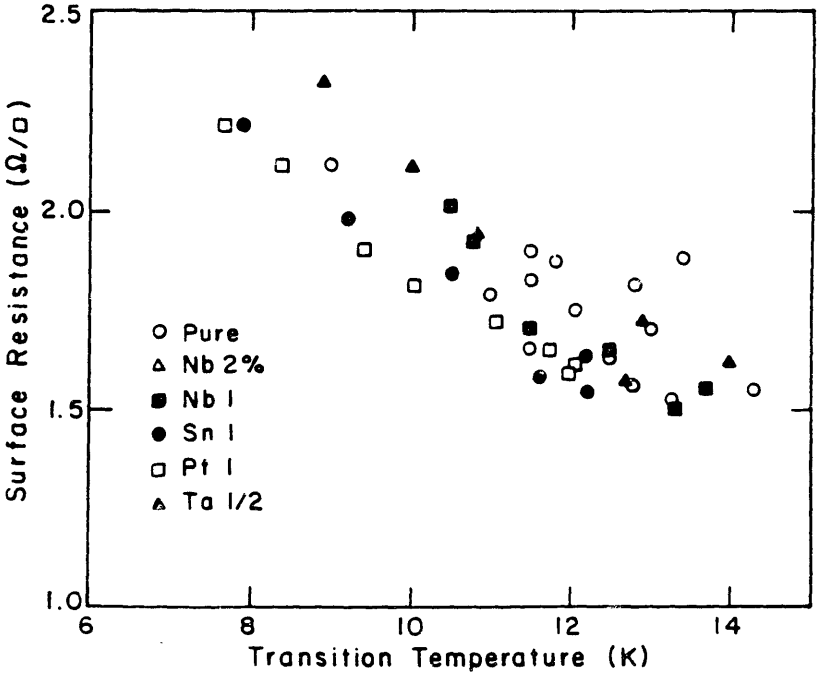

Fig. IV.2.2 Data showing correlation between T_c and the surface resistance of these 500nm thick films (e.g. $1\Omega/\Box = 50\mu\Omega - cm$).

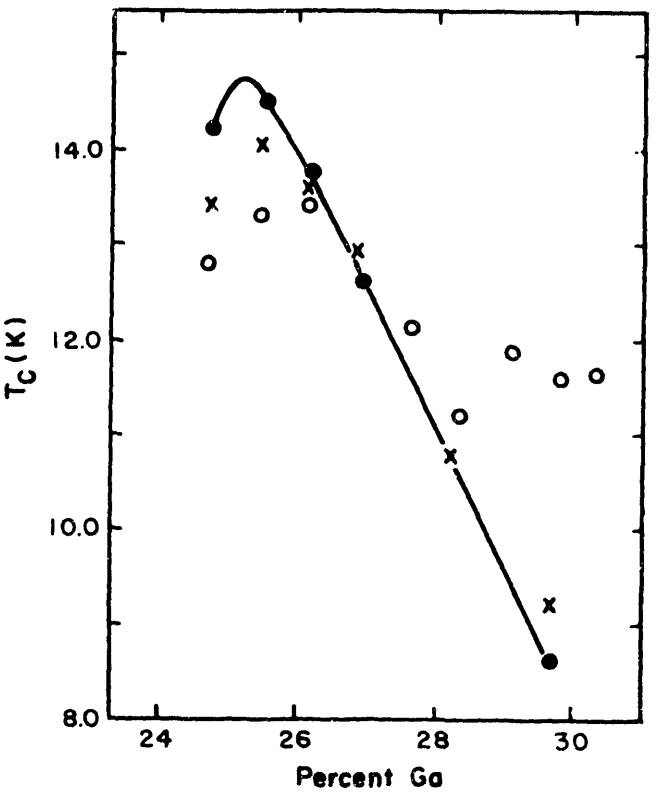

Fig. IV.2.3 Transition temperature verses Ga concentration for pure V-Ga films, —•—; V(2% Nb)-Ga films, o; and V(0.5% Ta)-Ga films, ×.

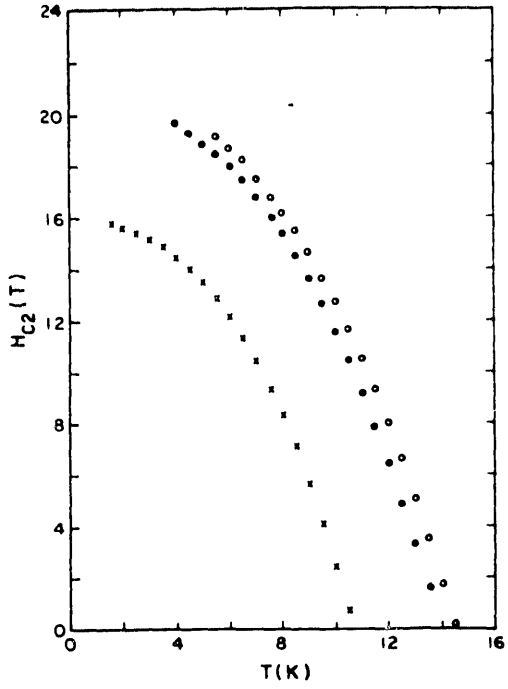

Fig. IV.2.4 Critical magnetic field of three V-Ga films. o – – – V_3Ga; • – – – $V_{0.735}Ta_{0.005}Ga_{0.25}$; × – – – $V_{0.72}Nb_{0.01}Ga_{0.27}$.

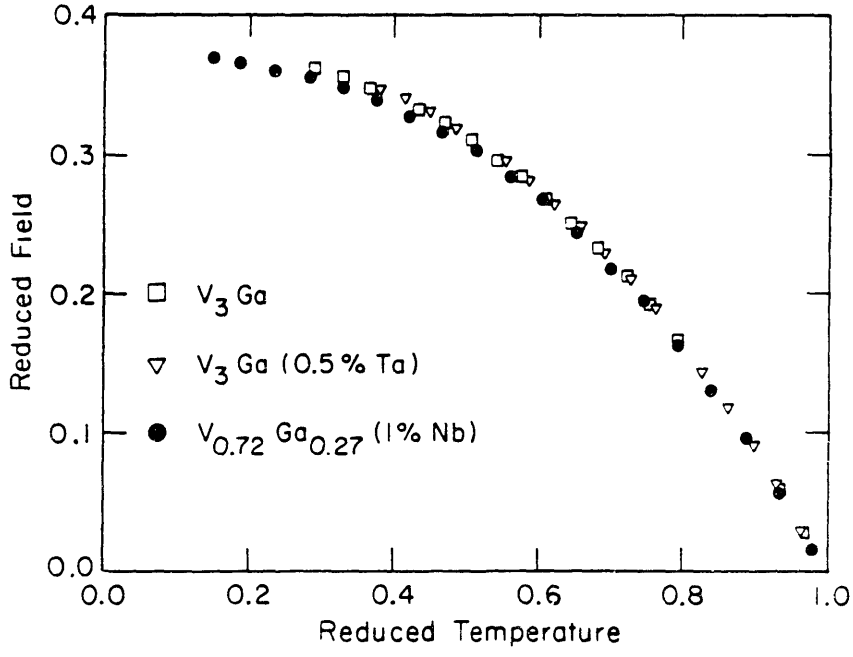

Fig. IV.2.5 Perpendicular critical fields of 500nm thick V-Ga with and without high Z elements. The reduced field is obtained by dividing H_{c2} by its $|dH/dT|_{T_c}$ and by T_c. The reduced temperature is T/T_c.

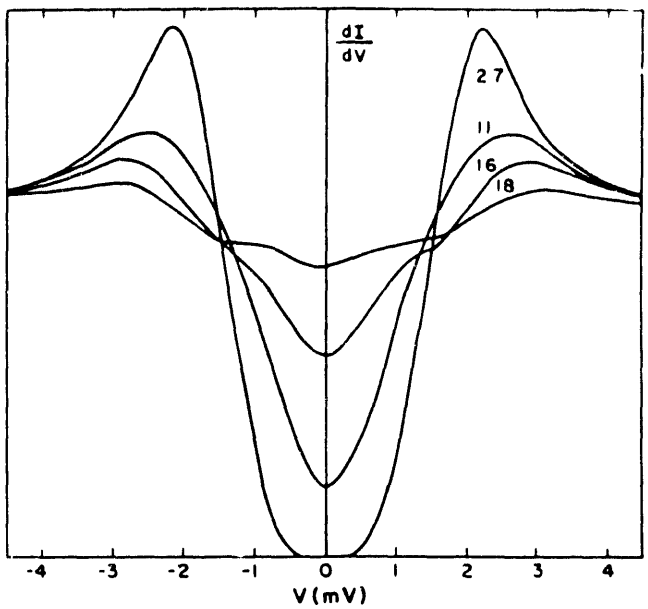

Fig. IV.2.6 Magnetic field dependence of the tunneling conductance vs. voltage of a $Pb - SiO - V_{0.76}Ga_{0.23}Pt_{0.01}$ junction. The magnetic field values are given in the figure in tesla.

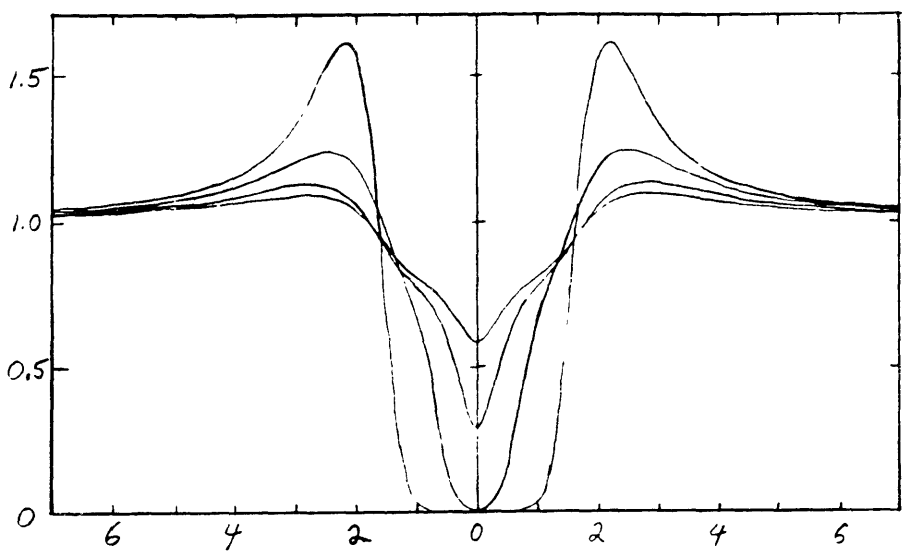

Fig. IV.2.7 The conductance calculated with the theory without corrections for vortices using parameters derived from the critical field of V_3Ga .

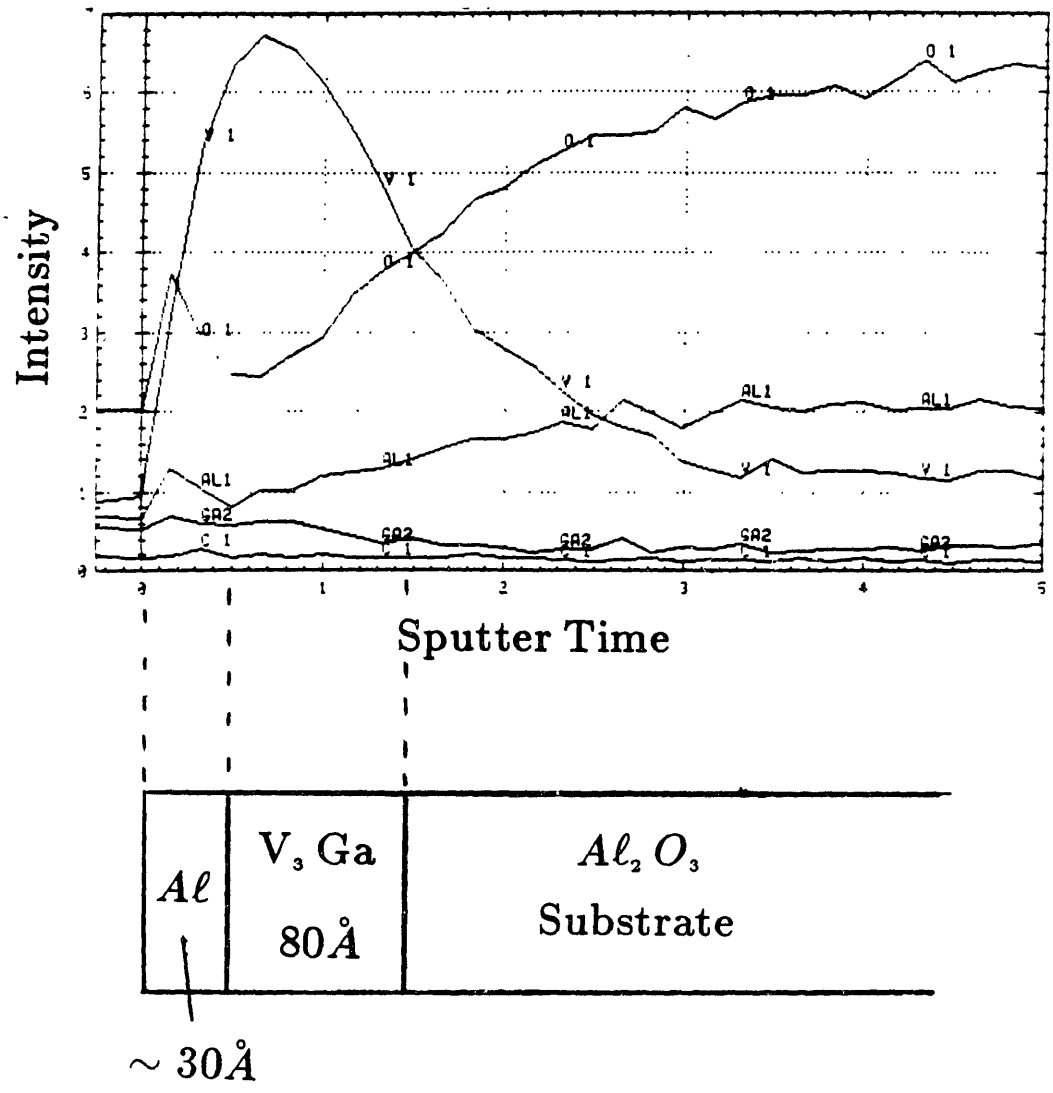

Fig. IV.2.8 A plot of the intensity of the x-ray photo emission peaks as a function of sputtering time.

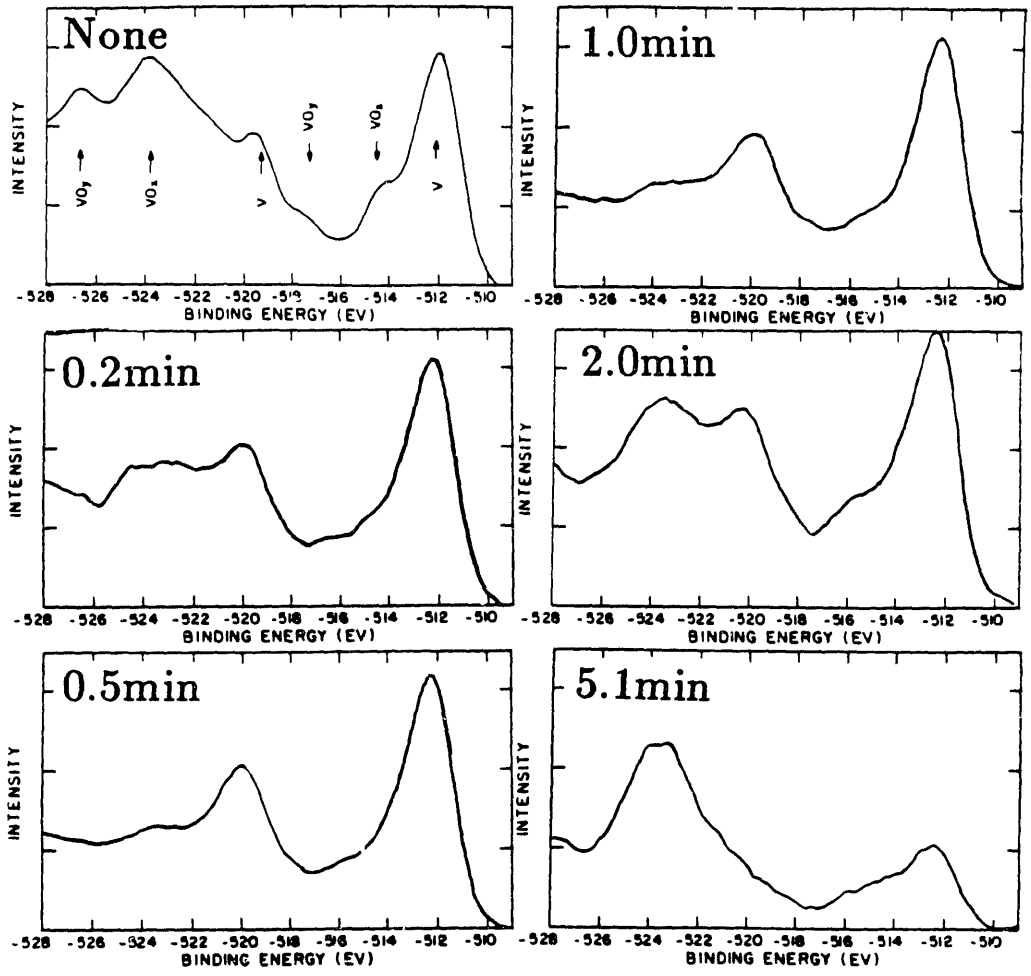

Fig. IV.2.9

The x-ray photoemission intensity verses energy after different values of the sputtering time. The previous figure indicates the approximate position in the film. According to the reference data, the peaks indicated by arrows can be associated with the presence of V, VO and VO_2. Note that the oxide peaks are largest at the sample surface and at the film/substrate interface.

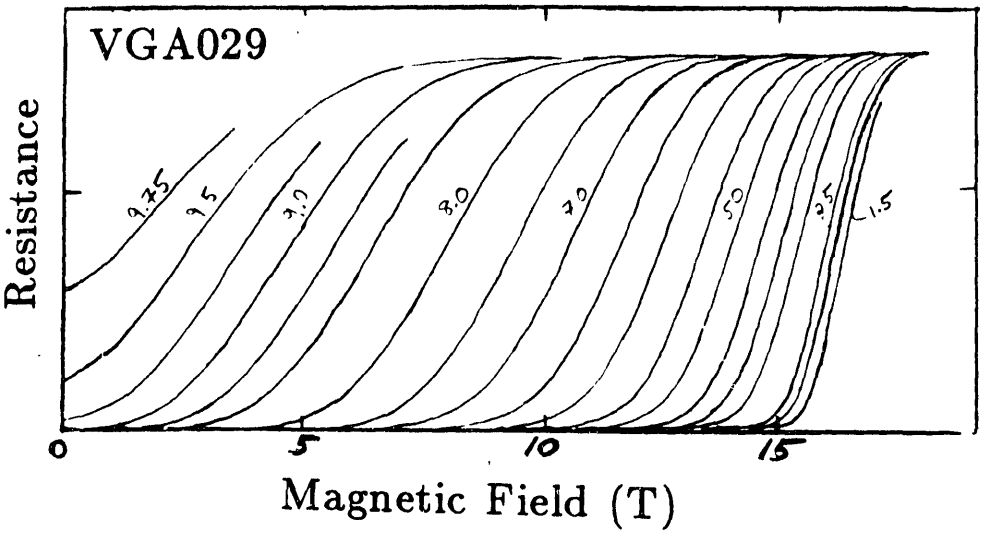

Fig. IV.2.10 The resistive transition of a (80nm) V_3Ga/(0.5nm) Ta/(6nm) Al film as a function of the applied field at constant temperature. (Sample VGA029 listed in Table 1).

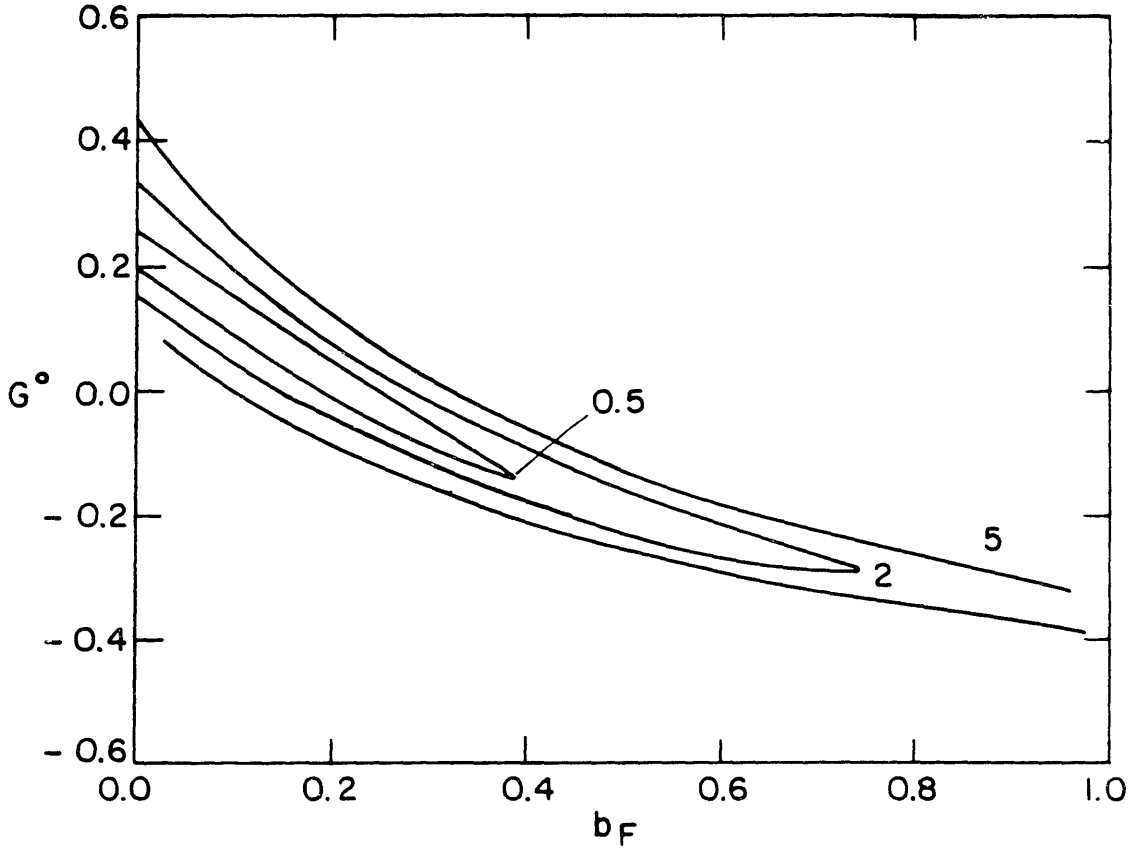

Fig. IV.2.11 Level curves of the variance minimized by adjusting $|dH/dT|_{Tc}$. Details as to the construction and meaning of this figure are found in the text.

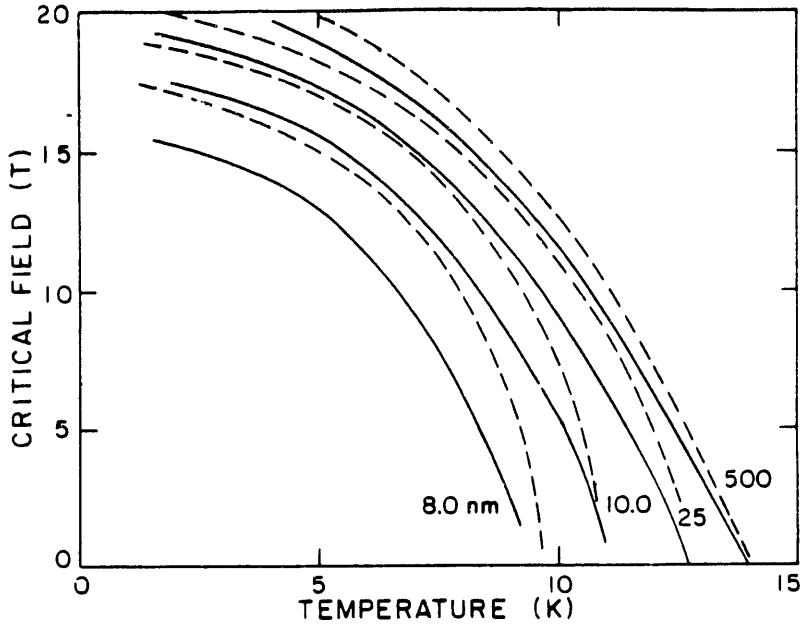

Fig. IV.2.12 Comparison of the perpendicular (solid) and parallel (dashed) critical fields for different thicknesses.

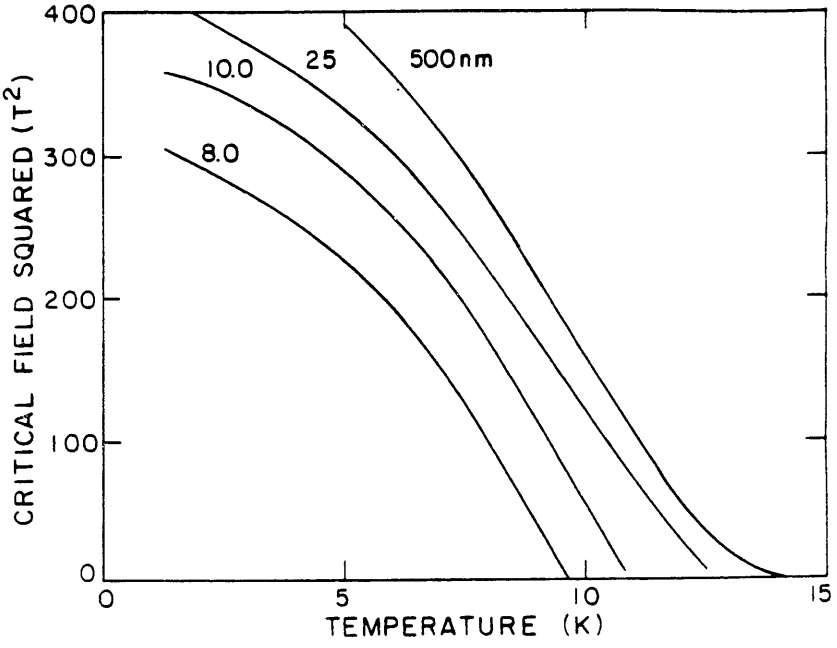

Fig. IV.2.13 The square of the parallel critical field is plotted as a function of temperature for V_3Ga films of various thicknesses. Two-dimensional behavior is characterized by the presence of a linear portion in the curves near T_c.

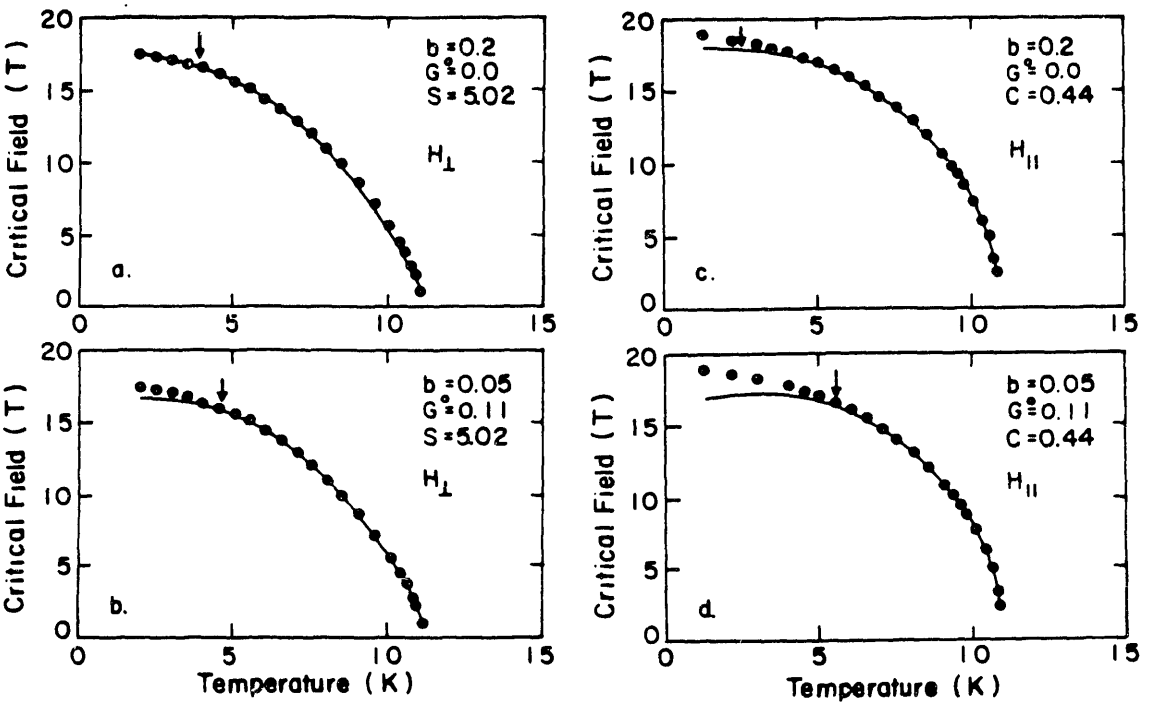

Fig. IV.2.14 Fits to the perpendicular and parallel critical field for two values of the spin-orbit scatting rate, $b = 0.2$ and 0.05. The orbital depairing is parameterized in the perpendicular case by the slope, S, of the critical field curve at T_c measured in tesla/K. The parameters c and G° are defined in the text. The arrows indicate the temperature below which the transition is first order.

Table IV—1 Analysis of Critical Fields

#	sample	T_c (K)	ΔT_c (K)	S (T/K)	b_{*o}	ξ (nm)	Variance ($T^2 \times 10^{-2}$)
—	Bulk[a]	15.1	0.23	4	0.22	2.7	
007	500nm, pure	13.90		3.9	0.26	3.0	0.59
006	500nm, 1% Nb	10.70		4.0	0.24	3.3	0.84
008	500nm, 0.5% Ta	14.51		2.9	0.25	2.9	0.94
014	20nm	12.60	0.4	4.3	0.25	2.9	0.58
018	10nm, 6nm Aℓ	10.55	0.7	5.4	0.23	2.8	0.38
060	10nm, 6nm Aℓ	11.26	0.4	5.1	0.20	2.9	2.05
070	10nm, 6nm Aℓ	10.64	0.6	5.3	0.22	2.9	0.2
067	0.5nm Ta, 10nm, 6nm Aℓ	11.32	0.6	4.8	0.27	2.9	0.19
030	8nm, 6nm Aℓ	9.5	1.5	5.8	0.22	2.9	1.20
029	8nm, 0.5nm Ta, 6nm Aℓ	9.95	1.0	5.8	0.20	2.8	1.39
087	6×(2nm, 1nm Ta), 6nm Aℓ[b]	9.84	1.0	5.1	0.25	3.0	0.86

[a] Values obtained from Foner et al, 1981.

[b] Alternating layers of V_3Ga and Ta.

Values of $T_c, S = |dH/dT|_{Tc}$ and $b_{*o} = \lambda_{*o}/1.123$ were taken from critical field fits. Fermi-liquid effects were neglected by taking $G^o = 0$. The statistical variance for the fits is given in the last column. The value of ΔT_c is the 90% - 10% width of the zero-field transiton.

Abrikosov, A.A., and L.P. Gor'kov, Sov. Phys. JETP **15**, 752 (1962).
Ackermann, B., and R. Feder, Solid State Comm. **49**, 489 (1984).
Alexander, J.A.X., T.P. Orlando, D. Rainer, and P.M. Tedrow, Phys. Rev. B, **31**, 5811 (1985).
Alexander, J.A.X., P.M. Tedrow, and T.P. Orlando, Phys. Rev. B **34**, 8157 (1986).
Anderson, P.W., Phys. Rev. Lett. **3**, 325 (1959).
Androes G.M., and W.D. Knight, Phys. Rev. Lett. **2**, 386 (1959).
Asik, J.R., M.A. Ball, and C.P. Slichter, Phys. Rev. **181**, 645 (1969).
Ball, M.A., J.R. Asik, and C.P. Slichter, Phys. Rev. **181**, 662 (1969).
Bending, S.J., M.R. Beasley, and C.C. Tsuei, Phys. Rev. B **30**, 6342 (1984).
Bergmann, G., Phys. Rev. Lett. **48**, 1046 (1982).
Bergmann, G., and C. Horriar-Esser, Phys. Rev. B **31**, 1161 (1985).
Chandrasekhar, B.S., Appl. Phys. Lett. **1**, 7 (1962).
Clogston, A.M., Phys. Rev. Lett. **9**, 266 (1962).
Dew-Hughes, D., Cryogenics, **15**, 435 (1975).
Dyson, F.J., Phys. Rev. **98**, 349 (1955).
Elliott, R.J., Phys. Rev. **96**, 266 (1954).
Eigler, D.M., and S. Schultz, Phys. Rev. Lett. **54**, 1185 (1985).
Eigler, D.M., and S. Schultz, Solid State Comm. **44**, 1565 (1982).
Engler, H., and P. Fulde, Phys. Kondens. Mater. **7**, 150 (1968).
Feher, G., and A.F. Kip, Phys. Rev. **98**, 337 (1955).
Feder, R., in *Polarized Electrons in Surface Physics*, edited by R. Feder, (World Scientific, Sinapore, 1985).
Ferrell, R.A., Phys. Rev. Lett. **3**, 262 (1959).
Ferrell, R.A., and R.E. Prange, Phys. Rev. Lett. **17**, 163 (1966).
Foner, S., E.J. McNiff, Jr., S. Moehlecke, and A.R. Sweedler, Solid State Comm. **39**, 773 (1981).
Friedel, J., Nuovo cimento supplemento **7**, 287 (1958).
Gibson, G., Ph.D. thesis, (unpublished), M.I.T. (1988).
Gossard, A.C., A.J. Heeger, and J.H. Wernick, J. Appl. Phys. **38**, 1251 (1967).
Griswold, T.W., A.F. Kip, and C. Kittel, Phys. Rev. **88**, 951 (1952).
Hake, R.R., Appl. Phys. Lett. **10**, 189 (1967).
Harrison, W.A., *Solid State Theory*, p. 200, (McGraw-Hill, Inc., NY, 1970).
Harrison, Phys. Rev. **181**, 1036 (1969).
Lindelof, P.E., and S. Wang, Phys. Rev. B **33**, 1478 (1986).
Ma, M., and E. Fradkin, Phys. Rev. Lett. **56**, 1416 (1986).
Maki, K., Physics **1**, 21 (1964).
Maki, K., Phys. Rev. **148**, 362 (1966).
Meservey, R., and P.M. Tedrow, Phys. Rev. Lett. **41**, 805 (1978).
Meservey, R., P.M. Tedrow, and R.C. Bruno, Phys. Rev. B **17**, 2915 (1978).
Neuringer, L.J., and Y. Shapira, Phys. Rev. Lett. **17**, 81 (1966).
Ohlsen, H., and J.L. Calais, Phys. Rev. B **35**, 7914 (1987).
Orlando, T.P., E.J. McNiff, Jr., S. Foner, M.R. Beasley, Phys.Rev.B **19**,4545 (1979).

Orlando, T.P., and M.R. Beasley, Phys. Rev. Lett. **46**, 1598 (1981).
Overhauser, A.W., Phys. Rev. **89**, 689 (1953).
Pines, D., and C.P. Slichter, Phys. Rev. **100**, 1014 (1955).
Reif, F., Phys. Rev. **106**, 208 (1957).
Schopohl, N., and K. Scharnberg, Physica **135B**, 482 (1985).
Stesmans, A., and J.R. Sambles, J. Phys. F **10**, L171 (1980).
Tachikawa, K., Y. Tanaka, K. Inoue, K. Itoh, T. Asano and Y. Iijima, IEEE Trans. Mag. **Mag-21**, 1048 (1985).
Takeuchi, T., Y. Iijima, K. Inoue, and K. Tachikawa, J. Appl. Phys. **60**, 1227 (1986).
Tedrow, P.M., and R. Meservey, Phys. Rev. Lett. **43**, 384 (1979).
Tedrow, P.M., and R. Meservey, Phys. Rev. B **25**, 171 (1982).
Tedrow, P.M., J.S. Moodera, and R. Meservey, Solid State Comm. **44**, 587 (1982).
Tedrow, P.M., J.E. Tkaczyk, R. Meservey, S.J. Bending and R. Hammond, IEEE Trans. Mag. **MAG-21**, 1144 (1985).
Tkaczyk, J.E., and P.M. Tedrow, in *Advances in Cryogenic Engineering Materials*, Vol. 32, edited by R.P. Reed and A.F. Clark, (Plenum Publishing Corp., 1986).
Tkaczyk, J.E., and P.M. Tedrow, IEEE Trans. Mag. **Mag-23**, 948 (1987).
Walker, M.B., Phys. Rev. B **3**, 30 (1971).
Werthamer, N.R., E. Helfand, and P.C. Hohenberg, Phys.Rev. **147**, 295 (1966).
Yafet, Y., Solid State Phys. **14**, 1 (1963).
Yafet, Y., J. Appl. Phys. **39**, 853 (1968).
Yosida, K., Phys.Rev. **110**,769 (1958).

Appendix A — Impurity Scattering in the Normal State

Presented here is a review of the formulae and theoretical techniques which serve as a description of electron scattering in metals. As will be shown, several subtleties of spin-orbit and exchange scattering appear in this context apart from those connected with superconductivity. Furthermore, the formalism, as applied in this familiar context, serves as an introduction to the treatment of scattering in superconductors. Calculative details are given when they don't appear explicitly in the reference literature or when they aid in obtaining formulae with the correct factors of 2, π and $\hbar$.

A.1 Relaxation Rate in Boltzmann Transport

In a perfectly periodic lattice, electrons within the Brillouin zones scatter constructively such that the current flow is unimpeded, and a complete set of Bloch waves provides the appropriate diagonalized basis for constructing wave packets. However, the crystal potential of a real metal contains defects. If the density of these is small, one may separate the potential into a periodic part and a part which provides matrix elements between Bloch states of differing wavenumber and band index. A solution to the Boltzmann equation approximately describes the resulting effect of transport phenomena. In the following discussion point defects will be considered.

Entering into the Boltzmann transport equation is the time rate of change of the quasiclassical distribution function due to collisional processes.

$$\left.\frac{\partial f(\vec{r},\vec{k})}{\partial t}\right|_{Coll} = \sum_{\vec{k}'}\{W(\vec{k}',\vec{k})f(\vec{k}')[1-f(\vec{k})] - W(\vec{k},\vec{k}')f(\vec{k})[1-f(\vec{k}')]\}$$

where $W(\vec{k}',\vec{k})$ specifies the rate at which scattering transfers electrons from "quasiclassical momentum state" $\vec{k}'$ to $\vec{k}$. In fact, the scattering rate generally taken is the transition rate between Bloch states calculated from perturbation theory. For elastic scattering, in the approximation that external fields simply displace the distribution function in $\vec{k}$-space, the collision term reduces to the form

$$\left.\frac{\partial f(\vec{r},\vec{k})}{\partial t}\right|_{Coll} = -\delta f/\tau_{tr}(\vec{k}).$$

Here $\delta f = f - f^{\circ}$ is the deviation from the equilibrium (i.e. Fermi-Dirac) distribution function appropriate for the local temperature $T(\vec{r})$. In this "relaxation time approximation" the variable $\tau_{tr}(\vec{k})$ takes the interpretation of the mean time between collisions (Ashcroft & Mermin).

$$\tau_{tr}(\vec{k})^{-1} = \int_{E=E(\vec{k})} d\Omega_{\vec{k}'}\frac{N(\vec{k}')}{|\nabla_{\vec{k}'}E|}W(\vec{k},\vec{k}')(1-\cos\theta) \qquad A.1.1$$

here $N(\vec{k})$ is the density of states in $\vec{k}$-space for one spin-direction (e.g. $N(\vec{k}) = k^2V/(2\pi)^3$). The current due to an applied electric field $\vec{E}$ becomes

$$\vec{J} = \frac{-e^2}{4\pi^3} \int \tau_{tr}(\vec{k})\vec{v}(\vec{k})\vec{v}(\vec{k}) \cdot \vec{E} \frac{\partial f^\circ}{\partial E} d\vec{k}.$$

The derivative of the Fermi function restricts the integration to the Fermi surface.

— T-matrix —

In order to complete the connection between the impurity potential and measureable transport coefficients, it remains to consider the derivation of the transition rate $W(\vec{k}', \vec{k})$. The treatment here summarizes that given by Gottfried for the case where the impurity has no internal degrees of freedom. The perturbation can be viewed as adding an inhomogeneous term to the time-dependent Schrödinger equation.

$$(i\hbar \frac{d}{dt} - H_o)\psi_k(t) = H' \ \psi_k(t)$$

The solution is constructed from the retarded Greens' function and the solution of the homogeneous equation $|k,t\rangle$ which in this case is the Bloch function with k (without an arrow) specifying both the wavevector and band index.

$$\psi_k(t) = |k,t\rangle + \int_{-\infty}^{+\infty} G_+(t-t')H' \ \psi_k(t')dt'$$

$$G_+(t-t) = \frac{-i}{\hbar}\Theta(t-t')e^{-iH_o(t-t')/\hbar}$$

Assuming a time-independent perturbation, the energy is a constant of the motion and a separation of the time variable can be performed.

$$\psi_k(t) = |\psi_k\rangle e^{iE_k t/\hbar}; \quad |k,t\rangle = |k\rangle e^{iE_k t/\hbar}$$

$$|\psi_k\rangle = |k\rangle - \frac{i}{\hbar}\int_{-\infty}^{0} dt e^{i(H_o - E_k)t/\hbar} H' \ |\psi_k\rangle$$

The integration is performed with the introduction of a convergence factor $e^{\epsilon t/\hbar}$ which corresponds to the boundary condition of outgoing scattered waves.

$$|\psi_k\rangle = |k\rangle + \frac{1}{E_k - H_o + i\epsilon} H' \ |\psi_k\rangle$$

Introducing the unit operator formed by the complete set of Bloch states, one obtains

$$|\psi_k\rangle = \left(1 + \frac{1}{E_k - H_o + i\epsilon} T\right)|k\rangle. \qquad A.1.2$$

where the T-matrix is defined as follows: $\langle k'|T|k\rangle \equiv \langle k'|H'|\psi_k\rangle$. Operating on equation A.1.2 with H' and taking the scalar product with $\langle k'|$ one obtains

$$T = H' + H' \frac{1}{E_k - H_o + i\epsilon} T$$

$$= H' + H' \frac{1}{E_k - H_o + i\epsilon} H' + \cdots \qquad A.1.3$$

In the Born approximation one takes $T_{k'k} = H'_{k'k}$.

— Fermi Golden Rule —

The transition rate from a state $|k\rangle$ to $|k'\rangle$ is usually referred to as the "Fermi Golden Rule" and is derived as follows. Consider that a initial state $|k\rangle$ evolves in time under the perturbed hamiltonian as $|\psi_k\rangle$. The probability amplitude at time t that the state $|\psi_k, t\rangle$ can be found in the (unperturbed) state $|k', t\rangle$ is given by the inner product. The desired expression for the transition rate is obtained after some algebra.

$$
\begin{aligned}
W(k',k) &= \frac{d}{dt}|\langle k',t|\psi_k,t\rangle|^2 = 2\Re e\{\langle\psi_k,t|k',t\rangle\frac{d}{dt}\langle k',t|\psi_k,t\rangle\} \\
&= \frac{2}{\hbar}\Im m\{\langle\psi_k,t|k',t\rangle\langle k',t|H'|\psi_k,t\rangle\} \\
&= \frac{2}{\hbar}\Im m\{\langle\psi_k|k'\rangle\langle k'|H'|\psi_k\rangle\} \\
&= \frac{2}{\hbar}\Im m\left\{\left(\delta_{kk'} + \frac{\langle k|T|k'\rangle}{E_k - H_o + i\epsilon}\right)\langle k'|T|k\rangle\right\} \\
&= \frac{1}{i\hbar}|T_{k'k}|^2\left\{\frac{1}{E_k - H_o + i\epsilon} + \frac{1}{E_k - H_o - i\epsilon}\right\} + \delta_{k'k}\frac{2}{\hbar}\Im m T_{kk} \\
W(k',k) &= \frac{2\pi}{\hbar}|T_{k'k}|^2\delta(E_k - E'_k) + \delta_{k'k}2/\hbar T_{kk}
\end{aligned}
$$

The delta function is a consequence of choosing a time-independent perturbation. The last step uses the Dirac relation $(x + i\epsilon)^{-1} = P(1/x) - i\pi\delta(x)$ where P stands for the principle value. The use of this expression in A.1.1 gives the "momentum transfer lifetime" associated, for example, with the Drude conductivity $\sigma = ne^2\tau_{tr}(k_F)/m$. Alternately, one defines the lifetime of a Bloch state $|k\rangle$ which differs from A.1.1 by the absence of the momentum transfer factor $(1 - cos\theta)$.

$$
\hbar/\tau_k \equiv 2\pi\sum_{k'\neq k}|T_{k'k}|^2\delta(E_k - E_{k'}) \qquad A.1.4
$$

When working in the Born approximation, it is convenient to include from the start the effect of forward scattering off the impurities. For the case of exchange scattering, the forward scattering causes an observable Zeeman splitting of the conduction states. The perturbation is redefined as $\widetilde{H}'_{k'k} \equiv H'_{k'k} - \delta_{k'k}H'_{kk}$ and the hamiltonian becomes $\widetilde{H}_{k'k} \equiv (H^o_{kk} + H'_{kk})\delta_{k'k} + \widetilde{H}'_{k'k}$. Similarly T is replaced by $\widetilde{T}$ and the sum in equation A.1.4 can be extended to $k' = k$ since $\widetilde{T}_{kk} = 0$.

— Born Approximation —

The assumption that the impurities are randomly distributed in the crystal leads to a simplification of the matrix elements in the Born approximation. It is assumed that the impurity potential can be written $H' = \sum_i u(\vec{r} - \vec{R}_i)$ where $\vec{R}_i$ is a lattice vector specifying the position of the i^{th} impurity. The Bloch wave has the form

$\langle \vec{r}|k\rangle = \frac{1}{\sqrt{V}} w_{n\vec{k}}(\vec{r}) e^{i\vec{k}\cdot\vec{r}}$ where the band index has been reintroduced. The function $w_{n\vec{k}}$ is invariant under translation by a lattice vector and has a normalization $\langle w_{n'\vec{k}}|w_{n\vec{k}}\rangle = V\delta_{n'n}$. One can choose the following decomposition of the matrix element into a product of a geometrical structure factor and a form factor. In this way the configurative information is isolated in the structure factor.

$$\langle k'|H'|k\rangle = S(\vec{k}-\vec{k}')F_{n'n}(\vec{k}',\vec{k})$$

$$S(\vec{q}) \equiv \frac{1}{N}\sum_i e^{i\vec{q}\cdot\vec{R}_i}; \quad F_{n'n}(\vec{k}',\vec{k}) \equiv \frac{1}{\Omega}\int d\vec{r} e^{i\vec{q}\cdot\vec{r}} w^{\dagger}_{n'\vec{k}'}(\vec{r})u(\vec{r})w_{n\vec{k}}(\vec{r})$$

Here $\Omega = V/N$ is the unit cell volume and $\vec{q} = \vec{k} - \vec{k}'$. This is the conventional volume independent form factor; for example, in the free electron case the $k' = k$ form factor becomes the spatial average of the impurity potential multiplied by N, the number of unit cells in the crystal.

Averaging the matrix element over the impurity positions selects out the forward scattering amplitude.

$$\overline{S(\vec{q})} \equiv \left(\prod_i \int \frac{d\vec{R}_i}{V}\right) S(\vec{q}) = \frac{1}{N}\sum_i \int \frac{d\vec{R}_i}{V} e^{i\vec{q}\cdot\vec{R}_i} = c\left(\frac{(2\pi)^3}{V}\delta^3(\vec{q})\right) \qquad A.1.5$$

$$\overline{\langle k'|H'|k\rangle} = \overline{S(\vec{q})}F_{k'k} = \delta_{k'k}cF_{kk} \qquad A.1.6$$

The bar designates the average of the impurity sites over all lattice vectors of the crystal and c is the atomic concentration of impurities. Similarly one averages $|S(\vec{q})|^2$ to determine $\overline{\hbar/\tau_k}$. The average disposes of the phase factors $e^{i\vec{q}\cdot\vec{R}_i}$ which are responsible for the coherent backscattering associated with weak localization effects (Bergmann, 1983).

$$\begin{aligned}
\overline{S^{\dagger}(\vec{q})S(\vec{q})} &\equiv \left(\prod_{i,j}\int \frac{d\vec{R}_i d\vec{R}_j}{V^2}\right) S^{\dagger}(\vec{q})S(\vec{q}) \\
&= \sum_{i,j}\frac{1}{(NV)^2}\int d\vec{R}_i \vec{R}_j e^{i\vec{q}\cdot(\vec{R}_j-\vec{R}_i)} \\
&= \sum_{i,j}\frac{1}{(NV)^2}[V^2\delta_{ij} + (2\pi)^3 V\delta^3(\vec{q})(1-\delta_{ij})] \\
\overline{S^{\dagger}(\vec{q})S(\vec{q})} &= c/N + (c^2 - c/N)(\frac{(2\pi)^3}{V}\delta^3(\vec{q}))
\end{aligned}$$

and

$$\overline{|\tilde{T}_{k'k}|^2} = \left(\overline{S^{\dagger}(\vec{q})S(\vec{q})} - |\overline{S(\vec{q})}|^2\right)|F_{n'n}(\vec{k}',\vec{k})|^2$$

$$\overline{\hbar/\tau_k} = 2\pi \sum_{k'} \overline{|\tilde{T}_{k'k}|^2}\delta(E_k - E'_k) \qquad A.1.8$$

Thus the impurity averaged scattering time is related to the correlation function $\tilde{\Gamma}(\vec{q},\omega = 0) = (\overline{S^\dagger(\vec{q})S(\vec{q})} - |\overline{S(\vec{q})}|^2|)$. For randomly distributed impurities, Γ has the constant value c/N except for $\vec{q} = 0$ where it vanishes. One makes an error of the order $1/N$ by letting the correlation function equal c/N at $q = 0$. In this case,

$$\overline{\hbar/\tau_k} = \frac{2\pi c}{N} \sum_{n'} \int_{E=E(\vec{k})} |F_{n'n}(\vec{k}',\vec{k})|^2 \frac{N(\vec{k}')d\Omega_{\vec{k}'}}{|\nabla_{\vec{k}'}E|}. \qquad A.1.9$$

For a single free electron band with effective mass m, and if the form factor depends only on the difference $\vec{q} = \vec{k} - \vec{k}'$ and equals the Fourier transform of the impurity potential divided by the unit cell volume, the scattering time is a integral over the spherical Fermi surface.

$$\hbar/\tau_k = 2\pi c(\Omega N_o) \int_{FS} \frac{d\Omega_{\vec{k}'}}{4\pi} |u(\vec{q})|^2; \qquad u(\vec{q}) = \frac{1}{\Omega}\int d\vec{r} e^{i\vec{q}\cdot\vec{r}} u(\vec{r}). \qquad A.1.10$$

Here $N_o = mk/2\pi^2\hbar^2$ is the usual density of states for a single spin direction having units of $(energy)^{-1}(volume)^{-1}$.

— Inelastic Scattering —

In generalizing these results to the case where the scattering center has internal structure (so that the scattering may be inelastic) one notes that

$$f_{\vec{k}}(1 - f_{\vec{k}'}) = -k_B T \frac{\partial f_o}{\partial E}\left[\frac{1}{1 - f_o(1 - e^{-\hbar\omega/k_B T})}\right] = -k_B T \frac{df_o}{\partial E}\left[\frac{2}{1 + e^{\hbar\omega/k_B T}}\right].$$

where $\hbar\omega = E'_k - E_k$ is the energy exchanged to the scattering center. The factor in the brackets describes the freezing out of the inelastic processes at low temperatures due to the Pauli exclusion principle. To retain the form of the relaxation time approximation it is appropriate to include this factor in the expression for the scattering rate (eqs. A.1.1, A.1.4).

$$\hbar/\tau_k = 2\pi \sum_{k' \neq k} |T_{k'k}|^2 \delta(E'_k - E_k - \hbar\omega)\left[\frac{2}{1 + e^{\hbar\omega/k_B T}}\right]$$

As in the elastic case, the scattering in the Born approximation can be related to the pair correlation function. Here the treatment follows Van Hove (1954). and Ashcroft & Mermin (Appendix N). The internal state of the impurities will be designated by $|m\rangle$. For example, in the case of exchange scattering, $|m\rangle$ designates the set of azimuthal quantum numbers $\{m_{S_i}\}$ for the impurity spins. Define the dynamical structure factor

$$\Gamma(\vec{q},\omega) = \sum_m \wp_m \sum_{m'} |\langle m'|\frac{1}{N}\sum_i e^{i\vec{q}\cdot\vec{R}_i}|m\rangle|^2 \delta[\omega + \frac{E_m - E'_m}{\hbar}]$$
$$= \int e^{i(\vec{q}\cdot\vec{r}-\omega t)}\Gamma(\vec{r},t)d\vec{r}\frac{dt}{2\pi}$$

It follows that

$$\hbar/\tau_k = \frac{2\pi}{\hbar}\sum_{k'}|F_{k'k}|^2\Gamma(\vec{q},\omega)\left[\frac{2}{1+e^{\hbar\omega/k_BT}}\right]. \qquad A.1.11$$

The quantity $\wp_m$ represents the probability of finding the impurity system in an initial configuration $\{m\}$. It arises from the T-matrix calculated with a density matrix. For example, for a thermal average $\wp$ represents the Boltzmann factor.

$\Gamma(\vec{r},t)$ is the pair distribution function.

$$\Gamma(\vec{r},t) = \frac{1}{(2\pi)^3}\int e^{i(\omega t - \vec{q}\cdot\vec{r})}\Gamma(\vec{q},\omega)d\vec{q}d\omega$$
$$= \frac{1}{(2\pi)^3}\sum_{m,m'}\wp_m\frac{1}{N^2}\sum_{i,j=1}^{N_i}\int d\vec{q}e^{-i\vec{q}\cdot\vec{r}}\langle m|e^{-i\vec{q}\cdot\vec{R}_i}|m'\rangle e^{iE_{m'}t/\hbar}$$
$$\langle m'|e^{i\vec{q}\cdot\vec{R}_j}|m\rangle e^{-iE_m t/\hbar}$$

$$\Gamma(\vec{r},t) = \frac{1}{(2\pi)^3}\frac{1}{N^2}\sum_{i,j=1}^{N_i}\int d\vec{q}e^{-i\vec{q}\cdot\vec{r}}\left\langle\left\langle e^{-i\vec{q}\cdot\vec{R}_i(0)}e^{i\vec{q}\cdot\vec{R}_j(t)}\right\rangle\right\rangle$$

where $\ll\gg = \sum_m \wp_m\langle m|\,|m\rangle$ and $\vec{R}_j(t)$ is the Heisenberg operator. The convolution theorem states that the "Fourier inverse transform of an (ordered) product of Fourier transforms is the convolution of the original functions" (G.Arfkin, 1970).

$$\Gamma(\vec{r},t) = \frac{1}{N^2}\left\langle\left\langle\sum_{i,j=1}^{N_i}\int d\vec{r'}\delta(\vec{r}+\vec{R}_i(0)-\vec{r'})\delta(\vec{r'}-\vec{R}_j(t)\right\rangle\right\rangle$$

For $t = 0$, all operators commute so that

$$\Gamma(\vec{r},t=0) = \frac{1}{N^2}\left\langle\left\langle\sum_{i,j=1}^{N_i}\delta[r-(\vec{R}_j(0)-\vec{R}_i(0))]\right\rangle\right\rangle.$$

A.2 Field Theoretic Description

The Boltzmann treatment of transport just described suffers from its reliance on 1)the independent electron approximation and 2) a quasiclassical picture. Pair-correlations are important in superconductors so that the former restriction precludes a Boltzmann type description of superconductivity. Field theory provides a convenient means of dealing with these correlations. The following discussion will explore the microscopic (as opposed to quasiclassical) formalism for the normal state (Abrikosov, Gor'kov, and Dzyaloshinski, 1963); however, a quasiclassical treatment of superconductivity is possible and, in fact, can provide considerable simplification in cases where spatial variations are on a scale of the coherence length.

Pair-correlations are described by the zero temperature, time ordered Green's function averaged over the ground state wavefunction.

$$\begin{aligned} G_{\alpha\beta}(\vec{r},\vec{r'},t,t') &\equiv -i\langle T\psi_\alpha(\vec{r},t)\psi^\dagger_\beta(\vec{r'},t')\rangle \\ &= \frac{1}{(2\pi)^8}\int d\vec{k}d\vec{k'}\,G(\vec{k},\vec{k'},\omega)e^{i\vec{k}\cdot\vec{r}-i\vec{k'}\cdot\vec{r'}-i\omega(t-t')} \end{aligned}$$

The field operator $\psi_\alpha(\vec{r},t)$ destroys a particle with spin α at point $\vec{r}$ and time t. T is the time ordering operator which orders the operators from left to right for increasing values of the time variable. The Green's function is identically the probability amplitude of finding an electron with spin α at position $\vec{r}$ and time t after putting in a electron with spin β at $\vec{r'}$ and t'. The impurity potential in second quantized notation is

$$H' = \sum_i \int d\vec{r}\psi^\dagger(\vec{r})u(\vec{r}-\vec{R}_i)\psi(\vec{r}).$$

The perturbative solution consists of expanding the Green's function in terms of the Green's function of the unperturbed system. The unperturbed system is assumed homogeneous so that the Green's function depends only on one momentum index.

$$G_0^{-1}(\vec{k},\omega) = \hbar\omega - \varepsilon_0(\vec{k},\omega) + i\delta sgn(\varepsilon_0 - E_F)$$

As in the calculation of the T-matrix in section A.1, the factor δ is a convergence factor set to zero at the end of the calculation. The expansion is conveniently represented by Feynman diagrams.

$$\overline{\overline{k \quad k'}} = \overline{\delta(k'-k)} + \overline{k \times k'} + \overline{k \times k'' \times k'} + \cdots$$

$$G^{-1} = G_0^{-1} + G_0^{-1}H'G_0^{-1} + G_0^{-1}H'G_0^{-1}H'G_0^{-1} \cdots$$

$$G^{-1} = G_0^{-1} + G_0^{-1}\Sigma G_0^{-1}$$

where $\Sigma = H' + H'G_0^{-1}\Sigma$ is the self-energy.

Consider the average over the impurity positions. The first diagram (one cross) in the self-energy reduces, upon averaging, to the forward scattering amplitude as in equation A.1.6. In accord with the discussion of section A.1, this term is best considered as part of the unperturbed hamiltonian. The second order term (two crosses) is associated with a term

$$u(\vec{k}'' - \vec{k})u(\vec{k}'\vec{k}'')e^{i(\vec{k}-\vec{k}'')\cdot\vec{R}_i + i(\vec{k}''-\vec{k}')\cdot\vec{R}_j}.$$

This vanishes, upon averaging, unless $\vec{R}_i = \vec{R}_j$ and $\vec{k}' = \vec{k}''$. This corresponds to the result of eq. A.1.7. Thus upon averaging over the impurity positions one regains the homogeneity of the system and $\overline{G(\vec{k},\vec{k}',\omega)} = G(\vec{q},\omega)\delta(\vec{k}' - \vec{k} - \vec{q})$. Edwards (1958) and Abrikosov and Gorkov (1959) introduced a special diagrammatic technique so as to account for the results of impurity averaging. It consists of joining pairs of $\times$'s in the diagrams corresponding to the same impurity with a dotted line.

$$\overline{\Sigma(k)} = \times\!\!=\!\!\times$$

In the Born approximation,

$$\overline{\Sigma(k)} = V\int \frac{d\vec{k}'}{(2\pi)^3}|u_0(\vec{q})|^2 G_0(k').$$

The principle part of this integration is real and shifts the chemical potential. The residue is of the form $i\ sgn(\omega)/2\tau$ where $\hbar/\tau$ is given by A.1.10. The Green's function becomes

$$G^{-1}(k) = \hbar\tilde{\omega} - \varepsilon - \frac{i\,\hbar\ sgn(\omega)}{2\tau}$$
$$G(\vec{r}-\vec{r}',t) = G_0(\vec{r}-\vec{r}')e^{-|\vec{r}-\vec{r}'|/2\ell}$$

indicating that correlations are reduced over a length scale of the mean free path $\ell = v_F\tau$. Treating the scattering beyond the Born approximation corresponds to keeping more crosses in the self-energy diagram acting at the same impurity site. The effect is to replace the Born scattering amplitude with the exact scattering amplitude.

A.3 Spin-Orbit Scattering

The spin-orbit interaction takes into account the fact that, in the rest frame of a particle moving through a region with electric fields, there is a magnetic field acting on the spin of the particle. This section is an attempt to explain the magnitude of spin-orbit scattering from surfaces and impurities. The matrix element of the spin-orbit interaction between hydrogenic wavefunctions of a atom shows a strong dependence on atomic number $\sim Z^4$. However, in multielectron atoms, because of screening of the nuclear charge by inner (core) electrons, the spin-orbit splitting of outer orbitals goes as $\sim Z^2$. In simple metals it appears that the atomic matrix element is the appropriate matrix element to substitute into the Fermi golden rule to obtain the scattering rate. This is because in the region near the core, where the spin-orbit interaction makes its strongest contribution, the Bloch wave is well described by an atomic wavefunction. Thus the spin-orbit scattering in s-p metals is expected to go as $\sim Z^4$ as suggested by Abrikosov and Gor'kov (1962) and found experimentally by Meservey and Tedrow (1978). Although some features of simple metals are described well by a pseudopotential picture, the pseudoelectron moves too slow near the core of the atom $(v/c)^4 \sim 10^{-8}$ and spin-orbit scattering, a relativistic effect, is absent. Finally, in d-band metals complications arise due to the fact that the d-bands have both local and itinerant character.

—Spin-Orbit Coupling in Atoms—

The Foldy-Wouthuysen transformation separates the large and small components of the Dirac spinor for a particle interacting with a electromagnetic field. This corresponds to a separation of the particle and antiparticle motions. Among the things one obtains are, for example, the g-factor of the electron and terms in the hamiltonian which couple the spin and orbital motions. (Itzykson and Zuber,p.71; Zeiger and Pratt).

$$H_{so}(\vec{r}) = \frac{\hbar}{2m^2c^2}\vec{s}\times(\vec{\nabla}V(\vec{r}))\cdot\vec{p} \qquad A.3.1$$

Here $\vec{s}$ is the electron spin operator, $V(\vec{r})$ is the electrostatic potential and $\vec{p} = -i\hbar\vec{\nabla}$ is the momentum operator which acts to the right. In a central field $\vec{\nabla}V(\vec{r}) = \frac{1}{r}\frac{\partial V(r)}{\partial r}\vec{r}$ and

$$H_{so}(r) = \frac{h^2}{2m^2c^2}\left(\frac{1}{r}\frac{\partial V(r)}{\partial r}\right)\vec{s}\cdot\vec{L}.$$

where $\hbar\vec{L} = \vec{r}\times\vec{p}$ is the angular momentum operator. In a hydrogenic atom with potential $V(r) = Ze^2/r$ the matrix element between states of total angular momentum $I = L + S = \ell \pm 1/2$ becomes (Gasiorowicz, p.274).

$$\langle n, I_\pm, I_z, L, s = 1/2|H_{so}|n, I_\pm, I_z, L, s = 1/2\rangle = \frac{1}{4}mc^2(Z\alpha)^4\frac{\left\{\begin{smallmatrix}\ell\\-\ell-1\end{smallmatrix}\right\}}{n^3\ell(\ell+1/2)(\ell+1)} \qquad A.3.2$$

This $(\alpha Z)^4$ dependence of this matrix element is usually contrasted with the weaker $(\alpha Z)^2$ dependence of the matrix element of the coulomb potential itself.

$$\langle n, L|\frac{Ze^2}{r}|n, L\rangle = \frac{1}{2}(mc^2)(Z\alpha)^2/n^2 = (13.6eV)Z^2/n^2 \qquad A.3.3$$

The factors of Z come from the fact that

$$\langle 1/r\rangle = Z/n^2 a_o;\ \langle 1/r^2\rangle = Z^2/a_o^2 n^3(\ell + 1/2)$$

$$V(r) \propto Z; \langle\vec{\nabla}\rangle \propto Z$$

where a_o is the Bohr radius.

In multielectron atoms, one may expect the core electrons to screen the nuclear potential, thereby greatly reducing the spin-orbit splitting of the valence electrons. Landau and Lifshitz (sect. 72) treat the screening with the Thomas-Fermi approximation. They conclude that screening effects do alter the $(\alpha Z)^4$ dependence of the spin-orbit splitting. Essentially their argument is that the main contribution to the spin-orbit splitting comes from within an unscreened region $r_o \sim a_o/Z$ from the nucleus. The potential there has a magnitude $V(r_o) \sim Z^2e^2/a_o$ so that

$$\Delta_{so} \sim \wp\frac{\hbar^2}{m^2c^2}\frac{U(r_o)}{r_o^2} \sim \wp mc^2(\alpha Z)^4.$$

For large Z, the Thomas-Fermi approximation gives the probability of finding the electron near the nucleus $\wp \sim Z^{-2}$ so that $\Delta_{so} \sim mc^2\alpha^4 Z^2$. The spin-orbit splitting of elements have been determined spectroscopically and are compiled for the valence p-shell by Yafet(1963). These are plotted in figure A.3.1, and the general trend (especially for the heavy elements) is that the data follow $\Delta_{so} \sim \frac{1}{10}mc^2\alpha^4 Z^2$.

—Plane Wave vs. Tight Binding—

In metals, the atomic-like regions of the crystal introduce spin-orbit coupling into the crystal hamiltonian. For weak spin-orbit interaction diagonalization of the crystal hamiltonian yields a term of the form $\mu_B \vec{S}\cdot\hat{g}\cdot\vec{B}$ where the g-factor is a tensor which has diagonal elements not necessarily equal to 2 due to the mixing of the spin and orbital degrees of freedom. The diagonal elements of the g-factor can be measured by a spin-resonance experiment where resonant absorption is detected at $\hbar\omega = g_{\alpha\alpha}\mu_B B_\alpha$. Terse and clear examples are given by White (chapt. 2). Non-periodicity in the crystal due to phonons, defects or surfaces cause spin-orbit scattering which broadens the resonance line in energy by $\sim \hbar/\tau_{so}$. At low temperatures, phonon modes are unpopulated, and spin-relaxation is due primarily to impurity and surface scattering.

In a perturbative treatment of scattering in simple metals one expects a plane wave basis to suffice. For example, the band structure of simple metals and the residual resistivity are well described by a free electron model(Harrison, 1966,1970,1980). The success of the free electron model in spite of the strong crystalline potential is explained in the pseudopotential theory by observing that for the valence electrons the attractive coulomb potential is compensated by an effective repulsive interaction

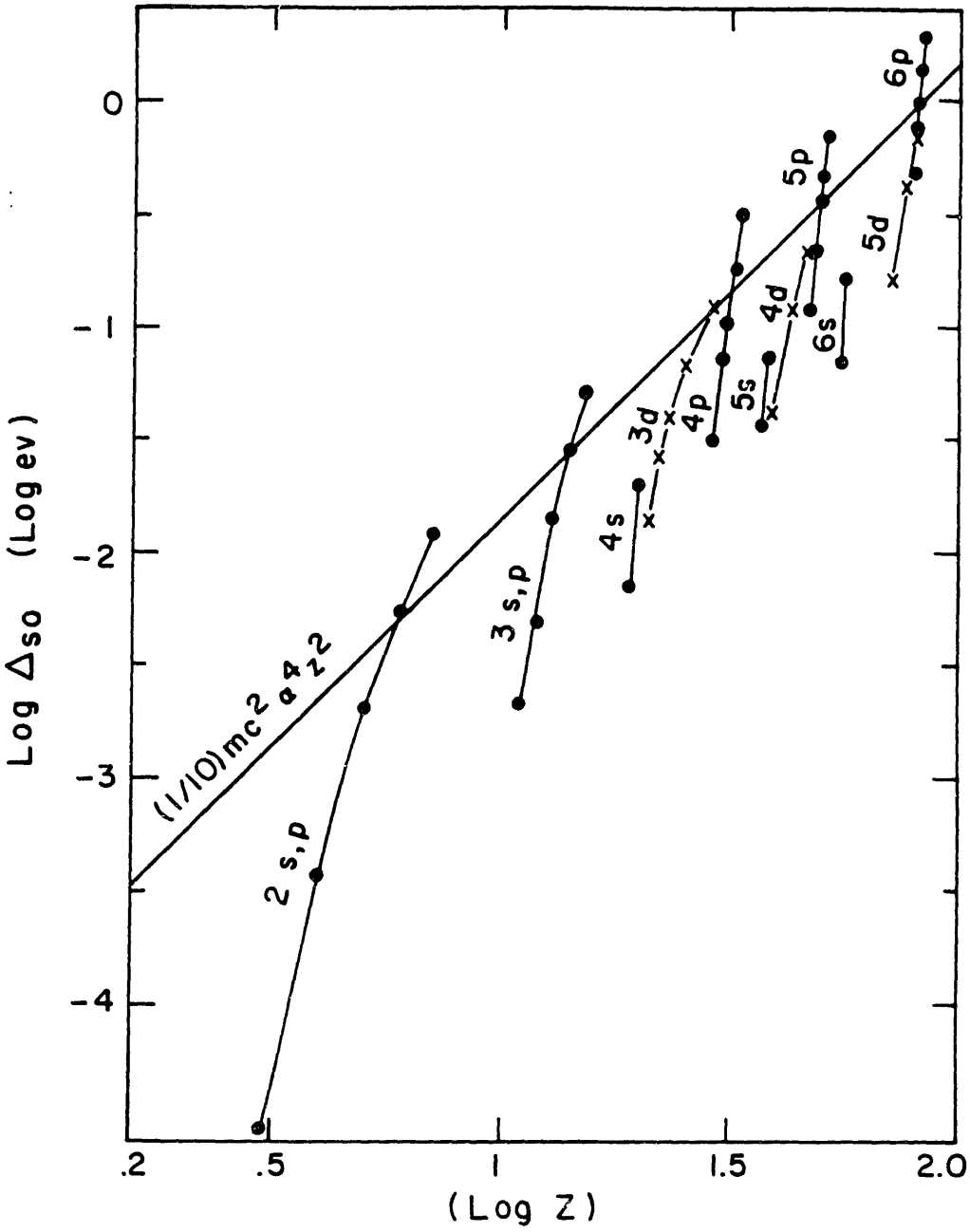

Fig. A.3.1 The base ten logarithm of the atomic valence p-orbital and metallic d-band splittings taken from Yafet (1963) and Mackintosh and Anderson (1980), respectively.

due to orthogonalization with the core states. As a result, the strong crystalline potential can be replaced by a weak pseudopotential, and the Bloch wave, which has strong oscillations near the atomic cores, replaced by a pseudo-wavefunction which is relatively smooth throughout the crystal. Perturbation theory with a plane wave basis is then used to obtain the band structure and residual resistivity of the metal. The smoothness of the pseudo-wavefunction means that the perturbation series will converge after including only a small number of plane waves. One can show that the band structure and residual resistivity obtained in this way are close to that which would be obtained from the real potential and Bloch wavefunction.

Consider the general form of the plane wave matrix element of the spin-orbit interaction.

$$\langle k'|H_{so}|k\rangle = \frac{\hbar}{2m^2c^2}\int d\vec{r}e^{-i\vec{k}'\cdot\vec{r}}[\vec{s}\cdot\vec{\nabla}V(\vec{r})\times(-i\hbar\vec{\nabla}_r)]e^{i\vec{k}\cdot\vec{r}}$$
$$= \frac{-i\hbar^2}{2m^2c^2}\int d\vec{r}e^{-i\vec{k}'\cdot\vec{r}}\vec{s}\cdot\vec{\nabla}V(\vec{r})\times i\vec{k}e^{i\vec{k}\cdot\vec{r}}$$

$$= \frac{\hbar^2}{2m^2c^2}\left\{\vec{s}\cdot\int d\vec{r}\vec{\nabla}(e^{-i\vec{k}'\cdot\vec{r}}V(\vec{r})e^{i\vec{k}\cdot\vec{r}})\times\vec{k} - (-i)\vec{s}\cdot(\vec{k}'\times\vec{k})\int d\vec{r}e^{i(\vec{k}-\vec{k}')\cdot\vec{r}}V(\vec{r})\right\}$$

The first term is a surface term and is neglected. The second term becomes

$$\langle k'|H_{so}|k\rangle = \frac{i\vec{s}\cdot(\vec{k}'\times\vec{k})}{k_F^2}\left[\frac{E_F}{mc^2}V(k-k')\right] \equiv \frac{i\vec{s}\cdot(\vec{k}'\times\vec{k})}{k_F^2}v_{so}. \qquad A.3.4$$

This is the form used throughout the literature on spin-orbit scattering in superconductors. However, note that the factor $v_{so} \sim E_F/mc^2$ so that $\hbar/\tau_{so} \propto (E_F/mc^2)^2 \sim (10eV/10^5eV)^2 = 10^{-8}$. The smallness of this factor follows directly from the fact that the spin-orbit interaction depends on the derivative of the wavefunction. Physically this is because the size of the magnetic field, acting on the electron spin in the electron rest frame, is proportional to the electron velocity relative to the crystal. For a plane wave $\beta = (v_F/c) \sim 10^{-2}$ and relativistic effects like spin-orbit scattering $\sim \beta^4$ are small.

It would appear that impurity scattering is unlikely to introduce spin-relaxation in "good pseudopotential metals". This, however, is not the case experimentally. The problem lies with the assumption that since the nearly free electron model describes well the band structure and residual resistivity, it will also describe spin-orbit scattering. In fact, plane waves provide a poor description of the true wavefunction in the core region $r \sim a_o/Z$ where the main contribution to the spin-orbit scattering is made. One expects that there the true Bloch state resembles closely the atomic wavefunction from which the band is derived. As a result one might consider a tight binding basis in a calculation of the spin-orbit scattering rate. Gallagher(1978) calculated the spin-relaxation time due to surface scattering in small particles and thin

films of s-p metals using the atomic spin-orbit splitting of Yafet and found factor of 5 agreement with experiment. For a tight binding basis $\langle \vec{r}|\vec{k},n\rangle = \frac{1}{\sqrt{V}} e^{i\vec{k}\cdot\vec{r}} w_{kn}(\vec{r})$ where $w_{kn}(\vec{r}) = \sqrt{V/N}\sum_R e^{-i\vec{k}\cdot(\vec{r}-\vec{R})}\psi_n(\vec{r}-\vec{R})$. Here $\psi_n(\vec{r})$ is a atomic orbital; n specifies the principle, orbital and spin quantum numbers. The $q = 0$ form factor for an impurity at lattice site $\vec{R}_o$ becomes

$$F_{n'n}(\vec{k},\vec{k}) = \frac{V}{N\Omega}\sum_{RR'}\int d\vec{r}\psi_{n'}(\vec{r}-\vec{R}')H_{so}(\vec{r}-\vec{R}_o)\psi_n(\vec{r}-\vec{R})$$

Since the spin-orbit interaction is large only near the core, it connects only atomic states at the same lattice site.

$$F_{n'n}(\vec{k},\vec{k}) = \int d\vec{r}\psi_n(\vec{r})H_{so}(\vec{r})\psi_n(\vec{r}) \equiv \Delta_{so}$$

The quantity Δ_{so} is the atomic matrix element which may be taken from figure A.3.1. The scattering rate becomes

$$\hbar/\tau_{so} = 2\pi c(\Omega N_o)|\Delta_{so}|^2 \qquad A.3.5$$

Disorder at the surface of a film causes diffuse scattering of the electron momentum and spin. In thin polycrystaline films, grain sizes are typically on the order of the film thickness L so that even for motion parallel to the film surface scattering centers are separated by a length L. Taking the region of disorder associated with grain boundaries or the film surface to be about one lattice constant thick, the effective impurity concentration c is of the order of the reciprocal of the film thickness measured in lattice constants. Here "impurity" refers to the non-periodic part of the crystal potential.

In this way Gallagher calculated the intrinsic spin-orbit scattering rate due to surface scattering in a number of s-p metals and found agreement with experiment to within a factor of 5. Using the free electron density of aluminum, $N_o = 1.18 \cdot 10^{22} cm^{-3} ev^{-1}$, a value $\Delta_{so}^{Al} = 1.38 \cdot 10^{-2} eV$ obtained from Yafet, and the lattice constant of bulk aluminum, $4.05\mathring{A}$, one obtains a value for the spin-orbit scattering rate of a $30\mathring{A}$ aluminum film from eq. A.3.5. $\hbar/\tau_{so} = 0.13meV$. The experimentally determined value is $\hbar/\tau_{so} = 0.05meV$. Since in a metal some delocalization of the electron is expected to occur, the use of the atomic matrix element may be expected to give an upper bound to the scattering rate. For scattering from a Au monolayer on the surface of a $30\mathring{A}$ film of Al, one may expect to use $\Delta_{so}^{Au} = 0.471eV \longrightarrow \hbar/\tau_{so} \approx 150meV$. This is consistent with the experimental fact that the spin-orbit scattering of a thin Al film is greatly enhanced by a surface layer of some heavy elements– for example, Pt (Tedrow and Meservey, 1979,1982).

The general trend of the matrix element Δ_{so} as a function of atomic number is shown in figure A.3.1. The erratic behavior can be attributed to the completion of atomic orbitals and the associated increase in effective screening. Overall, for large Z the matrix element follows the general trend $\Delta_{so} \sim (1/10)mc^2\alpha^4 Z^2$. As discussed previously, this is understood in the quasiclassical treatment of the multielectron

atom of Landau and Lifshitz where the screening is treated in the Thomas-Fermi Approximation. In a tight binding calculation of impurity scattering one then expects $\hbar/\tau_{so} \propto \Delta_{so}^2 \sim (\alpha Z)^4$. It is possible that this is the line of reasoning which lead Abrikosov and Gorkov to suggest that the ratio of the transport to spin-orbit scattering time was of the order $(\alpha Z)^4$ in samples where the scattering is dominated by surface collisions. This is in fact the dependence found by Meservey and Tedrow in a compilation of data on the spin-orbit scattering rate in many s-p metals.

(Alternatively, Gallagher points out that the ratio of the spin-orbit (A.3.2) to the (unscreened) coulomb (A.3.3) atomic matrix elements goes as $(\alpha Z)^2$ so that one may expect the ratio of the scattering rates to go as $(\alpha Z)^4$. He suggest that this may have been the line of reasoning followed by Abrikosov and Gorkov. However, after working out the implications of this view, Gallagher finds that the calculation of the ratio of the scattering rates is orders of magnitude different from the experimental data. He suggests an explanation which doesn't appear convincing. Rather, it is suggested that it is not accurate to calculate the transport scattering rate with a tight binding basis for the conduction states. Gallagher goes on to calculate, in the manner described above, the spin-orbit scattering rate, rather than the ratio, and finds agreement with experiment.)

—The pseudopotential and resonant scattering—

Whereas the residual resistivity of a simple metal can be calculated in a plane wave basis, it has been shown that the spin-orbit scattering rate is better calculated with a tight-binding basis. The success of the pseudopotential method for the former rests on the result that the attractive crystalline potential in the core region is compensated by the additional kinetic energy gained due to orthogonalization to core electrons. However, for the spin-orbit interaction there is no corresponding compensation effect. In fact, just the reverse occurs since the spin-orbit interaction involves the *product* of the electron velocity and the potential gradient. The pseudopotential W acting on the smooth (plane-wave-like) pseudo-wavefunction $|k\rangle$ has the form (Harrison,section 5)

$$W|k\rangle = U|k\rangle + \sum_t |t\rangle \left(\langle k| \frac{-\hbar^2 \nabla^2}{2m} |k\rangle + \langle k|W|k\rangle - E_t \right) \langle t|k\rangle. \qquad A.3.6$$

Here U is the true potential including the screened coulomb and the spin-orbit interactions $U = V + V_{so}$. The impurity scattering is calculated by treating the difference between the pseudopotential at the impurity and host sites as a perturbation. However, as is apparent in eq. A.3.6, the spin-orbit interaction appears only in matrix elements of the form $\langle k|V_{so}|k\rangle$. Since the pseudopotential is smooth, these matrix elements are smaller that typical atomic matrix elements by a factor $(v/c)^2 \sim E_F/mc^2 \sim 10^{-4}$. Thus the simple pseudopotential picture of metals fails to describe spin-orbit scattering. One must substitute from the start the form A.3.4 for V_{so} with v_{so} replaced with Δ_{so} the atomic matrix element.

A similar failure of the pseudopotential A.3.6 is found in the case of resonant scattering from impurities with unfilled d-orbitals. From the start the theory of transition metal pseudopotentials introduces a hybridization term $\langle k|\Delta|t\rangle$ which takes into

account the resonant mixing of the s-p conduction states with the more localized d-orbitals. For example, Friedel and coworkers (1952, 1954, 1958) showed experimentally that the residual resistivity due to 3-d transition metal impurities in Al followed a resonant dependence on the energy difference $E_d - E_F$ (fig. A.3.2). For Sc impurities the d-orbital is mostly empty and its energy lies above the Fermi level. For Cu, the d-orbital is mostly filled and its energy lies below the Fermi level. The peak in the resistivity occurs at Cr impurities which corresponds to the energy of the d-orbital crossing the Fermi energy. The resonant scattering of the itinerant electrons at the Fermi surface off the potential well represented by the impurity d-orbital is strong and cannot be treated by perturbation theory. Rather one uses phase shift analysis and a sum rule discovered by Friedel which relates the difference in valency of impurity and host z to the phase shifts.

$$z = \sum_{\ell} (2\ell + 1) sin^2(\delta_\ell)$$

By assuming only the $\ell = 2$ term, that is d-wave scattering, contributes one can calculate the order of magnitude as well as the dependence of the residual resistivity shown in figure A.3.2 using no adjustable parameters.

Yafet(1968) has introduced a similar resonant scattering type calculation for spin-orbit scattering. However, in the absence of a spin-orbit counterpart to the Friedel sum rule, this calculation involves the adjustable parameters $\varepsilon_d, (U - J)$ appearing in the Anderson model. Yafet finds the scattering time (for ℓ-wave scattering)

$$\hbar/\tau_{so} = n_i v_F \left[\frac{4\pi^3}{3k_F^2} \ell(\ell+1)(2\ell+1) \lambda_{eff}^2 \rho_d^2(\varepsilon_F) \right]$$

where the factor in the brackets is the cross section for one impurity. The parameters λ_{eff}, an effective spin-orbit scattering rate, and ρ_d, the d-orbital contribution to the density of states at the Fermi level, can be expressed in term of $\varepsilon_d, (U - J)$, and the atomic matrix element of the spin-orbit interaction Δ_{so}. Asik, Ball and Slichter(1969) used a somewhat different phase shift analysis to calculate the conduction electron spin-resonance relaxation time due to spin-orbit scattering from impurities in Li and Na. They find good agreement with the magnetudes and some trends across the periodic table for those impurities whose valence differs by 0,1, or 2 from the host. This theory does not account for an observed maximum as one moves across the periodic table.

These methods are approximate descriptions of scattering in s-p and 3d-metals. It may be expected that scattering in the 4,5-d metals and intermetallic compounds will be more complicated due to the intermediacy of the bands between local and itinerant character and the possibility of more than one type of atom per unit cell (e.g. V_3Ga). In fact, no approximation may prevent the necessity of solving the Schroedinger equation with methods like those used in band structure calculations. For example, the impurity scattering phase shifts discussed above could be calculated (Clogston, 1962) with a local, Wannier representation using the methods of Koster and Slater (1954). However, a common feature is expected to be that spin-orbit scattering and other relativistic corrections still have their major contribution from the core regions where

the Bloch wave resembles closely the associated atomic wavefunction. In fact, the quantum defect method (Brooks and Ham, 1958; Callaway, 1957) uses parameters obtained from atomic structure to determine the band structure. Other relativistic band calculations (Mackintosh and Anderson, 1980; Koelling and MacDonald, 1983) use relativistic dynamics to solve for atomic-like solutions inside the Wigner-Seitz cell and then match these to plane waves in the interstitial region. As shown in figure A.3.1, the resulting spin-orbit coupling in the metal is not very different from that in the atom.

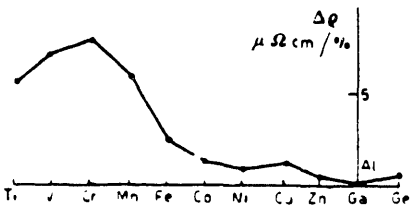

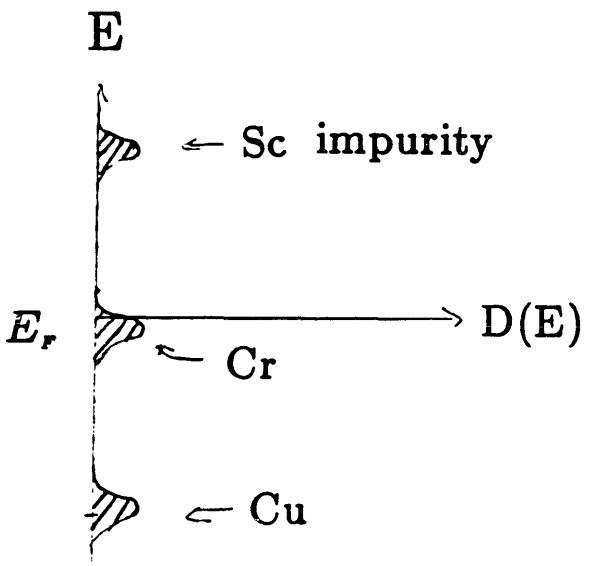

Fig. A.3.2 The residual resistivities of transitional impurities in Aℓ (from Friedel, 1958).

A.4 Exchange Scattering in the s-d Model.

The understanding of dilute solid solutions of magnetic impurities in metals has an involved but interesting history reaching back into the 1950's. However, rather than a historical perspective, a brief overview of the question of moment formation is given with the purpose of justifying the s-d exchange model. This is followed by an investigation of the s-d model in successively higher orders in perturbation theory leading up to the Kondo effect in third order. In second order, and in the s-d model a general expression for the scattering time in the Born approximation is obtained taking into account both spatial and temporal spin-correlations amongst the impurities.

—Moment Formation—

In insulators, an impurity generally assumes a definite valence state and retains the magnetic character of unfilled orbital shells as determined by Hund's rules. Effects due to neighboring ions of the solid are generally restricted to weak crystalline fields. However, in metal hosts, coulomb interactions and covalent mixing of local and itinerant electrons perturbs the ionic state. A general phenomenological picture emphasized by D.K.Wohlleben & B.R.Coles (1973) views the magnitude of the spin as always well defined but the axis direction as fluctuating. At high temperatures the axis motion is due to thermal fluctuations and the moment can be said to exist in the sense that the susceptibility follows a Curie law $\chi(T) \propto 1/T$. However, "there must exist a temperature T_f below which the motion of the axis of the moment is no longer dominated by thermal fluctuations $\cdots$ but by intrinsic fluctuations due to residual interactions with the conduction electrons." One expects a crossover to a regime where the susceptibility saturates $\chi(T) \propto 1/(T+T_f)$ and the moment is said to be quenched.

In the former case, the local and itinerant electrons are in some sense isolated from (orthogonal to) one another. One would like to consider the ionic and Block wavefunctions as a basis set and introduce a small effective coupling in a perturbative description. Of course such a description is only *useful* if the perturbation series converges in low order. If the series does not converge, then this means that the basis set is inappropriate. The Kondo effect is a case in point where the third order term in the perturbation series diverges at and below the "Kondo temperature". This suggests that the basis set does not span a large enough space to describe the physical system.

That the spin-dependent part of the effective coupling between two well separated groups of electrons can be expressed as the inner product of their spins $-J\vec{s}_1 \cdot \vec{s}_2$ is a non-trivial result whose validity and derivation are reviewed by Herring(1966), and the essential points are discussed by Callaway. An important concept is that the operator $(\frac{1}{2} + 2\vec{s}_1 \cdot \vec{s}_2)$ exchanges the spin indices of two distinguishable electrons.

$$(\frac{1}{2} + 2\vec{s}_1 \cdot \vec{s}_2)|1\uparrow\rangle|2\downarrow\rangle = (\frac{1}{2} + 2s_{1z}s_{2z} + s_{1+}s_{2-} + s_{1-}s_{2+})|1\uparrow\rangle|2\downarrow\rangle = |1\downarrow\rangle|2\uparrow\rangle$$

Thus the dot product of the spins enters in lowest order in the coupling of two electron wavefunctions where the antisymmetrize property of the total wavefunction must be preserved. That is, the appearance of this operator in the effective hamiltonian can

be understood as taking into account the fact that the basis functions treat the two electrons as distinguishable whereas in the true wavefunction they must be indistinguishable.

Herring derives a general expression for the exchange constant J. However, from elementary considerations (Zeiger and Pratt, sec.4.12.2) it can be seen that J will have positive (ferromagnetic) contributions arising from "direct" exchange and negative (antiferromagnetic) contributions from hybridization (Kondo,1962; Watson et al, 1965,1969). The direct term is of the form

$$J_{direct} = \int d\vec{r}_1 d\vec{r}_2 \psi_k^\dagger(\vec{r}_1)\phi_{loc}^\dagger \frac{e^2}{|\vec{r}_2 - \vec{r}_1|}\psi_k(\vec{r}_2)\phi_{loc}(\vec{r}_1).$$

This coupling is ferromagnetic since for parallel spin alignment the two electron wavefunction has a node between the electrons and the coulomb energy is reduced. The second order perturbative term in the coupling V_{dk} between the local and itinerant states contributes

$$J_{hyb} \propto -\frac{\langle k|V_{dk}|\phi_{loc}\rangle\langle\phi_{loc}|V_{dk}|k\rangle}{E_{loc} + U - \varepsilon_k}$$

. Here $\langle H' \rangle$ is the hybridization matrix element discussed by Watson et al (1969) and U is the on-site coulomb interaction

$$U = \int d\vec{r}_1 d\vec{r}_2 \phi_{loc}^\dagger(\vec{r}_1)\phi_{loc}^\dagger(\vec{r}_2)\frac{e^2}{|\vec{r}_2 - \vec{r}_1|}\phi_{loc}(\vec{r}_1)\phi_{loc}(\vec{r}_2).$$

Many of the ideas above are summarized in a model due to Anderson(1961) which starts with the hamiltonian

$$H = \sum_{k\alpha} \varepsilon_k c_{k\alpha}^\dagger c_{k\alpha} + \sum_\beta E_d c_{d\beta}^\dagger c_{d\beta} + U c_{d\uparrow}^\dagger c_{d\uparrow} c_{d\downarrow}^\dagger c_{d\downarrow} + \sum_{k,\alpha} V_{dk}(c_{k\alpha}^\dagger c_{d\alpha} + c_{d\alpha}^\dagger c_{k\alpha}).$$

Here $c_{k\alpha}^\dagger, c_{d\alpha}^\dagger$ are the creation operators for conduction and local electrons respectively. The local-itinerant coupling V_{dk} changes the local state into a virtual bound state or resonance of energy width $\Delta \sim \pi V_{dk}^2 N_o$ in analogy with the Fermi golden rule result of sections A.1 and A.2. In some sense Δ plays the role of the the intrinsic spin fluctuations $k_B T_f$ discussed at the beginning of this section. A zero-temperature, self-consistent Hartree-Fock calculation predicts a well-defined magnetic state of the ion when $\Delta \ll U, U \sim 2(\varepsilon_F - E_d)$. That is, when the energy broadening is small and the two "exchange split" local states sit symmetrically about the Fermi energy (Fig. A.4.1). By a variety of means one can show that in this limit the Anderson model reduces to a description equivalent to that of the s-d exchange hamiltonian $H_{s-d} = -J\vec{S}\cdot\vec{s}$. (Kondo,1962; Schrieffer and Wolff, 1966; Krishna-murthy et al, 1974). In the case of orbitally degenerate local states, the Anderson model can be suitably generalized and a similar correspondence can be made (Hirst,1972; *Coqublin

& Schrieffer,1969) to a generalized s-d exchange interaction in which both orbital and spin degrees of freedom are considered.

In most of the rare-earths there is considerable simplification from the general case. The 4f-shell is well shielded by outer shells(Taylor and Darby). The moment is well defined; the exchange coupling with conduction electrons is weak and positive and would appear to be primarily due to direct coulomb exchange. Lui(1961) has calculated the coulomb exchange integrals and concludes that the effect of the orbital degrees of freedom enters by simply replacing the ion spin by its projection onto the total angular momentum.

$$S \longrightarrow \frac{\vec{S}\cdot(\vec{L}+\vec{S})}{|\vec{L}+\vec{S}|^2} = (g_L - 1)(\vec{L}+\vec{S})$$

where g_L is the Lande g-factor. This is in accord with the ideas of DeGennes(1958) and Brout and Suhl(1959). In fact, the factor $(g_L - 1)(\vec{L}+\vec{S})$ is often called the DeGennes factor. However, a further complication is the fact that some rare-earth ions (Ce,Sm and Yb) have excited states close in energy to the ground state configuration. When in solid solution in a metal or in compounds, such ions may resonate between ionic states differing in valence. Since the different states have in general different ionic spin, these "valence fluctuations" introduce spin fluctuations and a relative high temperature T_f below which the moment is quenched. Since the Kondo effect produces similar quenching, the correct interpretation of experimental results may be difficult. A comprehensive theory would want to combine valence fluctuations, orbital degeneracy, crystal field effects, etc. into a suitably generalized Anderson type model treated non-perturbatively so as to deal with Kondo effects. On this point Anderson remarks "In fact, until recently I had come to think that the mixed valence problem was almost a trivial exercise in physical understanding, but more recently I have come to believe that there are real and very interesting complexities $\cdots$ which do indeed go beyond the primitive, fundamental understanding which one can achieve with simple physical concepts."(Anderson,1984).

—Zener model—

With this introduction, take the exchange interaction for rare-earth impurities to be the s-d model exchange hamiltonian and consider a perturbative calculation of the observable effects.

$$H_{ex} = -\sum_p J(\vec{r}-\vec{R}_p)\vec{S}_p\cdot\psi^\dagger(\vec{r})\vec{s}\psi(\vec{r})$$

where $\vec{s}=\vec{\sigma}/2$ is half the Pauli spin operator and $\psi^\dagger(\vec{r}) = (\psi_\uparrow^\dagger(\vec{r}),\psi_\downarrow^\dagger(\vec{r}))$ is a spinor operator with $\psi_\alpha(\vec{r}) = \sum_k \langle\vec{r}|k\alpha\rangle c_{k\alpha}$. Here $c_{k\alpha}$ is the annihilation operator for a Bloch state $|k\alpha\rangle = |\vec{k},n,\alpha\rangle$ with spin projection $\langle s_z\rangle = \alpha = \pm 1/2$. The local moments are described by a constant spin $S_p = S$ and a variable spin projection $\langle S_{zp}\rangle = m_p$. For convenience of notation the spin state of all the impurities $\{\prod_p |S,m_p\rangle\}$ will be designated by $|m\rangle$. The matrix element of the exchange hamiltonian becomes

$$\langle k'\alpha'm'|H_{ex}|k\alpha m\rangle = \langle k'\alpha'm'|c^{\dagger}_{k'\alpha'}J_{k'k}\vec{S}(\vec{q})\cdot\vec{s}_{\alpha'\alpha}c_{k\alpha}|k\alpha m\rangle$$

$$= J_{k'k}\langle m'|\vec{S}(\vec{q})|m\rangle\cdot\vec{s}_{\alpha'\alpha}.$$

The geometric structure factor is an impurity spin operator,

$$\vec{S}(\vec{q}) = \frac{1}{N}\sum_{p} e^{i\vec{q}\cdot\vec{R}_p}\vec{S}_p$$

and

$$J_{k'k} = \frac{1}{\Omega}\int d\vec{r}e^{i\vec{q}\cdot\vec{r}}w^{\dagger}_{\vec{k}',n',\alpha'}(\vec{r})J(\vec{r})w_{\vec{k},n,\alpha}(\vec{r})$$

is the form factor. Using the fact that $\vec{S}\cdot\vec{s} = S_z s_z + \frac{1}{2}(S_+ s_- + S_- s_+)$ one obtains a matrix element which clearly distinguishes the spin-flip and non-spin-flip processes.

Assuming no coupling between the impurity spins, the initial spin states are independently distributed among all possible configurations with a weight given by the Boltzmann factor $\wp_m = (1/Z)exp(-\eta m)$ where $\eta = g\mu_B B/K_B T$. In applying the thermal average the following relations are useful.

$$\sum_{m=-s}^{s} e^{-\eta m} = Z, \textit{ the partition function}$$

$$\sum_{m=-s}^{s} m\wp_m = -\frac{1}{Z}\frac{\partial Z}{\partial \eta} = -SB_S(\eta) \qquad A.4.1$$

$$\sum_{m=-s}^{s} m^2\wp_m = \frac{1}{Z}\frac{\partial^2 Z}{\partial \eta^2} = S(S+1) - SB_S(\eta)coth(\eta/2)$$

Here $B_S(\eta)$ is the Brillouin function.

In what may be called the Zener model(T.Kasuya, 1966), one considers only the spin-conserving part of the exchange interaction. This would represent the case where the impurity spins are aligned by a large external magnetic or internal (Weiss) field $\vec{B}$ so that spin-flip processes are frozen out. In first order, the perturbation is conveniently described by an spatially inhomogeneous, effective magnetic field. In the following, intraband coupling is considered; the generalization follows as in section A.1.

$$B_{ex}(\vec{q}) = -\langle\langle S_z(\vec{q})\rangle\rangle J(\vec{q})/g\mu_B$$

where

$$\langle\langle S_z(\vec{q})\rangle\rangle \equiv \left[\prod_{p'}\sum_{m_{p'}=-S}^{S}\wp_{m_{p'}}\right]\frac{1}{N}\sum_{p} m_p e^{i\vec{q}\cdot\vec{R}_p} = -SB_S(\eta)S(\vec{q})$$

where $S(\vec{q})$ is the (scalar) geometric structure factor defined in section A.1. If $J > 0$ (i.e. ferromagnetic coupling) then $\vec{B}_{ex}$ is in the same direction as the field $\vec{B}$. The average over the impurity configurations projects out the uniform exchange field $\overline{B_{ex}(q)} = B_{ex}(0)\delta_q = cSB_S(\eta)\delta_q/g\mu_B$. This spatially homogeneous field was used by Zener(1951) in a model of indirect coupling in ferromagnets.

The linear response of the conduction electron system is described by the static susceptibility which for a parabolic band is (H.G.Zeiger and J.W.Pratt, 1973).

$$\chi(\vec{q}) = \frac{g\mu_B^2}{2} N_o F(q/2k_F)$$

where

$$F(z) = \frac{1}{2}\left\{1 - \frac{1}{2z}(1-z^2)\ell n\left|\frac{1-z}{1+z}\right|\right\}$$

The conduction electron magnetization is

$$M(\vec{r}) = \int d\vec{r'}\chi(\vec{r}-\vec{r'})B_{ex}(\vec{r'}) = \sum_{\vec{q}} \chi(\vec{q})B_{ex}(\vec{q})e^{i\vec{q}\cdot\vec{r}} = -SB_S(\eta)\sum_{\vec{q}} \chi(\vec{q})J(\vec{q})S(\vec{q})e^{i\vec{q}\cdot\vec{r}}.$$

First consider the result in a totally localized limit. That is $J(\vec{q})$ independent of $\vec{q}$, and one impurity ($S(\vec{q}) \longrightarrow 1/N$).

$$M(\vec{r}) = (\frac{2}{\pi}k_F^3)(N_o\Omega)\ 2g\mu_B J(0)SB_S(\eta)\left(\frac{cosx}{x^3} - \frac{sinx}{x^4}\right)$$

where $x = 2k_F|\vec{r}|$. This localized oscillatory response is the RKKY (Ruderman el al, 1954) result following from the sharp Fermi surface and the delta function (i.e. q-independent) exchange potential and is a general feature of localized perturbations in an electron gas (Friedel, 1952,1954,1958). Since this expression is singular at the origin, the average magnetization is non-zero and equals $2(g\mu_B N_o J(0)SB_S(\eta))/N$. (Note that $\int_0^\infty dx(sinx - xcosx)/x^2 = 1$).

Alternatively consider the case of an uniform exchange field. For example, if one performs an average over the impurity positions, $\overline{S(\vec{q})} \longrightarrow c\frac{(2\pi)^3}{V}\delta(\vec{q})$. In the limit $q \longrightarrow 0, F(q/2k_F) \longrightarrow 1$ and $\chi(\vec{q})$ reduces to the Pauli paramagnetic susceptibility and the response is a uniform polarization of the conduction electrons.

$$\overline{M(\vec{r})} \longrightarrow cg\mu_B N_o J(\vec{q}=0)SB_S(\eta).$$

Thus, it is clear that with the indiscriminate use of the configurative average some physics is possibly lost, namely the local and oscillatory nature of the polarization.

—Exchange Scattering—

In a perturbative expansion, terms to second order represent scattering in the Born approximation. By applying a magnetic field to the system, one introduces

time-dependent spin-correlations which repress spin-flip scattering. Exchange scattering in the presence of spatial and temporal correlations among the impurity spins is discussed in the literature in the context of electrical resistivity (Dekker, 1965; VanPeski-Tinbergen and Dekker, 1963; DeGennes and Friedel, 1958), neutron scattering (Soukoulis, Grest and Levin, 1978), and the depairing of superconductivity (Soukoulis and Grest, 1980;Entel and Klose, 1974;Rainer, 1972). In the following the correspondence between these references is outlined. A general expression for the scattering rate is derived and shown to differ from that of Soukoulis et al by one term. This term arises due to the non-commutivity of the spin operators and is shown to be necessary in order for the general expression to reduce, in the limit of no spatial correlations, to the expression given by VanPeski-Tinbergen and Dekker. Physically this term takes into account the fact that the scattering rate for spin-up conduction electrons may be different than that for the spin-down ones.

As explained in section A.1 it is convenient to consider the forward scattering part of the perturbation as part of the unperturbed hamiltonian, that is, as adjusting the chemical potential. For exchange scattering this corresponds to the Zeeman splitting induced by the uniform exchange field and is *an observable effect.* The importance of treating this algebraically troublesome complication in detail is that the forward scattering acts differently on superconductivity from scattering which involves a momentum transfer. Thus a calculation of the scattering time requires an evaluation of the dynamical structure factor modified so as to remove the forward scattering part of the exchange interaction. As in section A.1 this is indicated by a tilde above.

$$\widetilde{\hbar/\tau_{k\alpha}} = \frac{2\pi}{\hbar}\sum_{k'}|J_{k'k}|^2\tilde{\Gamma}_\alpha(\vec{q},\omega)\left[\frac{2}{1+e^{\hbar\omega/k_BT}}\right] \qquad A.4.2$$

where

$$\tilde{\Gamma}_\alpha(\vec{q},\omega) = \sum_{\alpha' m' m}\wp_m\left|\langle\alpha' m'|\frac{1}{N}\sum_p e^{i\vec{q}\cdot\vec{R}_p}(\vec{s}\cdot\vec{S}_p - \vec{s}\cdot\langle\langle\vec{S}_p\rangle\rangle)\delta_q|m\alpha\rangle\right|^2\delta(\omega+\frac{E_m-E'_m}{\hbar})$$

$$\langle\langle\vec{S}_p\rangle\rangle \equiv \sum_{m_p}\wp_{m_p}\langle m_p|\vec{S}_p|m_p\rangle = SB_S(\eta)\hat{e_z}$$

Here $\delta_q = \frac{(2\pi)^3}{V}\delta(\vec{q})$. The reduction of the dynamical structure factor to a correlation function between impurity spins on different sites is best accomplished in the time domain and is similar to the calculation of DeGennes for elastic scattering.

$$\tilde{\Gamma}_\alpha(\vec{q},t) = \int d\omega e^{i\omega t}\tilde{\Gamma}(\vec{q},\omega)$$

$$= \sum_{m'm}\wp_m\frac{1}{N^2}\sum_{p,l}\langle\alpha m|e^{-i\vec{q}\cdot\vec{R}_p}(\vec{s}\cdot\vec{S}_p - \vec{s}\cdot\langle\langle\vec{S}_p\rangle\rangle\delta_q)|\alpha' m'\rangle e^{iE_{m'}t/\hbar}$$

$$\langle\alpha' m'|e^{i\vec{q}\cdot\vec{R}_l}(\vec{s}\cdot\vec{S}_l - \vec{s}\cdot\langle\langle\vec{S}_l\rangle\rangle\delta_q)|\alpha m\rangle e^{-iE_m t/\hbar}$$

$$\widetilde{\Gamma}_\alpha(\vec{q},t) = \frac{1}{N^2}\sum_{p,l} e^{i\vec{q}(\vec{R}_l-\vec{R}_p)} \left\langle\!\!\left\langle \left(\vec{s}\cdot\vec{S}_p(0) - \vec{s}\cdot\langle\!\langle\vec{S}_p\rangle\!\rangle\delta_q\right)\left(\vec{s}\cdot\vec{S}_l(t) - \vec{s}\cdot\langle\!\langle\vec{S}_l\rangle\!\rangle\delta_q\right) \right\rangle\!\!\right\rangle$$

Again the double brackets are introduced as an average over the initial spin-configuration of the system $\langle\!\langle\cdots\rangle\!\rangle \equiv \sum_m \wp_m \langle\alpha m|\cdots|\alpha m\rangle$. The term in the double angle brackets becomes

$$\left\langle\!\!\left\langle \left(\vec{s}\cdot\vec{S}_p(0)\right)\left(\vec{s}\cdot\vec{S}_l(t)\right) \right\rangle\!\!\right\rangle - \left\langle\!\!\left\langle \left(\vec{s}\cdot\langle\!\langle\vec{S}_p\rangle\!\rangle\right)\left(\vec{s}\cdot\langle\!\langle\vec{S}_l\rangle\!\rangle\right)\delta_q \right\rangle\!\!\right\rangle$$

Using the property of the Pauli spin operators $s^i s^j = (1/4)\delta_{ij} - (i/2)\epsilon^{ijk}s^k$ it follows that

$$\sum_{i,j} s^i \vec{S}_p^i(0) s^j \vec{S}_l^j(t) = \frac{1}{4}\vec{S}_p(0)\cdot\vec{S}_l(t) + \frac{1}{2}\vec{s}\cdot\vec{A}_{pl}(t).$$

where $A_{pl}^k(t) = -i\epsilon^{ijk}[S_p^i(0)S_l^j(t) - S_p^j(0)S_l^i(t)]$. That is $\vec{A}_{pl} = -i\vec{S}_p(0)\times\vec{S}_l(t)$. The dynamical structure factor and scattering time become for electrons with spin-up (+) and spin-down (−),

$$\widetilde{\Gamma}_\pm(\vec{q},t) = \frac{1}{N^2}\sum_{p,l} e^{i\vec{q}\cdot(\vec{R}_l-\vec{R}_p)}\frac{1}{4}\left(\langle\!\langle\vec{S}_p(0)\cdot\vec{S}_l(t) \pm A_{pl}^z(t)\rangle\!\rangle - \langle\!\langle\vec{S}_p\rangle\!\rangle\cdot\langle\!\langle\vec{S}_l\rangle\!\rangle\delta_q\right).$$

$$\widetilde{\hbar/\tau_{k\pm}} = \frac{2\pi}{\hbar}\sum_{k'}|J_{k'k}|^2\left[\frac{2}{1+e^{\hbar\omega/k_BT}}\right]\int\frac{dt}{2\pi}e^{-i\omega t}\widetilde{\Gamma}_\pm(\vec{q},t)$$

This is the general expression for the scattering time hypothesize by Soukoulis and Grest except for the term involving A_{pl}^z. The necessity of this term is evident if one considers that it is the only term in the above expression which differentiates between spin-up and spin-down conduction electrons. A similar expression occurs in the scattering of neutrons from the magnetic moment of the electron. As shown in the review of DeGennes (1963, section 3) the term involving A_{pl}^z drops out for unpolarized neutrons. Presumably, Soukoulis took this expression to apply to electron exchange scattering. However, this is not correct because of the factor in square brackets in the expression for the scattering rate above.

To check this expression for the scattering rate and to make contact with other calculations of the scattering rate (VanPeski-Tinbergen), this expression can be reduced in the case where spins at different sites are uncorrelated. If the correlations depend only on the distance between sites then one of the sums reduces to a counting of the number of impurity sites and thereby introduces the atomic concentration c.

$$\widetilde{\Gamma}_\pm(\vec{q},t) = \frac{c}{4N}\sum_p e^{i\vec{q}\cdot\vec{R}_p}\left(\langle\!\langle\vec{S}_0(0)\vec{S}_p(t) \pm A_{0p}^z(t)\rangle\!\rangle - \langle\!\langle\vec{S}_0\rangle\!\rangle\cdot\langle\!\langle\vec{S}_p\rangle\!\rangle\delta_q\right)$$

If the spins at different sites are statistically uncorrelated (i.e. the probability of an initial spin-configuration of the entire system $\{\prod_p |S_p, m_p\rangle\}$ is the product of probabilities for the individual spin states $\prod_p \wp_{m_p}$), then $\langle\langle \vec{S}_0(0)\vec{S}_p(t)\rangle\rangle = \langle\langle \vec{S}_0\rangle\rangle \cdot \langle\langle \vec{S}_p\rangle\rangle$ for $p \neq 0$. If one further averages the impurity sites over all lattice sites, then terms with $p \neq 0$ vanish.

$$\overline{\tilde{\Gamma}_\pm(\vec{q},t)} = \frac{c}{4N}(\langle\langle \vec{S}_0(0)\vec{S}_0(t) \pm A^z_{00}(t)\rangle\rangle - |\langle\langle S_0\rangle\rangle|^2\delta_q)$$

The bar designates, as in section A.1, the average over impurity sites. Note that the dynamic structure factor has been reduced to c times a factor accounting for time correlations at one site only.

In the expression for the scattering rate, the dependence on the energy transferred in inelastic processes is incorporated in two terms 1) $\tilde{\Gamma}(\vec{q},\omega)$ and 2) the term from the Fermi function $[2/1 + e^{\hbar\omega/k_BT}]$.

$$\overline{\tilde{\Gamma}_\pm(\vec{q},\omega)}\left[\frac{2}{1+e^{\hbar\omega/k_BT}}\right] = \int \frac{dt}{2\pi} e^{-i\omega t}\overline{\tilde{\Gamma}(\vec{q},t)}\left[\frac{2}{1+e^{\hbar\omega/k_BT}}\right]$$

$$= \frac{c}{4N}\int \frac{dt}{2\pi}(\langle\langle \vec{S}_0(0)\vec{S}_0(t) \pm A^z_0(t)\rangle\rangle - |\langle\langle S\rangle\rangle|^2\delta_q)\left[\frac{2}{1+e^{\hbar\omega/k_BT}}\right]$$

Note that $A^z_{00}(t) = (1/2)[S^+_0(0)S^-_0(t) - S^-_0(0)S^+_0(t)]$ so that

$$\vec{S}_0(0)\cdot\vec{S}_0(t) \pm A^z_{00}(t) = S^z_0(0)S^z_0(t) + S^\pm_0(0)S^\mp_0(t)$$

and

$$\int \frac{dt}{2\pi} e^{-i\omega t}\langle\langle \vec{S}_0(0)\vec{S}_0(t) \pm A^z_{00}(t)\rangle\rangle\left[\frac{2}{1+e^{\hbar\omega/k_BT}}\right] =$$

$$= \hbar \sum_{m_0=-S}^{S} \wp_{m_0}\langle m_0|S^z_0 S^z_0 + S^\pm_0 S^\mp_0\left[\frac{2}{1+e^{\mp\eta}}\right]|m_0\rangle$$

The factor of $\hbar$ comes from the fact that $\delta(\omega) = \hbar\delta(\hbar\omega)$. The matrix element is easily calculated if one makes the substitution $S^\pm S^\mp = S^2 - S^2_z \pm S_z$. Using equation A.4.1 yields

$$\overline{\tilde{\Gamma}_\pm(\vec{q},\omega)}\left[\frac{2}{1+e^{\hbar\omega/k_BT}}\right] = \frac{\hbar c}{4N}\left\{\left(S(S+1) - SB_S(\eta)coth(\frac{\eta}{2})\right)\right.$$

$$\left. + \left(SB_S(\eta)coth(\frac{\eta}{2}) \mp SB_S(\eta)\right)\left[\frac{2}{1+e^{\mp\eta}}\right] - |\langle\langle S\rangle\rangle|^2\delta_q\right\}.$$

$$= \frac{c\hbar}{4N}\left\{S(S+1) - SB_S(\eta)\left(coth(\frac{\eta}{2}) \pm (1 \mp coth(\frac{\eta}{2}))\left[\frac{2}{1+e^{\mp\eta}}\right]\right) - |\langle\langle S\rangle\rangle|^2\delta_q\right\}$$

$$= \frac{c\hbar}{4N}\left\{S(S+1) - SB_S(\eta)tanh(\frac{\eta}{2}) - |\langle\langle S\rangle\rangle|^2\right\} \qquad A.4.3$$

One uses: $2/(1+e^{\mp\eta}) = e^{\pm\eta/2}/cosh(\eta/2)$ and $[1 \mp coth(\eta/2)] = \mp e^{\mp(\eta/2)}/sinh(\eta/2)$, and $cosh^2 - 1 = sinh^2$.

Substituting this in A.4.2 yields the expression of VanPeski-Tinbergen and Dekker for the scattering rate. Note that in this limit there is no difference in the scattering rate for spin-up and spin-down electrons. If there are in addition no time correlations (i.e. $B = 0$), then one obtains the usual expression for the spin-disorder scattering rate $\hbar/\tau_k = 2\pi c \sum_{k'} |J_{k'k}|^2 (S(S+1)/4)$ which is easy to understand since the matrix element squared is $|H_{cx}|^2 \sim \langle\langle(\vec{s}\cdot\vec{S})^2\rangle\rangle \sim (1/3)s^2S^2 = (1/3)(3/4)S(S+1)$.

—Kondo Effect—

Finally the scattering of electrons from one impurity is calculated in the second Born approximation (i.e. third order in the exchange constant J). This yields the divergent term discovered by Kondo which signals the formation of a singlet state at low temperature(Kondo,1964). Consider the perturbation expansion of the T-matrix (Fig.A.4.2). There are two second order terms.

1) $$\langle k'\alpha'm'|c^\dagger_{k'\alpha'} J_{k'q} S^i s^i_{\alpha'\alpha''} c_{q\alpha''} G^\circ_{q\alpha''} c^\dagger_{q\alpha''} J_{qk} S^j s^j_{\alpha''\alpha} c_{k\alpha}|k\alpha m\rangle =$$

$$= \frac{J^2(1-f(\varepsilon_q))}{\varepsilon_k - \varepsilon_l}\langle\alpha', m'|S^i s^i_{\alpha'\alpha''} S^j s^j_{\alpha''\alpha}|\alpha m\rangle$$
$$= \frac{J^2(1-f(\varepsilon_q))}{\varepsilon_k - \varepsilon_l}\left(\frac{1}{4}S(S+1)\delta_{\alpha'\alpha} - \vec{s}_{\alpha'\alpha}\cdot\vec{S}/2\right)$$

2) $$\langle k'\alpha'm'|c^\dagger_{q\alpha''} J_{qk} S^i s^i_{\alpha''\alpha} c_{k\alpha} G^\circ_{q\alpha''} c^\dagger_{k'\alpha'} J_{k'q} S^j s^j_{\alpha'\alpha''} c_{q\alpha''}|k\alpha m\rangle =$$

$$= \frac{J^2}{\varepsilon_k - (\varepsilon_k - \varepsilon_q + \varepsilon'_k)}\langle\alpha', m'|(-1)c^\dagger_{q\alpha''} c_{q\alpha''} S^i s^i_{\alpha''\alpha} S^j s^j_{\alpha'\alpha''}|\alpha m\rangle$$
$$= \frac{J^2 f(\varepsilon_q)}{\varepsilon_k - \varepsilon_q}\langle\alpha', m'|S^i S^j s^j_{\alpha'\alpha''} s^i_{\alpha''\alpha}|\alpha m\rangle$$

After adding these two terms together, the term containing the Fermi function $f(\varepsilon_q)$

$$= \frac{J^2 f(\varepsilon_q)}{\varepsilon_k - \varepsilon_q}\langle\alpha' m|(S^j S^i - S^i S^j)s^i s^j|\alpha m\rangle.$$

The non-commutivity of the spin operators allows this term to be nonvanishing. The total second order contribution to the T-matrix is

$$T^{(2)}_{k'\alpha',k\alpha} = \sum_q \frac{J^2}{\varepsilon_k - \varepsilon_q}[\frac{1}{4}S(S+1) - \langle\alpha' m'|\vec{s}\cdot\vec{S}/2|\alpha m\rangle] + \sum_q \frac{J^2 f(\varepsilon_q)}{\varepsilon_k - \varepsilon_q}\langle\alpha' m'|\vec{s}\cdot\vec{S}/2|\alpha m\rangle.$$

The integral

$$N_o \int_{\epsilon_F - D}^{\epsilon_F} \frac{d\varepsilon}{\varepsilon_F - \varepsilon} \sim \ell n\left(\frac{\varepsilon_k + D - \varepsilon_F}{\varepsilon_k - \varepsilon_F}\right)$$

diverges logarithmically as ε_k approaches the Fermi energy. In the expression for the scattering rate $\hbar/\tau_k \propto |T|^2$, the cross term between the first and second order contributions of the T-matrix introduce a term proportional to $-J^3\ell n(T)$ which diverges as $T \longrightarrow 0$. An improved calculation results in a divergence at a temperature $T_K = De^{1/2JN_o}$ which plays the role of T_f below which the moment is quenched by a compensating conduction electron spin-polarization.

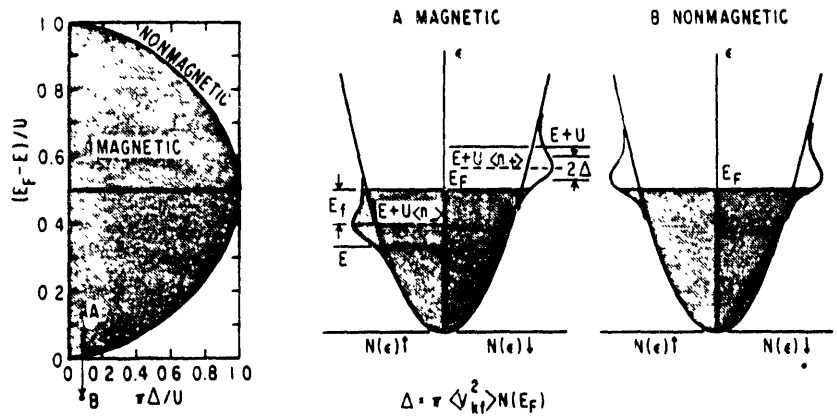

Fig. A.4.1 The phase diagram for the state of local moment in the Anderson model (from Maple, 1984).

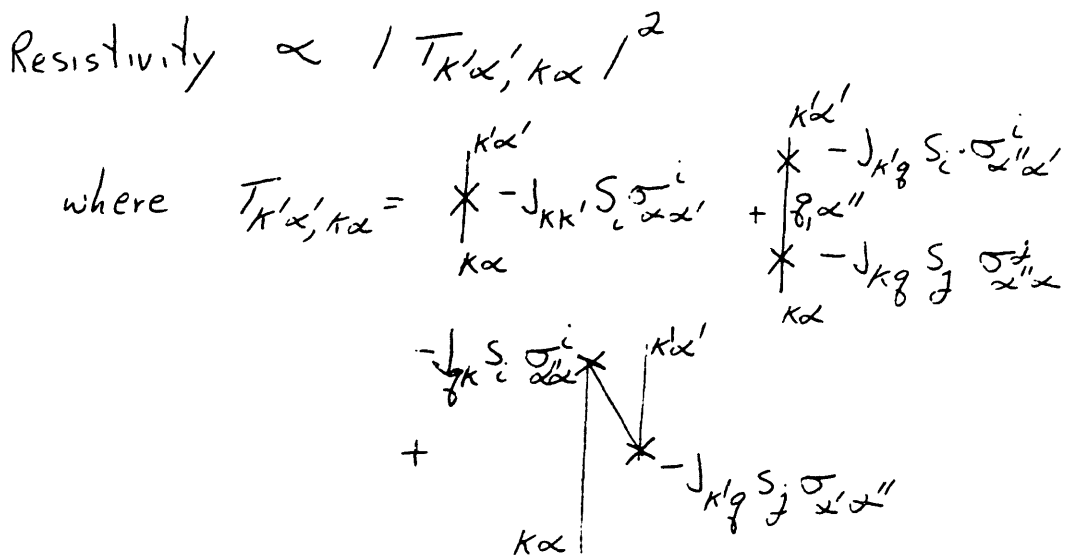

Fig. A.4.2 First and second order diagrams contributing to the kondo effect.

Abrikosov, A.A., and L.P. Gorkov, Sov.Phys. JETP **8**,1090 (1959).

Abrikosov, A.A., and L.P. Gorkov, Sov.Phys. JETP **15**,752 (1962).

Abrikosov, A.A., L.P. Gorkov, and I.E. Dzyaloshinski, *Methods of Quantum Field Theory in Statistical Physics*, English Trans. by R.A. Silverman, (Dover Publications, INC., NY, 1963).

Anderson, P.W., Phys.Rev. **124**,41 (1961).

Anderson, P.W., in *Moment Formation in Solids*, ed. W.J.L. Buyers, (Plenum Press, NY 1984).

Arfkin,G., *Mathematical Methods for Physicists*, 2^{nd} ed., (Academic Press, NY, 1970).

Ashcroft, N.W. and N.D. Mermin, Solid State Physics, (Saunders College , Philadelphia, 1976).

Asik, J.R., M.A. Ball, and C.P. Slichter, Phys.Rev **181**,645 and 662 (1969).

Bergmann, G., Phys.Reports **107**,1 (1984).

Brooks, H., and F.S. Ham, Phys.Rev. **112**,344 (1958).

Brout,R. and H. Suhl, Phys.Rev.Lett. **2**,387 (1959).

Callaway, J., Phys.Rev. **106**,868 (1957).

Callaway, J., *Quantum Theory of the Solid State*, (Academic Press, NY, 1974).

Clogston, A.M., Phys.Rev. **125**,439 (1962).

Coqblin, B. and J.R. Schrieffer, Phys.Rev. **185**,847 (1969).

DeGennes, P.G., in *Magnetism, Vol. III*, edited by G.T. Rado and H. Suhl, (Academic Press, NY, 1963).

DeGennes, P.G., and J. Friedel, J.Phys.Chem.Solids **4**,71 (1958).

Dekker, A.J., J.Appl.Phys. **36**,906 (1965).

Edwards, S.F., Phil.Mag. **3**,1020 (1958).

Entel, P., and W. Klose, J.Low Temp.Phys. **17**,529 (1974).

Friedel, J., Phil.Mag. **43**,153 (1952).

Friedel, J., Advan.Phys. **3**,446 (1954).

Friedel, J., Nuovo Cimento **7**,S287 (1958).

Gallagher, W.J., (unpublished) Thesis at MIT (1978).

Gasiorowicz, S., *Quantum Physics*, (J.Wiley & Sons, Inc. NY, 1974).

Gottfried, K., *Quantum Mechanics*, (Benjamin/Cummings Publishing Co., Reading, Mass. 1966).

Harrison, W.A., *Pseudopotentials in the Theory of Metals*, (Benjamin, NY, 1966).

Harrison, W.A., *Solid State Theory*, (McGraw-Hill, Inc. NY, 1970).

Harrison, W.A., *Electronic Structure and the Properties of Solids*, (W.H.Freeman, San Francisco, 1980).

Herring, C., in *Magnetism IIB*, ed. G.T. Rado and H.Suhl, (Academic Press, NY, 1966).

Hirst,L.L., Adv.Phys. **21**,759 (1972).

Itzykson, C., and J.B. Zuber, *Quantum Field Theory*, (McGraw-Hill Inc., NY, 1980).

Kasuya, T., in *Magnetism IIB*, ed. G.T. Rado and H.Suhl, (Academic Press, NY, 1966).

Koelling, D.D., and A.H. MacDonald, in *Relativistic Effects in Atoms, Molecules and Solids*, ed. G.L. Malli, (Plenum Press, NY, 1983).
Kondo, J., Prog.Theor.Phys. **28**,846 (1962).
Kondo, J., Prog.Theor.Phys. **32**,37 (1964).
Koster, G.F., and J.C. Slater, Phys.Rev. **96**,1208 (1954).
Krishna-murthy, H.R., K.G. Wilson, and J.W. Wilkins, Phys. Rev. Lett. **35**, 1101 (1975).
Landau, L.D., and E.M. Lifshitz, *Quantum Mechanics*, (Pergamon Press, NY, 1977).
Lui, S.H., Phys.Rev. **121**, 451 (1961).
Mackintosh, A.R., and O.K. Anderson, in *Electrons at the Fermi Surface*, ed. M. Springford, (Cambridge University Press, NY, 1980).
Maple, M.B., in *Magnetism V* ed. H. Suhl (Academic Press, NY 1973).
Maple, M.B., in *Moment Formation in Solids*, ed. W.J.L. Buyers, (Plenum Press, NY 1984).
Meservey, R., P.M. Tedrow, Phys.Rev.Lett. **41**,805 (1978).
Peski-Tinbergen, T., and A.J. Dekker, Physica **29**,917 (1963).
Rainer, D., Z.Physik **252**,174 (1972).
Ruderman, M.A., and C. Kittel, Phys. Rev. **96** , 99 (1954); T. Kasuya, Prog. Theor. Phys. Japan, **16**,45 (1956); K. Yosida, Phys.Rev. **106**,893 (1957).
Schrieffer, J.R. and P.A.Wolff, Phys.Rev. **149**,491 (1966).
Soukoulis, C.M., G.S. Grest, and K. Levin, Phys.Rev.Lett. **41**,568 (1978).
Soukoulis, C.M., and G.S. Grest, Phys.Rev.B **21**,5119 (1980).
Taylor, K.N.R., and M.I. Darby, *Physics of Rare-Earth Solids* (Chapman and Hall LTD, London, 1972).
Tedrow, P.M., and R. Meservey, Phys.Rev.B **25**,171 (1982).
Van Hove, L., Phys.Rev. **95**,249 (1954).
Watson, R.E., A.J. Freeman and S. Koide, **186**,625 (1969).
Watson, R.E., S. Koide, M. Peter and A.J. Freeman, Phys.Rev. **139**,A167 (1965).
White, R.M., *Quantum Theory of Magnetism*, second edition, (Springer-Verlag, NY, 1983).
Wohllenben, D.K., and B.R. Coles, in *Magnetism V*, ed. H. Suhl (Academic Press, NY 1973).
Yafet, Y., Solid State Phys. **14**,1 (1963).
Yafet, Y., J.Appl.Phys. **39**,853 (1968).
Zeiger, H.J., and G.W. Pratt, *Magnetic Interactions in Solids*, (Clarendon Press, Oxford, 1973).
Zener, C., Phys.Rev. **81**,440 (1951).

Appendix B— Critical Field Program

History

The HC2 routine was written by J.E. Tkaczyk and J.A.X. Alexander at the Francis Bitter National Magnet Laboratory, MIT. It includes orbital and paramagnetic pairbreaking, spin-orbit scattering and Fermi liquid effects. The last revision made by J.A.X. Alexander was on 6/21/83. This version had modified displays of the 5/30/83 version and contained the added pairbreakers PP0 and PP1. These pairbreakers are those found in Rainer's thin-film/parallel-field-tunneling program. Further modifications were made by J.E. Tkaczyk in 1984-1986. To this routine was added data overlaying and fitting capability. The data consists of temperature (in Kelvin) and critical field (in killogauss) associated in pairs. The critical field defined by G(T,H)=0 is found in this program by use of a modified linear interpolation procedure. The programs were written to run on the Dec 11/23-plus in Fortran 4.

Description

HC2 is the root of a routine which calculates and plots the critical field versus temperature curve given the various input parameters required. These parameters listed below are entered from the subroutine HCDISP. The subroutine HCFUNC uses a modified linear interpolation to calculate the correct value of H_{c2} for a given temperature.

HC2 prompts for a data file name, and you are prompted to view the data using the subroutine HCDATA. The first number in each data file should be the number of points. This is to be followed by the data points themselves (i.e. T(I),H(I), I=1,NPTS).

Both the calculated and experimental data are plotted in HCPLOT. Finally, one may choose to change the input parameters for a better fit, or run HCFIT which applies a gradient search to minimize the variance automatically. For best results try to get the best fit yourself before using HCFIT. It is possible that the gradient search will get stuck in a local minimum. The HCFIT program requires the calculation of the variance between your data and the theory. The variance is calculated by the subroutine HCHISQ.

Below the temperature T-first, which is calculated in the program HCFRST, the superconducting-normal phase transition is of first order (i.e. the H_{c2} calculation doesn't apply). Therefore all points below T-first are not included in the variance calculation. If while choosing parameters in HC2 you choose NPTS=0, the theory will be applied to the temperatures of your data and the variance and T-first will be displayed with the plot. An opportunity is presented in the program to save the theory generated curve and the associated best fit parameters.

The HC2 routine may be linked as follows:

```
Link/Prompt HC2,HCFIT,HCFRST
NCDATA/O:1
HCDISP/O:1
HCFUNC/O:1
HCPLOT/O:1
HCHISQ/O:1//
```

The input parameters to the program are:

IPAIRB The number signifying which pairbreaker is to be used. This depends on the geometry of your sample and its orientation relative to the field.

1-Bulk sample or a thin film oriented perpendicular to the field

2-Thin film oriented parallel to the field

3-Surface sheath (HC3)

PARAMS

1 SLOPE Slope of the critical field curve evaluated at T_c in killogauss/Kelvin (Internally converted to Gauss/K). This parameter is used with IPAIRB=1 and 3.

2 BFULDE spin-orbit scattering parameter used by Fulde

3 RENORM Renormalization factor for the Pauli field. Equals $(1 + G^o)$ where G^o is the $\ell = 0$ Fermi liquid parameter.

4 CFULDE Fulde's C parameter (used with IPAIRB=2)

5 PP0 Additional pairbreaker constnt with field

6 PP1 Additional pairbreaker linear in field

7 TC Critical temperature in zero field (Kelvin)

The reduced field $h = H/(TC \times SLOPE)$, and the reduced temperature $t = T/T_c$.

Putting the H_{c2} Program Together

There are 8 programs, each of which may be composed of one or more subroutines. These 8 programs may call one another as indicated by arrows in the diagram below.

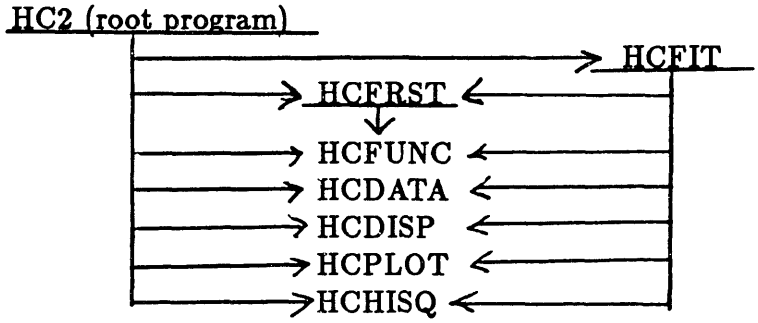

HCFRST only calls the program HCFUNC, while HC2 AND HCFIT call all the other programs. The five programs HCFUNC, HCDATA, HCDISP, HCPLOT, HCHISQ are all called independently and thus these may be overlayed into one storage location in internal memory. If you don't have enough computer memory, I suggest you forget about HCFIT. You may want to remove HCFRST also.

The Theory of Critical Fields

references:

J.A.X. Alexander, T.P. Orlando, D. Rainer, and P.M. Tedrow, Phys. Rev. B **31**, 5811 (1985)

T.P. Orlando, Ph.D. thesis, (unpublished), Stanford University, 1981.

T.P. Orlando, E.J. McNiff, Jr., S. Foner, M.R. Beasley, Phys. Rev. B **19**, 4545 (1979).

P. Fulde, Adv. Phys. **22**, 667 (1973).

(concerning the first order transition:) H. Engler, P. Fulde, Phys. Kondens. Mater. **7**, 150 (1968).

The Landau theory of phase transitions describes second order transitions and first order transitions close to a second order transition. The theory characterized by the expansion of the free energy in the order parameter:

$$f_s(T,H) = f_o(T,H)|\Delta|^2 + f_1(T,H)|\Delta|^4 + \text{higher order}$$

$$\begin{cases} f_1 > 0,\ f_o = 0, & \text{specifies } 2^{nd} \text{ order transition} \\ f_1 = 0, & \text{specifies a change in the order of the transition} \\ f_1 < 0, & \text{linearized theory doesn't apply} \end{cases}$$

Conventions: (SI units)

$t = T/Tc$ reduced temperature

$\Delta_o = (\pi/e^\gamma)k_B T_c = 1.764 k_B T_c$ the energy gap at zero temperature

$h = h_{Fulde} = (\mu_B H/\Delta_o)$ dimensionless magnetic field used by Fulde, not the same as used in program

$E = 1/(1+G^o)$ enhancement due to Fermi liquid effects, G^o is the $\ell = 0$, anti-symmetric Fermi liquid parameter

$b = \hbar/3\Delta_o\tau_{so}$ Fulde's spin-orbit scattering parameter

$\lambda_{so} = (2\Delta_o/\pi T_c)b = 1.123\ b$

$c_F = D(ed)^2\Delta_o/6\mu_B^2\hbar$ Fulde's c-parameter

$D = \ell v_F/3$ The electron diffusion constant

d is the film thickness

$S = \frac{dH_{c2}}{dT}\big|_{Tc} = 4k_B/\pi eD = 10.97(kG/K)/D(cm^2/sec).$

Pairbreakers:

thin film in a parallel field:

$$a = b + \frac{D}{6\Delta_o\hbar}(edH_{||})^2 = b + c_F h^2$$

bulk of film in perpendicular field:

$$a = b + \frac{DeH}{\Delta_o} = b + \frac{4k_B h}{\mu_B \pi S}$$

Surface superconductivity (H_{c3}):

$$a = b + (0.59)DeH/\Delta_o$$

The coefficients $f_o(T,H); f_1(T,H)$ must be calculated from the microscopic theory:

$f_o(T,H) = 0$ defines $H_{c2}(T)$:

$$\ell n(t) = \psi(1/2) - \frac{1}{2}\left(1 + \frac{b}{\sqrt{b^2 - h^2E^2}}\right)\psi\left(\frac{1}{2} + \frac{\Delta_o}{2\pi k_B T}[a - \sqrt{b^2 - h^2E^2}]\right)$$
$$- \frac{1}{2}\left(1 - \frac{b}{\sqrt{b^2 - h^2E^2}}\right)\psi\left(\frac{1}{2} + \frac{\Delta_o}{2\pi k_B T}[a + \sqrt{b^2 - h^2E^2}]\right)$$

where $\psi(x)$ is the digamma function $f_1(T, H_{c2}(T)) = 0$ defines the temperature below which the transition is first order.
$f_1^{\perp}(T,H) \propto$

$$(2\pi T_c)^3 \Re e \sum_{n=0}^{\infty} \left\{ \left(\frac{Z_n - ihE + a + b}{(Z_n + a)^2 - b^2 + h^2 E^2} \right)^3 - 2h^2 E^2 b^2 \frac{(Z_n + a + b)^2 + h^2 E^2}{((Z_n + a)^2 - b^2 + h^2 E^2)^4} \right\}$$

$$f_1^{\parallel}(T,H) \propto f_1^{\perp}(T,H) + (2\pi T_c)^3 \Re e \sum_{n=0}^{\infty} (b-a) \left(\frac{Z_n - ihE + a + b}{(Z_n + a)^2 - b^2 + h^2 E^2} \right)^4$$

where $Z_n = 2\pi k_B T/\Delta_o(n + 1/2)$.

```
C
C
C**********************************************************************
C       ROOT PROGRAM -- HC2 (version MAY  1985)
C       For fitting superconducting  critical magnetic field data
C**********************************************************************
C
C
C  DESCRIPTION   HC2
C           This program is the root of a routine which calculates and
C       plots the critical field versus temperature curve given the
C       various input parameters required
C       The following is a list of the variables used
C
C            INPUT PARAMETERS TO PROGRAM
C       IPAIRB          The number signifying which pairbreaker is to be used
C                  Which pairbreaker you use depends on the geometry of
C                  your sample and its orientation to the field
C            1 -   Bulk sample or a thin film oriented parallel to the fiel
C            2 -  Thin film oriented perpendicular to the fiel
C            3 -   Surface sheath (HC3)
C
C  Params
C     1  SLOPE          dHc2/dT Evaluated at Tc in kGauss/K
C                  (internally converted to Gauss/K)
C     2  BFULDE         spin orbit scattering parameter used by Fulde
C                         b-Fulde = lambda spin-orbit /1.122919
C                         where 1.122919=2/exp(Euler's constant= .5772157)
C     3  RENORM         Renormalization factor for pauli field
C     4  CFULDE         Fulde s C parameter
C     5  PP0       Additional pairbreaker constant with field
C     6  PP1       Additional pairbreaker proportionality constant
C                  linear with field
C     7  TC        Critical temperature in zero field (kelvin)
C
C
C
C
C            Variables internal to program
C
C       ANSWER          User s answer to program questions
C       NPTS       Number of points in the  urve
C       T          Reduced temperature     Temp(k) / Tc(k)
C       H          Reduced field     Field/ ((dHc2/dT)*Tc)
C       IDATA           If =1 uals one then plot data in addition to theory
C
C
C
      PROGRAM HC2
      BYTE ANSWER(1) FNAME ( )
C
C           The following asks if data will be overlayed to the calculation
C
      IDATA=0   !                          IDATA=1 Means data is to be overlayed
C
      TYPE 700
700   FORMAT (// '$Enter the data file name (just return if none) -- ')
      ACCEPT 710, FNAME
710   FORMAT (12A1)
      IF (FNAME(1) EQ ' ') GOTO 1000
      IDATA=1
      TYPE 715
715   FORMAT(//'$Do you wish to inspect the data file?  ')
      ACCEPT 720  ANSWER
720   FORMAT (1A)
      IF (ANSWER(1) EQ 'Y') CALL HCDATA(FNAME)
C
C
C
C
C
C           Initialise input parameters
C
      REAL PARAMS(7)
      EQUIVALENCE (PARAMS(1) SLOPE)
      EQUIVALENCE (PARAMS(2),BFULDE)
      EQUIVALENCE (PARAMS(3),RENORM)
      EQUIVALENCE (PARAMS(4) CFULDE)
      EQUIVALENCE (PARAMS(5) PP0)
      EQUIVALENCE (PARAMS(6) PP1)
      EQUIVALENCE (PARAMS(7) TC)
C
C
1000  IPAIRB=1
      NPTS=10
      SLOPE=-.20000
      BFULDE=0
      RENORM=1
      CFULDE=0
      PP0=0
      PP1=0
      TC=5.0
C
C           The following subroutine is the user interface for
C           entering the various parameters for the program
C
1150  CALL HCDISP(IDATA,IPAIRB,NPTS,PARAMS)
C
C
C
C           The following section increments temperature
C           and calls HCFUNC to recieve the critical field
C           for each value of the temperature
C
C
1510  TYPE 3100
3100  FORMAT (T5 /  Hc2 versus temperature /)
      TYPE 3110
3110  FORMAT (  Reduced temperature  T25  Reduced field  T45
     1'Temperature  T65  Field (kG) )
```

```
C
C
      REAL T2(50) H2(50),H(50)
      IF (NPTS NE 0) GOTO 3120
C           The following gets the data & temperature values
      OPEN (UNIT=1 TYPE='OLD' NAME=FNAME)
      READ (1 *) NPTS
      READ (1 *) (T2(I) H(I) I=1 NPTS) 'H=Data, H2=Calculated critical field
      CLOSE (UNIT=1)
      TSTEP=0
      GOTO 3125
C
3120  TSTEP=1./FLOAT(NPTS)
C
3125  DO 3550 N=1 NPTS
C
        IF (TSTEP NE 0 ) GOTO 3140
        T=T2(N)/TC                          Use the data temperature values
        GOTO 3150
C
3140    T=FLOAT(N)*TSTEP     'Start at small T and increment by TSTEP up to 1
        T2(N)=T*TC                                  'Store temperature in array
3150    H2(N)=HCFUNC(IPAIRB T2(N) PARAMS)
C                                          'Store field in array
C
3480    TYPE 3480  T ,(H2(N)*1000 /TC/SLOPE),T2(N),H2(N)
3480    FORMAT (5X F6 4 T25 F9 5 T47,F6 3 T65,F9 4)
3550  CONTINUE
C
C     H=Data, H2=Calculated critical field
      TFIRST=-1   ' This value indicates that TFIRST has not been calculated
      CHISQR=0 0
      IF (TSTEP NE 0 ) GOTO 3700
      TYPE 3600
3600  FORMAT(//  Calculating T first and the variance )
      TFIRST=HCFRST(IPAIRB PARAMS 1)
      CHISQR=HCHISQ (T2,H SIGMAY NPTS NPTS 1 0 H2 TFIRST)
C
3700  CALL HCPLOT(FNAME T2 H2 NPTS IPAIRB IDATA CHISQR
     (TFIRST,PARAMS)
C
C
C
C
C                What to do next after plotting'
C
4000  TYPE 4001
4001  FORMAT (///' Enter the number of the routine you desire  )
      TYPE 4010
4010  FORMA, (T20   1      Change the parameters )
      TYPE 4020
40.0  FORMAT (T20   2      Store fit values and parameters')
      TYPE 4030
40 0  FORMAT (T20   3      Run advanced plotting routines')
```



```
      TYPE 4040
4040  FORMAT (T20,' 4      Chi-Square fitting routine )
      TYPE 4050
4050  FORMAT ('$' T20   5      End program                    )
      ACCEPT * I
C
      IF (I EQ 1) GOTO 4100
      IF (I EQ 2) GOTO 4200
      IF (I EQ 3) GOTO 4300
      IF (I EQ 4) GOTO 4400
      GOTO 4500
C
C
4100  IF (TSTEP EQ 0 ) NPTS=0'          New parameters
      GOTO 1150
C
4200  TYPE 4210
4210  FORMAT ('1Enter the filename for storage )
      ACCEPT 4220, FNNAME
      BYTE FNNAME(12)
4220  FORMAT (12A1)
      OPEN (UNIT=1,TYPE='NEW' NAME=FNNAME)
      WRITE (1,*) NPTS
      WRITE (1,*) (T2(I),H2(I),I=1 NPTS)
      WRITE (1 *) IPAIRB,TC,SLOPE
      WRITE (1,*) BFULDE,CFULDE,RENORM
      WRITE (1 *) PP0,PP1
      CLOSE (UNIT=1)
      GOTO 4000
C
4300  TYPE 4310
4310  FORMAT( 'Not available yet')'      Advanced plotting routines
      GOTO 4000
C
4400  CALL HCFIT(FNAME IDATA IPAIRB NPTS PARAMS)
      NPTS=0'          Means that program will calculate curve at data points
      GOTO 4000
4500  END
```

```
C
C**********************************************************************
C       SUBROUTINE HCFIT
C**********************************************************************
C
C
C
C   DESCRIPTION   HCFIT
C       This is called from the root program HC2 which calculates
C       critical field   HCFIT fits data to the calculation in HCFUNC
C       by method of a chi-sqrare gradient search   See HC2
C       for more information on the input parameters
C
C       Functions and subroutines called
C       HCDATA - Enters the data points
C       HCGRAD - Chi-Square gradient search for data fitting
C       HCHISQ - Calculates chi-square  This is called in HCGRAD
C                and it must therefore be linked as described in HC2
C       HCPLOT - Plots data and fit
C       WHICH  - minor subroutine  Determines fitting parameters
C
C
      SUBROUTINE HCFIT(FNAME,IDATA,IPAIRB,NPTS,PARAMS)
      BYTE ANSWER,FNAME(12)
      PI=3.1415926535
      REAL PARAMS(7),DELTA(7),T(50),H(50)
C
C
      EQUIVALENCE (PARAMS(1),SLOPE)
      EQUIVALENCE (PARAMS(2),BFULDE)
      EQUIVALENCE (PARAMS(3),RENORM)
      EQUIVALENCE (PARAMS(4),CFULDE)
      EQUIVALENCE (PARAMS(5),PPO)
      EQUIVALENCE (PARAMS(6),PPI)
      EQUIVALENCE (PARAMS(7),TC)
C
C
C             The following asks for the data filename if IDATA=0
C
      IF (IDATA.EQ.1) GOTO 725
      IDATA=1   !IDATA=1 means data is to be overlayed (need for HCPLOT)
C
      TYPE 700
700   FORMAT (///,' $Enter the data file name      ')
      ACCEPT 710, FNAME
710   FORMAT (12A1)
      TYPE 715
715   FORMAT (' $Do you wish to inspect the data file?   ')
      ACCEPT 720, ANSWER
720   FORMAT (1A)
      IF (ANSWER.EQ.'Y') CALL HCDATA(FNAME)
725   OPEN (UNIT=1,TYPE='OLD',NAME=FNAME)
      READ (1,*) NPTS
      READ (1,*) (T(I),H(I),I=1,NPTS)
      CLOSE (UNIT=1)
C
C
C       The following section of code is the user interface for
C       Entering the various parameters for the program
C
C
C
      JPTS=NPTS     !Don't want NPTS to be changed in HCDISP subroutine
C
1150  CALL HCDISP(IDATA,IPAIRB,JPTS,PARAMS)
C
C
C       Determine which parameters are fit parameters
C
C
C
C
      DO 1810 I=1,7
1810  DELTA(I)=0.0  !Initialize array delta
C
      IF (IPAIRBB.NE.2) GOTO 1900
C
      TYPE 2030
2030  FORMAT (///,'$Is CFULDE a fit parameter? ')
      CALL WHICH(4,DELTA,PARAMS)
      GOTO 2005
C
1900  TYPE 2000
2000  FORMAT (//,' $Is SLOPE a fit parameter?  ')
      CALL WHICH (1,DELTA,PARAMS)
2005  TYPE 2010
2010  FORMAT (//,'$Is BFULDE a fit parameter?  ')
      CALL WHICH (2,DELTA,PARAMS)
      TYPE 2020
2020  FORMAT (//,'$Is RENORM a fit parameter (or ALPHA)? ')
      CALL WHICH(3,DELTA,PARAMS)
      TYPE 2040
2040  FORMAT (//,'$Is PPO a fit parameter?  ')
      CALL WHICH(5,DELTA,PARAMS)
      TYPE 2050
2050  FORMAT (//,'$Is PPI a fit parameter?  ')
      CALL WHICH(6,DELTA,PARAMS)
      TYPE 2060
2060  FORMAT (//,'$Is Tc a fit parameter?  ')
      CALL WHICH(7,DELTA,PARAMS)
      CALL TSERAS(3)
C
C
C
C       Calculate chi-square and compare to last value
C
C
      REAL HFIT(50),SIGMAY(50)
C       CSTORE -- Last chi-square value
C       CHISQR    - Latest chi-square value
C       HFIT      Array of calculated values of critical field
```

```
      CHISQR=0
      CALL HCGRAD(IPAIRB,T H SIGMAY,NPTS,7 0 PARAMS
     1DELTA,HFIT,CHISQR,0 0)
C
C
2200  CSTORE=CHISQR
C
      DO 2205 I=1 7
2205  DELTA(I)=DELTA(I)/2
C
      CALL HCGRAD(IPAIRB T H SIGMAY NPTS 7,0 PARAMS,
     1DELTA HFIT,CHISQR 0 0)
      IF (CSTORE EQ 0 0) GOTO 2200
      IF (ABS(CSTORE-CHISQR)/CSTORE GT 0 01) GOTO 2200
C
C          The fit is acceptible plot data and the calculated values
C
      TFIRST=HCFRST(IPAIRB PARAMS 1)
      CALL HCPLOT(FNAME T HFIT NPTS,IPAIRB,IDATA CHISQR,
     1TFIRST,PARAMS)
C
3050  RETURN
      END
C
C
C
C
C
C
      ***************          SUBROUTINES          ************
C
C
C
C
C
      SUBROUTINE WHICH(I DELTA PARAMS)
C          If a fitting parameter is not to be changed its  DELTA
C                              is set to zero
      REAL DELTA(7) PARAMS(7)
      BYTE ANSWER
      ACCEPT 2500,ANSWER
2500  FORMAT (1A1)
      IF (ANSWER EQ 'Y ) GOTO 2502
      DELTA(I)=0 0
      GOTO 2510
C
2502  TYPE 2504
2504  FORMAT( XEnter divisor which determines the parameter increments )
      TYPE 2506
2506  FORMAT( 1Increment=Parameter value/ divisor     (Start with 20)   )
      ACCEPT * DIVSOR
      IF (DIVSOR LE 2 ) GOTO 2502
      DELTA(I)=PARAMS(I)/DIVSOR
2510  END
C
```



```
C
C
C
C
C
C
C
C
C**************************************************************
C       SUBROUTINE HCGRAD
C**************************************************************
C
C       ORIGIN   PROGRAM 11-3 GRADLS
C             FROM  BEVINGTON, PHILIP R
C             DATA REDUCTION AND ERROR ANALYSIS
C             FOR THE PHYSICAL SCIENCES
C
C             However, the program has been specifically
C             modified for use with the root program HCFIT
C             which fits critical field data
C
C
C       PURPOSE
C        Make a gradient-search least-squares fit to data with a
C          specified function which is not linear in coefficiences
C
C       USAGE
C        Call HCGRAD(IPAIRB X Y SIGMAY,NPTS,NTERMS,MODE,
C            A,DELTAA,YFIT  CHISQR,NPRINT)
C
C
C       Description of parameters
C         X    - Array of data points for independent variable
C         Y    - Array of data points for dependent variable
C         SIGMAY - Array of standard deviations for Y data points
C         NPTS   - Number of pairs of data points
C         NTERMS - Number of parameters
C         MODE     - Determines method of weighting least-squares fit
C            +1 (INSTRUMENTAL) WEIGHT(I) = 1 /SIGMAY(I)**2
C            0  (NO WEIGHTING) WEIGHT(I) = 1
C            -1 (STATISTICAL)  WEIGHT(I) = 1 /Y(I)
C         A    - Array of parameters
C         DELTAA - Array of increments for parameters A
C         YFIT     - Array of calculated values of Y
C         CHISQR - reduced chi-square for fit
C         NPRINT - if NPRINT=1 suppress typed output to the vidieo screen
C
C       Subroutines and function subprograms required
C
C         HCFUNC (IPAIRB T A)
C           Evaluates the critical field at temperature T with parameters A
C         HCHISQ (X Y SIGMAY, NPTS  NFREE  MODE  YFIT TFIRST)
C           Evaluates reduced chi square for fit to data
C
```

```
C
      SUBROUTINE HCGRAD(IPAIRB,X,Y,SIGMAY,NPTS,NTERMS
     1MODE, A, DELTAA YFIT CHISQR NPRINT)
C
      REAL X(50) Y(50) SIGMAY(50) A(7) DELTAA(7), YFIT(50)
      REAL GRAD(7)
C
C           EVALUATE CHI SQUARE AT BEGINNING
C
  110 NFREE=NPTS - 3
C
      IF (NPRINT) GOTO 200
      TYPE 120  NFREE
  120 FORMAT (//  The number of degrees of freedom is NPTS-3=     I2)
C
  200 IF (NPRINT) GOTO 215
      TYPE 210
  210 FORMAT (// 'Evaluate chi square at beginning  CHISQR1=  ')
  215 IF (CHISQR EQ 0 ) GOTO 220
      CHISQ1=CHISQR
      IF (NPRINT) GOTO 310
      TYPE * CHISQ1
      GOTO 310
C
  220 TFIRST=HCFRST(IPAIRB A 1)
      DO 230 I=1 NPTS
      IF (X(I) LT TFIRST) GOTO 230  'Such points are ignored in HCHISQ
C                          because the transition is first order
      YFIT(I) = HCFUNC(IPAIRB X(I) A)
  230 CONTINUE
      CHISQ1 = HCHISQ (X Y  SIGMAY  NPTS  NFREE  MODE  YFIT TFIRST)
      IF (NPRINT) GOTO 310
      TYPE * CHISQ1
C
C           EVALUATE GRADIENT OF CHI SQUARE
C
  310 SUM = 0
  320 DO 390 J=1  NTERMS
C
      IF (DELTAA(J) NE 0 ) GOTO 330
      GRAD(J)=0 0 'This parameter is not being varied
      GOTO 390
C
      BYTE FLAG
  330 FLAG=0 'The meaning of this variable indicated below
C
      REAL DSTORE(6)
      DSTORE(J)=DELTAA(J) 'We don t want to change the value of DELTAA(J)
C                  since it will effect the value outside HCGRAD
C
   50 DELTA = 0 15 * DSTORE(J)
      A(J) = A(J) + DELTA
      TFIRST=HCFRST(IPAIRB A 1)
      DO 360 I=1  NPTS
      IF (X(I) LT TFIRST) GOTO 360
```



```
      YFIT(I) = HCFUNC(IPAIRB X(I),A)
  360 CONTINUE
      A(J)= A(J) - DELTA
      GRAD(J) = CHISQ1-HCHISQ(X,Y  SIGMAY, NPTS  NFREE
     1MODE, YFIT TFIRST)
C
      IF (NPRINT) GOTO 365
      MM=J
      IF (FLAG EQ 0) TYPE *, MM, 'Foward direction, CHISQR= '
     1 CHISQ1-GRAD(J)
      IF (FLAG EQ 1) TYPE *, MM 'Reverse direction  CHISQR= '
     1 CHISQ1-GRAD(J)
      TYPE *
C
  365 IF (GRAD(J) GE -1 0E-5) GOTO 390
C     If grad(j) is negative that means the chisqr has increased with
C     the change "A(J)=A(J)+DELTA"  So lets look in the other direction
C               (only if FLAG=0 )
C
      IF (FLAG) GOTO 370 'If we have already looked in the reverse directio
      FLAG=1
      DSTORE(J)=-DSTORE(J)
      GOTO 350
C
C     We looked in both directions and found that chisqr has increased
C     in both directions  Divide DSTORE(J) by 10 and start again
  370 DSTORE(J)=DSTORE(J)/10
      FLAG=0
      IF (NPRINT) GOTO 350
      TYPE *   Divide DELTAA(I) by a factor of 10
      GOTO 350
C
  390 SUM = SUM + GRAD(J)** 2
C
      IF (SUM GT 1 0E-5) GOTO 410
      IF (NPRINT) RETURN
  400 TYPE *,' No change in CHISQR
C     PAUSE
      RETURN
C
C
  410 DO 420 J=1,NTERMS
  420 GRAD(J) = DSTORE(J) * GRAD(J)/SQRT (SUM)
      IF (NPRINT) GOTO 510
      TYPE 500
  500 FORMAT (//  Parameters are incremented along
     1 the following gradient //)
      TYPE *  SLOPE--   GRAD(1)  BFULDE--  GRAD 3)
      TYPE *  RENORM-   GRAD(3)  CFULDE    GRAD(4)
      TYPE *  PP0   --  GRAD(5), PP1  --   GRAD(6)
      TYPE *  TC    --  GRAD(7)
C
C           EVALUATE CHI SQUARE AT NEW POINT
C
  510 DO 560 J=1  NTERMS
```

```
520     A(J) = A(J) + GRAD(J)
        TFIRST=HCFRST(IPAIRB A,1)
530     DO 540 I=1, NPTS
        IF (X(I) LT TFIRST) GOTO 540
        YFIT(I) = HCFUNC(IPAIRB X(I) A)
540     CONTINUE
        CHISQ4 = HCHISQ (X Y SIGMAY  NPTS, NFREE, MODE, YFIT TFIRST)
        IF  CHISQ4 EQ CHISQ2) GOTO 710
        CHISQ2=CHISQ4
        IF (NPRINT) GOTO 610
        TYPE 560
560     FORMAT (//  Follow gradient in chi-square   )
        TYPE * CHISQ2
C
C            MAKE SURE CHI SQUARE DECREASES
C
610     IF (CHISQ1 - CHISQ2) 620  620  710
620     DO 640 J=1  NTERMS
        A(J) = A(J) - GRAD(J)
640     GRAD(J) = GRAD(J) / 10
        IF (NPRINT) GOTO 510
        TYPE 650
650     FORMAT (//  Must decrease increments by a factor of 10 )
        GO TO 510
C
C                  INCREMENT PARAMETERS UNTIL CHI SQUARE STARTS TO INCREASE
C
710     DO 720 J=1  NTERMS
720     A(J) = A(J) + GRAD(J)
        TFIRST=HCFRST(IPAIRB A 1)
        DO 740 I=1  NPTS
        IF (X(I) LT TFIRST) GOTO 740
        YFIT(I) = HCFUNC(IPAIRB X(I) A)
740     CONTINUE
[illegible] CHISQ3 = HCHISQ (X Y  SIGMAY  NPTS  NFREE  MODE  YFIT TFIRST)
        IF (NPRINT  GOTO 7[illegible]
        TYPE * CHISQ[illegible]
[illegible] IF (CHISQ[illegible]  CHISQ[illegible]) [illegible]
[illegible] CHISQ1 = CHISQ2
[illegible] CHISQ2=CHISQ3
        GO TO 710

             FIND MINIMUM OF PARABOLA DEFINED BY LAST THREE POINTS

[illegible] IF (NPRINT) [illegible]
        TYPE [illegible]
[illegible] FORMAT [illegible] min[illegible] of parab[illegible] is defined by last
          three [illegible]
[illegible] IF (CHISQ3 EQ CHIS[illegible]
[illegible] DELTA = [illegible]
        [illegible] NTERMS
[illegible] A(J) = A(J) - DELTA*GRA[illegible]
        TFIRST HCFRST(IPAIRB A 1)
        DO [illegible] NPTS
        IF (X(I) LT TFIRST) [illegible]
```



```
        YFIT(I) = HCFUNC(IPAIRB X(I),A)
950     CONTINUE
C
        CHISQR = HCHISQ (X Y SIGMAY, NPTS  NFREE  MODE  YFIT TFIRST)
1010    IF (CHISQ2 - CHISQR) 1020  1100  1100
1020    DO 1030 J=1  NTERMS
1030    A(J) = A(J) + (DELTA-1 ) *GRAD(J)
        TFIRST=HCFRST(IPAIRB A 1)
1040    DO 1050 I=1  NPTS
        IF (X(I) LT TFIRST) GOTO 1050
        YFIT(I) = HCFUNC (IPAIRB X(I) A)
1050    CONTINUE
C
1060    CHISQR = CHISQ2
1100    IF (NPRINT) RETURN
        TYPE 1110
1110    FORMAT ( $Final CHISQR for this iteration is  )
        TYPE *,CHISQR
        END
```

```
C
C*************************************************************************
C       Function HCFBST FOR
C*************************************************************************
C
C
C            This subroutine calculates the temperature below which the
C            superconducting transition is first order
C
C
C       Subroutines needed
C            FONEFN- calculates the value of F-One which when zero
C                 defines the change from the second to first order
C                 transition   (see Fulde P  High field supercon-
C                 ductivity in thin films)
C            HCFUNC- calculates the value of
C                 critical field defined by f0=0 (see Fulde)
C            MDLNIN- modified linear interpolation to find this root
C
C
      FUNCTION HCFBST(IPAIRB PARAMS,NPRINT)
C
C          NPRINT=1 means no printing
      LOGICAL PRINT
      PRINT= TRUE
      IF (NPRINT NE 0) PRINT= FALSE
C
      REAL PARAMS(7)
      TC=PARAMS(7)
C
C     CALL TSERAS(2)
C
      T=TC* 3
      TSTEP=TC/5
      H=HCFUNC(IPAIRB T PARAMS)
      FONE=FONEFN(T IPAIRB PARAMS H)
      IF (PRINT) TYPE *  T=   T  FONE=   FONE
C
      IF (FONE) 200 200 300
C
200   TROOT=T
      GOTO 1000
C
C          FONE is already less than zero  so increase T
220   TSTEP=-TSTEP
C
300   FSAVE=FONE
      T=T-TSTEP
      IF (T/TC GT 0 005) GOTO 370
      IF (T GT 0 00001) GOTO 350
C
C          T/Tc is equal to or less than 0 00001  so increase it
      T=T+TSTEP
      TSTEP=TSTEP/2 0
      GOTO 400
C
C          T/Tc is between 0 00001 AND 0 005
350   TROOT=0 0
      GOTO 1000
C
C          T/Tc is greater than 0 005  so check the value of FONE
370   H=HCFUNC(IPAIRB,T PARAMS)
      FONE=FONEFN(T IPAIRB PARAMS H)
      IF (PRINT) TYPE * 'T= '.T  FONE=   FONE
C
      IF (FONE*FSAVE) 600 400 300
C
C     Fone= zero at this T
400   TROOT=T
      GOTO 1000
C
C
C          FONE has changed sign  goto modified linear interpolation
C
600   IF (PRINT) TYPE 610
610   FORMAT (//' Modified linear interpolation ')
C     CALL MDLNIN(IPAIRB PARAMS,T,T+TSTEP,FONE FSAVE TROOT 0 05 0 0.15,1)
C
C
C
C
C
C
C
C
C     SUBROUTINE MDLNIN (IPAIRB PARAMS X1 X2 F1 F2 XB XTOL FTOL NLIM I)
C
      X1=T
      X2=T+TSTEP
      F1=FONE
      F2=FSAVE
      XTOL=0 05
      FTOL=0 0
      NLIM=15
C
C
C
C
C
C
C
C
C
C
C*************************************************************************
C       SUBROUTINE  MDLNIN= Modified linear interpolation
C*************************************************************************
C       MODIFIED FOR CALL FROM HCFBST''''''''''''''
C
C       SUBROUTINE MDLNIN (IPAIRB PARAMS X1 X2 F1 F2 XB XTOL FTOL NLIM I)
```

```
      REAL PARAMS(7)
C
C     Subroutine for root finding by modified linear interpolation
C
C     Origin  Curtis F  Gerald  Applied Numerical Analysis  2ED
C          Addison-Wesley 1980  pg 46
C
C     Parameter are -
C     X          The independent variable for the interpolation
C                It is the temperature in this case
C     FONEFN          This calculates the values of FONE  It requires
C                the following arguments  X,TC ,IPAIRB PARAMS H
C     X1 X2           Initial values of X  F(x) must change sign at these
C                points
C     XB         Returns the root to main program
C     XTOL FTOL  Tolerance values for X F(x) to terminate interations
C     NLIM       Limit to number of interations
C     I
C          I=1  meets tolerance for X values
C          I=2  meets tolerance for F(x)
C          I=-1 NLIM exceeded
C          I=-2 f(x1) not opposite in sign to f(x2)
C
C     When the subroutine is called, the value of NPRINT
C     indicates whether to print each value of not   NPRINT=0
C     means print them   NE  0 means NO-PRINT
C
      NPRINT=1
      LOGICAL PRINT
      PRINT= TRUE
      IF (NPRINT NE 0) PRINT= FALSE
      IF ( NOT PRINT) GOTO 2500
C
C
C          F1 AND F2 were passed over from HCFRST
C     H=HCFUNC(IPAIRB X1 PARAMS)
C     F1=FONEFN(X1 IPAIRB PARAMS H)
      IF (PRINT) TYPE *  FOR T=   X1   F(ONE)=   F1
C     H=HCFUNC(IPAIRB X2 PARAMS)
C     F2=FONEFN(X2 IPAIRB PARAMS H)
      IF (PRINT) TYPE *, FOR T=   X,   F(ONE)=   F,
C
2500  IF (F1*F2 GT 0) GOTO 2050
C
C
C
C
C
      FSAVE=F1
C
      DO 2020 I=1 NLIM
      XR=X2-F2*(X, X1)/(F2 F1)
      IF ( NOT PRINT) GOTO 2600
      TYPE *
      TYPE *  X1 X2   F1 F,
```



```
2600  H=HCFUNC(IPAIRB,XB,PARAMS)
      FB=FONEFN(XB,IPAIRB PARAMS H)
      XERR=ABS((X1-X2)/X2)       'Different than book
C
      IF ( NOT PRINT) GOTO 2005
      TYPE 2199  J XR FB
2199  FORMAT (1H 13HAt iteration   I4  5H T =  E12 5
     1  12H  F(ONE() =  E12 5)
C
2005  IF (XERR LE XTOL) GOTO 2060
      IF (ABS(FB) LE FTOL) GOTO 2070
      IF (FB*F1 LT 0) GOTO 2010
C
      X1=XB
      F1=FB
      IF (FB*FSAVE GT 0) F2=F2/2
      FSAVE=FB
      GOTO 2020
C
2010  X2=XB
      F2=FB
      IF (FB*FSAVE  GT  0) F1=F1/2
      FSAVE=FB
C
2020  CONTINUE
C
C
C
C          When loop is normally completed  NLIM is exceeded
      I=-1
      IF ( NOT PRINT) GOTO 2700
      TYPE 2200  NLIM XB FB
2200  FORMAT (1H0  26HTolerance not met   After   I4
     1 15H Iterations X=   E12 5   12H And F(X) =  E12 5)
      GOTO 2700
C
C
C
C
C     This section for return when f(X1) and f(X2) not opposite in sign
2050  I=-2
      IF ( NOT PRINT) GOTO 2700
      TYPE 2201
2201  FORMAT (1H0, 35HFunction has same sign at X1 and X2)
      GOTO 2700
C
C
C
C
C     This section returns after meeting XTOL
2060  I=1
      IF   NOT PRINT) GOTO 2700
      TYPE 2202  J XR FB
2202  FORMAT (1H0   Tolerance met in    I4   Iterations   X =
     1  F12 5  8H F(X) =   E1. 5)
```

```
      GOTO 2700
C
C
C
C
C     This section returns after meeting F(x) tolerance
2070  I=2
      IF ( NOT PRINT) GOTO 2700
      TYPE 2203  J,XR FR
2203  FORMAT (1H0  19HF Tolerance met in   I4,10H
     1iterations  X =   F12 5  8H F(X) =   E12 5)
C     RETURN
C     END
C
C
C
C
C
C
C
C
C
C
C
2700  TROOT=XR
      IF (I GE 0) GOTO 1000
      IF (I LT -1) GOTO 700
C
C          I=-1
      TYPE *   Number of iterations exceeded in
     1the linear interpolation
      GOTO 1000
C
700   TYPE *   FONE did not change sign
      STOP
C
1000  HCFRST=TROOT
1050  RETURN
      END
C
C
C**********************************************************************
C     FUNCTION FONEFN FOR
C**********************************************************************
C
C     This function is called from HCFRST FOR which calculates
C     where in the H vs T phase field the S C  first order transition
C     occures   The first order transition occures when F-fone =0
C     (see P  Fulde  Adv  Phys  2,  667 (1973))
C
C
C
      FUNCTION FONEFN T IPAIRB PARAMS H)
C
      REAL PARAMS(7)
110   SLOPE=PARAMS(1)
```



```
      BFULDE=AMAX1(PARAMS(2),0 0) 'Must be non-negative
      BENORM=PARAMS(3)
      CFULDE=AMAX1(PARAMS(4) 0 0) 'Must be non-negative
      PP0=PARAMS(5)
      PP1=PARAMS(6)
      TC=PARAMS(7)
C
C
      H=H/(14 897*1 7639*TC) 'REDUCED H where 14 897
C           is K-Boltzman/Bohr magneton in kG/K
C
C
      IF (IPAIRB NE 2) GOTO 300
      AFULDE=BFULDE+CFULDE*H**2
      GOTO 400
C
300   AFULDE=BFULDE+4*14 897*H/(3 14159265359*SLOPE)   ' IPAIRB=1 3
C
C
400   AFULDE=AFULDE+(PP0/1 7639)+H*PP1
      FACTOR=2*3 14159265359*T/(1 7639*TC)
      H=H/BENORM   ' This is the renormalised  H  seen by the spins only
C                  It does not enter into the pairbreaker
      STORE=0
      SUM=0
      TERM3=0
500   DO 600 I=0 9999
      ZN=FACTOR*( 5+FLOAT(I))
      DENOM=(ZN+AFULDE)**2-BFULDE**2+H**2
      X=(ZN+AFULDE+BFULDE)
      TERM1=(X**3-3*X*H**2)/DENOM**3
      TERM2=-2 *H**2*BFULDE*(X**2+H**2)/DENOM**4
      IF (IPAIRB NE 2) GOTO 510
C          Included next term in thin film  parallel case only
      TERM3=(BFULDE-AFULDE)*(X**4-6*X**2*H**2+H**4)/DENOM**4
510   SUM=SUM+TERM1+TERM2+TERM3
      NN=I
C     TYPE *,'I SUM  NN.SUM
C     TYPE *  'STORE= ' STORE
C     TYPE *  'ABS((SUM-STORE)/SUM)  ABS((SUM-STORE)/SUM)
C          To be safe the sum is carried out to at least
C     29 terms before applying the difference test   This
C     was found necessary at low temperatures because the
C     sum starts out negative and becomes more negative
C     and then turns around and increases again until it
C     becomes positive   The difference test fails prematurely
C     at the turn around
C
      IF (I LT 30) GOTO 550
      IF (ABS((SUM-STORE)/SUM) LT 0 001) GOTO 2000
550   STORE=SUM
600   CONTINUE
C
C
2000  FONEFN=SUM
      RETURN
```

```
C
C*************************************************************************
C       FUNCTION HCFUNC(IPAIRB T2,PARAMS)
C*************************************************************************
C
C       This subroutine calculates the critical field
C       for a given temperature T2  by using a  modified linear interpolation
C       proceedure'  This program has grown out of the routine HC2-8/21
C       written by J A X  ALEXANDER
C       The accual equations used to calculate Hc2 come
C       from T P Orlando s Thesis(Standford)
C       The present version of this program is the fault of J E  TKACZYK
C
C       The following is a list of the variables used
C            Inputs to program
C
C       T2          Input temperature
C       IPAIRB          The number signifying which pairbreaker is to be used
C  PARAMS
C    1  SLOPE           dHc2/dT Evaluated at Tc in KGauss/K.
C                    Internally converted to Gauss/K
C    2  BFULDE          b-Fulde  Fulde's spin-orbit parameter
C                       (a negative value is set = 0)
C    3  RENORM          Renormalisation factor for pauli field
C    4  CFULDE          C Fulde, Fulde's C parameter
C    5  PP0         Additional pairbreaker constant with field
C    6  PP1         Additional pairbreaker proportionality constant
C                    Linear with field
C    7  TC          Critical temperature
C
C
C
C            Important variables internal to program
C
C       Note   Some of these are essentially the same as those listed
C            above   I have converted to these because the accual
C            equations which are used to calculate Hc2 come from
C            T P  Orlando s Thesis which was written when the
C            following parameters were the fashionable ones to use  J E T
C       THICK           Thickness of film in cm
C       SLAMDA          Lambda spin orbit
C       HP          Pauli field
C       ALFA        Alpha
C       HZERO           Field at T=0 if BFULDE=0
C       T           Reduced temperature     TEMP(K) / Tc(K)
C       H           Reduced field     Field/ ((dHc2/dT)*Tc))
C       HBAR        H*4/(PI**2)   Where PI=3 14  etc
C       BISECT          2*Bisect = Maximum reduced H
C       PI          3 14159265 35
C       G           G=0 Defines the Hc2 Curve
C
C            Subroutines required
C       HCFNYP
C       HCFNF
```



```
C
      FUNCTION HCFUNC(IPAIRB T2 PARAMS)
      REAL PARAMS(7)
      SLOPE=PARAMS(1)
      BFULDE=AMAX1(PARAMS(2),0 0)
      RENORM=PARAMS(3)
      CFULDE=AMAX1(PARAMS(4) 1E-5)
      PP0=PARAMS(5)
      PP1=PARAMS(6)
      TC=PARAMS(7)
C
C
C
C
C     Switch to parameters used in T P Orlando's thesis
C
      PI=3 14159265359
      THICK=1 E-7
1100  IF (IPAIRB NE 2) GOTO 1500
      SLOPE=-( 0120*TC*1000 /CFULDE)' SLOPE in G/K
      PARAMS(1)=SLOPE
C
C
1500  SLAMDA=BFULDE*1 122919
      HP=18572 906985*TC*RENORM
C     18572 906985 = SQRT(2) * PI * K / MU / e / (e to the Euler constant)
C     where e = 2
      ALFA=-(SLOPE*TC* 979587372345/HP)
C                    979587372345= (2)**1/2 * PI**2 / (8*e to the euler
C                                                                constant)
        T=T2/TC' use reduced temperature
        IF (T LT 1 0) GOTO 3300
        H=0 0  'Temperature equal or above Tc
        GOTO 3700
C
C
C
C
C
C
C
C
C           The critical field is defined by the condition G(T H)=0
C     In the following we first find the field, H  at which
C     the value of G changes sign and then pass to the modified linear
C     interpolation  The values (HSTORE HSTORE)  (H G) are the values
C     of (H,G) on either side of the zero of G
C
C           Choose initial value of H BISECT and GSTORE
3300    HZERO=0 592672873757/SQRT (1+ALFA**2) '  h(t=0) FOR (BFULDE=0)
        IF (IPAIRB NE 2) GOTO 3320
          HZERO=SQRT(-12 76671236742E-7/SLOPE/TC/THICK**2))
C         ' 2 76671236742E-7 = ***
3320    H=HZERO*(1-T)  'Line between H=0 and H(t=0)=HZERO
        H=AMAX1(H HZERO* 05)  'Convergence is bad if H starts too small
```

```
          BISECT=H/2
          GSTORE=0 0
          HSTORE=0 0
C
C            Bisection loop
3360      HBAR=H*4 /PI**2
          Y= MCFNYP(IPAIRB HBAR TC THICK SLOPE)
     1*PP0* 5/PI-PP1*H*SLOPE/PI/0 .000033575
          G=ALOG(T) - MCFNF(T HBAR Y ALFA SLAMDA)
C
C            Test to see  BISECT is small compared to H
          IF ((BISECT/H) LT 5 0E-6) GOTO 3700
C            If G changes sign goto modified linear interpolation
          IF (GSTORE*G LT 0 0) GOTO 3500
          GSTORE=G
          HSTORE=H
C         TYPE *  H G=   H G
          IF (G) 3630 3700 3600
C
C            NOTE  can t have H<0
3600      H=H-BISECT  'H IS TOO LARGE G>0
          IF (H GT 0 0) GOTO 3360  'H MUST BE >0
          BISECT=BISECT/2
          H=H+BISECT
          IF (H LT 5E-12) GOTO 3700
          GOTO 3360
C
C
3630      H=H+BISECT  'H IS TOO SMALL G<0
          GOTO 3360
C
C
C
3500      XTOL=5 0E-6
          FTOL=0 0
          NLIM=15
          NPRINT=1 'NO PRINT
          X1=HSTORE
          X2=H
          F1=GSTORE
          F2=G
C         CALL MDLNIN (IPAIRB T TC THICK SLOPE
C         1 PP0 PP1 ALFA SLAMDA
C         1HSTORE H GSTORE G XB XTOL FTOL NLIM NPRINT)
C
C
C
C
C
C
C
C
C
C
C*****************************************************************
```



```
C         SUBROUTINE  MDLNIN= Modified linear interpolation
C*****************************************************************
C         MODIFIED FOR CALL FROM MCFUNC!!!!!!!!!!!!!!
C
C         CALL MDLNIN (IPAIRB T TC THICK SLOPE
C         1 PP0 PP1 ALFA SLAMDA
C         1HSTORE H GSTORE G XB XTOL FTOL NLIM NPRINT)
C
C         SUBROUTINE MDLNIN (IPAIRB T TC THICK SLOPE
C         1 PP0 PP1 ALFA SLAMDA
C         1X1 X2 F1 F2 XB XTOL FTOL NLIM NPRINT)
C         REAL PARAMS(7)
C
C         Subroutine for root finding by modified linear interpolation
C
C         Origin  Curtis F  Gerald. Applied Numerical Analysis. 2ED
C              Addison-Wesley 1980  pg 48
C
C         Parameter are -
C         X          The independent variable for the interpolation
C                    It is the field in this case
C         X1,X2           Initial values of X  F(x) must change sign at these
C                    points
C         XB         Returns the root to main program
C         XTOL,FTOL Tolerance values for X F(x) to terminate interations
C         NLIM       Limit to number of interations
C         I
C              I=1  meets tolerance for X values
C              I=2  meets tolerance for F(x)
C              I=-1 NLIM exceeded
C              I=-2 f(x1) not opposite in sign to f(x2)
C
C         When the subroutine is called  the value of NPRINT
C         indicates whether to print each value of not   NPRINT=0
C         means print them   NE  0 means NO-PRINT
C
          LOGICAL PRINT
          PRINT= TRUE
          IF (NPRINT NE 0) PRINT= FALSE
C
C
C
2500      IF (F1*F2 GT 0) GOTO 2050
C
C
C
C
          FSAVE=F1
C
          DO 2020 J=1 NLIM
          XB=X2-F2*(X2-X1)/(F2-F1)
          IF ( NOT PRINT) GOTO 2600
          TYPE *
          TYPE *  X1 X2    X1 X2
C
```

```
2000    PI=3.14159265359
        HBAR=XR**4 /PI**2
        Y= HCFNYP(IPAIRB HBAR TC THICK,SLOPE)
        1+PP0* 5/PI-PP1*XR*SLOPE/PI/0 000033579
        FR=ALOG(T) - HCFNF(T HBAR Y ALFA SLAMDA)
C
        XERR=ABS((X1-X2)/X2)        'Different than book
C
        IF ( NOT PRINT) GOTO 2005
        TYPE 2199  J XR FR
2199    FORMAT (1H 13HAt iteration   I4  5H T =  E12 5
        1  12H  FONE(T) =  E12 5)
C
2005    IF (XERR LE XTOL) GOTO 2060
        IF (ABS(FR) LE FTOL) GOTO 2070
        IF (FR*F1 LT 0) GOTO 2010
C
        X1=XR
        F1=FR
        IF (FR*FSAVE GT 0) F2=F2/2
        FSAVE=FR
        GOTO 2020
C
2010    X2=XR
        F2=FR
        IF (FR*FSAVE  GT  0) F1=F1/2
        FSAVE=FR
C
2020    CONTINUE
C
C
C
C            This section when NLIM is exceeded
        I=-1
        IF ( NOT PRINT) GOTO 2700
        TYPE 2200, NLIM XR FR
2200    FORMAT (1H0  26HTolerance not met   After   I4
        1 15H Iterations X=   E12 5   12H And F(X) =  E12 5)
        GOTO 2700
C
C
C
C
C       This section for return when F(X1) and F(X2) not opposite in sign
2050    I=-2
        IF ( NOT PRINT) GOTO 2700
        TYPE 2201
2201    FORMAT (1H0  35HFunction has same sign at X1 and X2)
        GOTO 2700
C
C
C
C
C       This section returns after meeting XTOL
2060    I=1
```



```
        IF ( NOT PRINT) GOTO 2700
        TYPE 2202, J,XR,FR
2202    FORMAT (1H0,' Tolerance met in    I4   Iterations   X =
        1  F12 5, 8H F(X) =   E12 5)
        GOTO 2700
C
C
C
C
C       This section returns after meeting F(X) tolerance
2070    I=2
        IF ( NOT PRINT) GOTO 2700
        TYPE 2203  J,XR FR
2203    FORMAT (1H0  19HF Tolerance met in   I4 18H
        1Iterations  X =   F12 5  8H F(X) =   E12 5)
C       RETURN
C       END
C
C
C
C
C
C
C
C
C
C
2700    H=XR
        IF (I GE 0) GOTO 3700
        IF (I LT -1) GOTO 700
C
C            I=-1
        TYPE *,  Number of iterations exceeded in
        1the linear interpolation
        GOTO 3700
C
700     TYPE *  'FONE did not change sign
        STOP
C**********************************************************************
C**********************************************************************
C       Out of Modified linear interpolation
C
C
C
C
C
3700    HCFUNC=H*TC*SLOPE/(-1000 )
C
C
        END
C
C       This function is called from HC2 which was written by J A A
C       ALEXANDER   The last revision was made by her 6/21/83
C       It was adapted to fortran by J E  TEA.ZYE ON 9/84
C
C
```

```
      FUNCTION HCFNF(T,HBAR,V,ALFA,SLAMDA)
      A=ABS (SLAMDA* 3/(HBAR*ALFA))
      IF (A GE 1 ) HCFNF=FNFBEA(T,HBAR,V,
     1ALFA,SLAMDA)
      IF (A LT 1) HCFNF=FNFIMA(T HBAR V ALFA SLAMDA)
      END
C
C
      FUNCTION FNFBEA(T,HBAR V ALFA SLAMDA)
      X=SQRT((SLAMDA* 25)**2 )-((HBAR*ALFA* 5)**2 ))
      P=SLAMDA* 25/X
      IF (P LT 2 E0) GOTO 8410
        P=EXP (ALOG( SLAMDA)- ALOG (6 *X))
8410  Q=Y/T+(SLAMDA* 25-X)/T*0 5   '       Grouping is important if
C                                          SLAMDA is large
      B=0 5*Y/T+(SLAMDA* 25+X))/T
      FNFBEA=FNPSI(Q 5)-(1 -P)* 5*FNPSI(Q)-(1 -P)* 5*FNPSI(B)
      END
C
C
      FUNCTION FNFIMA(T HBAR Y ALFA SLAMDA)
      REAL L E
      INTEGER VMAX,V
      PI=3 14159265359
      ERR=0 01
      L=6 *Y/(ERR*T)
      IF (L GT 10001 ) L=10001 0
      ALFAH=ALFA*HBAR
      E=2 *Y*(SLAMDA+2 *Y)+ALFAH**2 0
C     CALCULATE DELTA
C     Delta is the error in terminating the sum after L terms
C        where L=2V+1
8540  BOTTOM=L*((L*T)**2 +(SLAMDA+6 *Y)*T*L+E)
      FIRST=ALOG((L*T)**2 *L/BOTTOM)*0 5
      CHI = SQRT(6 *ALFAH**2 -SLAMDA**2 )
C          TRIG FUNCTIONS HAVE ARGUMENTS IN RADIANS
      ANGLE=ATAN((2 0*L*T+6 0*Y+SLAMDA)/CHI)
      FACTOR=PI* 5-ANGLE
      SECOND=SLAMDA*FACTOR/CHI
      DELTA=-(FIRST+SECOND)
      IF (L GE 10001 0) GOTO 9040
C                              Maximum value for L is reached
      IF (DELTA LT ERR) GOTO 9040    Correct value for L found
      L=L+5 0     '     Increase L and recalculate delta
      GOTO 8540
8840  VMAX=INT((L-1 )* 5)
      SUMM=0
C
      DO 8720 V=0 VMAX '                    Loop to sum PSI series
      L=2 *FLOAT(V)+1
      TOP=2 *Y*T*L+E
      BOTTOM=L*((L*T)**2 +(SLAMDA+6 *Y)*T*L+E)
      SUMM=SUMM+TOP/BOTTOM
8720  CONTINUE
C
```



```
      IF (V GT 4999) TYPE *, ' FNFIMA   V> 4999    SUM ERROR =   DELTA
C          TKACZYK   The above IF/THEN statement was removed from
C                the do loop  V=1 to VMAX
      FNFIMA=-2 0*SUMM
      END
C
C
C
C
C
      FUNCTION FNPSI(Z0) '      Called by function FNFBEA
C          Calculates the digamma function
      IF ((Z0 LE 2 ) AND (Z0 GE 1 )) FNPSI=FNPSI1(Z0)
      IF (Z0 LT 1 ) FNPSI=FNPSI2(Z0)
      IF ((Z0 LT 50 ) AND (Z0 GT 2 )) FNPSI=FNPSI3(Z0)
      IF (Z0 GE 50 ) FNPSI=FNPSI4(Z0)
      END
C
C
      FUNCTION FNPSI1(Z1) ' Called by functions PSI, PSI2, AND PSI3
C          1(=Z1(=2
C          REF  "APPROXIMATIONS FOR THE PSI(DIGAMMA) FUNCTION "
C               W J MOODY  1988
      S=Z1-1
      S7=S**7
      SUM1= 0469933333*(S-S7)- 2020319l*(S**2 -S7)+ 0820943J3*(S**3 -S7)
      SUM2=-( 03591065*(S**4 -S7))+ 01405925*(S**5 -S7)
      1- 0067205*(S**6 -S7)
      FNPSI1=S/(1 +S)- 5772156649+S7* 5+SUM1+SUM2
      END
C
C
      FUNCTION FNPSI2(Z2) ' Called by FN PSI
C          Z2(1
      FNPSI2=FNPSI1(1 +Z2)-1 /Z2
      END
C
C
      FUNCTION FNPSI3(Z3) 'Called by FN PSI
C          2(Z3(50
      INTEGER WHOLE,VAU
      WHOLE = INT (Z3)
      FRAC=Z3-FLOAT(WHOLE)
C          CALCULATE PSI(WHOLE+FRAC)
      PSUM=0   ' INITIALIZE SUM PSUM TO ZERO
      DO 9070 VAU=1 (WHOLE-1)
          PSUM=PSUM+1 /(FLOAT(WHOLE-VAU)+FRAC)
9070  CONTINUE
      FNPSI3=PSUM+FNPSI1(1 +FRAC)
      END
C
C
      FUNCTION FNPSI4(Z4) '  Called by FN PSI
C          Z4)=50
      FNPSI4=ALOG (Z4)  5/Z4 1 /(12 *Z4**2 )+1 /(120 *Z4**4 )-1 /
```

```
      1.252 *Z6**6 )
      END
C
C          The following function is called from HC2
C     HC2 and this function program were written by J A R
C     Alexander as last modified by her 6/21/83   It was
C     Adapted to fortran by J E  Thacker on 8/86
C
C
C
      FUNCTION HCFHYP(IPAIRB HBAR TC THICK SLOPE)
      PI=3.1415926535
      IF (IPAIRB EQ 1) GOTO 9040
      IF (IPAIRB EQ 2) GOTO 9200
C
C 9100  PAIRBREAKER  2
      HCFHYP=HBAR* 39010* 5
C      39010 is derived on page 88 of TYPE II SUPERCONDUCTIVITY by
C     Saint-James, Thomas  and Sarma
      GOTO 9000
C
C     PAIRBREAKER  1
9040  HCFHYP=HBAR* 5
C                    Bulk of thin film perpendicular to field
      GOTO 9000
C
C
C          PAIRBREAKER        Thin film parallel to field
C     Y2=(HBAR**2)*(PI**2)**(1/2)*HP*ALFA*GAMMA* THICK**2)/(12*Flux quantum
C     Y2=(PI**2)*( SLOPE*(TC*(THICK**2)**HBAR**2))/(3*Flux quantum
9080  HCFHYP=(1)12)017 (0278*SLOPE*TC*THICK**2 *HBAR**2 )
C     2123017 (0278= PI**2 / 3) * Flux quantum (Gauss cm**2)
C     GOTO 9000
C
C
9000  END
```

```
C
C
C*************************************************************
C       FUNCTION HCHISQ
C*************************************************************
C
C
C
C       ORIGIN  BEVINGTON PHILIP R
C            DATA REDUCTION AND ERROR ANALYSIS
C            FOR THE PHYSICAL SCIENCES
C
C            However  this program has been modified for use
C            with the root program HC2 which calculates
C            critical fields
C
C
C
C       PURPOSE
C            EVALUATE REDUCED CHI SQUARE FOR FIT TO DATA
C            HCHISQ = SUM ((Y YFIT)**2 / SIGMA**2) / NFREE
C
C       USAGE
C            RESULT = HCHISQ (X Y  SIGMAY  NPTS  NFREE  MODE  YFIT TFIRST)
C
C       DESCRIPTION OF PARAMETERS
C            Y    -ARRAY OF DATA POINTS
C            SIGMAY     ARRAY OF STANDARD DEVIATIONS FOR DATA POINTS
C            NPTS -NUMBER OF DATA POINTS
C            NFREE      NUMBER OF DEGREES OF FREEDOM
C            MODE -DETERMINES METHOD OF WEIGHTING LEAST SQUARES FIT
C                  +1 (INSTRUMENTAL) WEIGHT(I) = 1 /SIGMAY(I)**2
C                   0 (NO WEIGHTING) WEIGHT(I) = 1
C                   1 (STATISTICAL)  WEIGHT(I) = 1 /Y(I)
C            YFIT -ARRAY OF CALCULATED VALUES OF Y
C
C
      FUNCTION HCHISQ (X Y  SIGMAY  NPTS  NFREE  MODE  YFIT TFIRST)
C     DOUBLE PRECISION CHISQ  WEIGHT
      DIMENSION X(50) Y(50) SIGMAY(50) YFIT(50)
110   CHISQ = 0
      NSKIP=0
120   IF (NFREE) 130 130 200
130   HCHISQ = 0
      GOTO 400
C
C     ACCUMULATE CHI SQUARE
C
200   DO 305 I=1 NPTS
           Test to see if this point lies in the region where
C          the transition is first order   If so don t include this point
      IF (X(I) GT TFIRST) GOTO 210
      NSKIP= NSKIP+1
      GOTO 305
C
```

```
210     IF (MODE) 220,270,290
220     IF (Y(I)) 250,270,230
230     WEIGHT = 1   / Y(I)
        GOTO 300
250     WEIGHT = 1   / (-Y(I))
        GOTO 300
270      WEIGHT = 1
        GOTO 300
290     WEIGHT = 1 /SIGMAY(I)**2
300     CHISQ=CHISQ + WEIGHT*(Y(I)-YFIT(I))**2
305     CONTINUE
C
C            DIVIDE BY NUMBER OF DEGREES OF FREEDOM
C
310     FREE=FLOAT(NFREE-NSEIP)
320     HCHISQ=CHISQ/FREE
400     END
```



```
C
C
C*************************************************************
C            SUBROUTINE HCDISP
C*************************************************************
C
C
C
C
C
C
C
C   DESCRIPTION   HCDISP
C       This is called from the root program HC2 which calculates
C       critical field.  This program displays the parameters used and
C       allows their modification.  See the HC2 for more details on the
C       parameters themselves.  The parameters are displayed in the
C       subroutine DISPLA
C
C
C
C
C
C
      SUBROUTINE HCDISP(IDATA IPAIRB NPTS PARAMS)
      BYTE ANSWER(1)
      REAL PARAMS(7)
      SLOPE=PARAMS(1)
      BFULDE=PARAMS(2)
      BENORM=PARAMS(3)
      CFULDE=PARAMS(4)
      PP0=PARAMS(5)
      PP1=PARAMS(6)
      TC=PARAMS(7)
C
C
C
C
C       The following section of code is the user interface for
C       entering the various parameters for the program HC2 and HCFIT
C
C
C
C
1150    PARAMS(1)=SLOPE
        PARAMS(2)=BFULDE
        PARAMS(3)=BENORM
        PARAMS(4)=CFULDE
        PARAMS(5)=PP0
        PARAMS(6)=PP1
        PARAMS(7)=TC
C
        CALL DISPLA(IPAIRB NPTS PARAMS)
        TYPE 1330
1330    FORMAT (  Enter the number of the parameter you wish to alter /
        1   (   11 if you are satisfied with these parameters ) )
        ACCEPT 1340 ICHNGE
1340    FORMAT (I2)
```

```
C
      IF (ICHNGE EQ 1) GO TO 1401
      IF (ICHNGE EQ 2) GO TO 1420
      IF (ICHNGE EQ 3) GO TO 1430
      IF (ICHNGE EQ 4) GO TO 1440
      IF (ICHNGE EQ 5) GO TO 1450
      IF (ICHNGE EQ 6) GO TO 1460
      IF (ICHNGE EQ 7) GO TO 1490
      IF (ICHNGE EQ 8) GO TO 1500
      IF (ICHNGE EQ 11) RETURN
      GOTO 1150
C
C
1401  TYPE 1402
1402  FORMAT (//' What is the pairbreaker number? ')
      TYPE *,'  1     Bulk of thin film perpendicular to field'
      TYPE * ,'  2     Thin film parallel to field'
      TYPE * ,'  3     Surface sheath'
      TYPE 1404
1404  FORMAT ('0Enter the number of the pairbreaker  then return  //)
      ACCEPT 1406, IPAIRB
1406  FORMAT (I1)
      IF (IPAIRB EQ 1) GOTO 1435  'Enter the slope
      IF (IPAIRB EQ 2) GOTO 1430  'Enter C-Fulde
      IF (IPAIRB EQ 3) GOTO 1435  'Enter the slope
      GOTO 1150
C
1420  TYPE 1422
1422  FORMAT (//' What is Tc  (K)' ///
      ACCEPT * TC
      GOTO 1150
C
1430  IF (IPAIRB NE 2) GOTO 1435
      TYPE 1431
1431  FORMAT (// 'What is c fulde'   ///
      ACCEPT * CFULDE
      GOTO 1150
C
1435  TYPE 1437
1437  FORMAT (//  What is the slope (dG/K)' ///
      ACCEPT * SLOPE
      SLOPE=-ABS(SLOPE)*1000  ' convert to G/K  make slope negative
      GOTO 1150
C
1440  TYPE 1442
1442  FORMAT (// 'Enter b-Fulde   ///
      ACCEPT * BFULDE
      GOTO 1150
C
1450  TYPE 1452
1452  FORMAT (//  Enter the renormalization for Hp' ///
      ACCEPT * RENORM
      GOTO 1150
C
1460  TYPE 1462
```



```
1462  FORMAT (//' How many points in the plot? ///)
      IF (IDATA EQ 1) TYPE *,'Enter zero if you want the calculation
     1done at the data points '
      ACCEPT 1466,NPTS
1466  FORMAT(I3)
      IF ((IDATA EQ 0) AND (NPTS EQ 0)) GOTO 1480
      IF (NPTS LT 50) GOTO 1488
      TYPE 1465
1465  FORMAT (//     points must be (=50   press return to
     1 acknowledge //)
      PAUSE '  Change dimension statement if more than 50 points are needed
      GOTO 1460
1488  IF (NPTS EQ 0) GOTO 1150
      TSTEP=1/FLOAT(NPTS)
      GOTO 1150
C
1490  TYPE 1492
1492  FORMAT (//' Enter the value of PP0  additional pairbreaker
     1 constant with field'//)
      ACCEPT *,PP0
      GOTO 1150
C
1500  TYPE 1502
1502  FORMAT (//' Enter PP1  proportionality constant for
     1pairbreaker linear with field //)
      ACCEPT * PP1
      GOTO 1150
C
      END
C
C
C
C
C
C
C
      SUBROUTINE DISPLA (IPAIRB,NPTS PARAMS)
C
      REAL PARAMS(7)
      SLOPE=PARAMS(1)
      BFULDE=PARAMS(2)
      RENORM=PARAMS(3)
      CFULDE=PARAMS(4)
      PP0=PARAMS(5)
      PP1=PARAMS(6)
      TC=PARAMS(7)
C
C
C
      CALL TSERAS(2) 'Erase screen
C
C
      TYPE 1300 IPAIRB PP0
1300  FORMAT(' I  Pairbreaker =    I2 T40  '  PP0 =   F5 2//
      TYPE 1301,TC,PP1
```

```
1301    FORMAT(' 2  Tc =   F5.2 T40  0  PP1 =   F5.2/)
C
        IF (IPAIRB NE 2) GOTO 1303
        TYPE 1302 CFULDE
1302    FORMAT (' 3  Cfulde =   F9.6/)
        GOTO 1305
C
1303    TYPE 1304 SLOPE*1E 3
1304    FORMAT (  )  Slope =   F9.6  kG/K /)
C
1305    TYPE 1306 BFULDE
1306    FORMAT (' 4  b-Fulde =   F6.3/)
        TYPE 1308 BENORM
1308    FORMAT (' 5  Benorm =   F5.3/)
C
        IF (NPTS NE 0) GOTO 1309
        TYPE 1311
1311    FORMAT (' 6  At data points  T39  11  Continue ///)
        RETURN
C
1309    TYPE 1310 NPTS
1310    FORMAT (  6    points =   I2.T39  11  Continue ///)
        RETURN
        END
```



```
C
C*****************************************************************************
C       SUBROUTINE HCPLOT(FNAME.T2.H2 NPTS.IPAIRB IDATA CHISQR TFIRST PARAMS)
C*****************************************************************************
C
C   DESCRIPTION  HCPLOT
C       Called from HC2 or HCFIT this program plots the superconducting
C       critical field vs temperature
C
C   VARIABLES       See HC2 for most of the input variables
C       T2() Input temperature array
C       H2() Input(theory) critical field array
C       T()  Data temperature array
C       H()  Data critical field array
C       IDATA       If equals one then plot data in addition to theory
C       H2MAX       Maximum critical field needed for drawing the grid
C
        SUBROUTINE HCPLOT(FNAME.T2 H2.NPTS IPAIRB.
        1IDATA.CHISQR.TFIRST.PARAMS)
        REAL T2(50).H2(50)
        REAL T(50).H(50)
        BYTE FNAME(12) IDATA
        REAL PARAMS(7)
        SLOPE=PARAMS(1)
        BFULDE=PARAMS(2)
        BENORM=PARAMS(3)
        CFULDE=PARAMS(4)
        PP0=PARAMS(5)
        PP1=PARAMS(6)
        TC=PARAMS(7)
C
C       Fill arrays
C
C       REAL TARRAY(50) HARRAY(50) H3(50) ***Not used
C       DO 5 I=1.NPTS
C       TARRAY(I)=T2(I)/TC '                    STORE REDUCED TEMPERATURE IN ARRAY
C       HARRAY(I)=H2(I)*(-1000 )/TC/SLOPE       STORE REDUCED FIELD IN ARRAY
C5      H3(I)=H2(I)**2 '                        STORE FIELD SQUARED IN ARRAY
C
C
        IF (IDATA EQ 0) GOTO 30
C
C       Gather data from disk data file if IDATA =1
C
        OPEN (UNIT=1 NAME=FNAME.TYPE='OLD')
        READ (1.*) NPTS
        READ (1.*) (T(M) H(M).M=1 NPTS)
        CLOSE (UNIT=1)
C
C
C       DRAW GRID
C
30      H2MAX=H2(1)
        DO 40 I=2 NPTS
40      H2MAX=AMAX1(H2(I) H2MAX)
```

```
C
      CALL TSGRID(0 TC.0 H2MAX*1 3  Hc2
     1 vs Temperature', 'Temperature (K)  'Critical field (kG)  1)
C
C     Display parameters
C
      IF (IDATA EQ 0) GOTO 125
C
      TYPE *
      TYPE 100,FNAME BFULDE
100   FORMAT (X,T8 12A1,T40  b-Fulde  T62 F8 6)
      GOTO 175
C
125   TYPE *
      TYPE 150,BFULDE
150   FORMAT (/X T40  b-Fulde  T62 F8 6)
C
175   IF (CHISQB EQ 0 ) GOTO 179
      TYPE 176 CHISQB
176   FORMAT (8 T8, Variance  T25 F8 3)
      TYPE 177 RENORM
177   FORMAT (X,T8  Renorm  T25,F6 4)
      GOTO 210
C
179   TYPE 200 RENORM
200   FORMAT (X T40  Renorm  T47 F8 6)
C
210   TYPE 250 TC
250   FORMAT (8 T8  Tc  T26 F5 2   K )
      TYPE 275 PP0 PP1
275   FORMAT (X,T8  PP0  T16 F6 3 T26  PP1  T31 F6 3)
C
      IF (IPAIRB NE 2) GOTO 340
      TYPE 320 CFULDE
320   FORMAT (T8  c-Fulde  T26 F7 2)
      GOTO 400
C
340   TYPE 350 SLOPE/1000
350   FORMAT (T8  Slope at Tc  T21 F7 2   KG/K )
C
400   TYPE 550 IPAIRB NPTS
550   FORMAT (8 T8  Pairbreaker    I1 T15  Npts  T31 I
      IF (TFIRST LT 0 0) GOTO 900
      TYPE 600 TFIRST
600   FORMAT(8 T8,'T-first  T16 F8 2)
C
800   CALL TSRPLT(T2 0 0 H2 NPTS 1)
      IF (IDATA EQ 1)      CALL TSRPLT(T 0 0 H NPTS 0)
      IF (TFIRST GE 0 0) CALL TSTEXT(TFIRST H,MAX
     1H2MAX* 04 0 0      1)
      ACCEPT 1000
1000  FORMAT()
      CALL TSEBAS(1)
      CALL TSOFF
      RETURN
      END
```

```
C
C     This is called from the root program HC2 which calculates
C     critical field   The program HCDATA displays a data file of
C     critical field values   See HC2 for more details
C
C*************************************************************
      SUBROUTINE HCDATA(FNAME)
C*************************************************************
      BYTE FNAME(12)
      REAL T(50),H(50)
C
      OPEN (UNIT=1,NAME=FNAME TYPE='OLD')
      READ (1,*) NPTS
200   READ (1,*) (T(I),H(I), I=1,NPTS)
      CLOSE (UNIT=1)
C
      TYPE *,'NPTS = ',NPTS
      TYPE 15
      DO 20 M=1,NPTS
      IF (FLOAT(M/10) NE FLOAT(M)/10 ) GOTO 17
      PAUSE
      TYPE 15
15    FORMAT (/T6,' I',T13,'TEMP ',T28,'HC2')
17    N=M
20    TYPE *, N,T(M),H(M)
      PAUSE
      RETURN
      END
```

Appendix C

Proc. 18th Int. Conf. on Low Temperature Physics, Kyoto, 1987
Japanese Journal of Applied Physics, Vol. 26 (1987) Supplement 26-3

Tunneling at High Magnetic Fields and ^{3}He Temperatures Using a Squeezable Tunnel Junction Apparatus

J.E.Tkaczyk and P.M.Tedrow,

Francis Bitter National Magnet Laboratory**, M.I.T.
Cambridge, MA , USA

An apparatus similar to that described by Moreland and Hansma has been constructed; However, the junction gap is mechanically adjusted without use of an electromagnet, allowing for a compact design. High quality Pb-Pb junctions with conductances showing phonon structure have been obtained. A crossover from ohmic to tunneling conduction across the junction gap is observed as the squeezing force on an Al-normal metal junction is decreased. The tunneling conductance of an Al-ferromagnet junction measured in an applied magnetic field and 0.4K shows the asymmetry due to spin-polarized tunneling. This is the first observation of spin-polarized tunneling in a junction with a mechanically adjustable gap. Application to bulk samples will be discussed.

INTRODUCTION

The recent development of vacuum tunneling techniques, such as scanning tunneling microscopy, has given new hope that tunneling can be applied in previously unmanagable situations. In particular, the squeezable method[1] developed by Moreland, Hansma and co-workers can be applied to a variety of sample configurations including thin films, bulk samples, and filaments[2]. The basic idea is that two substances can be controllably brought together to a separation suitable for tunneling by bending the two with sightly different radii of curvature. We have constructed a variation of the squeezable apparatus for which the squeezing force is supplied mechanically rather than with the use of an electromagnet. This allows for a compact design suitable for ^{3}He cryogenics and for use in high magnetic fields.

The design is such as to provide common-mode rejection of vibration yielding good stability of the spacing between the electrodes. This feature is necessary due to the exponential relationship between the spacing and tunneling resistance.

EXPERIMENTAL RESULTS

The conductance curve vs bias voltage for a Pb-Pb squeezable electron tunneling (SET) junction obtained at 4.2K and zero applied field is shown in Fig. 1. The thickness of each of the Pb films was 150nm. The conductance shows the features typical of a high quality S-I-S junction: the peaks at the sum of the energy gaps of the two films are sharp, the conductance in the sub-gap region is flat and there is little leakage. Phonon induced structure is visible at higher voltage.[3] This curve took several minutes to obtain demonstrating the stability of the junction.

Figure 2 shows a sequence of conductance curves for an Al-normal metal thin film junction as the squeezing pressure is changed. The normal metal is a 20nm thick vanadium-titanium alloy. The Al film was 6 nm thick. The number to the right of each curve indicates the order in which the curves were taken. The nature of the conduction process across the junction could be changed continuously by adjusting the squeezing force. For a large squeezing force a large area of the films are in ohmic contact; that is, the conductance is constant as a function of bias voltage. When the squeezing force is reduced, the contact area is reduced with a resulting decrease in conductance. For junctions with resistance above 5 kohm an increasingly large portion of the conduction is due to tunneling. This is evident from the appearance of structure associated with the 0.3mV superconducting gap of the thin Al film. The relative proportion of tunneling to ohmic conductance across the junction can be readily determined due to the fact that at 0.4 K the contribution to the conductance from tunneling at zero bias voltage is zero. The junction leakage, that is ohmic conduction, decreases as the junction resistance increases. In addition the conductance peak associated with the singularity in the BCS density of states becomes sharper and more pronounced.

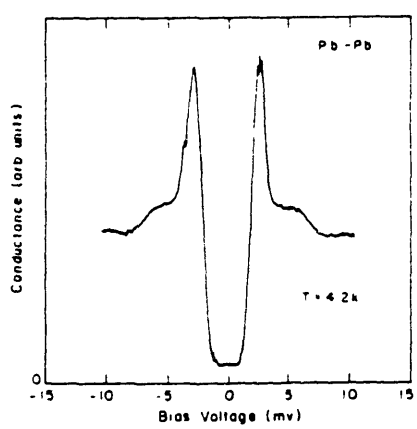

Fig. 1 Conductance of a Pb-Pb SET junction.

* Supported by US DOE Contract No. DE-FG02-84ER45094.
** The Francis Bitter National Magnet Laboratory is supported by the US National Science Foundation.

The conductance curves in Fig.3 are those for an Al-Fe thin film junction at a temperature of 0.4K in zero magnetic field and in an applied magnetic field of 1.8 tesla provided by a water-cooled Bitter magnet. The asymmetry which develops with the magnetic field applied is the result of spin-polarized tunneling[4] which is a consequence of both the Zeeman splitting of the Al density of states and the ferromagnetic polarization of the Fe conduction electrons at the Fermi surface.

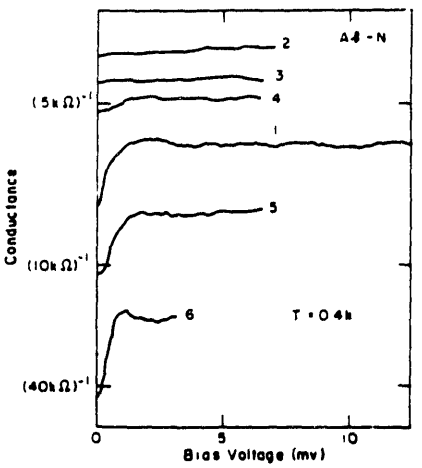

Fig. 2 A sequence of conductance curves for an Al-normal metal SET junction for different squeezing forces. The number at the right indicates the order in which the curves were taken.

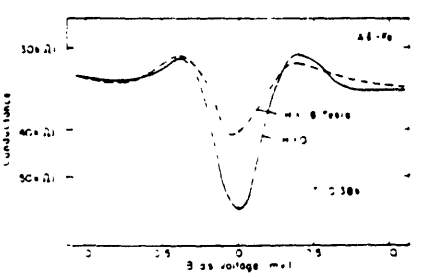

Fig. 3 Two conductance curves of an Al-Fe SET junction. The curve taken with an applied field shows the asymmetry assocciated with spin-polarized tunneling.

Figure 4 shows conductance curves for a junction between a Pb film and a sintered pellet of the high T_c superconductor $Ba_2YCu_3O_{7-\delta}$ which has a transition temperature of 92.5 K[5]. The Pb film was 130nm thick. The pellet was made at the Francis Bitter National Magnet Laboratory[6]. Conductance curves were taken in a superconducting magnet to a maximum field of 7 tesla. The size of the BCS gap for a T_c of 92.5K is indicated on the figure. The structure at lower voltage is approximately the proper form for tunneling between two Pb films. The voltage peaks correspond to those in Fig. 1. Presumably some Pb has been transfered to the pellet. Since the bulk critical field of Pb is 800 Oe, the observation of superconductivity at 7 tesla suggests either that the transfered Pb is in the form of very small particles, or is proximity-coupled to the $Ba_2YCu_3O_{7-\delta}$.

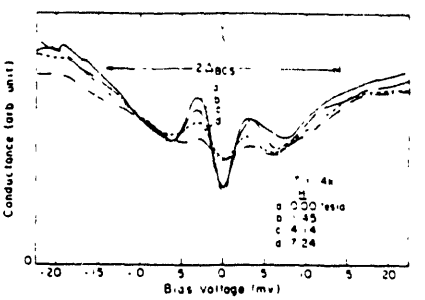

Fig. 4 Conductance curves of a Pb-$Ba_2YCu_3O_{7-\delta}$ SET junction for several values of the applied magnetic field.

SUMMARY

We have constructed a versatile squeezable tunnel probe which allows study of thin film and bulk samples in fields up to 20 T and temperatures down to 0.4K. Spin-polarized tunneling between Al and magnetic films gives information about the spin density of states of the magnetic material and, in addition, has served as an invaluable tool for studying Pauli limited superconductors[7]. The observation of spin-polarized tunneling in a mechanically adjustable tunneling device, reported here for the first time, may lead to application of this technique to an increased variety of materials.

ACKNOWLEDGMENT

We would like to thank Dr. J.S. Moodera for supplying us with samples of high T_c superconductors.

REFERENCES

1) J.Moreland and P.K.Hansma: Rev. Sci. Instrum. 55(1984) 399; J.Moreland, S.Alexander, M.Cox, R.Sonnenfeld, and P.K.Hansma: Appl.Phys.Lett. 43(1983) 387.
2) J.Moreland and J.W.Ekin: Appl. Phys. Lett. 47(1985) 175.
3) W.L.McMillan and J.M.Rowell: Phys. Rev. Lett. 14(1965) 108; W.L.McMillan and J.M.Rowell: Superconductivity, ed. R.D.Parks, (Marcel Dekker Inc., New York, 1969) Vol. 1, p.561.
4) P.M.Tedrow and R. Meservey: Phys.Rev.B, 7(1973) 318.
5) M.K.Wu, J.R.Ashburn, C.J.Torng, P.H.Hor, R.L.Meng, L.Gao, Z.J.Huang, Y.Q.Wang and C.W.Chu: Phys. Rev. Lett. 58(1987) 908; R.J.Cava,B.Batlogg, R.B.van Dover, D.W.Murphy, S.Sunshine, T.Siegrist, J.P.Remeika, E.A.Rietman, S.Zahurak, and G.P.Espinosa: Phys. Rev. Lett. 58(1987) 1676.
6) J.S.Moodera et al: preprint.
7) J.A.X.Alexander, T.P.Orlando, D.Rainer, P.M.Tedrow: Phys. Rev.B, 31(1985) 5811.

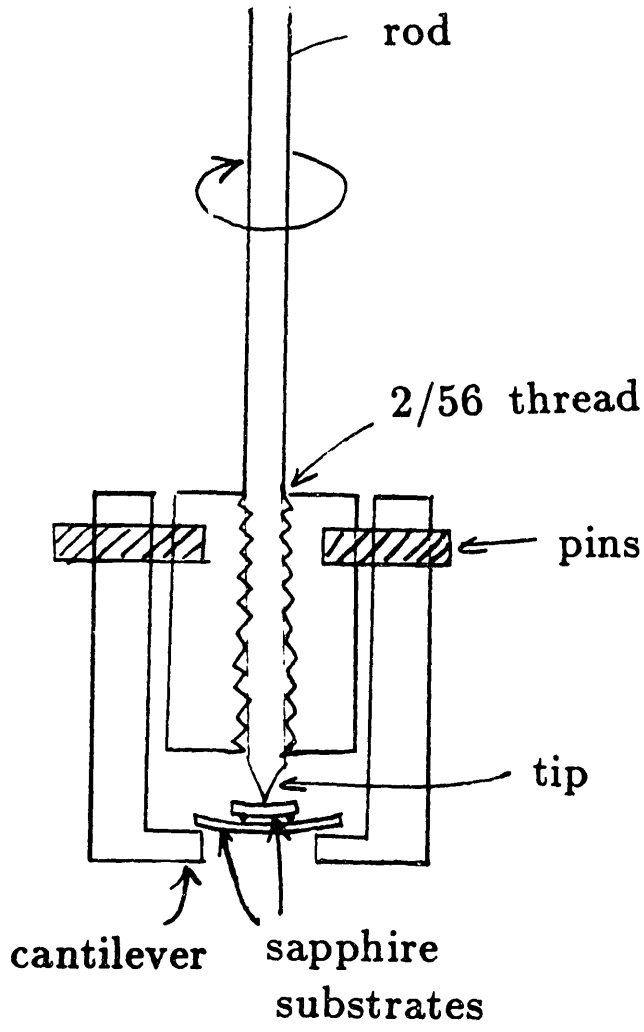

Fig. C.1 Simplified drawing of the squeezing apparatus. A stop (not shown) prevents the whole apparatus from turning as the rod is turned. Rather, the result of turning the rod is to lower the tip and raise the cantilever so as to increase the curvature of the substrates. Note that vertical vibration along the rod vibrates the whole apparatus and not just the tip.